Shock induced bubble explosions in liquid cyclohexane

vorgelegt von
Diplom-Ingenieur
Konstantinos Mitropetros
aus Pireas, Griechenland

Von der Fakultät III – Prozesswissenschaften
der Technischen Universität Berlin
zur Erlangung des akademischen Grades

Doktor der Ingenieur-Wissenschaften
- Dr.-Ing. -

genehmigte Dissertation

Promotionsausschuss:

Vorsitzender: Prof. Dr.-Ing. G. Fleischer
Berichter: Prof. Dr.-Ing. J. Steinbach
Berichter: Priv.-Doz. Dr. rer. nat. B. Plewinsky

Tag der wissenschaftlichen Aussprache:
14. April 2005

Berlin 2005

D 83

Abstract in English

In this work the influence of shock waves on organic liquids with and without bubbles is investigated. The experiments were performed in a new experimental setup with the help of high speed photography and pressure measurements. The apparatus consisted of a cylindrical autoclave with a bubble generator at its bottom. For the creation of a detonation wave a tube was installed on the top of the autoclave.

The following parameters were varied: The distance between neighboring bubbles, the composition of the gaseous mixture inside the bubbles, the initial pressure of the system, the initial bubble size, and the organic liquid (cyclohexane, 2-ethylhexanal, cumene, and methanol).

Two different types of bubble explosion were observed. Their main difference is the length of their ignition delay. The bubble explosion type I takes place during the first oscillation after the shock wave impact. Further important results about this type of explosion refer to:

- the explosion range in relation to the composition of the gas mixture within the bubble as well as to the initial bubble size.
- the direct ignition of a bubble by a shock wave emitted by a nearby bubble explosion. Such a phenomenon is experimentally observed for the first time.
- the shock induced ignition of gas bubbles containing an initially non explosive fuel-lean gas mixture. Optical recordings of jet penetration into the bubble prove that shock wave induced enrichment in vapor of the surrounding liquid is an important stage before the ignition.
- the observation of bubble explosion type I in all the investigated liquids.
- the mechanism of bubble explosion type I.

The bubble explosion type II takes place with much longer ignition delay. It was observed under certain conditions only. An explosion mechanism is proposed on the basis of the experimental results. According to this mechanism, even non explosive fuel-rich gaseous bubbles can become explosive due to partial condensation of the fuel.

A further group of results refer to cavitation phenomena inside the liquid and to shock induced phenomena on the surface. Additionally, the explosion limits of gaseous cyclohexane in pure oxygen at elevated pressures and temperatures were determined.

The safety engineering aspects of the experimental results are discussed.

Abstract in German

In dieser Arbeit wird der Einfluss von Stoßwellen auf organische Flüssigkeiten mit und ohne Gasblasen untersucht. In einer neu aufgebauten Apparatur wurden Untersuchungen mit Hilfe der Hochgeschwindigkeitsfotografie und mit Druckmessungen durchgeführt. Die Apparatur bestand aus einem zylindrischen Autoklav mit einem Blasegenerator an seinem Boden. Zur Erzeugung einer Detonationswelle war oberhalb des Autoklavs eine Rohstrecke angeflanscht.

Die folgenden Parameter wurden variiert: Die Entfernung zwischen benachbarten Gasblasen, die Zusammensetzung der Gasmischung in den Blasen, der Anfangsdruck des Systems, die Anfangsgröße der Blasen und die organische Flüssigkeit (Cyclohexan, 2-Ethylhexanal, Cumol und Methanol).

Zwei verschiedene Typen von Blasenexplosion wurden beobachtet. Ihr Hauptunterschied ist die zeitliche Verzögerung der Zündung. Die Blasenexplosion des Typs I findet während der ersten stoßinduzierten Blasenschwingung statt. Folgende Ergebnisse bzw. Aussagen wurden erhalten:

- Die Explosionsgrenzen hinsichtlich der Zusammensetzung der Gasmischung innerhalb der Blase und der Anfangsgröße der Gasblase wurden ermittelt.
- Die Stoßwelle, die bei der Explosion einer Blase erzeugt wird, kann einer Nachbarblase zünden. Ein derartiger Zündmechanismus wurde erstmalig in der vorliegenden Arbeit beobachtet.
- Gasblasen, die eine anfangs nicht explosionsfähige, magere Gasmischung enthielten, können durch Stoßwellen gezündet werden. Optische Aufzeichnungen von Flüssigkeitsjets in der Gasblase zeigen, dass auf diese Weise eine stoßinduzierte Anreicherung mit Dampf unmittelbar vor der Zündung stattfindet.
- Blasenexplosionen des Typs I wurden in allen untersuchten Lösemitteln festgestellt.
- Der Mechanismus von Blasenexplosion des Typs I wurde beschrieben.

Die Blasenexplosion vom Typ II findet mit einer viel längeren Zündverzögerung statt. Sie wurde nur unter bestimmten Bedingungen beobachtet. Ein Explosionsmechanismus wurde auf der Basis der Beobachtungen vorgeschlagen. Nach diesem Mechanismus können sogar Gasblasen, die anfangs eine nicht explosionsfähige, brennstoffreiche Gasmischung enthalten, durch teilweise Kondensation des Brennstoffs explosionsfähig werden.

Weitere Untersuchungen beziehen sich auf Kavitationsphänomene innerhalb der Flüssigkeit und auf die Wechselwirkung zwischen der Flüssigkeitsoberfläche und einer Stoßwelle. Ferner wurden die Explosionsgrenzen von Cyclohexan in reinem Sauerstoff bei erhöhten Drücken und Temperaturen bestimmt.

Die sicherheitstechnischen Aspekte der Versuchsergebnisse werden diskutiert.

Acknowledgements

This dissertation is based on the experiments performed in the frame of my work in the Federal Institute for Materials Research and Testing (BAM) in Berlin.

Very special thanks for trusting me this interesting and challenging task and for their expert supervision are due to Professor Dr. J. Steinbach of the Technical University of Berlin and to Priv. Doz. Dr. B. Plewinsky of the Free University of Berlin.

I would like to acknowledge also that through the course of writing this dissertation, I have benefited from many discussions I had with Dr. H. Hieronymus and with Dr. P. A. Fomin on various aspects of this work. Mr. H.-J. Seeger, Mr. J. Bender and Mr. S. Seifert, the three technicians of the group "Explosion dynamics" of BAM, I would like to thank for their interest in and for their devotion to the successful execution of this research project. I should like to thank also Mr. J. Dengel, Mr. K. Nisch and Mr. W. Apel from the TU-Berlin, who assisted me in the frame of their student research projects and diploma theses.

Further, I want to express my gratitude to the Deutsche Forschungsgemeinschaft (DFG), which financed this project. Thanks are also owed to the company BASF AG, and in particular to Dr. H.-P. Schildberg, for kindly offering the liquid cyclohexane for the experiments.

In the frame of international scientific events, fruitful discussions with experts in various fields offered me valuable information and comments which influenced this work. Of these persons, a warm thanks goes especially to Dr. W. Proud of the Cambridge University (England), Dr. H. Förster of the Physikalisch-Technische Bundesanstalt (Germany) and Professor S. Umezu of the Oita National College of Technology (Japan).

Finally, I would like to thank my friends for their support; and also members of my family for their encouragement and patience while the manuscript was being developed.

Table of contents

Nomenclature

LATIN LETTERS

- A Area
- α Spherical bubble radius, constant in time
- C concentration of gaseous cyclohexane inside a bubble
- C_P The specific heat capacity at constant pressure
- C_V The specific heat capacity at constant volume
- c_P The molar heat capacity at constant pressure
- c_V The molar heat capacity at constant volume
- D Molecular diffusion coefficient
- d Equivalent bubble diameter
- R The molar gas constant (R = 8.314 J / (mol K))
- r Equivalent bubble radius
- L Distance from a bubble's center
- T Absolute temperature
- t Time
- M Molecular weight
- m Total mass
- P Pressure
- p_1^* Critical value of shock strength above which a bubble in the front of the initiating shock wave is ignited
- $\dot{Q}$ Radiative flux of energy
- V Volume

GREEK LETTERS

- a_i The molar fraction of the compound i
- γ Adiabatic coefficient of the gas
- κ Thermal diffusivity
- ρ Density
- σ The Stefan-Boltzmann constant ($\sigma = 5.67051 \cdot 10^{-8} \cdot \frac{W}{m^2 \cdot K^4}$)
- τ_D The characteristic time of the diffusion process

- λ Thermal conductivity
- β Gas holdup in the liquid
- τ_C The characteristic time of the conduction process
- τ_{SW} Duration of the incident shock wave

INDEXES

"0"	"Initial"	"ign"	"At the moment of ignition"
"1"	"Final", unless stated otherwise	"max"	"Maximum"
"av" or "aver"	"Arithmetic average"	"ref"	"Refracted"
"ad"	"Under the assumption of an adiabatic process"	"SW"	"Of the shock wave"
"b"	"Emitted by the bubble"	"v"	"Of the vapor"
"eql"	"At equilibrium"	"l"	"of the liquid"
		"g"	"of the gas"

Abbreviations

BAM	Bundesanstalt für Materialforschung und -prüfung (Federal Institute for Materials Research and Testing)
C-J	Chapman Jouguet
DW	Detonation wave
fps	Frames per second
RW	Reflected wave
SW	Shock wave

1 Introduction

In the chemical industry many liquid phase oxidation processes are carried out in essentially similar ways. A gaseous oxidizer, usually air, is fed into the liquid and the reaction is carried out inside the bubbly medium under the necessary conditions [1].

In such heterogeneous systems an explosion behavior that is multifold and more complex than in homogeneous systems is known to exist. Special risks arise from aerosol explosions [2], film detonations [3], surface explosions ([4] - [6]), and foam explosions ([7] -[9]).

A few decades ago an additional kind of explosion was discovered and was added to the list above: The explosion of the bubbles in the liquid ([10] - [12]). During a bubble explosion, chemical energy release within the bubble causes an abrupt expansion of the bubble's volume. This leads to the emission of spherical pressure waves into the surrounding medium with high initial pressure peaks. One significant finding was that, under certain conditions, a self sustaining wave of sequential explosion of bubbles can be formed. Such a wave can contain pressure peaks as high as a few hundred bar and can propagate through the complete volume of a bubbly liquid.

It should be noted that the advance of air oxidation over the last decades as a major process route has been accompanied by a continuing increase in explosion hazard. Factors which have contributed to this rise in loss potential include increases in size of plant, severity of operating conditions and the use of pure oxygen in place of air [13].

Although the systems consisting of an organic liquid and dispersed oxidizer bubbles are of high interest to the industry, there is still today a serious lack of proven knowledge of the bubble explosion behavior in these systems. The aim of the present work is to contribute to the elimination of this lack of experimental information.

Scope

The investigations were focused on the explosion behavior of single bubbles or of small bubble clusters. This was chosen as a first step in order to solve the problem of the bubble detonation wave initiation and propagation. Three main objectives were pursued in the frame of this study:

I. To create and optimize an experimental setup for the investigation of bubble explosions. This included the use of a new autoclave, the integration of all the necessary measurement techniques, and the design of experimental procedures which allowed a safe remotely controlled operation.

II. To investigate the bubble explosion behavior right after a shock wave impact. This included the detailed examination of the bubble explosion stages, the estimation of the conditions inside the bubble at the moment of ignition and the investigation of parameters that influence the bubble explosion phenomenon.

III. To examine the behavior of the system in later stages after a shock wave impact. The primary goal here was to reveal possible new phenomena that could add new aspects to the hazard assessment of bubble systems.

A critical analysis of the obtained results, in respect to their connection with safety engineering, has been a primary concern throughout this work, too.

The investigated system

In this study the explosion behavior of gas bubbles dispersed in liquid cyclohexane, under normal conditions was investigated. The bubbles were created by oxygen injection into the liquid. For comparison, additional experiments were performed in which parameters of the system, e.g. the organic solvent, the gas phase composition of the bubbles and the initial pressure, were varied.

The investigated system corresponds to the oxidation of cyclohexane to cyclohexanone and cyclohexanol, which is a raw material for the production of nylon [14]. This process is a common chemical reaction in the industry and is known to include usually air bubbles as oxidizer. On the other hand, the examination of the patents from the chemical industry shows that the trend is towards the use of pure oxygen bubbles, moving away from air bubbles predominant 30 years ago [15], to 90 % oxygen bubbles a few years ago [16]. This justifies the choice of pure oxygen bubbles for these investigations.

2 Review of the literature

Since the first observation of bubble ignition more than 40 years ago, many investigators have conducted research with the goal to understand and to describe the processes that drive all the phenomena involved. Still today, there is no complete theory that can fulfill this task in a satisfactory manner. Moreover, there are indications that the known information may not be adequate to validate such a theory, even if it would be proposed.

The lack of proven knowledge is linked to the fact that only a portion of the practice-relevant bubbly systems and conditions has been investigated. Another factor is related to the limitations of the previously used measurement techniques. Due to recent technological breakthroughs –like for example, that of the digital high speed photography– better tools are now at the disposal of the scientific community for such investigations.

Because of this lack of experimental information important basic questions, like the one of the clarification of the bubble detonation wave propagation mechanism, have not yet been satisfactorily answered. Some of those questions will be discussed at relevant positions of this chapter. It should be noted also that experimental investigations add new aspects occasionally to the general problem which, in their turn, result in new questions. Such a situation appeared in the course of this study when a new type of bubble explosion was observed (see §5.4).

Throughout this work, the following grouping of bubbly (liquid (L) - bubble (B)) systems, proposed by Sychev (1986) [17], has been used:

0.	L: non reacting	- B: non reacting gas	(e.g. L: H_2O - B: N_2)
1.	L: non reacting	- B: active gas	(e.g. L: H_2O - B: (C_2H_2 / O_2))
2.	L: fuel (or oxidant)	- B: gas oxidant (or fuel)	(e.g. L: C_6H_{12} - B: O_2)
3.	L: explosive	- B: non reacting gas	(e.g. L: N_2H_4 - B: N_2)
4.	L: explosive	- B: active gas	(e.g. L: H_2O_2 - B: (H_2 / O_2))

The systems 1 - 4 describe chemically active media, in which an explosion is possible. As will be shown in Chapter 5, the system investigated in this work consisted of a liquid fuel that contained active gas bubbles; i.e. a system that lies between systems 1 and 2. The bubble explosions in systems 3 and 4 have a different mechanism and therefore will not be considered in this literature review.

Apart of the systems mentioned above, further variations in which three phases are combined, are also possible. In this case, inside a liquid ‘hot spots’ created by compressed bubbles ignite a solid explosive (Wlodarczyk (1992) [18] and [19]). From the point of view of the explosion mechanism these new systems are similar to the systems 3 and 4 and consequently they will not be discussed further.

Many important aspects of the bubble explosion behavior are closely related to shock induced dynamics of inert bubbles. Therefore, before reviewing the properties of the systems 1 and 2, some important information about the shock induced behavior of inert bubbles inside non combustible liquids (systems 0) are summarized below.

2.1 Shock induced dynamics of inert bubbles

The most important shock induced phenomena, directly related to bubble explosions, are bubble collapse, bubble breakage, and liquid jet penetration through the bubble. In this section a short review on these phenomena is presented.

2.1.1 Bubble collapse and bubble breakage

Experiments have shown that interaction between a bubble and a shock wave leads to the compression of the bubble. During this interaction, instabilities are created on the bubble's surface and the bubble shape is distorted. At a certain compression stage of the bubble, a liquid jet may be formed. Kornfeld & Suvorov (1944) [20] were the first to suggest that a bubble might collapse asymmetrically and produce a liquid jet. The jet forms by involution of one side of the bubble. It passes across the bubble and penetrates the far surface. The experiments of Naude & Ellis (1961) [21], using spark-induced bubbles, were the first to give clear evidence of this jet formation. Since then, several other researchers have provided photographic confirmation of the jet penetration (e.g. Benjamin & Ellis (1966) [22], Brunton (1967) [23], Lauterborn (1979) [24], Beylich et al. (1990) [25]).

As a result of the jet penetration, the bubble may directly break up (Pinaev & Sychev (1986) [26] and (1995) [27]). In the absence of jet formation or when the jet fails to destroy the bubble at once, bubble breakage can occur due to the Rayleigh-Taylor instabilities at the gas-liquid interface during the bubble expansion phase (Dupre (1999) [28]). A few fluctuations of the bubble may be observed before this type of collapse take place (Pinaev and Sychev (1986) [26] and (1995) [27]. Interaction phenomena between neighboring bubbles or a nearby solid surface have an influence on these processes too (Tomita et al. (1984) [29], Dear & Field (1988) [30], and Shima (1996) [31]).

Theoretical calculations for the collapse of cavitation bubbles have shown that pressures as high as 10^4 bar can be locally produced (Plesset & Prosperetti (1971) [32], Mørch (1979) [33]). Such pressures have clearly damage potential as was experimentally demonstrated by several authors (e.g. Brunton (1967) [23], Tomita et al. (1986) [34]). These pressures, however, decline very quickly within a few bubble radii (Hickling & Plesset (1964) [35]). Bruckert et al. (1994) [36] found that even small changes in the time-development of the applied pressure (shape of the pressure signal), including the strength of the reflected waves, can cause significant variations in the dynamics of a single bubble. This was reported for inert as well as chemically active single bubbles under shock wave impact.

From the two mechanisms of bubble destruction mentioned above, the one based on the formation of a liquid jet in the bubble offers important information about the development of bubble explosions. Accordingly, the next paragraph is focused on this topic only.

2.1.2 Jet formation

According to Dear & Field (1988) [30], there are two general situations that can lead to jet formation inside a single bubble. The first is where jet formation takes place in an asymmetrical pressure field as produced, e.g. near a solid surface during cavitation phenomena. This effect has been theoretically examined first by Plesset & Chapman (1971) [37]. In their model the liquid was considered incompressible and with negligible small viscosity. The jet formation, according to this model, is most pronounced for cavitation bubbles closest to the solid surface. Experiments by Lauteborn (1979) [24] using laser-induced bubbles formed at various distances from a solid wall, confirmed these predictions.

The second situation is when a shock wave passes over the bubble, causing a jet in the direction of the shock wave. It differs from the first situation in that the distant side of the bubble, from the approaching shock wave's point of view, is initially not aware of the collapse process. Consequently the dynamics of the collapse and the pressure profile around the bubble surface differ from the Plesset & Chapman hydrostatic studies. This kind of jet formation can be observed for single bubbles under shock wave impact. Several researchers have tried to simulate this process (e.g. Mader (1979) [38], Lesser (1984) -the model is described in [30]-, Brennen (2001) [39]).

In the system investigated in the present study, both of the above two mechanisms for jet creation inside a bubble are likely to play a role. This is because in a group of bubbles under shock wave impact, pressure waves emitted by collapsing nearby bubbles, will distort the pressure field around neighboring bubbles influencing thereby their jet formation.

Several investigations have been carried out (e.g. Lauterborn (1979) [24], Bruton (1967) [23], Chaudhri et al. (1982) [40], Tomita et al. (1984) [29], Dear & Field (1988) [30], Shima (1996) [31]) to study the influence of the interaction between two chemically inert bubbles on the direction of the jet. The investigated cases include the situation where the two bubbles are of the same or different diameters, near, away or on a solid wall. In these experiments it was observed that the direction of the jet propagation was not normal to direction of the shock wave.

Fujiwara & Hasegawa (1981) [41] and (1982) [42] investigated the influence of the initial shape of the bubble on the jet formation. They found that initially oblate bubbles had a different behavior from initially prolate bubbles under the same conditions. The jet velocity was also found to differ significantly. The one in oblate bubbles was measured to be more than three times higher than in the prolate bubbles, reaching values that exceeded 400 m/s.

Concerning the properties of the jet, investigations by Nakoryakov and Donstov (1995) [43]) revealed that the jet structure increases with the pressure wave amplitude and that the jet

entrains the whole gas bubble when the pressure wave intensity is above a certain limit ($\Delta p / p_0 \geq 50$ for the system of water-glycerin solutions with inert bubbles of 1 mm - 2 mm in diameter). They also found that the velocity of the jet depends on the amplitude of the shock wave, but not on the viscosity of the liquid, surface tension, or the bubble's size.

2.2 Shock induced bubble explosions

Information about shock induced bubble explosions has been obtained by experiments carried out with single bubbles, bubble rows and bubble columns. The mechanism of the explosion of a single reactive gas bubble in an inert liquid (systems 1) was first studied by Solouhkin (1961) [10]. An experimental and theoretical investigation on a linear array of reactive bubbles was made by Hasegawa and Fujiwara (1982) [11], who observed that the explosion of one bubble was followed by the explosion of the next one and consequently a sequential explosion of bubbles was produced. Sychev (1985) [12] investigated bubble columns and was the first to experiment with oxygen containing bubbles in liquid fuel (systems 2) and to provide a confirmation on the existence of a self-sustaining bubble detonation wave. All the above experiments showed that both in systems 1 and 2 there exists a critical value of shock strength (p_1^*) above which a bubble in the front of the initiating shock wave is ignited.

The basis of the bubble explosion mechanism is the well known [44] mechanism of transformation of pressure waves in inert bubble media: Energy from the incident shock wave is absorbed from the bubble. This energy is consumed for an increase in temperature of the shrinking bubble and is then re-emitted by the bubble during its oscillation. Apparently, when attaining the ignition temperature the bubble explodes. In this case, the energy produced by bubble explosions may compensate the losses in the shock wave and provide the existence of a self-sustaining regime, the so-called bubble detonation wave.

This term was used in the literature for the first time by Hasegawa & Fujiwara (1984) [45]. There still exists no official definition of this term. Sychev (1986) [17] justified it based on the following observation. The bubble explosions release energy which forms a shock wave inside the liquid. This shock wave has a steady-state, supersonic velocity independent of the conditions of initiation of the bubble explosions. Therefore this process can be called a detonation process and the shock wave can be called bubble detonation wave.

Below an overview follows on the experimental findings for bubble explosions in systems 1 and in systems 2, as well as some important findings for bubble detonation waves.

2.2.1 Bubble explosions in systems 1

Experimental investigations about bubble explosions in systems 1 have been described by many researchers. Several liquids, explosive gaseous mixtures for the generation of the bubbles, and other parameters have been investigated in these works. It was found that a shock induced bubble explosion in systems 1 is a stochastic phenomenon.

When the ignition of the reactive bubble occurred, this happened during the first fluctuation after the shock wave impact on the bubble (e.g. Dupre (1999) [28]). The compression period before the ignition t_{ign} was shown to depend on the initial bubble diameter• (Sychev (1985) [46], (1995) [27], (1997) [47]). Many studies revealed a pattern in the explosion behavior of bubbles according to which a bubble ignites generally when $d_0/d_c = 3-4$ (see e.g. Sychev (1985) [46] and Bruckert et al. (1994) [36]). Additionally, Sychev ((1985) [46], and (1995) [27]) reported that the mean bubble surface velocity during the compression phase (from $d/d_0 = 0.9$ to the ignition point) was found to be less than the velocity measured during the subsequent expansion (from the instant of ignition to $d/d_0 = 0.9$).

In the same papers, Sychev argued that the process of compression of an individual bubble in the shock wave, and thus its ignition, is a collective phenomenon. That is, in a bubble column each individual bubble is compressed in the pressure field formed by shock waves that come by several bubble explosions. Direct optical recordings of the interaction effects between nearby exploding bubbles are not described in the literature at the present time, but they are presented and discussed in Chapter 5.

Light emission during the bubble explosion is a very important aspect of the phenomenon, because it is often used as one of the main criteria to identify optically the existence of a bubble explosion. Hasegawa and Fujiwara (1982) [11] were the first to publish a photo of an exploding bubble of systems 1, where the light emission was visible. Light emission in a single-stage was reported also by many other researchers (e.g. Pinaev & Sychev (1986) [17] and Gülhan & Beylich (1989) [48], [49]). According to these observations the light emission was found to last a few μs.

2.2.1.1 Parameters that influence the initiation of bubble explosion in systems 1

In the literature, the parameters known to influence the phenomenon of bubble explosion in systems 1 are (i) the initial bubble diameter (d_0); (ii) the viscosity of the liquid (μ); as well as (iii) the gaseous mixture, and (iv) the initial pressure (p_0) in the bubble.

Although other parameters have been considered occasionally, like solid particle dispersion or polymer additions in the liquid (e.g. Rubach, et al. (1993) [50]), it is commonly accepted by the scientific community that the above mentioned parameters play the most significant role in the phenomenon. The main findings about the influence of these parameters on the critical initiating shock pressure p_1^* are summarized below.

• Experimental values: t_{ign} = 10-15, 15-20, 20-30 and 30-40 μs for bubbles with an equivalent diameter of 1.9 ± 0.1 , 2.5 ± 0.2, 3.9 ± 0.2 and 5.1 ± 0.3 mm respectively (gas bubbles of C_2H_2 + 2.5 O_2 inside a water-glycerine solution, where the molar fraction of glycerine was 0 % or 25 % or 50 %, for each of the four bubble diameters) [27], [47]

(i) Influence of the initial bubble diameter

A wide agreement can be found in the literature concerning the dominant role of the initial bubble diameter on the bubble explosion behavior (e.g. Sychev (1995) [27], Dupre (1999) [28]). In [26] it was reported for example that in the system L: (0.5 H_2O + 0.5 glycerin) - B: (C_2H_2 + 2.5 O_2), and for bubbles with d_0 = 3 mm to 4 mm (β_0 = 2 %) the critical shock wave pressure was p_1^*=10 bar, while at d_0 = 0.5 mm to 1.0 mm no ignition was observed for pressure waves up to 80 bar.

Buckert et al. (1994) [36] suggested the existence of lower and upper diameter explosion limits for single bubbles under shock wave impact. They offered an explanation for the lower limit based on the assumption that heat losses from the bubble surface are large enough to prevent the bubble temperature to reach the ignition value. Similarly they explained the existence of the upper limit by the assumption that the bubble collapse becomes highly asymmetric, also preventing a sufficient temperature rise. In their investigations (single chemically active bubbles under mechanically generated shock wave impact) they measured the lower limit, but not the upper one. Sychev (1995) [27] encountered both limits investigating the influence of the bubble diameter on the existence of a self-sustaining bubble detonation wave inside bubble columns.

(ii) Influence of the viscosity of the surrounding liquid

The viscosity of the liquid phase as important factor for the bubble explosions was investigated mainly by Sychev. It was reported that this factor has a great influence on the process of bubble ignition [27]. More precisely, the critical pressure of the initiating shock wave p_1^* increases with decreasing viscosity of the liquid. The explanation provided by the author was that with increasing viscosity, the development of instability of bubble surface perturbations is hindered during the compression process. Bubble heat losses then decrease and as a result the critical parameters for bubble explosion are lowered.

(iii) Influence of the gas mixture inside the bubble

Gülhan & Beylich (1989) [48] found experimentally that a decrease of the adiabatic index γ of the gaseous mixture inside the bubble increases the critical pressure required for ignition. Earlier, Pinaev & Sychev ((1986) [26] and (1987) [12]) had reported that a reduction in the ignition induction period of the gaseous mixture inside the bubble leads into reduction of p_1^*. They observed moreover that p_1^* was increased when the gas mixture was lean or enriched. Their experiments showed also that the amount of inert gas in the bubble, has a big influence on the detonation range. For example in water - glycerol solution (glycerol concentration 50 %) systems containing acetylene-air bubbles, shock waves with amplitudes up to 90 bar failed to initiate a bubble explosion.

(iv) Influence of initial pressure of the bubble

An increase in the initial pressure of the bubble p_0 is equivalent (for the same bubble diameter or for unchanged gas hold-up in bubble columns) to an increase of the mass concentration of the gas inside the liquid, and thus of the energy capacity of the medium. It was found experimentally that an increase in p_0 leads to an increase in p_1^* in bubbly media (Pinaev & Sychev ((1986) [26] and (1987) [51]).

2.2.2 Bubble explosions in systems 2

The investigations of bubble explosions in systems 2 are very rare. Sychev`s few related publications are practically the only source of experimentally gained information for these systems (see Table 2-1). It is interesting to note though that these papers are not dedicated solely to systems 2. Additionally, the lack of some important information in these papers, make it very difficult for an external researcher to understand the reported results in depth, to reproduce them, or to compare them with other results.

One important information that is systematically missing, is the exact organic liquid that was used in the reported investigations. The problem rises mainly from the fact that Sychev mentions in his publications only the empirical formula of the liquids he used (see Table 2-1), and not their chemical name or any information about their structure. Thus, for example, under the empirical formula C_7H_{16}, which is a liquid that was used in [26] and [12], at least nine different liquids can be described (the liquids Nr. 595 - 598, 860, 861, 1193, 1194, and 1844 in [54]).

Apart from that, in Sychev's publications ([26], [12]-[53]) and PhD thesis [55] only some of the important properties of the liquids are mentioned -usually the density, the viscosity, the vapor pressure and the sonic velocity-, but without the temperature at which these values were measured. Other properties of the liquids that could be relevant to the understanding of the involved phenomena are not mentioned at all. Such properties are for example: the surface tension, the ignition temperature, the flash point, and the lower and upper explosion limit.

It is interesting to note also that until today only the possibility of a bubble explosion after a relatively short time, i.e. only during the first bubble oscillations after the passage of the incident shock wave, has been investigated. This has left open the question of the explosion behavior of a single bubble in later stages after the shock wave loading. For systems 2 this question is important because the interaction between the liquid and the gas phase of the bubble plays a critical role for the explosion behavior of the latter. The importance of the question is enhanced by the fact that hydrocarbons can have explosion regimes with a variety of explosion mechanisms and explosion parameters [56].

Despite the limitations discussed above, important experimental observations about the bubble explosion behavior in systems 2 have been reported. These observations are briefly summarized below.

Table 2-1: Organic liquids inside which ignition of oxygen bubbles has been reported.

Organic liquid (as reported in the references)	Initial system pressure bar	Initial bubble diameter mm	References
o C_7H_{16} o C_9H_{20} o $C_{13}H_{28}$ o $C_{16}H_{34}$	1	3.0 - 3.5	[12] (1983)
o Vacuum oil (VM-3)	1	2 - 4	[51] (1986), [52], [53] (1994)
o C_7H_{16} o $C_{16}H_{34}$ o Vacuum oil (VM-3) o capacitor oil o 20V industrial oil	1 -7	2 - 4	[26] (1985)

One finding was that the bubble ignition mechanism differs between bubbly systems 1 and 2. In systems 1 compression of the bubble can lead to a rise of the temperature of the gas in the bubble, sufficient for igniting the explosive gas phase of the bubble. In systems 2 the bubble contains an initially non explosive gaseous mixture. Sychev (1985) [12] suggested the following explosion mechanism. An explosive mixture inside the bubble is formed during the compression phase. During this phase the liquid jet that penetrates the bubble (see §2.1.2) enriches the gas phase of the bubble in fuel. As a result of this enrichment and the increased temperature of the gas in the bubble, an explosive gas mixture is formed and ignited.

Sychev supported that the qualitative difference between systems 1 and 2 is the presence in the latter of the mixture formation processes, which hinder and retard the ignition of the bubbles.

When this process comes to an end, systems 1 and 2 become in principle identical from the viewpoint of the generation mechanism of the bubble explosion behavior.

Concerning the light emission during the bubble explosion he reported that apart from the emission of the type and duration observed in systems 1, additionally a two-stage light emission can appear. He made this experimental observation in oil-O_2 systems. It was confirmed by optical studies and by analysis of the corresponding oscillograms in [26]. The two-stage character of the light emission was explained by the two authors of that paper as double ignition upon repeated compression of the bubbles in such systems (due to incomplete combustion in the first stage). This would mean that the two stage character of bubble ignition is a distinctive feature of systems 2 with high viscosity. The duration of these light emissions was found to be a few μs for the first compression and significantly longer (50 μs - 100 μs) for the second.

Shock induced bubble explosions were found to be a stochastic phenomenon also in systems 2. The eventual ignition of the bubbles in systems 2 was found to occur during the first fluctuation after the shock wave impact. Other common points with the behavior in systems 1 are that the compression period before the ignition t_{ign} depends on the initial bubble diameter and that a bubble ignites generally when $d_0/d_c = 3-4$.

2.2.2.1 Parameters that influence the initiation of bubble explosion in systems 2

The source of information about the parameters that influence the critical initiating shock pressure p_1^* in systems 2 are investigations carried out with small bubble columns. The reported parameters are identical to those discussed for systems 1: (i) the initial bubble diameter (d_0); (ii) the viscosity of the liquid (μ); as well as (iii) the gaseous mixture and (iv) the initial pressure (p_0), inside the bubble.

(i) Influence of the initial bubble diameter

According to the experimental results in [51] the role of the initial bubble diameter to the bubble explosion behavior in systems 2 is the same as the one reported for systems 1.

(ii) Influence of the viscosity of the surrounding liquid

The viscosity of the liquid phase has the same influence on the process of detonation wave initiation in systems 2 like in systems 1. For example, the system L:VM-3 - B:O_2 is more reactive ($p_1^* \approx 10bar$, at $\beta_0 = 1\%$, $p_0 = 1bar$) than the system L:$C_{16}H_{34}$ - B:O_2 ($p_1^* \approx 40bar$, under the same conditions). In the first system a bubble detonation wave was formed after 1 m from the surface of the bubbly liquid. In the second this distance was about 3.5 m. The explanation provided by Sychev in [26] was that with increase in μ, development of instability of bubble surface perturbations is hindered during the compression process. Bubble heat losses then decrease and as a result the critical parameters for bubble explosion are lowered.

It was also observed by the same author that the concentration detonation limits for bubbles containing fuel gas (systems 1) and of those containing oxidant (systems 2) become closer as μ decreases; and he claimed that each system has a μ_{min} at which the detonation vanishes. His explanation for this was that after a certain viscosity value, the bubble ignition delay (which is connected to the total heat losses during the compression phase) can become greater than the compression time, which allows the bubble not to ignite. Such limits have not been measured yet though.

(iii) Influence of the gas mixture inside the bubble

It was experimentally observed in systems 2 that p_1^* increases when the inert gas content increases. Also that the amount of inert gas in the bubble, has a big influence on the detonation range, i.e. the range inside which a bubble detonation wave can be created. For example no detonation was found in the VM-3 system containing oxygen-nitrogen bubbles with up to 65 % oxygen [53].

(iv) Influence of initial pressure of the bubble

An increase in the initial pressure of the bubble p_0 is equivalent (for the same bubble diameter or for unchanged β_0 in bubble columns) to increase in the mass concentration of the gas inside the liquid, and thus in the energy capacity of the medium. It was found experimentally that an increase in p_0 leads to an increase in p_1^* in bubbly media of system type 2 ([26], [51]). For example in the system L:VM3 - B:O_2 , at p_0=1 and 7 bar (β_0=1 %) the critical initiating shock pressure was p_1^*= 10 and 30 bar respectively [26].

2.3 Pressure waves in bubbly liquids

The investigation of the self sustaining bubble detonation wave was not included in the objectives of this study (see Chapter 1). During the experimental part, information was revealed though that is related to the propagation mechanism of such waves. For this reason, a short review on pressure waves in inert bubbly media and on bubble detonation waves in chemically active bubbly media is included.

2.3.1 Pressure waves in inert bubbly liquids

Campbell & Pitcher (1958) [57] carried out the first qualitative experiments on shock waves in inert bubbly liquids. They established that the Mach number of the wave must be greater than unity for a shock wave to exist. The Mach number is defined as the velocity at which the shock propagates divided by the sonic velocity of the medium ahead of the shock. Other researchers have investigated pressure profiles in bubbly columns under weak, moderate or strong shock waves (e.g. Noordzij & van Wijngaarden (1973) [58] and (1974) [59], Borisov et al. (1983) [60], V.E. Nakroyakov et al.

(2000) [61]). From these investigations it is known that in chemically inert media, the propagating shock waves have an oscillatory structure. Pressure oscillations behind the wave front are caused by the inertia of the combined mass of bubbles. As it propagates, the shock wave decays into a series of combined waves moving at various speeds proportional to their amplitudes. Many researchers have presented theoretical studies on the structure and properties of shock wave propagation in inert bubble media (e.g. Noordzij & van Wijngaarden (1970) [62], (1973) [58], and (1974) [59], Nigmatulin & Shagapov (1974) [63], Borisov et al. (1983) [60], Beylich & Gülhan (1990) [25]).

2.3.2 Pressure waves in chemically active bubbly liquids

When a shock wave hits the surface of a chemically active bubbly liquid, an initiating shock wave (non steady state wave) is formed and starts propagating through the bubbly media. Hasegawa and Fujiwara (1984) [45] were the first to report that also this initiating shock wave has an oscillatory structure. Provided that the amplitude of the wave is high enough, a certain zone forms with its propagation, in which bubbles explode synchronously (Kedrinskii (1997) [64]). After a certain distance L, the initiating shock wave is being separated into two parts. A precursor wave propagating with the sonic velocity in the liquid and a main disturbance (the bubble detonation wave) having the form of a wave train that travels at a stationary velocity (Pinaev & Sychev (1986) [26]). The duration of pressure pulsations both in the wave and in the precursor and in the perturbations behind the wave was found to be in the order of magnitude of a few μs (Pinaev & Sychev (1986) [26], and Beylich (1995) [65]). For further experimental information about the precursor wave, the reader is encouraged to refer to the investigations of Hasegawa and Fujiwara (1984) [45], Gülhan & Beylich (1989) [48], Pinaev & Sychev (1986) [26], and other.

2.3.2.1 The bubble detonation wave

Experimental studies of shock wave propagation inside chemically active bubbly media revealed that a self-sustaining, quasi-stationary bubble detonation wave forms at some distance L from the surface of the medium. This distance decreases with increase in the amplitude of the incident shock wave p_1. The distance L was found to be generally in the range of 1 m to 3.5 m in the experiments of Pinaev & Sychev ((1986) [17] and [26]).

The bubble detonation wave was found to have a wave train structure and a duration which, in a monodispersed medium, is proportional to the bubble diameter [64]. For example in [(1986) [26]], the duration of the bubble detonation wave was found to be 40 - 80 μs with pressure pulsations, the amplitude of which reached 70 - 100 bar, and an additional short peak of 150 - 400 bar. These measurements were performed in the system: L: saturated C_7H_{16} or $C_{16}H_{34}$ or VM-3 or capacitor oil or 20V industrial oil, B: O_2 or air, at an initial pressure of 1 bar. Similar pressure amplitudes were reported also by other authors (e.g. [49], [66]) who investigated systems 1. An essential amplification of the bubble detonation wave amplitude was claimed to be possible according to

theoretical calculations by Kedrinskii et al. (1989) [67]. Such an amplification was explained by effects of collective pulsation of bubbles at a certain width of the bubble layer.

After its departure from the initiating shock wave, the combustion zone (bubble detonation wave) was found to accelerate to a constant velocity D, higher than that of the following shock wave V. This stable (bubble detonation) wave propagates with velocity exceeding the shock wave velocity in passive media and is less than the sonic velocity in the liquid. An explanation on the mechanism of the departure of the bubble detonation wave from the initiating shock wave, was offered by Pinaev & Sychev ((1986) [17] and [26]), as follows: The presence of energy liberation (due to bubble explosion) during the first bubble oscillation leads to an abrupt increase in pressure in the medium with increase in wave amplitude and, consequently, wave propagation velocity. As a result the bubble detonation wave removes itself from the initiating shock wave.

The difference between a bubble detonation wave and a wave propagating in chemically inert bubble media is that the latter is formed as a result of simultaneous manifestation of the non linear and dispersion properties of the medium. The existence of a bubble detonation wave, which is also a combined wave, is caused by energy liberation in the medium.

2.3.2.2 Parameters that influence the bubble detonation wave's properties

Beylich and Gülhan ((1990) [25], [49] and (1995) [65]) suggested that there exist at least three important physical length scales that influence the bubble detonation wave properties: the tube diameter, the inter-bubble distance (related to the gas hold-up) and the bubble diameter. These scales have been referred also as macroscale, mesoscale and microscale respectively. Beylich and Gülhan used ensemble averaging of pressure profiles to obtain quantitative information on the bubble detonation wave properties.

It is not known whether such an averaging procedure is meaningful or not, i.e. if the physics it retains are truly the governing ones. Also it is not known at the present time how the single bubble dynamics are related to the propagation and structure of a bubble detonation wave. Whether the bubble detonation wave depends on single bubble dynamics or on averaged fluid properties is crucial for the understanding of the phenomenon.

The parameters according to which limits for the existence of a self-sustaining bubble detonation wave can be defined are, according to the literature, the same parameters that influence the single bubble explosions, i.e.: the initial bubble diameter, the viscosity of the liquid, the gaseous mixture inside the bubble, and the initial pressure; with the addition of the gas hold-up.

Outside the areas which define these limits, it is reported that a shock wave may ignite the first bubbles, but no self-sustaining detonation wave is formed. In this case, the shock wave weakens as it propagates and the ignition ceases (Sychev (1994) [52]).

Although additional parameters have been occasionally considered and experimentally investigated, e.g. the tube diameter (e.g. Scarini et al. (1991) [68]), the tube's walls strength (e.g.

Barbone et al. (1997) [69]), and the mode of production of the initiating shock wave amplitude (methods that were tested include: discharge inside the bubbly liquid, ignition of an explosive gas mixture above the surface of the liquid, and breakage of a diaphragm); it is commonly accepted that the above mentioned parameters play the most significant role in the phenomenon.

3 Fundamentals

An important basis for a discussion - especially in the field of safety engineering - is a system of clear definitions of the terms used. Therefore the most important terms used in this work are defined below.

3.1 Definitions

One difficulty for the description of explosion phenomena in heterogeneous systems of the type liquid-gas, arises from the fact that there exist no norm, in which these phenomena are defined. Because of this, the definitions of the terms to follow will be based on the corresponding definitions for gaseous systems, with some adaptations where necessary. Generally, the European norm EN 1127-1 (1997) [70], and in special cases, the international standard ISO 13943 (2000) [71] will be used for this purpose. The European norm mentioned will be used also for the definition of those terms of this work that refer only to the gas phase.

3.1.1 Combustion

In chemistry, the word *combustion* generally refers to a very rapid oxidation that is accompanied by intensive heat and light emission [72]. In the international standard ISO 13943 the term *combustion* is defined as "exothermic reaction of a substance with an oxidizer". The same definition is used in this work.

3.1.2 Explosion and bubble explosion

The word *explosion* is commonly used to describe a sudden release of energy in a violent manner. An explosion causes pressure waves in the local medium in which it occurs. Explosions are categorized as deflagrations if these waves are subsonic and detonations if they are supersonic (shock waves).

In the European norm EN 1127-1, the term *explosion* is defined as: "Abrupt oxidation or decomposition reaction producing an increase in temperature, pressure, or in both simultaneously". The same definition is used in this study to describe the explosion inside a gas bubble, i.e. a bubble explosion.

3.1.3 Deflagration

The word *deflagration* describes a relatively slow explosion, generating only subsonic pressure waves in contrast to a detonation, where the pressure waves are supersonic. In the European norm EN 1127-1, the term *deflagration* is defined as: "Explosion propagating at subsonic velocity". According to Hieronymus and Plewinsky [73] the above definition of the term *deflagration* can be used without any change for heterogeneous systems of the type investigated in this work.

3.1.4 Detonation

Although the word *detonation* has been in common use for at least 200 years, it has been claimed (e.g. in [74]) that a concise but precise definition of this word is a very difficult task. In earlier times the word detonation referred to the sudden decomposition of certain chemicals and mixtures with the production of considerable noise "like thunder", even though these materials were unconfined when they decomposed.

At the present time the term *detonation* is applied only to processes where shock-induced combustion wave is propagating through a reactive mixture or pure exothermic compound. Since a shock wave is always observed to precede the reaction front in a detonation, the propagation velocity of such a combustion wave is always supersonic relative to the undisturbed media [75].

The term *detonation* is defined in the European norm EN 1127-1 as: "Explosion propagating at supersonic velocity and characterized by a shock wave". This definition without any change will be used to describe the detonation also inside heterogeneous systems of the type investigated in this work, as suggested in [72].

3.1.5 Chapman Jouguet pressure, temperature and velocity

The first experimental evidence for the supersonic nature of gaseous detonation waves was obtained in 1881, when Berthelot and Vieille and independently Maillard and Le Chatelier observed supersonic combustion waves, while studying flame propagation in tubes filled with gaseous combustible mixtures. In 1899 Chapman and independently also Jouguet in 1905 were the first to present a theory describing this supersonic combustion wave, propagating at a unique velocity [75].

The Chapman Jouguet (C-J) theory [74] treats the detonation wave as a discontinuity with infinite reaction rate. The conservation equations for mass, momentum and energy across the one-dimensional wave give a unique solution for the detonation velocity (*C-J velocity*). Based on the C-J theory it is possible to calculate the detonation pressure (*C-J pressure*) and temperature (*C-J temperature*) if the gas mixture is known. The C-J theory does not require any information about the chemical reaction rate (i.e. chemical kinetics).

During World War II, Zeldovich, Döring and von Neumann improved the C-J model by taking the chemical reaction rate into account. Again in this theory the leading shock is treated as a discontinuity but, in contrast to the C-J model, no reaction occurs in the flow immediately behind the shock (see Fig. 3-1). The reaction follows an incubation period, during which a pool of chemically active species is formed at a finite rate at the high temperature and pressure of the shocked medium, before the combustion is triggered [74]. The Zeldovich, Döring and von Neumann (ZND) theory gives the same detonation and pressures as the C-J theory. The difference between the two models is the thickness of the wave, which is given by the reaction rate in the ZND model.

It is known that the C-J theory, when applied to detonations inside gaseous mixtures that are not near their explosion limits, predicts detonation wave velocities which agree with the

experimentally measured propagation velocities within a few percent [75]. However it should be noted that an actual detonation wave is a three-dimensional shock wave followed by the reaction zone. A further weakness of the C-J and ZND theories is that they predict the detonation velocity and pressure independently of the geometrical conditions. In reality, the propagation of a detonation is limited by the geometrical conditions.

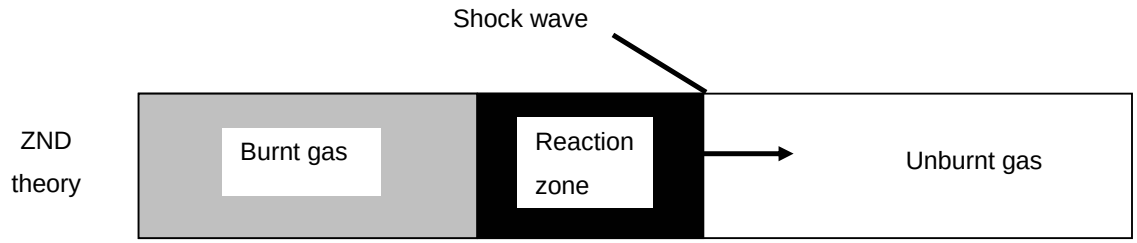

Fig. 3-1: A detonation wave can be described as a shock wave immediately followed by a flame (ZND theory).

3.1.6 Explosion limits

Virtually every fuel-oxidizer combination will support an explosion only when the fuel concentration is within a certain range, bounded by some upper and lower limit concentration. Outside these limits a flame does not propagate a long distance from an ignition source. The initial pressure and temperature of the mixture affect the upper and lower concentration limits. Increasing the temperature always widens the limits because it causes the flame temperature to increase. Increasing pressure has little effect on the lower or lean limit but causes the upper limit to increase. The addition of inert gases to the mixture causes the limits to narrow and eventually with sufficient added inert all fuel – oxidizer mixtures are non explosive. In general, the addition of an inert such as He, N_2, H_2O, or CO_2 to the mixture narrows the limits because such mixtures have a lower flame temperature than the original fuel-air mixture [75],[76].

In this work, the definition found in the European norm EN 1127-1, will be used for the term *explosion limits.* According to this, *explosion limits* are "the limits of the explosion range". According to the same source, the *explosion range* is "the range of the concentration of a flammable substance in air, within which an explosion can occur".

The above definition from the European norm EN 1127-1 of the term *explosion limits* can be used also in connection with bubble explosions induced by shock wave impact. It must be noted though, that in this case the above definition of the term *explosion range* is not adequate. The following broadened definition will be used instead: *Explosion range* is "the range of one variable parameter, all the other parameters being constant, within an explosion can occur".

Examples of such a variable parameter for bubble explosion ranges are: the composition of the gaseous mixture inside the bubble, the bubble diameter and properties of the shock wave used to compress and ignite the bubble.

3.1.7 Ignition

In the absence of a corresponding definition in a European norm, the definition found in the international standard ISO 13943 [71] is used. According to this definition, *ignition* is called the "initiation of combustion".

3.1.8 Ignition temperature and ignition delay

After a shock wave impact, the bubble shrinks rapidly and therefore the temperature in its interior increases. This temperature increase continues during the bubble compression phase until the bubble is ignited. The temperature inside the bubble at the moment just before its ignition will be called in this work *ignition temperature*. The estimation of the ignition temperature inside the bubble in the case of an adiabatic or nearly adiabatic compression is an important task of this work (see §5.3.2).

It should be noted at this point, that the above definition of the term *ignition temperature* defers from the definition that is usually found in standards and norms for gaseous systems. For instance, the *ignition temperature* of a combustible gas or of a combustible liquid is defined for gaseous systems in [71] as "the lowest temperature of a heated wall as determined under specified test conditions, at which the ignition of a combustible substance in the form of gas or vapor mixture with air will occur". The difference in the definition should be taken into consideration especially during the discussion of the experimental results, where the reader is tempted to compare known ignition temperatures of e.g. cyclohexane with the corresponding measured values from bubble explosions.

Accordingly, the term *ignition delay* of a bubble explosion is defined as the time elapsed between the shock wave impact and the ignition of the gas phase inside the bubble.

3.1.9 Flash point

In the discussion part, one of the organic liquid's properties that is used in the flash point. The *flash point* is, according to the definition in the European norm EN 1127-1, the "minimum temperature at which, under specified test conditions, a liquid gives off sufficient combustible gas or vapor to ignite momentarily on application of an effective ignition source".

3.1.10 Shock wave

A *shock wave* in a gas is defined in [77] as a fully developed compression wave of large amplitude, across which density, pressure, and particle velocity change dramatically. Additionally, the thickness of a shock wave is of the order of the mean free path and may be treated as a discontinuity [78].

A *shock wave* propagates at supersonic velocity relative to the gas immediately ahead of the shock, i.e., the gas ahead is undisturbed by the shock. The propagation velocity of the shock wave depends on the pressure ratio across the wave. Increasing pressure gives higher propagation velocity.

3.1.11 Equivalent bubble diameter

The bubbles created in the experiments were typically of non spherical shape. To solve this problem for the calculations that need the bubble diameter as input, the concept of the *equivalent diameter* was used to define the size of the bubbles. The *equivalent diameter* is defined by the equation: $d_e = (ab^2)^{1/3}$, where a and b are the minor and major axes of the bubble, respectively. The assumption behind this calculation is that the bubble has the form of an ellipsoid (see Fig. 3-2, with b = c).

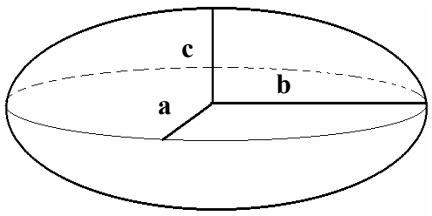

Fig. 3-2: For the calculation of the bubble equivalent diameter, an ellipsoid form was assumed.

3.2 Processes in the bubble that can influence its explosion behavior

Shock induced processes can influence the temperature, the pressure and the gas composition inside the bubble. Such changes are very important for the bubble explosion behavior. In this section an overview over these processes is presented. Their mechanism and their relevance to the experimentally observed bubble explosion behavior is analyzed.

There are generally four different categories of such processes / phenomena that could influence the shock induced explosion behavior of a bubble. These are: (i) mass transfer from and to the gas phase of the bubble; (ii) heat transfer from and to the gas phase of the bubble; (iii) compression of the bubble; and (iv) chemical reactions inside the bubble.

Although the phenomena that correspond to the above four categories can in principle take place simultaneously (e.g. heat and mass transfer, during bubble compression), these categories will be considered as separate groups, in which their processes function independently.

3.2.1 Mass transfer from and to the bubble

In the bubble a concentration gradient can be created by (i) dissolution and (ii) vaporization / condensation processes. In this case mass transfer by diffusion occurs. Additionally fluid flows may be involved, because of which mass transfer by convection can occur.

Dissolution

If the bubble contains a gaseous substance in which the surrounding liquid is not saturated, then dissolution of this substance into the liquid takes place at the bubble wall. The saturated levels in the liquid x' can be calculated by the well known *Henry's law*:

$$x' = p_{gas} \cdot H \,, \qquad \text{(eq. 3-1)}$$

where x' is the mole or mass concentration of the gas in the liquid, p_{gas} is the partial pressure of this gas. The multiplication factor H is called in both cases "Henry coefficient", despite the fact that they are two different physical quantities.

During dissolution there is a continuous movement (diffusion) of the gaseous component from the gas phase of the bubble into the surrounding liquid. *Fick's* law can be used in both phases to describe the process.

During mass transfer between the two phases due to dissolution, the controlling part is the diffusion of the gas molecules inside the liquid, which is much slower than the diffusion process within the gas phase. Generally the diffusion coefficient of gas molecules in a liquid phase is one to two order of magnitudes less than inside a gas. Therefore, dissolution from the bubbles towards the liquid can be neglected for the time scale of the experimental observations of this study.

Vaporization/Condensation

Apart from the dissolution, also vaporization and condensation can take place inside the bubble. These processes can take place either on the bubbles surface, or inside the bubble's entire volume.

In the first case, the phenomenon can be described by the well known *Fick's* law for molecular diffusion with the assumption that the vaporization process is much faster than the diffusion process. The upper limit of the concentration of the surrounding organic solvent in the gas phase is given by the vapor pressure of the latter at the temperature inside the bubble. As will be shown later (in Chapter 5), this process defines the composition of the gaseous mixture inside the bubble. The equations that describe the enrichment of a bubble in vapor of cyclohexane due to molecular diffusion are presented in Appendix A. The possibility that mass transfer occurs additionally due to convection processes inside the bubble was not taken into account in the calculations just mentioned. As a result of convection processes the rate of mass transport would be increased, but this would not change the information derived by these calculations.

During and after a shock wave impact, processes of vapor condensation and liquification into micro-droplets or droplets vaporization can take place inside the bubble's volume. These processes are mainly connected to the existence of a liquid jet in the bubble. Micro-droplets in the bubble can be introduced by the penetration of a shock induced jet through the bubble. Several

parameters are needed to be measured experimentally (e.g. diameter of droplets, number of them) before any estimation on these processes is possible. This kind of vaporization and condensation processes had to be ignored in this work due to lack of information.

3.2.2 Heat transfer

The shock induced compression of a bubble, results into a rapid internal temperature increase. During this process, heat flows from the (hotter) bubble to the (cooler) surrounding liquid. It is important for the interpretation of the experimental results to know if and when an adiabatic bubble compression can be assumed. The answer to this question depends of course on the duration and the intensity of the heat losses from the bubble during its compression.

There are four distinct ways by which this transference of heat can take place: (i) conduction; (ii) convection; (iii) radiation of the body; and (iv) phase change. In the following paragraphs they are considered separately.

Heat transfer by conduction

Heat losses due to conduction take place from the walls of a hot bubble. The well known Fourier's law is the fundamental differential equation for heat transfer by conduction. The temperature decrease inside an initially hot bubble due to heat conduction to the surrounding liquid is mathematically described in Appendix B. Apart from that, the equations for the calculation of the characteristic time of the conduction process and important properties of the gaseous mixture inside the bubble at different conditions and gas compositions are also derived and presented in Appendix B. This system of equations was used for the corresponding calculations about the conditions inside the bubble at the moment of ignition, in Chapter 5.

Heat transfer by convection

Heat-transfer coefficients due to convection can be calculated with the help of Nusselt number which depends among others on Reynolds number in the gas phase of the bubble. Since there is not adequate information about the flow of the gas in the bubble, convection will be completely ignored.

Heat transfer by radiation of the body

The system of equations for the calculation of the maximum rate of temperature decrease inside an initially hot bubble due to radiation is presented in Appendix C. The corresponding results of this calculation are presented in Chapter 5.

Heat transfer by phase change

In systems like a gas bubble in a liquid, where a liquid phase contacts a gas phase, transference of heat can take place also together with mass transfer due to change of phases (vaporization, condensation). The vaporization of a liquid is an endothermic process, i.e. it takes energy from the surrounding

media, and mainly from the gas phase. Condensation on the contrary, offers energy mainly to the gas phase of the bubble. Heat transfer by phase change is expected to be important due to vaporization of micro-droplets from the jet penetration, before the explosion. It can also play a role in the behavior of a saturated hot bubble which is over-enriched in fuel and it cools down. In this case, as it cools down, the vapor pressure of the organic solvent decreases, and condensation starts. Since condensation is an exothermic process, the bubble loses its temperature at slower rates. This is an interesting aspect which will be discussed in the results and discussion chapter.

3.2.3 Compression of a bubble

When a bubble is shrinking due to external pressure rise, its gas phase is being compressed. In case of an adiabatic bubble compression, the well known (slightly modified) Poison equation can be applied:

$$P_{ad} = P_0 \cdot \left(\frac{r_0}{r} \right)^{3 \cdot \gamma} \qquad \text{(eq. 3-2)}$$

$$T_{ad} = T_0 \cdot \left(\frac{r_0}{r} \right)^{3 \cdot \gamma - 3} \qquad \text{(eq. 3-3)}$$

In these equations P_{ad} and P_0 are the calculated and initial pressure; T_{ad} and T_0 the calculated and initial temperature; r and r_0 the current and initial bubble radius and γ the adiabatic index of the gas mixture respectively. The adiabatic index is assumed to be constant in this consideration. It follows that the behavior of the temperature inside the gas bubble is very sensitive on the value of γ.

For an adiabatic compression during which high temperatures are reached, e.g. in the case of shock induced bubble compression, the temperature dependence of the adiabatic index should be taken into account in the calculation of these temperatures. One way to do this for the case of a shrinking bubble, is to divide the compression process in many virtual bubble compression stages and calculate the temperature, the pressure and the adiabatic index for each stage separately (see Fig. 3-3). In this calculation the adiabatic index is assumed to be constant during a compression stage.

In this case the temperature and the pressure inside the bubble at the end of each compression stage will be:

$$P_{j+1} = P_j \cdot \left(\frac{r_j}{r_{j+1}} \right)^{3 \cdot \gamma_j} \qquad \text{(eq. 3-4)}$$

$$T_{j+1} = T_j \cdot \left(\frac{r_j}{r_{j+1}} \right)^{3 \cdot \gamma_j - 3} \qquad \text{(eq. 3-5)}$$

where the index "j" has as first value zero and denotes the number of each virtual bubble compression stage; γ_j is the adiabatic index at T_j and P_j.

In the case that the radius is reduced from r_0 to $\alpha \cdot r_0$ in *n* stages so that at the end of each step the radius is reduced $\frac{(1-a)}{n} \cdot r_0$, then: $r_{j+1} = r_j - \frac{(1-\alpha) \cdot r_0}{n} = (1 - \frac{(j+1) \cdot (1-\alpha)}{n}) \cdot r_0$ and the temperature and the pressure inside the bubble, in case of adiabatic compression can be calculated by the equations:

$$P_{ad} = P_n = P_0 \cdot \prod_{j=0}^{n-1} \left(\frac{n - j \cdot (1-\alpha)}{n - (j+1) \cdot (1-\alpha)} \right)^{3 \cdot \gamma_j} , \quad \text{(eq. 3-6)}$$

and

$$T_{ad} = T_n = T_0 \cdot \prod_{j=0}^{n-1} \left(\frac{n - j \cdot (1-\alpha)}{n - (j+1) \cdot (1-\alpha)} \right)^{3 \cdot \gamma_j - 3} , \quad \text{(eq. 3-7)}$$

where *n* is the total number of the virtual compression stages into which the compression process is divided and $\alpha \cdot r_0$ is the bubble radius at the end of the compression process.

It should be noted that before T_{ad}, P_{ad} can be calculated, all the intermediate compression stages must be calculated first. This is because for the calculation of γ_j it is necessary to know the temperature T_j, and pressure P_j.

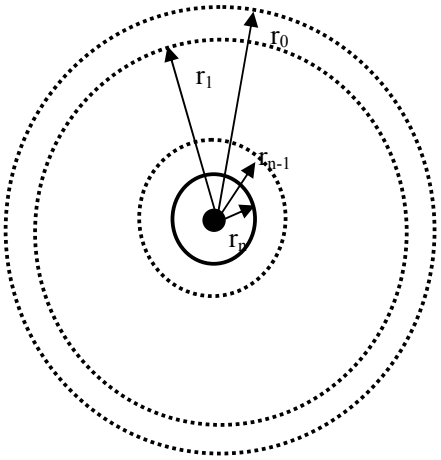

Fig. 3-3: Schematic of a bubble of initial radius r_0 compressed in *n* stages reaching a final radius r_n.

3.2.4 Chemical reactions

In a gaseous mixture containing for example oxygen and cyclohexane, chemical reactions (e.g. partial oxidations) will start to take place at temperatures that are significantly lower than the ignition temperature [56]. Such reactions can take place also in non explosive mixtures (e.g. fuel over-enriched mixtures). Depending on the conditions and their duration, such effects can become important for the explosion behavior, since they change the content of the mixture prior to its ignition. This effect demonstrates itself especially at high temperatures near the upper explosion limit [80].

Additionally, as the temperature and pressure inside the bubble approaches the ignition point during the compression of for example an oxygen – cyclohexane bubble, intermediate chemical compounds (e.g. CO and OH) are produced. Therefore the chemical composition of the bubble's gas is changed, so that at the ignition point the ignited gas contains apart from only cyclohexane and oxygen, a pool of different species.

The changes of the gaseous mixture inside the bubble before the explosion due to chemical reaction, including dissociation processes during the combustion process are not taken into account in this work.

3.3 Duration of bubble collapse

The time that a bubble needs to collapse under shock wave impact, gives a very good approximation of the time scale of the phenomena that are involved. The estimation of this quantity is based on the analysis of bubble motion, i.e. on the laws of conservation of mass, momentum, and energy.

Under the assumption of an incompressible liquid and neglecting the role of the liquid's surface tension and viscosity, the Rayleigh equation for the growth and collapse of a single vapor bubble can be derived [17]:

$$r \cdot \ddot{r} + \frac{3}{2} \cdot \dot{r}^2 = \frac{1}{\rho_{liquid}} \cdot P_{\infty}, \qquad \text{(eq. 3-8)}$$

where r is the bubble radius, P_{∞} the pressure in the liquid, and ρ_{liquid} the density of the liquid.

Assuming further that a pressure equal to the peak pressure of a shock wave is imposed suddenly and that it remains constant in the liquid during the complete collapse process, it can be shown that the total collapse time of the bubble $t_{collapse}$ is [17]:

$$t_{collapse} = 0.915 \cdot r_0 \cdot \sqrt{\frac{\rho_{liquid}}{P_{SW}}}, \qquad \text{(eq. 3-9)}$$

where r_0 is the initial diameter of the bubble before the impact. The factor 0.915 has no units.

For the conditions of the investigated system, the above calculation results into bubble collapse durations in the order of tenths of microseconds. An example of such a calculation is presented in §5.3.1.2.

4 Methodology

In this chapter, the experimental setup, the experimental procedure and the data treatment are described. Furthermore, a discussion about the limitations of the methods used is included.

4.1 Experimental setup

As part of this work a new experimental setup was installed (see Fig. 4-1). The central component of the apparatus is a vertical tubular autoclave inside which the experiments take place (A). On the wall, right from the autoclave, the signal amplifiers can be seen (B). Each amplifier corresponds to one pressure sensor installed in the autoclave.

The optical bank seen on the left of the autoclave holds the light source and the optical components (lenses, mirror) necessary for the generation of a parallel light beam (C). The light beam enters the autoclave through one of its windows and is then focused into the cameras, two of which can be installed at the two optical banks. The lenses that were used for the generation of the parallel light beam were achromatic. The generated light beam had a diameter of 100 mm and the mirrors a diameter of 150 mm. For the simultaneous use of more than one camera, semitransparent mirrors can be used for the division of the light beam. In the case that a flash lamp was used as light source, it was installed directly in front of the autoclave's back window.

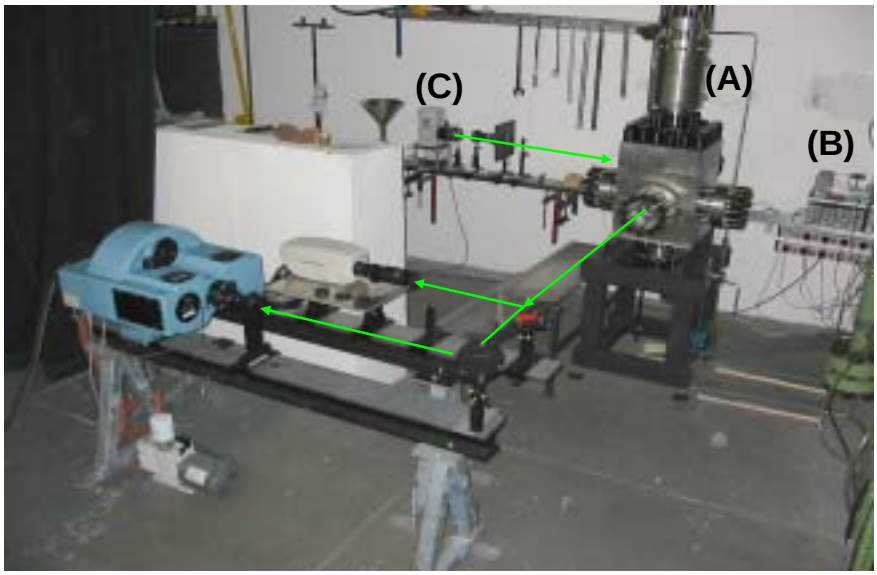

Fig. 4-1: General overview of the experimental arrangement.

The path of the light beam from the light source up to the cameras can be seen. In this configuration, parallel light, a high speed video (Kodak) and a rotating drum (Cordin) camera were used.

The autoclave is designed pressure resistant for up to 1 100 bar at 200 °C. The pressure resistance of the feeding pipes and connections is higher. The pressure resistance of the flanges and the adapters for pressure and optical measurements were designed in accordance with the instructions in the references [81], [82] and [83]. Nevertheless, for safety reasons the apparatus is operated under remote control. The mixer for the preparation of the gaseous mixtures can be seen in Fig. 4-2. The compressed gas cylinders for the preparation of the detonable mixture and for the buffer vessel are located in a separated room (see Fig. 4-3(A)). A second control room was used to operate the experimental setup (Fig. 4-3(B)).

For safety reasons, the apparatus as well as the pipes had to be frequently tested for leakage. Apart from that, during the preparation of the detonable mixture the procedures had to be followed very carefully, since the gas mixture of acetylene – oxygen can be easily ignited. Such an unwanted ignition causing an explosion took place once during the experimental phase. As a result of this accident the internal parts of the gas mixer were destroyed (see Fig. 4-2). The repair of the apparatus took about 6 weeks. After this accident the mixing process was performed at a pressure of 5 bar instead of 12 bar previously, to increase the safety.

In the next sections the most important elements of the experimental setup are described in detail.

Fig. 4-2: The high pressure vessel for the mixing of gases and components of it that were destroyed inside it by an explosion caused by an unwanted ignition.

(A) **(B)**

Fig. 4-3: Control rooms for the performance of the experiments.

(A) Control room for the preparation of the gas mixtures; (B) Part of the control room for the performance of the experiments.

4.1.1 The autoclave

The autoclave consists of mainly three parts (see Fig. 4-4). In the bottom part (part I) the bubble generator is installed. Additionally, part I contains four adapters for pressure transducers and windows. The diameter of the openings hosting these adapters is 100 mm. The inner diameter of the bottom part can be either 200 mm or 100 mm. In the experiments reported in this work, only the diameter of 100 mm was used. The middle part (part II) and the upper part of the autoclave (part III) have an inner diameter of 100 mm, too. On the upper part, the ignition source is installed. As ignition source, an exploding wire was used. For its ignition 380 V were applied (see Fig. 4-5). The wire is made from Nickelin (31 % Ni, 56 % Cu, 13 % Zn) and has a diameter of 0.1 mm. Some experiments were performed also with an incandescent wire. The total length of the autoclave is 1070 mm. The bubble generator in the bottom of the autoclave consists of an orifice with two side openings of 0.35 mm diameter each. The outlet for the liquid is installed in the bottom part of the autoclave too (see Fig. 4-6 and Fig. 4-13).

A mass flow meter (*Model 5850E)* coupled with a control and read out equipment (*Model 5875)*, both from the company *Brooks Instruments*, were used to measure the gas flow for the generation of the bubbles. The device is calibrated for the gases N_2, O_2 and air and for flows in the range of 3 ml_n/min to 30 l_n/min with an accuracy of ± 1 % and repeatability of 0.25 % of rate. The index n refers to a pressure of 1 bar and a temperature of 25 ^oC. The device can be used at operating pressures up to 100 bar. It allowed to significantly increase the reproducibility and controllability of many of the parameters in the experiments. The following parameters were possible to be controlled: The bubbles properties (form, diameter), their spatial distribution (distance between bubbles), and the gas holdup of the system. Most of the experiments were performed with a gas flow of about 180 ml/min. Experiments have been performed up to 6 l/min.

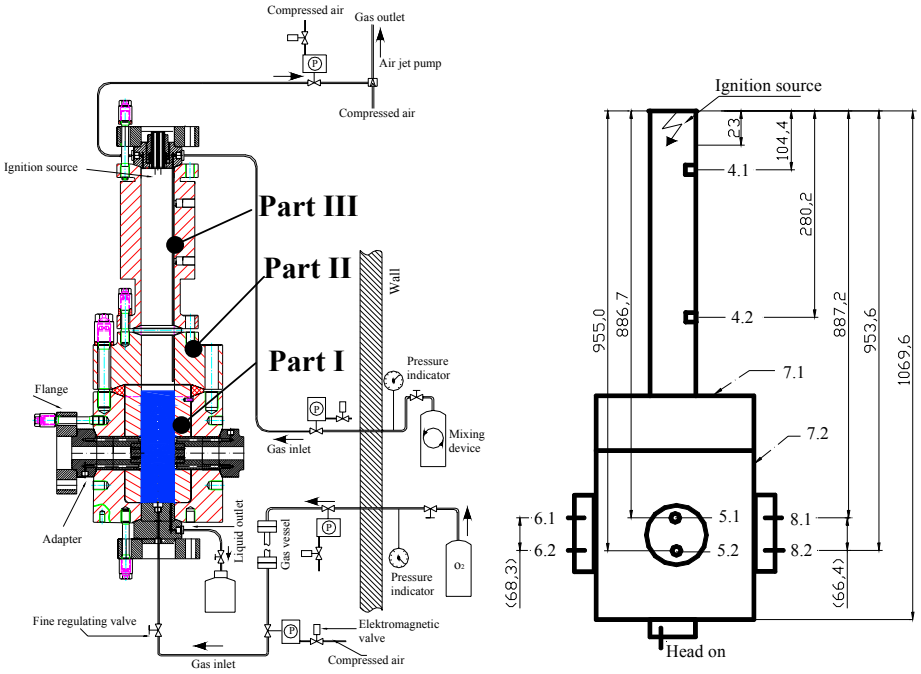

Fig. 4-4: Two schematics of the autoclave. On the right one the positions of the pressure sensors are annotated.

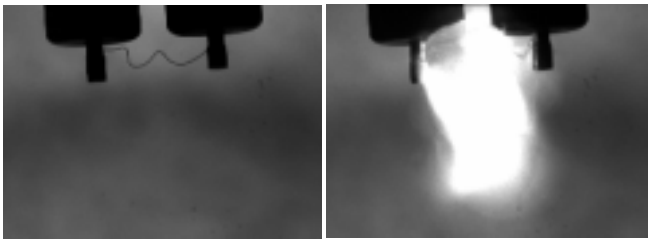

Fig. 4-5: Ignition device; recording of the exploding wire.

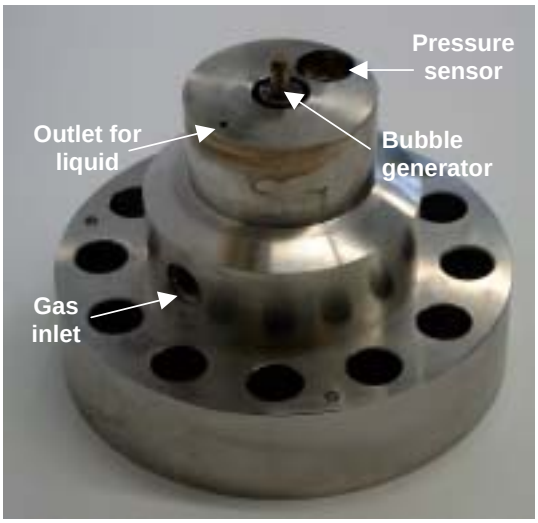

Fig. 4-6: The bubble generator mounted on the top of the adapter.

The detonation pressure in the gas phase was measured from the pressure sensors at the positions indicated by 4.1 and 4.2 in Fig. 4-4. Mostly the resulting shock wave in the liquid was monitored at two positions on each adapter (see Fig. 4-4). The pressure signals inside the liquid phase at the level of the windows, which are presented in this work, were recorded at the position 8.1 in Fig. 4-4, if nothing else is stated.

The length of the acrylic glass window was either 40 mm, 144 mm, or 184 mm. Metallic sealing gaskets were used on the two longer windows on the right, as seen in Fig. 4-7. At 184 mm the windows filled almost completely the corresponding openings of the autoclave, so that the volume of the liquid inside had a cylindrical form. Some of the most significant autoclave parts that were developed in the frame of this work, are presented in Fig. 4-8 – Fig. 4-14.

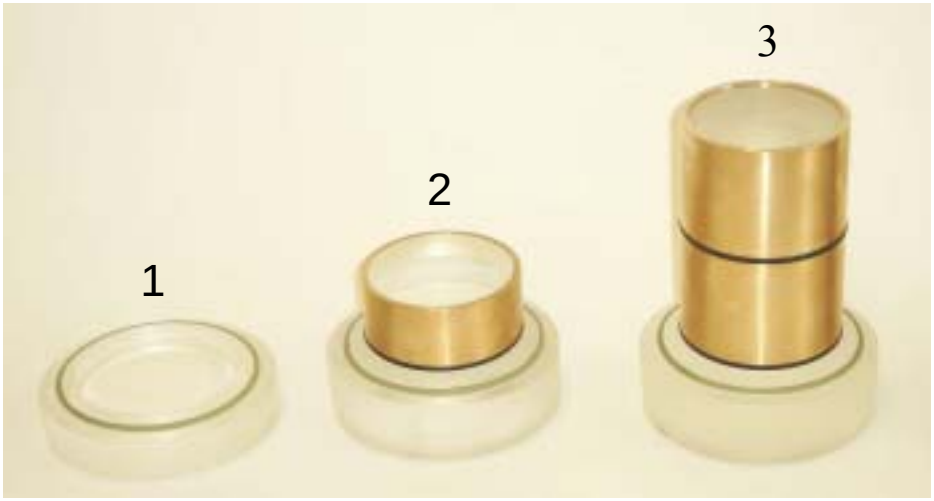

Fig. 4-7: Three different acrylic glass windows.

The window type 1 offers an observation area of 10 cm in diameter. Due to the metallic sealing gaskets that are installed, the windows of type 2 and 3 offer an observation area of 9 cm in diameter.

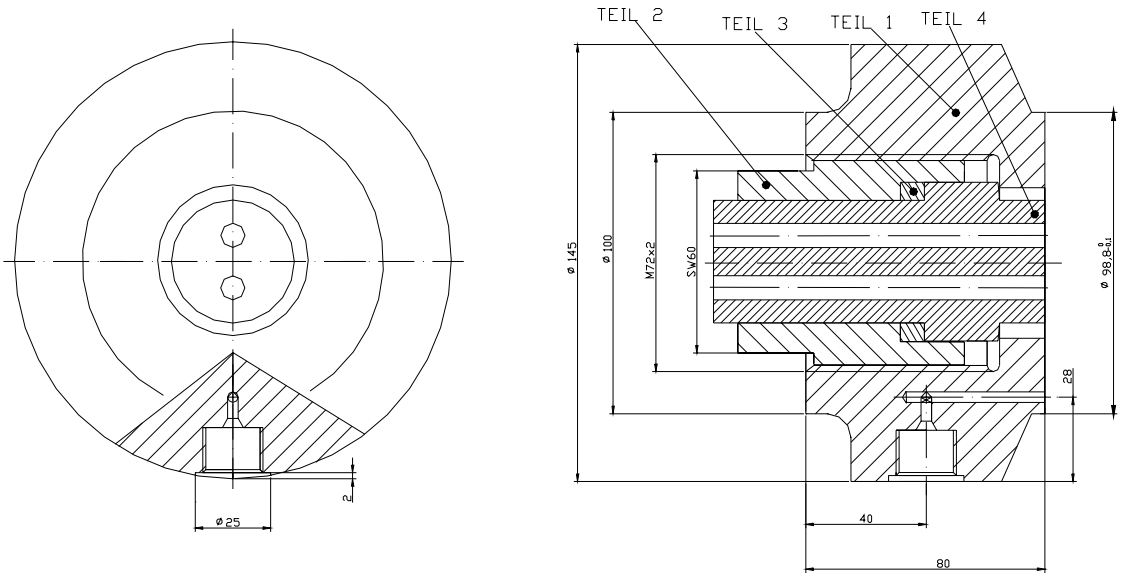

Fig. 4-8: Drawing of the adapter for the ignition device.

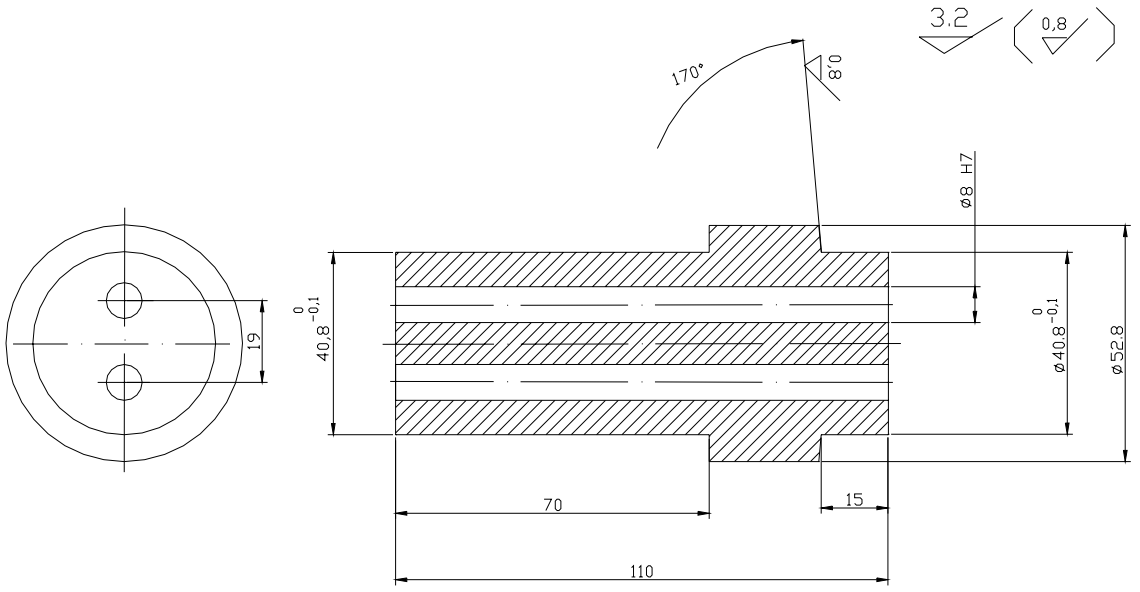

Fig. 4-9: Drawing of the adapter for the exploding wire.

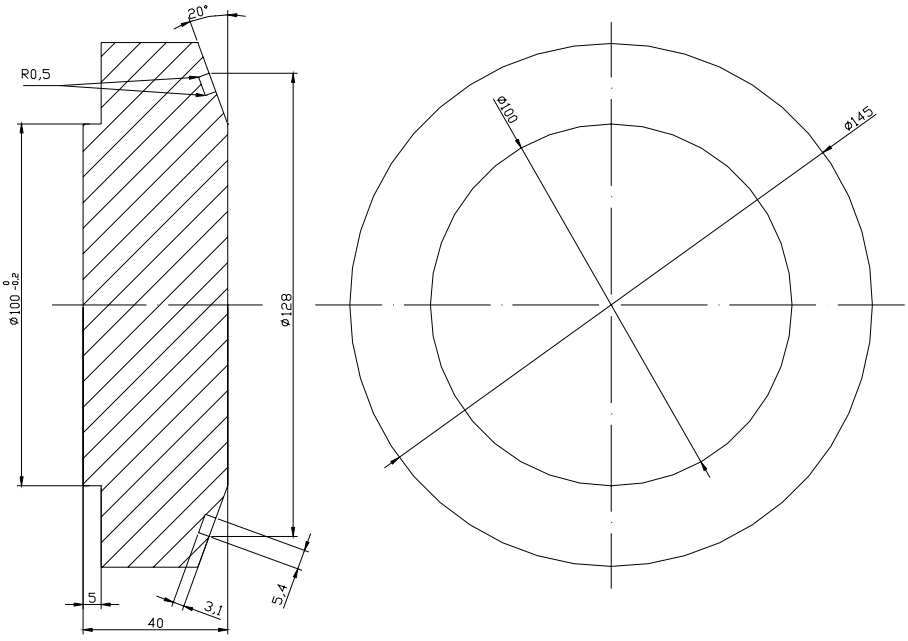

Fig. 4-10: Drawing of the acrylic glass window type 1 (see Fig. 4-7).

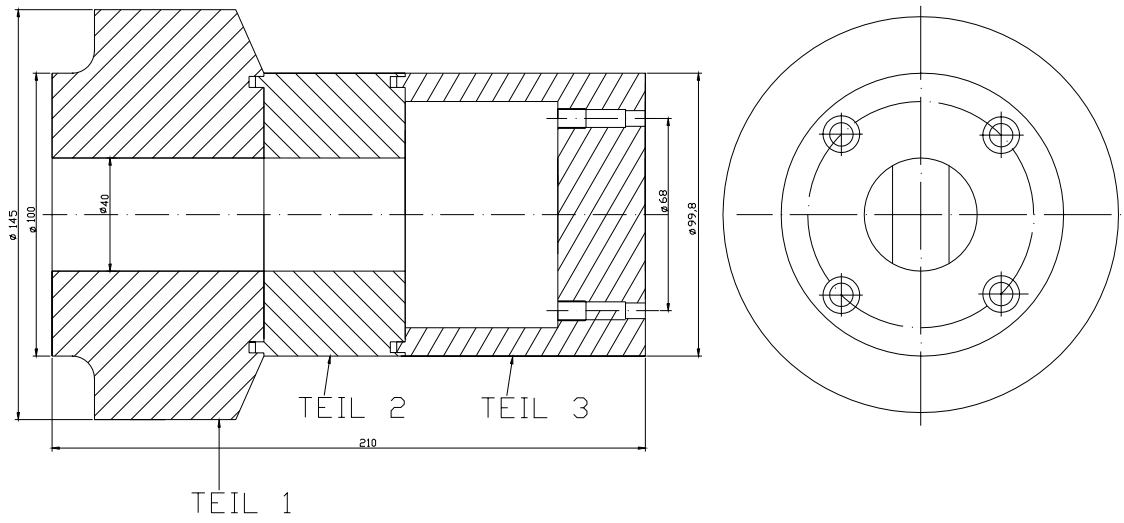

Fig. 4-11: Drawing of the adapter for the pressure sensors.

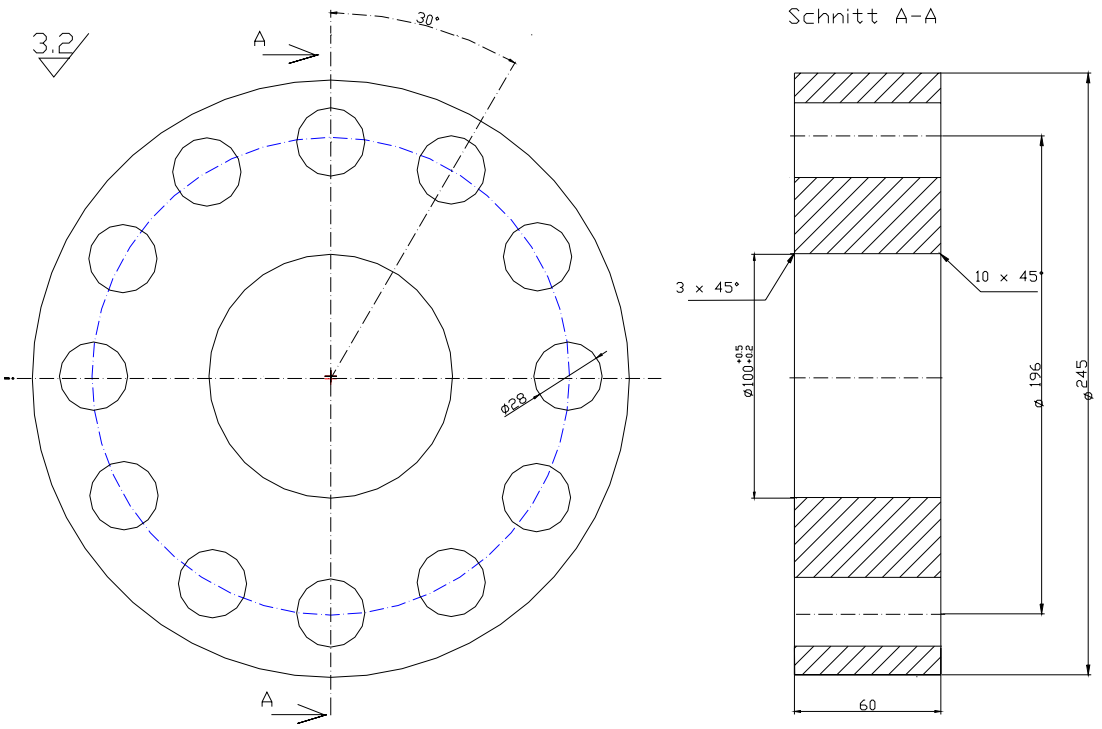

Fig. 4-12: Drawing of the a flansh.

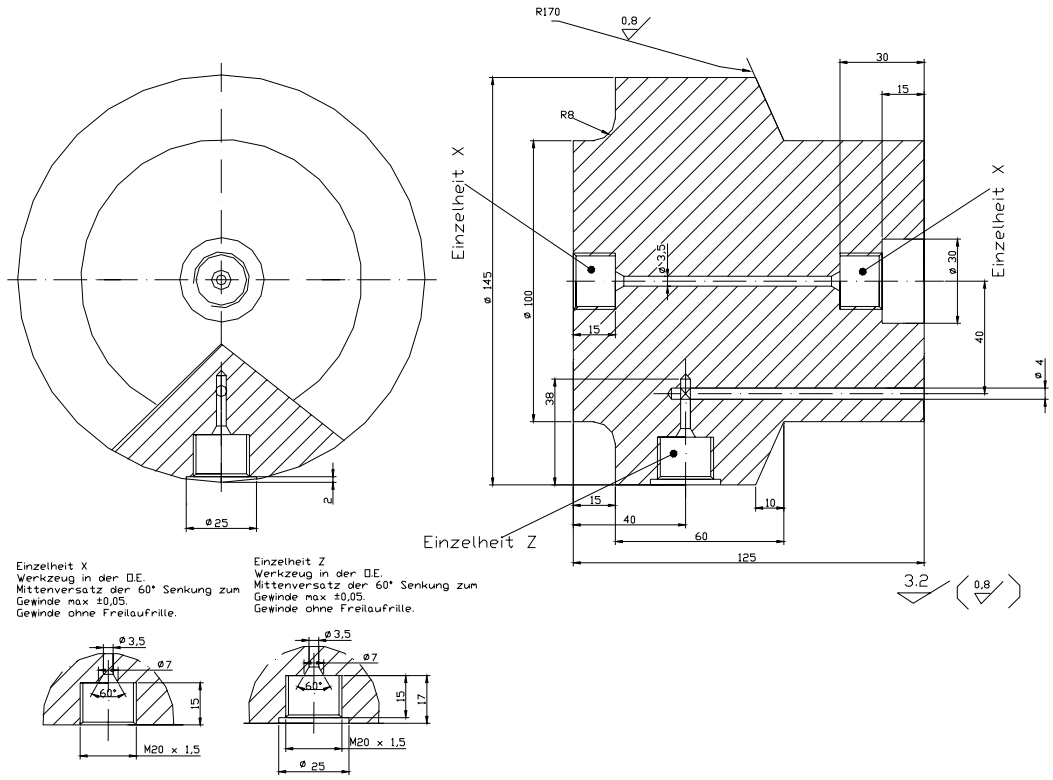

Fig. 4-13: Drawing of the adapter for the bubble generator.

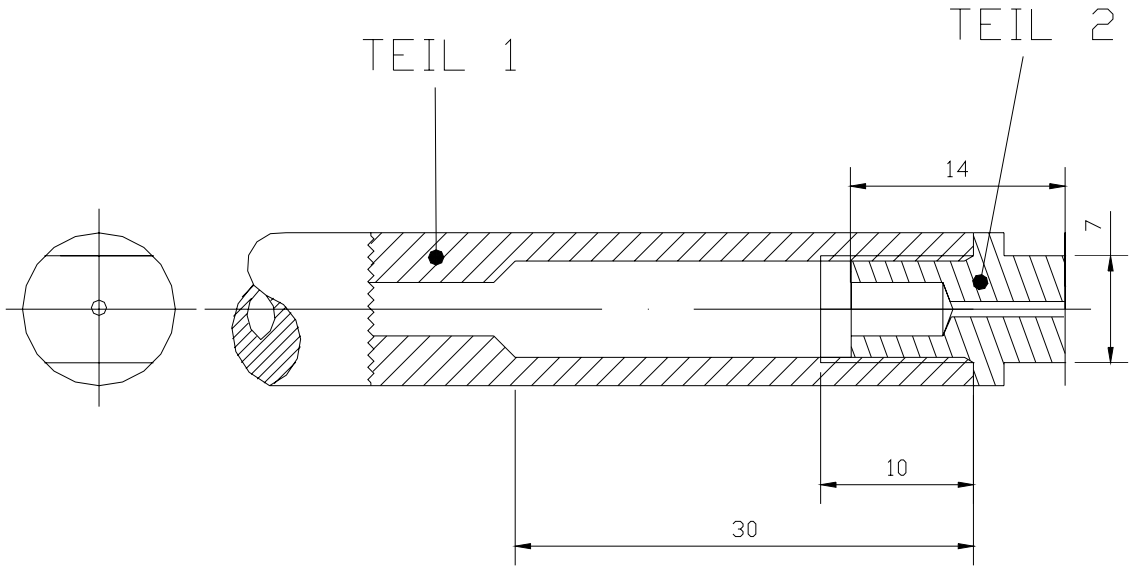

Fig. 4-14: Drawing of the basic version of the bubble generator.

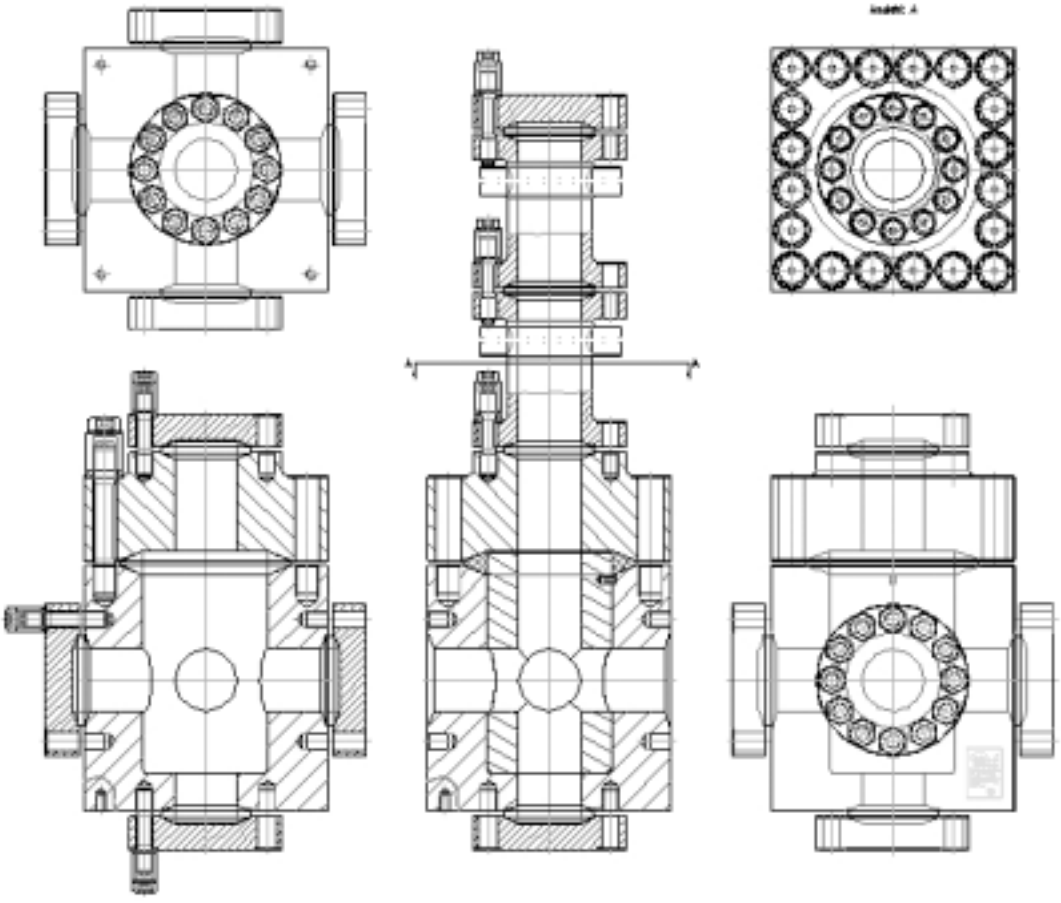

Fig. 4-15: Drawing of main parts of the autoclave, which were delivered by an external company.

4.1.2 Pressure measurements

For the pressure measurements, piezoelectric pressure transducers (Kistler 601H) in combination with a multi-channel transient recorder operating at a sample rate of 1 MHz were used. These type of pressure transducers can measure pressures up to 1 000 bar at a temperature of up to 200 °C. They have a natural frequency of 150 kHz. The produced signal from the pressure transducers was passed through an electronic amplifier of the type Kistler 5001 SN. The signal was intensified there, so that it could be recognized by the transient recorder. The transient recorder automatically translated the measured voltage signals into pressure signals which were saved in a digital form. The transient recorder used in this work was the model TRA 800 from the company *W + W Instrumente AG Basel*. A maximum of 6 different pressure sensors were installed in the autoclave, each of them corresponding to one measurement channel of the transient recorder. Although it is possible to operate and trigger each of the channels separately, they were triggered simultaneously, directly by the manual triggering signal (see Fig. 4-23).

4.1.3 Optical measurements

The interaction between the bubbly liquid and the incident shock wave was observed with the help of acrylic glass (Plexiglas®) windows (see Fig. 4-7) using different types of high speed photography. Continuous diffuse light, a flash lamp or parallel light were used as external light sources. A setup was created that allows the use of up to three different cameras simultaneously. A system with lenses and mirrors (normal and semitransparent) was used for this purpose (see Fig. 4-1 and Fig. 4-16). The light sensitivity of the optical measurements was varied by the appropriate configuration of the cameras and additional filters when necessary (e.g. for the recordings of the behavior of the surface).

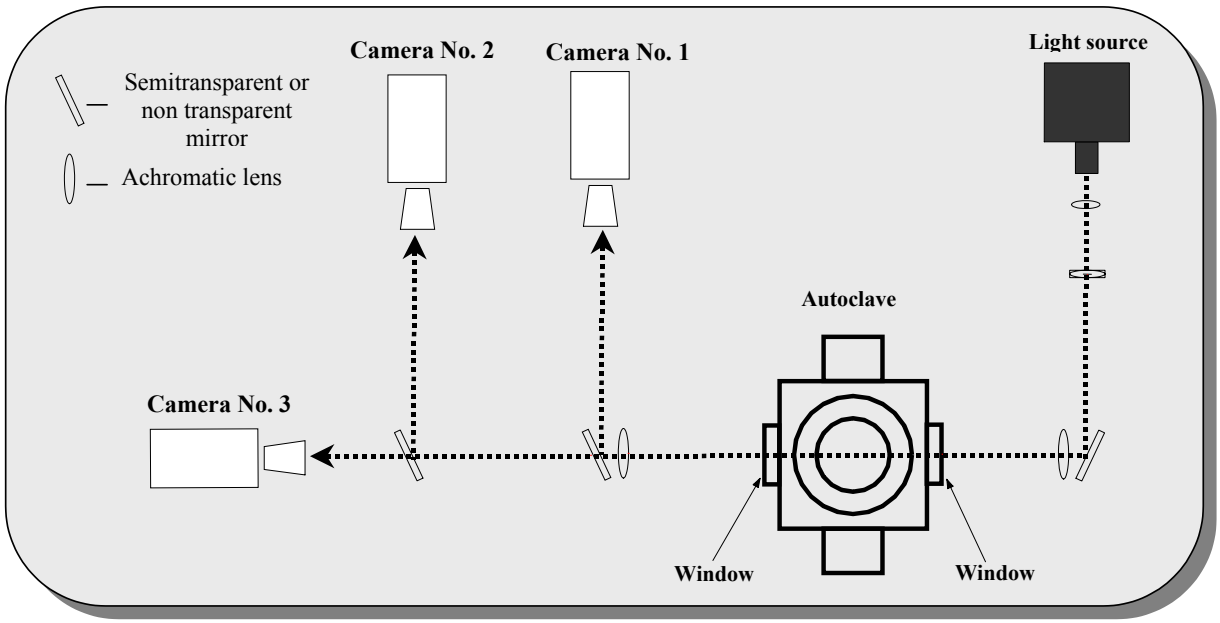

Fig. 4-16: Diagram of the optical configuration.
In this diagram the configuration for parallel light (shadow photography) and use of three cameras is illustrated.

4.1.3.1 Cameras

For the needs of the experiments a total of three different cameras was used: Two high speed digital framing cameras and one rotating drum camera. The rotating drum camera is the model 374 of the company Cordin (see Fig. 4-17). It offers framing rates up to 100 000 fps. The frames are recorded on a 70 mm black and white film at four rows, as shown in Fig. 4-18. A maximum of 500 frames (10 mm x 6.9 mm) can be recorded during an experiment. The exposure time of each frame is 20 % or 30 % of the time interval between the recording of two sequential frames and can be configured directly on the camera.

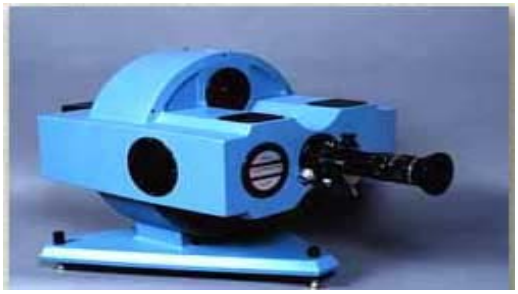

Fig. 4-17: Rotating drum camera Cordin model 374

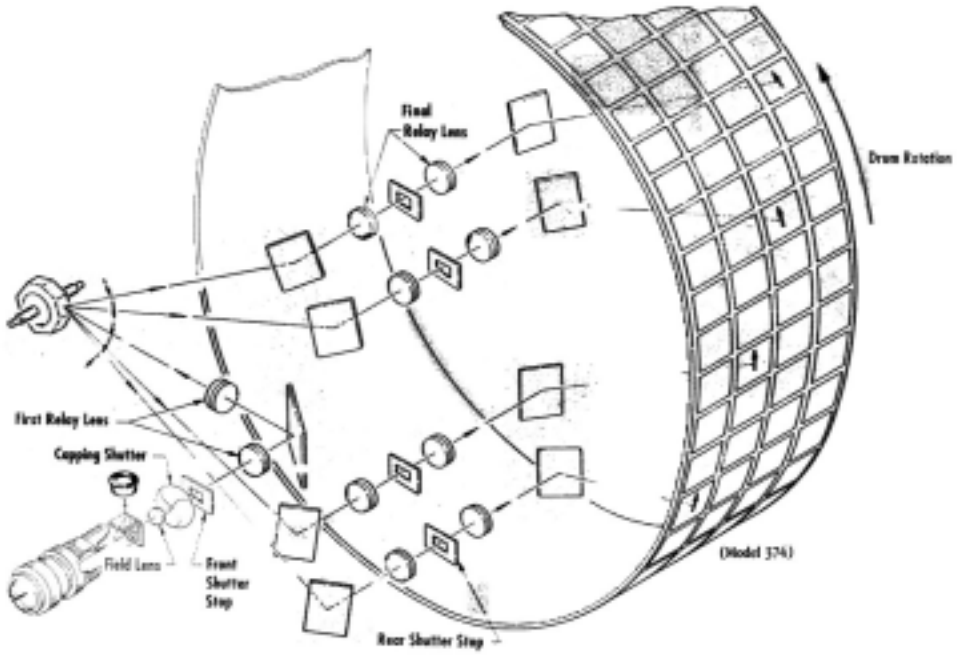

Fig. 4-18: The path of the light beam inside the rotating drum camera

The recorded frames were digitized with the help of a flatbed film scanner (Cordin model 1820). This scanner is intended for black and white films just over one meter long and 70 mm wide. The digitization was performed with a video camera that provided an image resolution of 768 x 494 pixels, through a 55 mm Nikon Micro-Nikkor lens. Backlighting for the film was provided by two fluorescent tubes. The camera and its motor were mounted on a 1350 mm profile slide, which was in turn mounted on a light box. The operation was controlled by a software program that generates camera movement with two stepper motors in lengthwise and crosswise directions. A separate program called IMAQ (by National Instruments Corporation) acquires the images in either .TIFF or .BMP format.

The first of the digital cameras was the high speed video camera (Kodak Ektapro HS coupled with the Kodak Ektapro HS processor 4540) shown in Fig. 4-19. This camera has a maximum framing rate of 4 500 fps at a resolution of 256 x 256 pixels. The framing rate can be increased up to 40 500 fps, but with corresponding lower resolutions, as seen in Table 4-1. The exposure time of each frame is the time between the recording of two sequential frames. The camera can recognize 256 different gray scales .

Table 4-1: The modes of the high speed digital video camera Kodak HS.
(fps stands for frames per second)

Mode No.	X axis pixels	Y axis pixels	fps	Number of photos	Exposure time per frame in µs	Total recording time in s
1	256	256	4 500	3 072	222.22	0.682
2	256	128	9 000	6 144	111.11	0.682
3	128	128	13 500	12 248	74.07	0.682
4	256	64	18 000	12 248	55.56	0.682
5	128	64	27 000	24 576	37.04	0.682
6	64	64	40 500	49 152	24.69	0.910

(A) **(B)**

Fig. 4-19: Kodak Ektapro HS camera (A), and processor (B).

The second digital camera was a prototype of the company Shimadzu (model ISIS V2, see Fig. 4-20). This camera was not commercially available during the time this work was performed. It offers a maximum framing rate of 1 000 000 fps at a resolution of 312 x 260 pixels. The exposure time of the frames is the interval time between the recording of two sequential frames. The camera offers a total of 104 digital frames.

Fig. 4-20: The camera Shimadzu-ISIS V2 with its control unit.

4.1.3.2 Light sources

For the generation of parallel light a high pressure, mercury-vapor, lamp from the company Oriel Instruments (see Fig. 4-21) was installed. The power of this light source was 100 W. The light beam was expanded to a beam of parallel light of 100 mm in diameter and sent through the windows of the autoclave. Behind the autoclave the light was focused.

Fig. 4-21: Photo and drawing of the mercury lamp.

For the generation of diffuse light a Xenon-flash lamp (model 659 of the company Cordin, see Fig. 4-22) was used. This lamp produces a light flash with a duration of 0.5 ms to 11 ms. Alternatively for the generation of continuous diffuse light, a halogen lamp with a power between 500 W and 2 000 W was also used. To make the light homogeneous a frosted glass between the lamp and the autoclave was used.

Fig. 4-22: Flash lamp and its control unit.

4.1.3.3 Trigger arrangement

The synchronization of the cameras and the light sources with the passage of the incident shock wave in front of the observation window becomes more difficult as the camera's framing rate increases and as the total number of produced frames decreases. The rotating drum camera and the Kodak Ektapro HS digital camera - even at maximum framing rate - offer relatively long recording time (more than 5 ms). Therefore, they can be triggered directly with the ignition of the gas mixture above the liquid.

This method is ineffective though, when the second digital camera (Shimadzu) is to be used. At maximum framing rate (1 000 000 fps), this camera offers a time window of 100 μs. The solution in this case is to use the pressure signal that the shock wave produces in front of the observation window as triggering signal. For the translation of the pressure signal into a triggering signal for the Shimadzu camera, an electronic device was developed in BAM. In order to be able to see the complete phenomenon, a pre-trigger had to be used. That is, the camera kept a certain amount of frames *before* the trigger point. This number depends on the propagating velocity of the shock wave inside the liquid, as well as the framing rate. Since only the Shimadzu-ISIS V2 camera provided the possibility for pre-triggering, this system was used only with this camera. The other two cameras were triggered independently of the Shimadzu camera.

A further point that should be considered is that the cameras and the flash lamp have their own response times, as most of the electronic parts that are used for the triggering system. The response time of the digital cameras (Kodak and Shimadzu) is negligibly small. The response time of the Cordin rotating drum camera is about 6.3 ms, and that of the Cordin flash lamp 0.5 ms. The time delay between the manual trigger signal and the initiation of the explosion in the gas phase was 2.7 ms to 3.7 ms, when an exploding wire was used as ignition source. To this time an additional delay of 3.7 ms was artificially added, when the Cordin rotating drum camera was used (see Fig. 4-23).

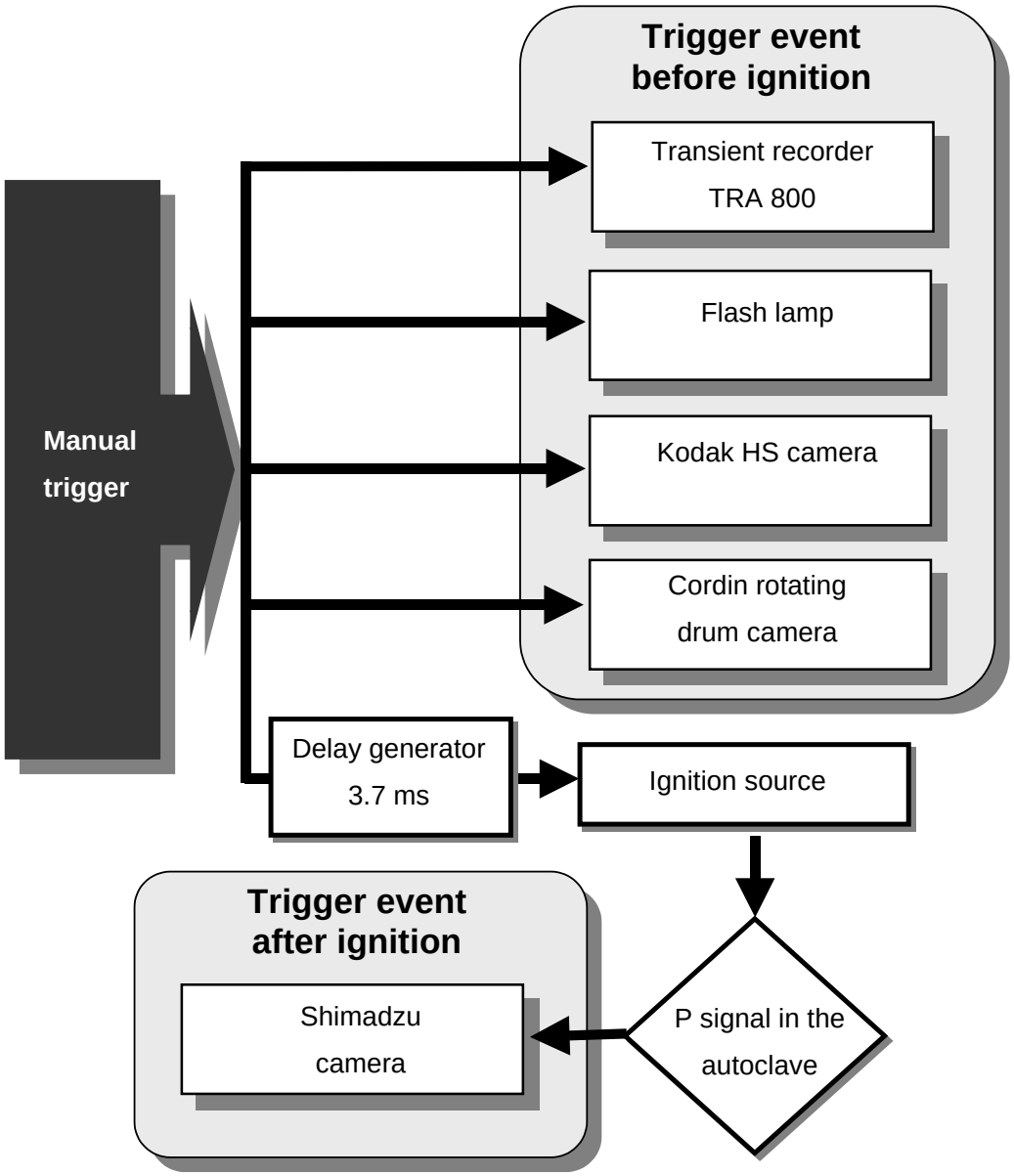

Fig. 4-23: Diagram of the trigger arrangement.

4.2 Experimental procedure.

After the preparation of the needed gas mixtures, the appropriate volume of liquid was filled into the autoclave. Then the explosive gas mixture (usually acetylene – oxygen) was fed in from the upper gas inlet. Bubbles were created by injecting gas (oxidizer or inert) into the liquid phase through the bubble generator at the bottom. A shock wave in the liquid was generated by the impact of a gas detonation of an explosive gas mixture above the liquid. The gas detonation was ignited by an incandescent or by an exploding wire in the top flange (see Fig. 4-4, Part III). The gas and liquid outlets were used for the

evacuation of the autoclave at the end of the experiment. The cyclohexane was then stored. When adequate amount was collected, it was distilled and could be used again.

Before the filling of the autoclave with the explosive gas mixture, all persons had to leave the room, which was then closed. From that point on, nobody was allowed to enter the room and the necessary operations were performed under remote control from two observation rooms. The entrance into the autoclave's room was allowed again after the experiment had been finished. The configuration of the setup and other important information (e.g. room temperature) were written down in a standard protocol and the measured data were saved in digital form.

4.3 Data treatment

In this section the treatment of the experimentally recorded data will be described.

4.3.1 Pressure measurements

The recorded pressure signals were analyzed and evaluated with the help of the computer program FAMOS - version 3.0 Rev.2 (Integrated Measurement & Control (IMC)). With the help of the integrated tools, the signals were mathematically treated (application of moving average). All pressure signals were saved and archived in electronic form.

4.3.2 Optical measurements

The recorded frames were treated in electronic form with the help of the computer program IrfanView - version 3.80. The treatment was limited only to the improvement of the optical quality of the photos (e.g. contrast, gamma correction) when this was necessary for the evaluation. The measurement of the bubble diameter and of the distances between bubbles was performed by direct measurements on the printed form.

4.4 Limitations

In this section important aspects of the methodology limiting or influencing the accuracy of the pressure and of the optical measurements will be discussed.

4.4.1 Pressure measurements

Frequent impacts of shock waves on the pressure sensors can influence their accuracy. To minimize this influence, a calibration was performed regularly. The calibration of the pressure transducers was performed according to the work instructions in [84].

Another source of inaccuracies is the natural oscillations of the pressure sensors. All the pressure data were recorded by the transient recorder described above, with a time resolution of 1 μs. In order to reduce the influence of the natural oscillations the signals were smoothed with a moving average of 20 points. Averaging over 20 points corresponds to 3 oscillation periods of the pressure transducers (their natural frequency is 150 kHz).

4.4.2 Optical measurements

For the distance measurements (e.g. bubble diameter) the limiting factor is the resolution (in mm/pixel) of the recorded frames. From Table 4-2 this resolution can be calculated. With this kind of calculation the minimum resolvable area can be estimated. Per distance measurement the maximum error corresponds to two pixels.

Table 4-2: The resolution (in mm per pixel) of the cameras for the experimental conditions.

		resolution of the cameras (in mm/pixel)								
	Pixels	**for an observation length of:**								
camera	**Per axis**	**9 cm**	**8 cm**	**7 cm**	**6 cm**	**5 cm**	**4 cm**	**3 cm**	**2 cm**	**1 cm**
Cordin x-axis	768	0.117	0.104	0.091	0.078	0.065	0.052	0.039	0.026	0.013
Cordin y-axis	494	0.182	0.162	0.142	0.121	0.101	0.081	0.061	0.040	0.020
ISIS x-axis	312	0.288	0.256	0.224	0.192	0.160	0.128	0.096	0.064	0.032
ISIS y-axis	260	0.346	0.308	0.269	0.231	0.192	0.154	0.115	0.077	0.038
Kodak x,y-axis	256	0.352	0.313	0.273	0.234	0.195	0.156	0.117	0.078	0.039
Kodak x,y-axis	128	0.703	0.625	0.547	0.469	0.391	0.313	0.234	0.156	0.078
Kodak x,y-axis	64	1.406	1.250	1.094	0.938	0.781	0.625	0.469	0.313	0.156

A problematic situation can arise in the rare case when one shadow corresponds to two or more bubbles, which are situated on the same optical axis. This leads to a confusion for the measurement of diameters and light emission durations. The bubbles that corresponded to this situation were not included into the evaluation procedure. Such a bubble overlapping demonstrates itself by the emitted shock waves that follows the bubble expansion phase (with or without explosion). If more than one shock wave originates from virtually the same center, this is a strong indication that there is an overlapping of at least two bubbles. Such an effect was observed a few times in the experiments. An example recorded during the Exp. Nr. 137 can be seen in Fig. 5-36 at 30 μs. From the two spherical shock waves with the same center, it can be assumed that the bubble denoted with the label 1 corresponds to 2 bubbles!

The measurement of time (e.g. for the light emission during bubble explosions) was performed by direct observation of the recorded frames. This means that only a positive deviation from the real time can take place. This is the case when the light emission covers only a part of the exposure time of the frames. The maximum error of this kind corresponds to the time of less than two frames. This time can be calculated from the corresponding framing rate of the camera.

Another point is that at the explosion limits the bubbles emit very weak light, making the quality of the used optical method critical. If the sensitivity of the method is not high enough, bubble explosions would not be registered by light emission and this would influence the measurement of the bubble explosion limits. The ability to distinguish between light illuminations and light emission caused by weak bubble explosion is important too.

Experiments were performed to investigate the light emission of bubble explosions with different background light intensities (power of light source: 0 W, 100 W, 500 W, 2 000 W), different cameras (different recording methods and parameters: digital or chemical, recording frame rate, exposure times, etc) and variation of their properties (gain, gamma correction, light intensifier, external filters). An example of these investigations can be seen in Fig. 4-1. The influence of the light emitted above and on the liquid's surface, induced by a gas detonation and its reflection, was investigated too (see §5.1).

In the experiments the sensitivity of the optical method was also varied according to the kind of information that should be revealed. An example of these experiments is presented in Fig. 4-25. At high sensitivity the relatively weak waves from the autoclave's walls into the liquid can be visualized. On the other hand the incident wave has a very complicated structure. This makes it impossible to clearly record the shock induced bubble dynamics. Such effects were taken into account.

Based on the practice followed in the literature concerning the experimental errors in experiments with bubble explosions (see e.g. [36], [45], [46], and [48]), and on the measures described above for the identification and minimization of such errors, the assumption can be made that experimental errors did not significantly influence the conclusions of this work.

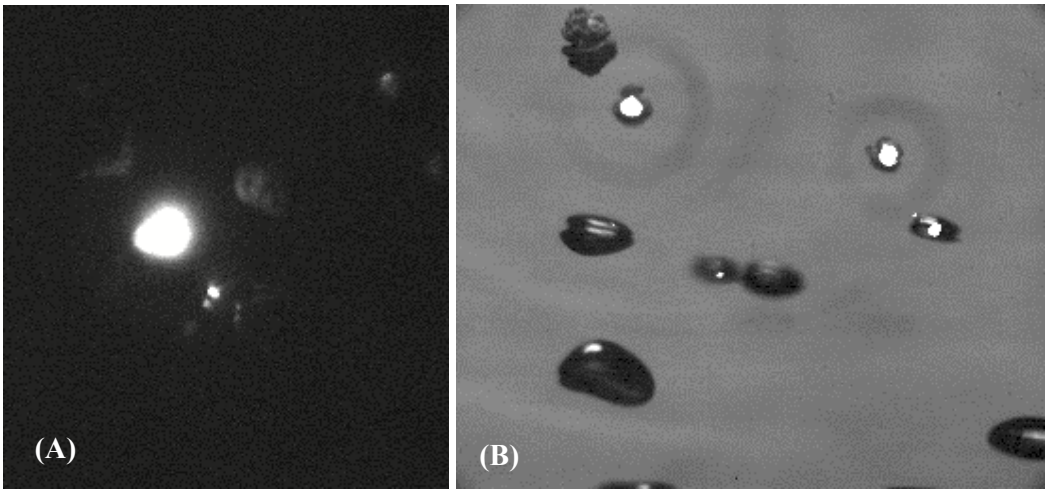

Fig. 4-24: Bubble explosions without and with external light source.

A: Recording without background light. The illumination of the explosion on the nearby bubbles is visible. Exposure time 2 µs (Exp. Nr. 64); B: Recording with background light. Non exploding bubbles are visible at different stages of shock induced behavior. Exposure time 2 µs (Exp. Nr. 94).

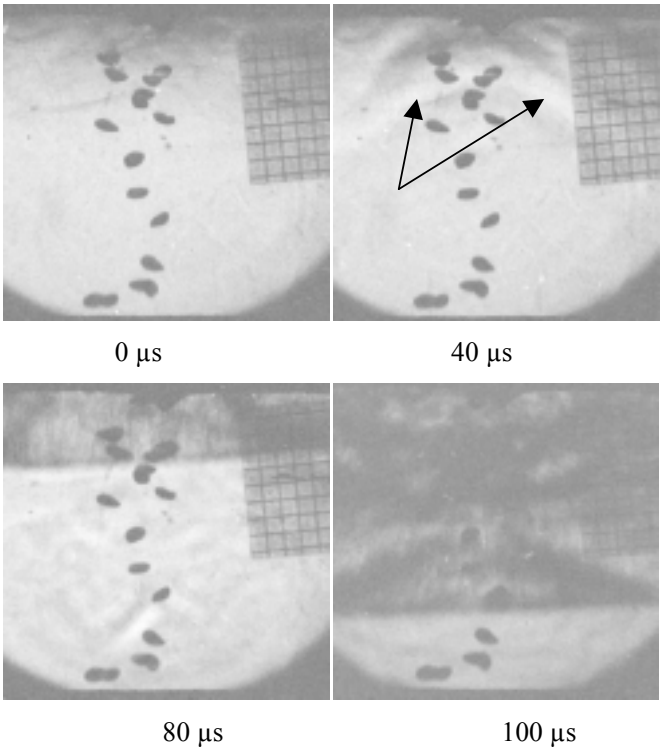

Fig. 4-25: An example of shadow photography at high sensitivity.

Oxygen bubbles under shock wave impact. The weak waves from the autoclave's walls are visualized (see the arrows). The dark layer corresponds to the incident shock wave. The Cordin rotating drum camera was used at 100 000 fps. Exposure time 3 µs per frame (Exp. Nr. 56).

5 Experimental results and discussion

During this study, 176 experiments and 35 auxiliary experiments were performed. The auxiliary experiments were necessary in order to gain basic know-how on several important issues, like the generation of bubbles and the application of the optical methods. Apart from that, during the auxiliary experiments new constructions for the apparatus (e.g. the bubble generator) were tested and improved too. The process of testing new ideas for improvements continued during most of the experimental phase.

The performed experiments are grouped in Table 5-1. At the beginning of the experimental phase, the explosive gaseous mixture for the detonation above the liquid phase had to be chosen. Additionally, some safety related questions had to be considered. The most important of these questions was to determine the initial pressures at which optical measurements can be safely applied. The experiments belonging to the groups I and II served this purpose.

The behavior of the liquid's surface, which is the position at which the gas detonation created the shock wave in the liquid phase, was systematically observed in the experiments of group III. The experiments of group IV were focused on the observation of the shock induced behavior of inert (nitrogen) bubbles.

The explosion behavior of oxygen-containing bubbles in organic solvent, which is the core subject of this study, was investigated in two groups. In group V, bubbles created by injection of pure oxygen into different organic liquids were investigated. The bubble diameter and several other parameters were varied in these experiments. In group VI, mixtures of nitrogen/oxygen were used for the bubble generation with the purpose to find the corresponding explosion limits in liquid cyclohexane. The bubbles' diameter in these experiments was kept constant at about 3 mm. A few experiments were carried out with the ignition of an explosive but not detonable gaseous mixture above the liquid, to investigate if bubbles can be ignited also in this case. These experiments correspond to the final group (group VII).

All in all, more than 40 000 digital frames and more than 1 000 pressure signals were archived during the experimental phase (the auxiliary experiments are not included in these figures). The evaluation and interpretation of this material was a long process and provided such an amount of information that a selection was at the end necessary to keep the size of this work inside some acceptable limits.

Table 5-1: The experiments of this study, in seven groups.

- **Group I: Gas phase only** (8 experiments)

These experiments involved only a gas phase. An explosive gaseous mixture of H_2 / O_2 or C_2H_2 / O_2 was ignited at several initial pressures (1, 2, 2.5, and 5 bar).

- **Group II: Gas detonation above a liquid without bubbles** (8 experiments)

These experiments involved a gas detonation above a liquid phase. Three of the experiments were performed with distilled water as liquid at 5 bar initial pressure. In the other experiments, liquid cyclohexane at an initial pressure of 1, 2, or 3 bar was used.

- **Group III: Behavior of a liquid's surface after detonation wave impact** (14 experiments)

These experiments involved a gas detonation above a liquid phase whose surface was situated at the middle of the windows. Apart from three early experiments performed with ethanol as liquid, the other experiments were performed at 1 bar and with liquid cyclohexane (one experiment at 2.5 bar).

- **Group IV: Gas detonation above a liquid containing N_2 bubbles** (28 experiments)

These experiments involved a gas detonation above liquid cyclohexane which contained nitrogen bubbles. The initial pressure was 1, 2, or 3 bar.

- **Group V: Gas detonation above a liquid containing O_2 bubbles** (96 experiments)

These experiments involved a gas detonation above liquid cyclohexane which contained oxygen bubbles. The initial pressure was 1, 2, or 3 bar. Liquid methanol, cumene or 2-ethylhexanal at an initial pressure of 1 bar, were used instead of cyclohexane in 11 of the experiments.

- **Group VI: Gas detonation above a liquid containing (O_2 / N_2) bubbles** (12 experiments)

These experiments involved a gas detonation above liquid cyclohexane which contained bubbles created by a mixture of nitrogen and oxygen. The initial pressure of the system was 1 bar.

Because of this reason, the following filtering of the results was performed during the preparation of this chapter: (i) Experimental observations that describe well known phenomena (e.g. detonation of C_2H_2 /O_2 mixtures) are reported only if they are necessary for the discussion; (ii) the report of observations from experiments involving nitrogen bubbles is kept to a minimum and is discussed always in connection to the bubble explosion phenomena; (iii) those experiments in which an explosive but not detonable gaseous mixture was ignited above the bubbly liquid, are not discussed in

this work. This decision was taken because on the one hand bubble explosion was not observed during these experiments, on the other hand time limitations did not allow a thorough investigation in this direction that would support this information with confidence. Finally (iv) only the information from the auxiliary experiments that are of direct use for the discussion are reported.

All the other results are described and discussed in this chapter. The order of presentation is according to the effects that are reported, which was chosen as the most compact variation. Frames recorded from the Cordin camera are not presented in this chapter, because it was possible to show the same experimental observations at higher optical quality offered by the two digital cameras. An example of recording with the Cordin camera was presented though in Chapter 4 (see Fig. 4-25)

When no other information is given for the respective experiment in discussion in this chapter, the initial pressure was 1 bar and the digital camera of the company Shimadzu (model ISIS V2) was used to record the presented frames. The initial temperature of the system was always between 20 ^{o}C and 25 ^{o}C, i.e. equal to the room temperature.

5.1 Pressure waves in the gas phase and behavior of the liquid's surface

In this section experimental information about the detonation waves in the gas phase, and the behavior of the liquid's surface induced by a detonation wave impact, are presented. This information is important to understand the experimental results presented later, because:

i) In the experiments, the shock wave that was used as igniter for the bubble explosions in the liquid phase, was created by the impact of a gas detonation on the surface.

ii) At the surface, light emissions take place after the ignition of the gas detonation and its reflection on the liquid's surface. This is important because light emission is one of the criteria to recognize optically a bubble explosion (the other is the bubble expansion). So, in order to ensure the correctness of this study's conclusions, -especially at the explosion limits-, a discussion of these emissions on the surface and their eventual illumination on the investigated bubbles is necessary.

Apart from these reasons, a more general motivation stems from the fact that the phenomena induced by the impact of shock waves at the contact surface between the different phases is of high interest for the safety assessment of multiphase systems. The surface of the bubbly liquid investigated in this work is an example of such a contact surface. At this position one or more shock induced phenomena like the creation of aerosol clouds and surface instabilities as well as high temperatures and pressures, could appear. Such phenomena have a significant role in a wide range of safety related problems, ranging from the mechanism of surface explosions up to the properties of the reflected wave in the gas phase and of the respective shock wave in the liquid phase.

In all the experiments, which are related to the behavior of the surface of the liquid, the observation area had the same diameter as the windows used. The level of the liquid's surface was the one shown in Fig. 5-1.

The recorded pressure signals were analyzed and evaluated with the help of the computer program FAMOS - version 3.0 Rev.2 (Integrated Measurement & Control (IMC)). With the help of the integrated tools, the signals were mathematically treated (application of moving average). All pressure signals were saved and archived in electronic form.

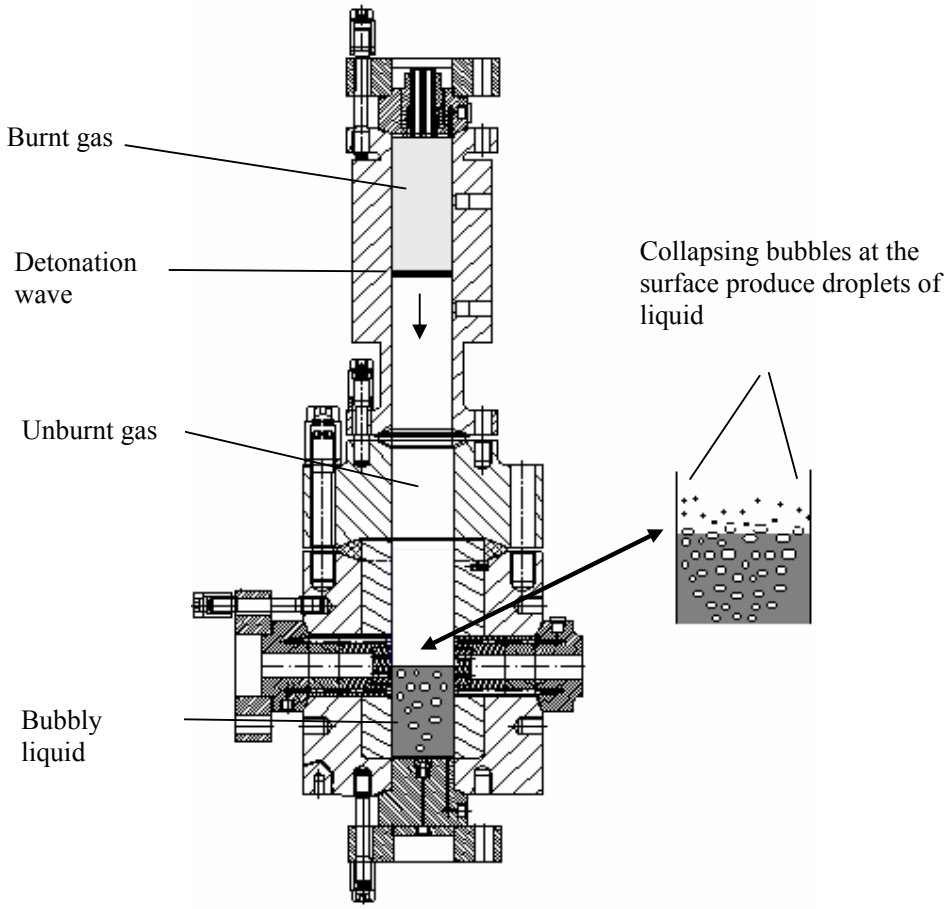

Fig. 5-1: Propagation of a detonation wave inside the autoclave containing bubbly liquid.

In this drawing the liquid reaches the middle of the observation windows. This height of the liquid was used for the experiments for the investigation of the behavior of the liquid's surface after detonation impact. On the right a magnification of the liquid's surface and the generation of liquid droplets due to bubble collapse are illustrated.

5.1.1 Detonation waves in the gas phase

The detonation phenomenon in the gas mixtures used is well investigated in the literature (see e.g. [75] and [74]). Thus only experimental observations that are useful for the discussion will be reported here. The pressure in the gas phase above the liquid was measured at the positions 4.1 and 4.2, as denoted in Fig. 4-4. Additionally pressure measurements in the gas phase were conducted at the position 8.1 in those experiments in which the surface of the liquid was below that position. The detailed information about the investigated system in each experiment (explosive gas mixture above the liquid, initial pressure, bubble's gas phase, liquid) is summarized in Appendix D, Table 7-4. From this table it can be seen that the following explosive gaseous mixtures were used:

i. H_2 / O_2, with a H_2 molar fraction of 0.66, at 1, 2, and 5 bar initial pressure (7 experiments);
ii. C_2H_2 / O_2, with a C_2H_2 molar fraction of 0.25, at 1, 2, 2.5, 3, and 5 bar initial pressure (162 experiments);
iii. $C_2H_2 / O_2 /$ He, with a C_2H_2 molar fraction of 0.20 and O_2 molar fraction of 0.60 at 1 bar initial pressure (1 experiment); and
iv. $C_2H_2 / O_2 /$ He, with a C_2H_2 molar fraction of 0.10 and O_2 molar fraction of 0.30 at 1 bar initial pressure (5 experiments).

The initial pressure of 1 bar was applied in most of the experiments (i.e. 86 %). Some explanation should be given concerning the choice of the gaseous mixtures listed above. The mixture (i) was chosen because its explosion generates no soot. Between the explosive mixtures (i) and (ii) the second was preferred because the deflagration to detonation transition distance of this mixture is shorter. In this mixture the oxygen content is higher than stoichiometric with the goal to reduce the generated soot during the explosion. The mixtures (iii) and (iv) were used only for a small number of experiments with the purpose to create deflagration waves in the gas phase. The mixture (ii) was used in most of the experiments (i.e. 92 %). Due to the large number of the conducted experiments with mixture (ii), the rest of this section focuses only on this mixture, at an initial pressure of 1 bar. These conditions correspond to 154 of the experiments.

At this initial pressure, the calculated Chapman-Jouguet conditions for this gas mixture give a detonation wave pressure of 31.6 bar with a propagation speed of 2 329 m/s[•].

The experimentally measured shock wave peak pressure at the position 4.2 for each experiment is shown in Appendix D, Table 7-6. Of the relevant 154 experiments, 148 provided adequate information for this measurement. The examination of these experiments showed that the

[•] The calculation of the Chapman-Jouguet conditions was kindly performed by Dr. P. A. Fomin.

average value of the detonation pressure was 44.1 bar. Moreover in 97 % of these experiments the detonation pressure was above the value of 31.6 bar.

The experimental propagation velocity in the gas phase in each experiment was calculated with the help of the measured pressure signals at the positions 4.1 and 4.2 of Fig. 4-4. The results are presented in Appendix D, Table 7-7. Of the above mentioned 154 experiments, 143 provided adequate information for this calculation. The examination of these experiments showed that the average value of the propagation velocity was 2 586 m/s. Moreover in 97 % of the experiments the propagation velocity was above the calculated value of 2 330 m/s.

The above mentioned values of the peak pressure measurements and of the calculated detonation velocities show that overdriven detonations were created in the gas phase. This effect is common especially in short tubes and is well known in the literature (e.g. [85]). An additional influence on the measured detonation wave parameters originates from the enrichment of the gas mixture with vapor of cyclohexane.

5.1.2 Impact of a detonation wave on the surface of a liquid without bubbles

At this point the 14 experiments in which the liquid's surface was at the middle height of the observation windows (see Fig. 5-1) will be discussed. The main goal of these experiments was to investigate the interaction of the detonation wave in the gas phase with the surface of the liquid. The experiments are discussed in two groups. The first, which is discussed below, contains the experiments in which no bubbles were generated inside the liquid; the second contains those of the 14 experiments where bubbles existed in the liquid (§5.1.3).

One of the nine experiments conducted, in which the liquid cyclohexane did not contain any bubbles, is presented in Fig. 5-2. In this experiment the gas phase above the liquid consisted of C_2H_2 / O_2, with a C_2H_2 molar fraction of 0.25 at 1 bar. Its ignition created a detonation wave with a peak pressure of 41 bar (see Fig. 5-6(1)). The detonation wave reached the undisturbed surface of the cyclohexane in 20 μs in Fig. 5-2. This can be seen by the weak light emission near the surface of the liquid.

The front of the reflected wave in the gas phase can be seen propagating towards the upper part of the autoclave at 40 μs. The reflected wave had a peak pressure of 75 bar (see Fig. 5-6(1)) and therefore a higher temperature [86]. This resulted in a higher light emission, as expected.

About 130 μs after the reflection (see Fig. 5-2, 150 μs), the formation of a structure starts to become visible on the surface. This structure has two parts, both of them are indicated by arrows in Fig. 5-2. The first part is the apparent height of the surface (pointed by the lower arrow). It increases with the time, due to surface phenomena between the material of the windows and the liquid, enhanced by the high pressure of the gas phase. This apparent height was 3.2 mm before the reflection of the detonation wave and reached 7.6 mm 780 μs after the reflection (Fig. 5-2, 800 μs). On the top of this first part, a cloud of droplets detached by the surface edges appears. The formation of this cloud can be explained by shock induced turbulence at this position. This cloud reached a maximum height

of 9.5 mm within 460 μs and started to shrink (reaching 4.4 mm 340 μs later). This two part structure is expected to appear only at the edges of the surface.

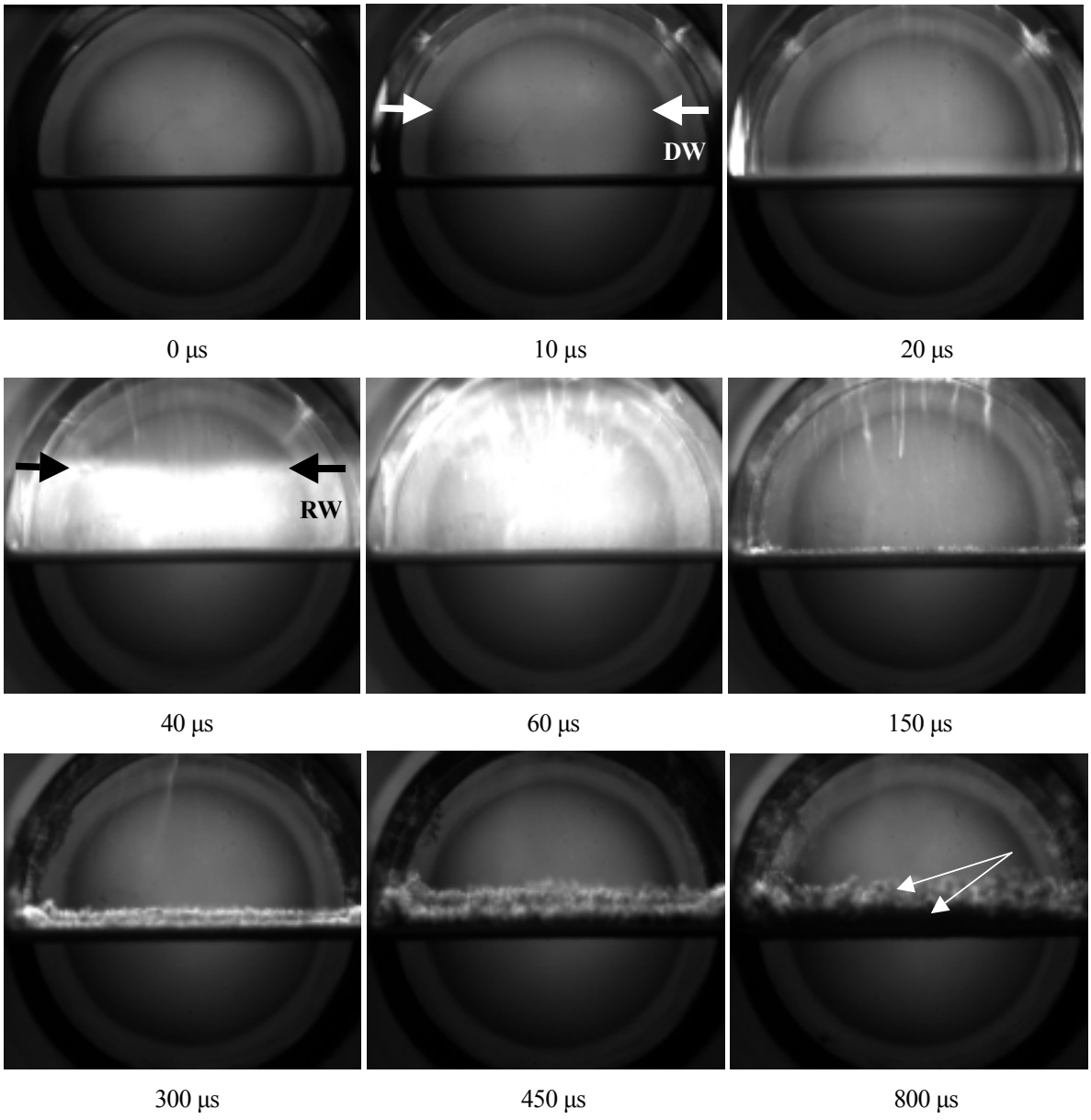

Fig. 5-2: The surface of cyclohexane without bubbles under detonation wave impact.

The framing rate was 100 000 fps. The exposure time for each photo was 10 μs. The arrows at 800 μs indicate the two parts of the formed structure on the surface. The detonation wave (DW) and the reflected wave (RW) in the gas phase are denoted with arrows. (Exp. No. 140)

5.1.3 Impact of a detonation wave on the surface of a bubbly liquid

Experiments in which bubbles were present near the surface before the impact of a detonation wave, were performed also. In these experiments the number of bubbles in the liquid as well as the time between the first bubble creation and the ignition in the gas phase were varied.

In Fig. 5-3 the results of an experiment similar to the one in Fig. 5-2, but in which the liquid cyclohexane contained oxygen bubbles, is presented. There were two more differences between the two experiments: In the experiment presented in Fig. 5-3, the framing rate of the camera was five times higher and the light sensitivity was changed, so that the detonation wave in the gas phase could be visible.

In this figure the light emission caused by the propagating detonation wave in the gas phase can be seen at 6 μs. The dark sports in the gas phase after the frame at 22 μs, appeared after the passage of the detonation wave and were located relatively close to the surface. They are interpreted to be the result of soot formation.

The detonation wave reached the surface at 22 μs. In the next two frames the generation of the reflected wave in the gas phase and the incident wave in the liquid phase were recorded. The shock wave in the liquid phase can be clearly seen on the frame at 34 μs. The passage of the reflected wave creates higher light emission in the gas phase than the detonation wave and at 70 μs the complete visible gas area appears to emit strong light. This light is significantly weaker at 160 μs and thereafter.

In Fig. 5-4 an experiment with the same system and gas flow for the generation of the bubbles, but with longer observation time, is presented. The light sensitivity of the optical method was also changed so that the observation of the liquid's surface was possible all the time, despite the strong light emission by the reflected shock wave.

The detonation wave reached the surface of the liquid at 20 μs. After its passage, spots of soot similar to the ones in Fig. 5-3 were seen. After the shock wave reflection a strong aerosol structure appears at the position of the bubbles on and near the surface (see Fig. 5-4, 150 μs – 800 μs). As expected, this structure becomes stronger as the gas flow for the generation of bubbles increases.

For illustration, in Fig. 5-5 an experiment in which the gas flow was about 65 times higher than in the experiments of Fig. 5-3 and Fig. 5-4 is presented. As a result of the higher flow not only the aerosol structure was more intense and reached higher levels above the surface, but also a liquid film was formed on the windows too. The liquid film is seen after the frame at 40 μs being removed by the pressure waves in that area. The maximum height of the aerosol structure varied from experiment to experiment, and can exceed 5 cm.

Although the three experiments presented in Fig. 5-3, Fig. 5-4 and Fig. 5-5, have shown similar phenomena to the experiment without bubbles (Fig. 5-2), the existence of the bubbles has resulted into some additional observed phenomena.

The presence of bubbles near and on the surface caused considerable instabilities. These instabilities become more intense as the flow of the rising bubbles increases. Before the shock wave impact, the bursting of the bubbles on the surface obviously enriched the gas phase with droplets of cyclohexane (see Fig. 5-1).

The existence of these liquid droplets explains the spatial distribution and the intensity of the soot formation after the detonation front, seen in Fig. 5-4, Fig. 5-5 and Fig. 5-3. It explains also the absence of soot in Fig. 5-2.

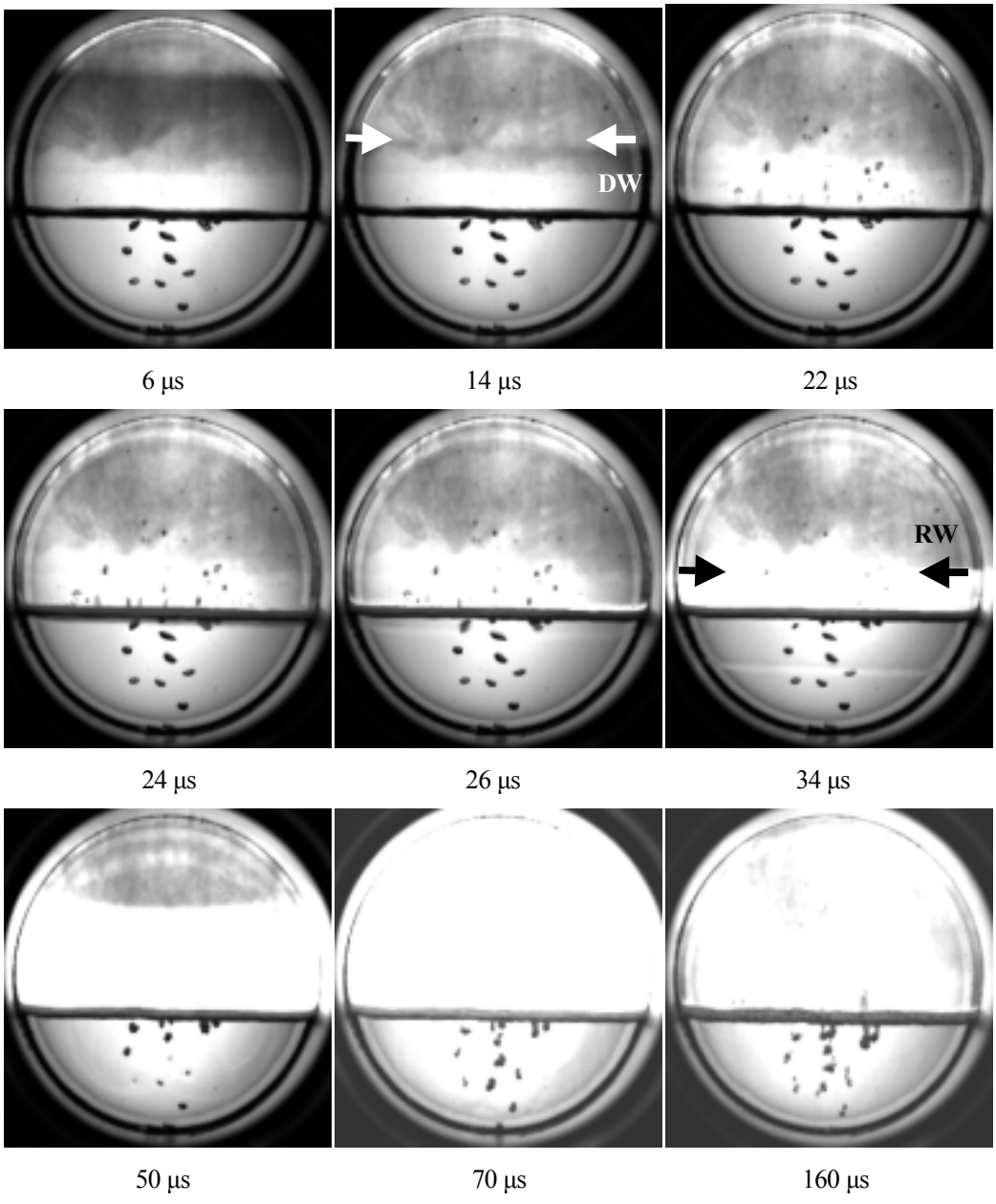

Fig. 5-3: The surface of cyclohexane containing oxygen bubbles under detonation wave impact.

Gas flow for the generation of the bubbles: 0.18 L / min for 50 s. The framing rate was 500 000 fps. The exposure time for each photo was 2 μs. The detonation wave (DW) and the reflected wave (RW) in the gas phase are denoted with arrows. (Exp. No. 89)

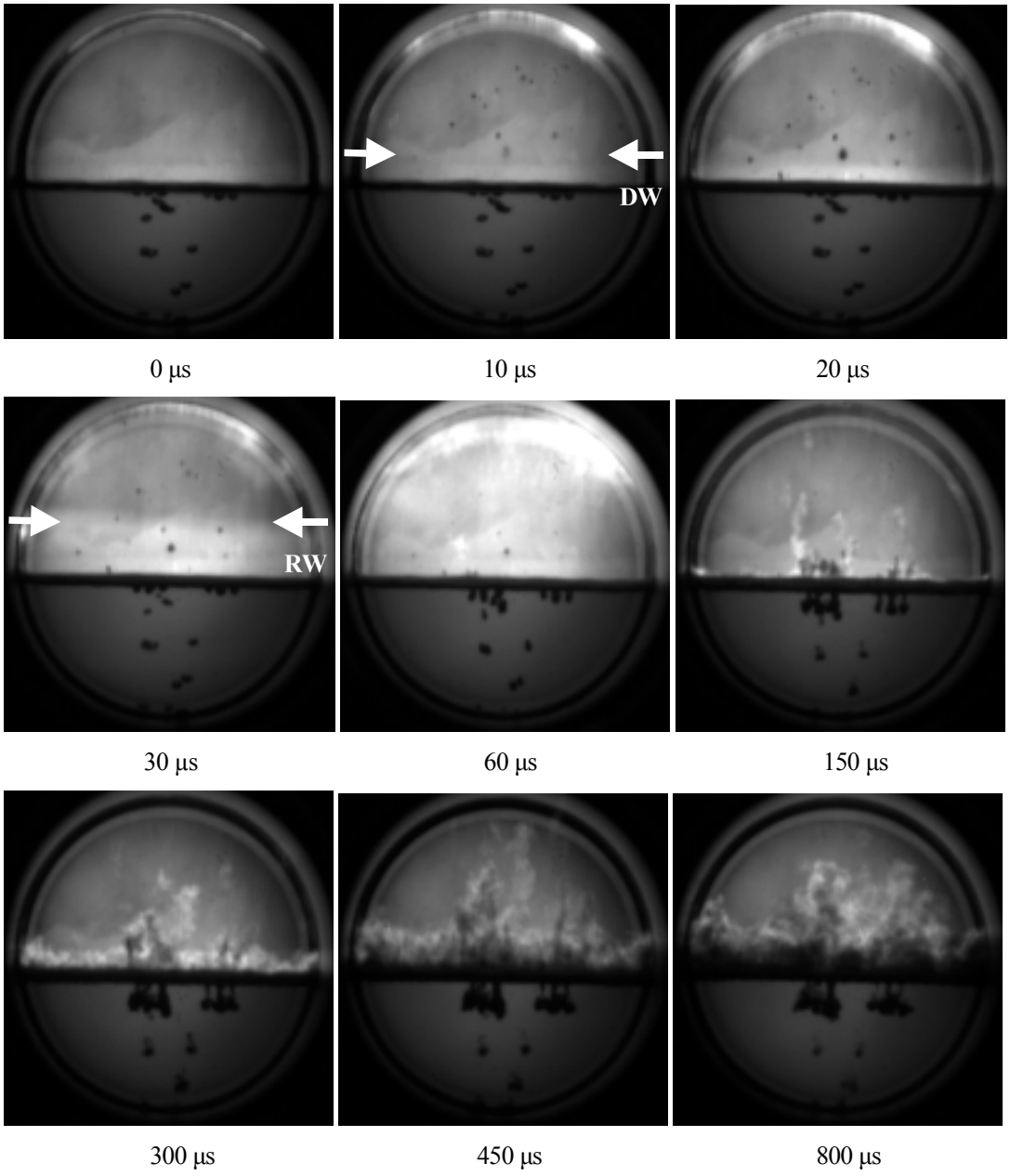

Fig. 5-4: The surface of cyclohexane containing oxygen bubbles under detonation wave impact.

Gas flow for the generation of the bubbles: 0.18 L / min for 10 s. The framing rate was 100 000 fps. The exposure time for each photo was 10 μs. The detonation wave (DW) and the reflected wave (RW) in the gas phase are denoted with arrows. (Exp. No. 88)

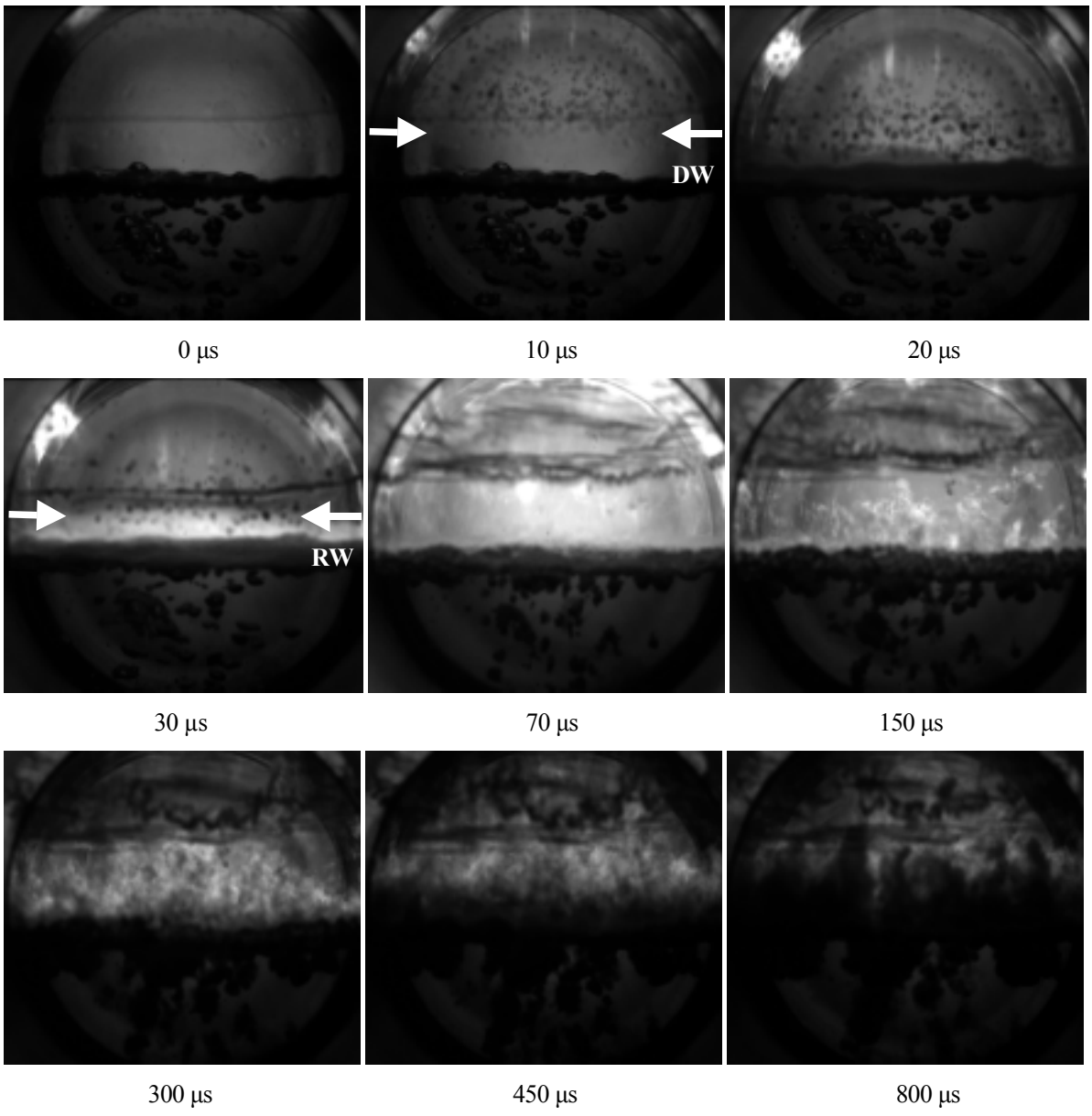

Fig. 5-5: The surface of cyclohexane with oxygen bubbles under detonation wave impact.

Gas flow for the generation of the bubbles: 12 L / min for 120 s. The framing rate was 100 000 fps. The exposure time for each photo was 10 µs. The detonation wave (DW) and the reflected wave (RW) in the gas phase are denoted with arrows. (Exp. No. 141)

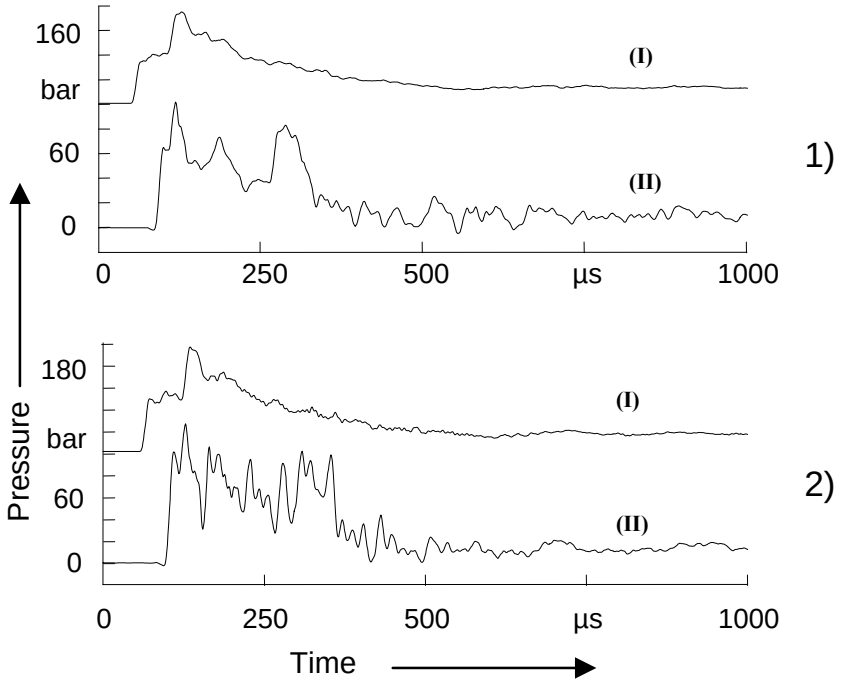

Fig. 5-6: Measured pressure signals near the surface.

The pressure signals 1) and 2) were recorded during the experiments presented in Fig. 5-2, and Fig. 5-5 respectively. The pressure curves (I) correspond to the gas phase and were measured 35 mm above the surface of the liquid. The pressure curves (II) correspond to the liquid phase and were measured 35 mm below its surface. For a better distinction a pressure of 100 bar is artificially added to all pressure signals in the gas phase.

5.1.4 Summary

In the 176 performed experiments the ignited gas phase above the liquid, had one of six different compositions. The mixture C_2H_2 / O_2, with a C_2H_2 molar fraction of 0.25, was used in most (92 %) of the experiments. The initial pressure of 1 bar was applied in 86 % of the experiments. The peak pressure measurements and the calculated detonation wave propagation velocities show that overdriven detonations were created in the gas phase.

From the investigations of the impact of a detonation wave on the surface of cyclohexane, the following conclusions can be drawn. The gas detonation and especially its reflection on the surface of the liquid, produces a strong, inhomogeneous and time dependent light emission that can be illuminated by the bubbles inside the liquid. Shock induced phenomena that involve the presence of bubbles near the liquid's surface influence these light emissions too. This is an information that must be considered during the evaluation of the experiments showing bubble explosions in this system.

The existence of bubbles near the liquid's surface added local sources for aerosol creation. When the number of the bursting bubbles was adequate, a liquid film on the walls around the surface was observed too.

5.2 Chemical composition inside the bubble before the shock wave impact

The amount of time that a bubble has at its disposal to rise inside the liquid before the impact of the incident shock wave occurs, is an important information for the estimation of the chemical composition inside that bubble. This time can be calculated if the rising velocity of the bubble is known.

For this reason, auxiliary experiments were performed to measure the rising velocity of bubbles 2.0 mm to 5.0 mm in equivalent diameter [87]. These investigations were performed in liquid H_2O with variable viscosity (solution with different amounts of Sedipur® was used for increasing the viscosity). This range of bubble diameters covers most of the bubble sizes that were created in the experiments, the diameter around 3 mm being the most common of them. The rising velocity of these bubbles depends, as is well known, on the bubble diameter and liquid's viscosity. It also depends on the current position of the bubble inside the liquid, reaching its maximum value at the middle of the distance to the surface ([88], [89]). In the auxiliary experiments this velocity was measured in the area around the middle of the distance between the bubble generator and the surface of the liquid. During these measurements, as well as the main experiments, the geometry and the scale of the vessel that was covered with liquid, did not allow wall effects to influence the bubble velocity [90]. The measured velocities were in the range of 17 cm/s to 30 cm/s. Thus, even at the maximum rising velocity measured, a bubble needs more than 500 ms to reach the middle level of the windows of the autoclave.

As is shown in Appendix A, the characteristic time of diffusion τ_D is a necessary information for the estimation of the composition inside the bubbles. In order to calculate this quantity for the case of an oxygen bubbles that initially did not contain any gaseous cyclohexane, the diffusion coefficient of gaseous cyclohexane in oxygen D is a necessary input. As system´s conditions 300 K temperature and 1 bar pressure will be assumed, i.e. the initial conditions of the system that was investigated in this study. The experimentally measured value of the diffusion coefficient of cyclohexane in oxygen is D = 0.0744 cm^2/s [91]. This value corresponds to a temperature of 288 K and a pressure of 1 bar. A correction of this value is necessary for the temperature of 300 K.

For a binary gas mixture, and for temperatures up to about 1000 K and pressures of maximum 70 bar the Chapman-Enskog equation provides good estimates of the influence of temperature and pressure on D [91]. From that equation it follows that:

$$D_{P_1,T_1} = \frac{P_0}{P_1} \cdot \left(\frac{T_1}{T_0} \right)^{3/2} \cdot D_{P_0,T_0} \qquad \text{(eq. 5-1)}$$

With the help of (eq. 5-1) and the above mentioned experimental value of D = 0.0744 cm^2/s, it is found that at a temperature of 300 K and at a pressure of 1 bar:
D = 0.0791 cm^2/s

For this D, pressure and temperature, and with the help of (eq. 7-4) in Appendix A, the characteristic time for the diffusion process τ_D can be calculated as function of the bubble's radius. In Table 5-2 the calculation for some typical bubble sizes is presented.

Table 5-2: Characteristic times of the diffusion process of cyclohexane inside an oxygen bubble, as function of bubble radius at 300 K and 1 bar.

r mm	τ_D ms	r mm	τ_D ms
0.25	1	2.00	51
0.50	3	2.50	80
0.75	7	3.00	115
1.00	13	3.50	157
1.50	29	4.00	205

After a time $3\tau_D$ the concentration of cyclohexane inside the bubble has reached 97 % of the saturation level, i.e. it can be considered practically saturated. For the bubbles created in the experiments this time is beween 29 ms (bubble 2 mm in diameter) and 471 ms (bubble 7 mm in diameter). This means that the time of at least 500 ms that each bubble needed to reach the center of the observation window was enough for the mixture to be practically saturated in cyclohexane vapor.

The surface tension influences the total pressure inside the bubble [92]. But this effect is negligible for the bubble sizes discussed in this work, so that the initial total pressure inside the bubble can be assumed to be equal to the initial pressure inside the surrounding liquid. The initial cyclohexane partial pressure inside the gas phase of the bubble is the vapor pressure at ambient temperature. The vapor pressure of cyclohexane at 25 ^{o}C is 0.13 bar [93]. Therefore at atmospheric pressure the molar fraction of cyclohexane in the bubble before the shock wave impact is 0.13. In this case the explosive mixture is nearly stoichiometric, if pure oxygen is used as oxidizer. Therefore the oxygen bubbles in these experiments contained an explosive mixture of cyclohexane / oxygen already before the shock wave impact.

At this point, it is interesting to estimate at which time the gaseous phase inside the bubbles entered the explosion range, due to this diffusion process. The lower explosion limit of cyclohexane in pure oxygen at 1 bar and at 298 K is 1.1 % [see Table 5-10]. This means that the bubble enters the explosion range from the point at which $C_{av} > 1.1$ %. For a saturation concentration of $C_{eql} = 13$ %, the bubble is explosive when $C_{av}/C_{eql} > 0.085$. According to Table 7-1 the bubble needs about 1 % of the characteristic time of diffusion (i.e., $0.01\tau_D$) to reach this concentration. Thus, according to the characteristic times shown in Table 5-2 the bubbles of the experiments, i.e. with 2.4

to 7.2 mm in diameter, must have needed between 130 μs (bubble 2 mm in diameter) and 1.57 ms (bubble 7 mm in diameter).

5.3 Bubble explosion type I

The shock wave that was generated in the liquid by the impact of the gas detonation on the surface, compressed and often ignited bubbles that contained oxygen. The experimental observations of this behavior will be described and discussed in this section. For a first general illustration of this phenomenon, an example is presented in Fig. 5-7. The frames of this figure show what happened to a line of bubbles created by pure oxygen, after the passage of a shock wave in liquid cyclohexane. The shock wave impacted the first two bubbles at 4 μs. On the frames at 28 μs – 78 μs the light emissions from sequential bubble explosions can be observed.

As will be shown later in this section, this kind of bubble explosion occurs during the first shock induced bubble oscillation after the shock wave impact. It will be called from this point *bubble explosion type I*, to distinguish it from explosions that occur at times much after the first bubble oscillation (i.e. bubble explosions type II) and which will be discussed in §5.4. The present section focuses on the bubble explosion type I.

5.3.1 The stages of the bubble explosion behavior

The basis of the bubble explosion during the first shock induced oscillation is the well known mechanism of transformation of pressure waves in inert bubble media: Energy from the incident shock wave is absorbed by the bubble. This energy is consumed for an increase in internal energy of the gas, namely, the temperature of the shrinking bubble and is then re-emitted by the bubble during its expansion phase. When attaining the ignition temperature the bubble explodes [44].

In Fig. 5-8, frames recorded during the experiment No. 94 showing oxygen bubbles in cyclohexane under shock wave impact are presented. At time 0 μs, the incident shock wave is seen in the middle of the observation window. After the shock wave impact a bubble compression phase follows. During this phase, jet penetration through the bubble can occur as can be seen for example in Fig. 5-8 at 17 μs and 18 μs (bubble No. 5). During the collapse of the pointed bubble, a jet started to form penetrating from its left side. The frame at 17 μs, shows this bubble at the time when the jet reached the other side of the bubble wall. Two edges on the bubble wall, one at the point of the jet penetration on the left and one of the jet impact on the right can be clearly recognized on that frame. A black thin line that connects these two edges is interpreted to be the continuous stream of the liquid jet that was flowing through the bubble's volume at that time. Ignition or explosion was recorded at 17 μs – 18 μs inside the bubbles No. 2, 3, 4 and 6 (see Fig. 5-8). Spherical shock waves emitted by bubble explosions are also seen on these two frames (see for example Fig. 5-8 at 18 μs). Such spherical shock waves are observed for the first time. The explosion results into an expansion phase of the bubble, as can be seen in this figure.

The following three general stages of the shock induced bubble explosion behavior were recognized by the examination of the experiments (see Fig. 5-8):

i) Shock induced bubble compression and jet penetration through the bubble;

ii) Maximum levels of bubble compression and eventual bubble ignition; and

iii) bubble expansion.

In the following paragraphs, experimental observations about each of the above three general stages of shock induced bubble behavior will be presented.

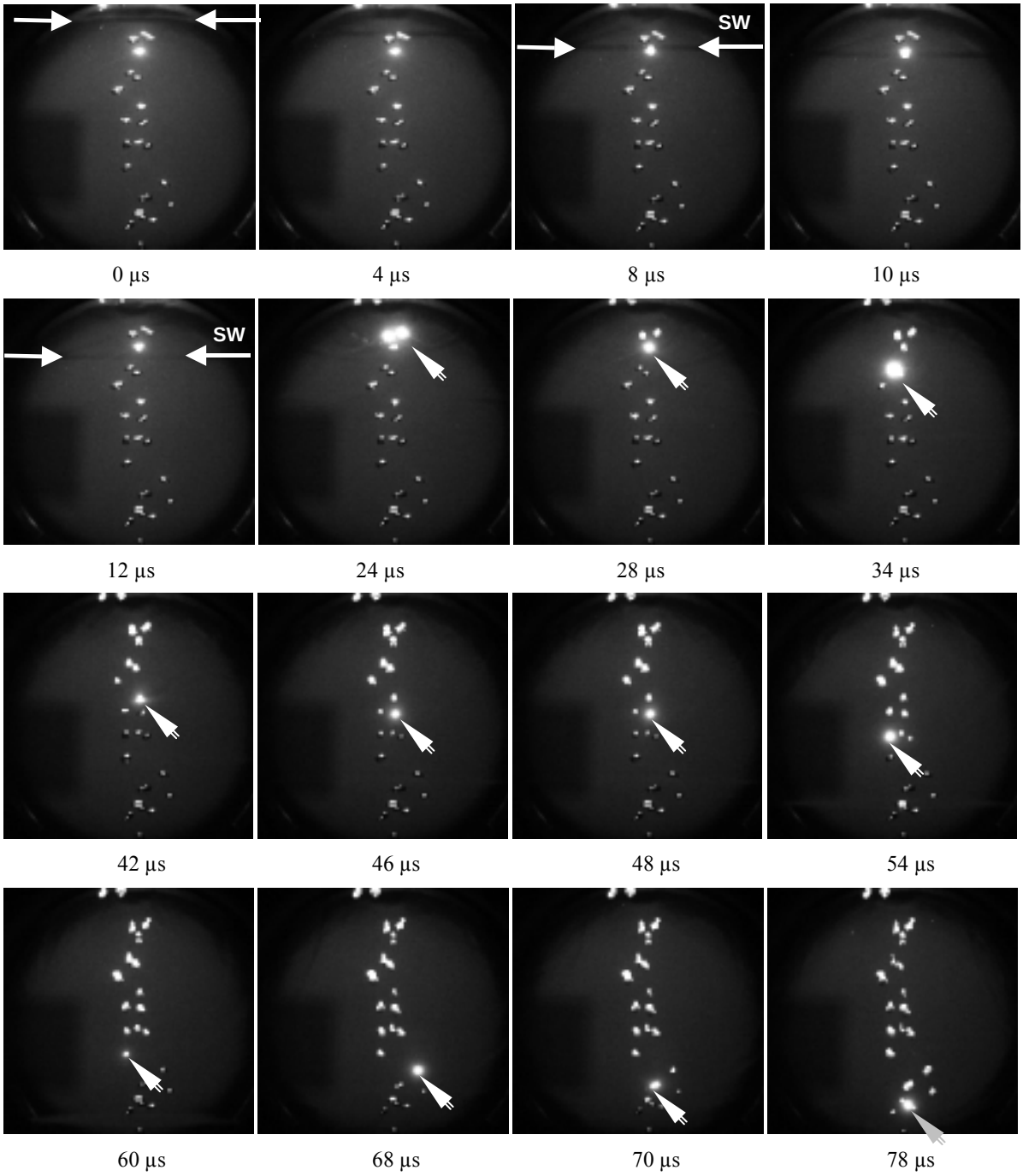

Fig. 5-7: Shock induced sequential bubble explosions.

Oxygen bubbles in cyclohexane under shock wave impact. The intense light emission from the third bubble from above at 0 µs – 24 µs is the only one not related to a bubble explosion. The two white arrows show the position of the incident shock wave (SW) inside the liquid. With the single arrow the exploding bubbles are shown. Diffuse light was used as external light source. Framing rate: 500 000 fps. (Exp. No. 59)

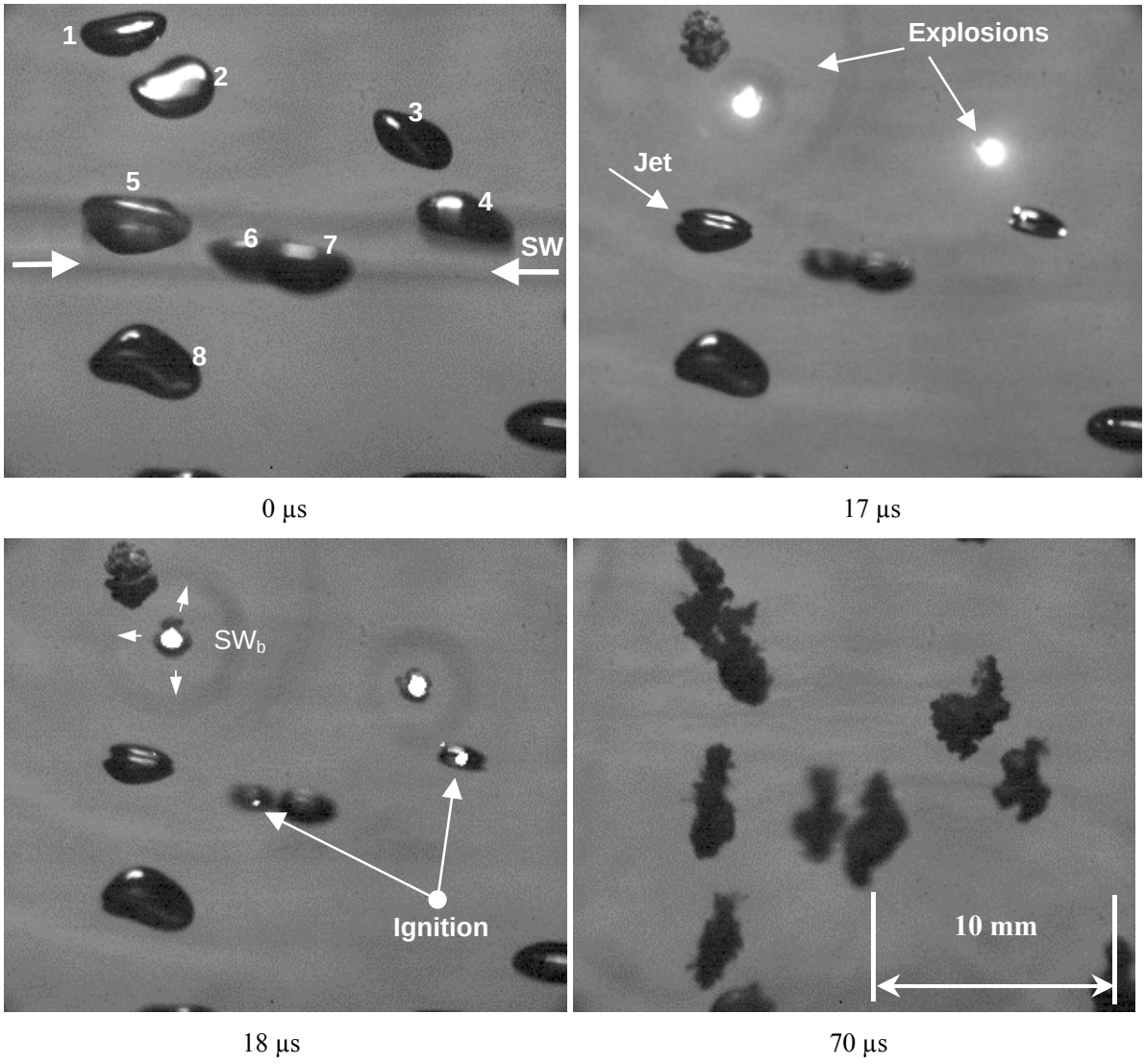

Fig. 5-8: The stages of a bubble explosion.

Oxygen bubbles in cyclohexane under shock wave impact. The arrows at 0 µs show the position of the incident shock wave (SW). Jet penetration, bubble ignition and explosion and shock wave emission can be recognized on the frames at 17 µs - 18 µs. (Exp. No. 94)

5.3.1.1 Shock induced bubble compression and jet penetration through the bubble

After a shock wave impact on a bubble, the latter starts to collapse. A number of experiments were performed to investigate this type of bubble collapse in more detail. In Fig. 5-9 the radius change of a bubble due to shock wave impact is shown. The figure corresponds to a bubble that can be seen in Fig. 5-15 (bubble No. 2), and according to the estimations performed in §5.2, it contained a nearly stoichiometric mixture of gaseous cyclohexane and oxygen. In this figure, time zero is the point when the shock wave exerts impact on the bubble wall. On the curve the following three phases of the bubble behavior between the shock wave impact and the bubble ignition can be distinguished.

At first, following the shock wave impact, the bubble does not start to shrink immediately. It can be seen from the curve (point 1 in Fig. 5-9), that between the time of the incident shock wave impact and the beginning of the compression phase there is a time delay of about 8 µs. Typically in the experiments it was observed that this initial phase during which practically no bubble compression takes place, had a duration in the order of 10 µs.

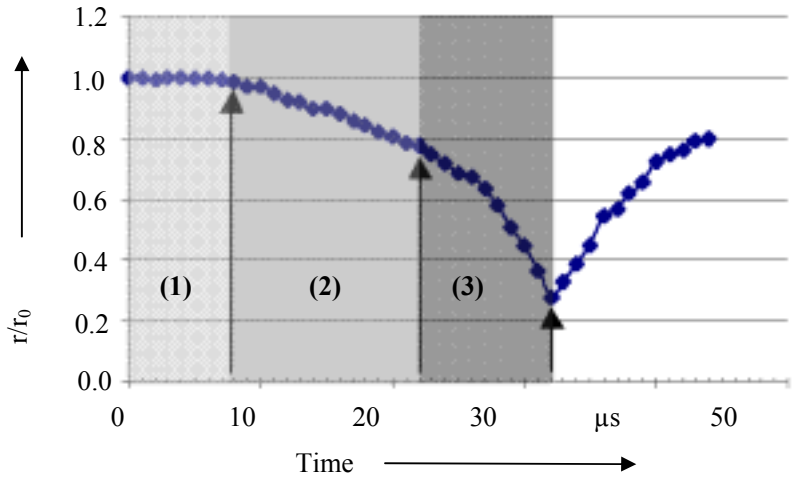

Fig. 5-9: The three stages of the bubble compression and the expansion.

Shock induced dynamics of a bubble 4.1 mm in equivalent initial diameter. Time zero corresponds to the moment of the shock wave exerts impact. The pressure in the liquid during the complete compression phase had a peak value of 61 bar and an average value of 46 bar. The figure corresponds to the bubble No. 2 in Fig. 5-15.

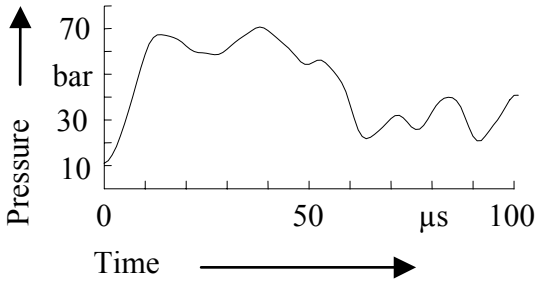

Fig. 5-10: Pressure in liquid cyclohexane after shock wave impact.

The first 100 µs of the incident shock wave of the experiment presented in Fig. 5-15.

After this delay time, the bubble shrinks noticeably. This is the second step of the bubble pro-ignition behavior. As already described and shown (in Fig. 5-8, at 17 μs), during this compression step a jet forms, which penetrates the bubble. The third step starts at the point of the jet penetration (point 2 in Fig. 5-9) and ends at the point of ignition (point 3 in Fig. 5-9). In this example, after the jet formation the bubble compression proceeds at higher rates, dr(t)/dt (r being the equivalent radius of the bubble and t being the time), than before (see Fig. 5-9). The same behavior was observed in all the experiments. These higher rates were usually between 50 m/s and 100 m/s.

The jet formation is interpreted to be the result of an inhomogeneous pressure field in the liquid near the bubble, as well as surface instabilities and the non symmetrical bubble form. It seems in the experiments of this work, that bubbles which are very near of other bubbles tend to form the jet earlier. In the experiments the jet was formed when the bubble radius r reached the range: $0.5 \leq r/r_0 \leq 0.9$, where r_0 is the initial equivalent bubble radius.

During the time between the jet penetration and the bubble ignition, mass and heat transfer phenomena are intensified, influencing the explosion behavior of the oxygen bubbles. This time was found to be between 2 μs and 18 μs and is generally longer when the jet is formed earlier. It should be noted that the same stages of bubble behavior described here were observed also in bubbles with all pure gases or gaseous mixtures that were used for bubble creation in the experiments.

5.3.1.2 Maximum levels of bubble compression and eventual bubble ignition

In order to observe the maximum possible levels of bubble compression, experiments with nitrogen bubbles were performed. Additionally oxygen-containing bubbles that occasionally did not explode, were used too.

In Fig. 5-11 an example of the behavior of nitrogen bubbles after a shock wave impact can be seen. At the time 8 μs, the incident shock wave is located at about the middle of the observation window. After the impact, the bubbles start to shrink, as described in previous experiments. At 26 μs the bubble No. 1 has reached a minimum diameter which is then followed by an expansion phase. The same happened to the other bubbles at different times. During the expansion phase bubble breakage was observed in some cases too. An example of this can be seen in Fig. 5-11 at 130 μs. The bubbles No. 2 and No. 4 broke into two parts. The breakage is interpreted as indication of a strong jet formation during the compression of the bubble. The jet inside the bubble No. 2 and No. 4 is pointed with an arrow at 32 μs and at 42 μs respectively. It is expected that such a strong jet can eventually divide the bubble into two parts already during the final stages of the compression phase.

Not only nitrogen bubbles but also oxygen-containing bubbles which did not explode, showed this behavior, i.e. following the compression phase the bubble was either broken up into two parts, or it remained unbroken. In both cases an expansion phase followed. Compared to its initial

value, r_0, the bubble radius during the compression phase, reached typically a minimum value that was between $0.2 \leq r/r_0 \leq 0.3$. In some cases higher values were occasionally observed too.

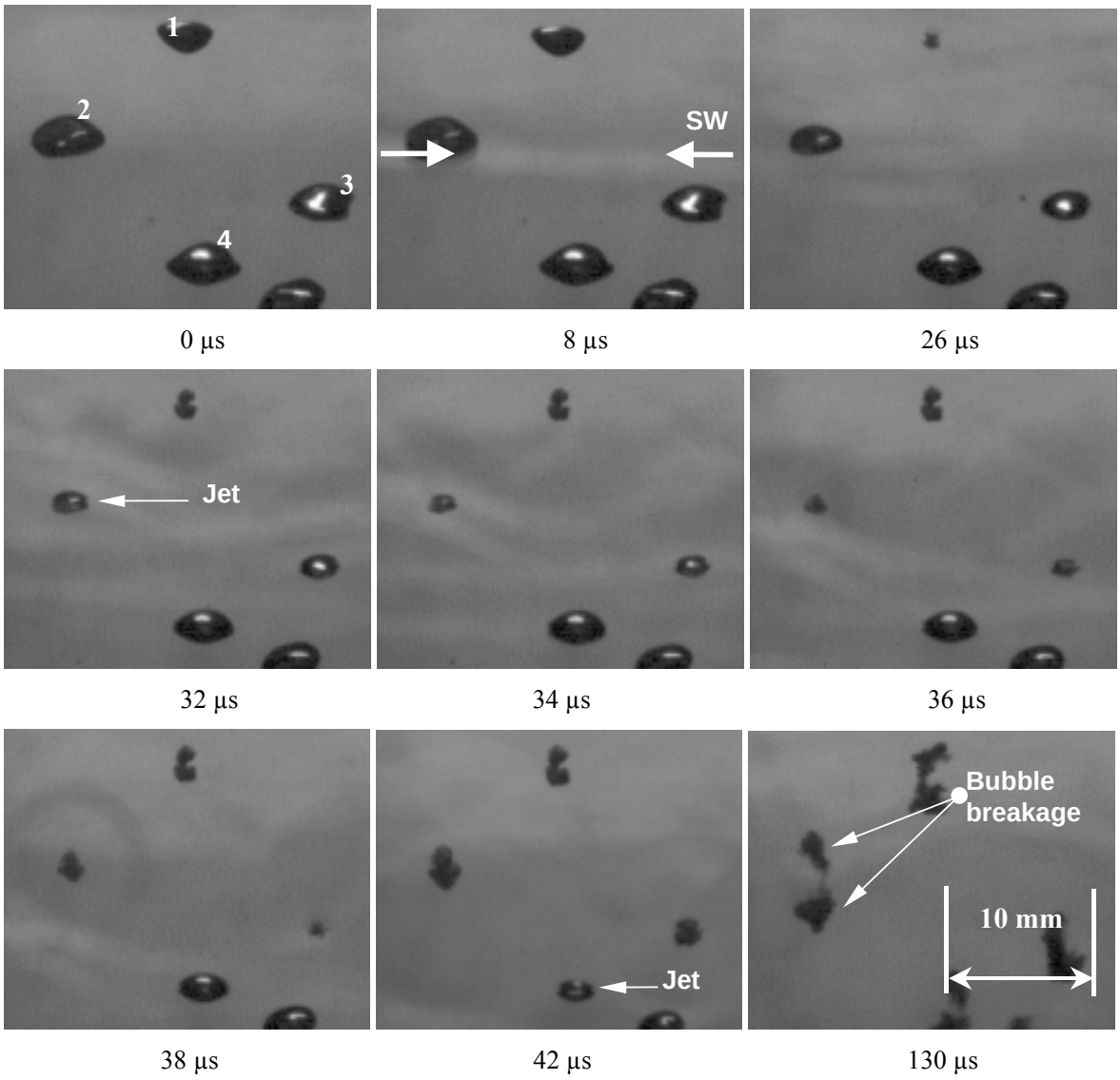

Fig. 5-11: Examples of bubble breakage due to shock induced jet penetration.

Nitrogen bubbles in cyclohexane under shock wave impact. (0 µs): Just before the entrance of the incident shock wave into the observation window; (8 µs): The incident shock wave is in the middle of the observation window; (26 µs): Maximum levels of compression for the bubble No. 1; (32 µs): Strong jet formation inside the bubble No. 2; (130 µs): The bubble No. 2 and No. 4 are broken into two parts. Framing rate: 500 000 fps. (Exp. No. 92)

A special attention was given to clearly record the ignition process inside the bubble by optical means. For this reason bubbles created by injection of pure oxygen in liquid cyclohexane were ignited by shock wave impact. During these experiments the ignition delay and the duration of the light emission of the bubble explosions were measured too.

A first example of bubble ignition during the compression phase has been already illustrated in Fig. 5-8. The detailed evaluation of the experiments showed that when ignition during the first shock induced oscillation was observed, the bubble was not previously broken up. The ignition of this type took place at a bubble compression level of $0.20 \leq r/r_0 \leq 0.56$. The measured ignition delays (time from the incident shock wave impact to bubble ignition), t_{ign}, were in the range of 15 μs to 60 μs. A relationship between the length of the ignition delay and the bubble radius was found. Between two bubbles with significant difference in size, the smaller one has the shorter ignition delay. On the other hand, the bigger the bubble is, the longer the compression phase lasts and the more asymmetric the compression process becomes. This is evident by optical recordings of experiments that due to space limitations are not presented in this work.

If the bubble ignition occurs at a bubble compression level that is close to the maximum possible one, then the duration of the ignition delay is close to the duration of the total compression phase, $t_{collapse}$, of a similar inert bubble under the same experimental conditions. For this reason, it is interesting to be able to calculate this time theoretically.

In Fig. 5-9 experimental measurements of the radius of an oxygen bubble 4.1 mm in initial diameter under shock wave impact in cyclohexane are presented. Time zero for the presented measurements is the time of shock wave impact on the bubble. It can be seen on the curve of that figure that the time between the shock wave impact and the ignition of the bubble, was 30 μs.

In §3.3 (eq. 3-9) was presented. This equation can be used for a rough estimation of the duration of the bubble compression after a shock wave impact. The corresponding calculated value according to (eq. 3-9) is: $t_{collapse}$ = 23.6 μs. This calculation assumes a 4.1 mm diameter bubble, cyclohexane as liquid, 1 bar initial pressure and 50 bar shock wave pressure. It is obvious that a deviation between the experimental and the calculated value exist.

The deviation between the experimentally measured values and those calculated is caused by the difference between the assumptions of the calculation and the experimental conditions. In reality the liquid is both compressible and viscous and within the bubbles there is a mixture of vapor and gas. The bubbles are not collapsing necessarily symmetrically and the pressure change which causes the collapse takes place not abruptly but at some finite speed. These assumptions can only decrease the rate of collapse of the bubble. This explains why the calculated value was smaller than the experimentally measured one. Therefore, taking into account the above comments it is expected that the calculated values should correlate reasonably well with the bubble ignition delays.

In Fig. 5-12 a further example of ignition inside an oxygen bubble in liquid cyclohexane is presented. The bubble had 7.2 mm in initial diameter. After the shock wave impact at 0 μs, the bubble started to shrink according to the pattern described in previous section. A local light emission is clearly recorded inside the bubble 50 μs later. This local light in the bubble is interpreted to be the ignition of the bubble's gas phase. During the following two microseconds the light emitting area covered the complete volume of the bubble. When the bubble wall were reached, a spherical shock

wave was emitted into the liquid (see at 53 µs). At this point the bubble expansion phase started and the light emission gradually disappeared (see at 53 µs - 55 µs).

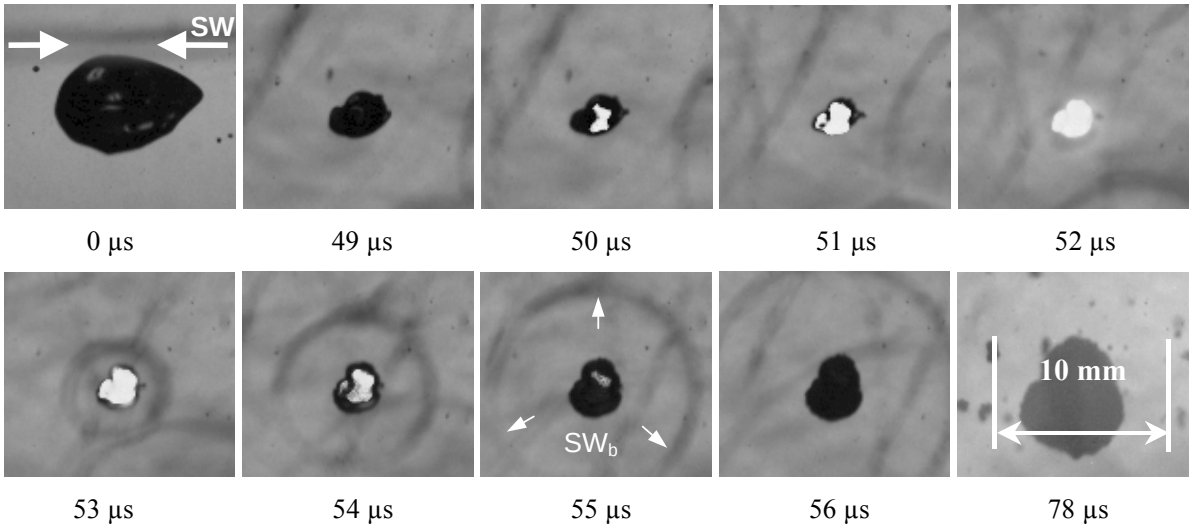

Fig. 5-12: Light emission during a bubble explosion after shock wave impact.

Oxygen bubble in cyclohexane. Initial equivalent bubble diameter d_0 = 7.2 mm. The incident shock wave exerts impact on the walls of the bubble at t = 0 µs. The framing rate of the camera was 1 000 000 fps. (Exp. No. 130)

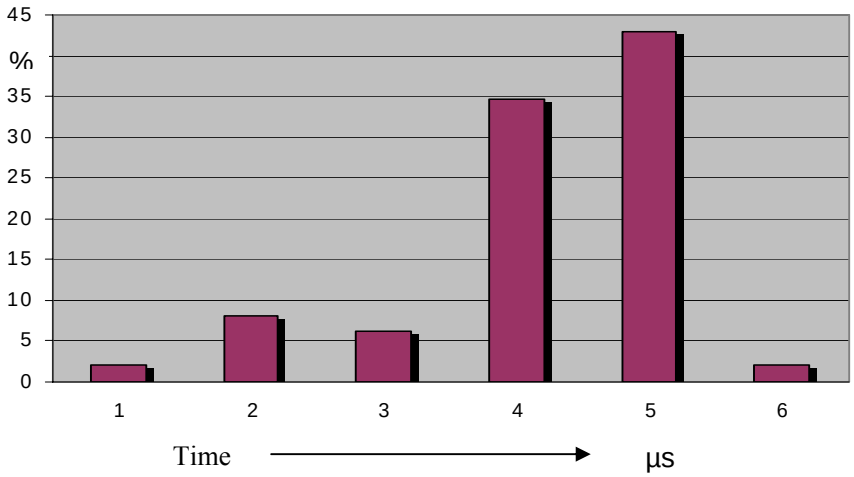

Fig. 5-13: Distribution of the light emission durations during bubble explosion.

Oxygen bubbles in cyclohexane. The figure represents the measurements from 49 single bubbles. (Exp. No. 91, 93-97, 129-130 and 135-136)

It follows from the examination of the experiments, that the behavior described just above is typical. Directly after the bubble ignition, light emission from the complete bubble volume and a strong spherical shock wave emission follows and results into the bubble expansion phase. The duration of

this light emission was between 1 μs and 6 μs, and typically about 4 μs – 5 μs (see Fig. 5-13). In a few cases the bubble continued to shrink for 1 μs - 2 μs after its ignition, until the explosion front in the bubble reached the walls, (as seen e.g. in Fig. 5-12, frames at 50 μs – 52 μs).

5.3.1.3 Bubble expansion phase

The behavior of the bubbles during the first shock induced compression phase, is discussed in the previous sections. The goal of this section is mainly to investigate if there is a difference in the behavior after the compression phase between those bubbles that exploded and those that did not.

Two frames recorded in the same experiment, showing oxygen containing bubbles in liquid cyclohexane, are presented in Fig. 5-14. The first frame (on the left) corresponds to a time prior to the shock wave impact and the second frame (on the right) corresponds to 180 μs after the shock wave propagation in front of the observation window. The white circles in the frames serve two purposes. They indicate the bubbles that exploded and they serve as reference points to observe the spatial displacement of the bubbles after the shock wave impact. Apart from the spatial displacement of many bubbles, which is obvious in Fig. 5-14, some bubble collisions (e.g. see the bubbles marked by the two arrows) and bubble breakage (e.g. bubble No. 1, in Fig. 5-14) were also observed.

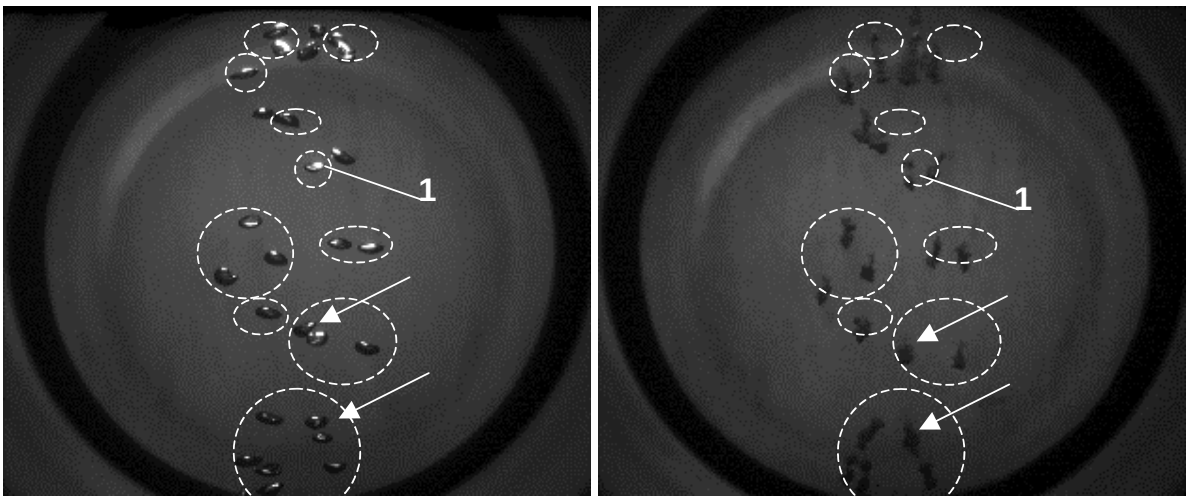

BEFORE SHOCK WAVE IMPACT AFTER SHOCK WAVE IMPACT

Fig. 5-14: Observed behaviors after the end of the bubble expansion phase.

Oxygen bubbles before and 180 μs after the incident shock wave impact. The circles indicate the bubbles that exploded. The liquid was pure cyclohexane. (Exp. No. 123)

The experiments show that bubbles which are very near to each other do not collide during the compression phase, such collision can though occur during the expansion phase that follows.

According to the performed experiments the only observed difference in the behavior between bubbles that exploded and bubbles that did not explode was as follows. When an oxygen-containing bubble did not explode during the compression phase directly after a strong shock wave impact, then it was often broken into two parts at the beginning of or during the subsequent expansion phase. This kind of breakage is interpreted to be the result of strong jet penetration through the bubble. Bubbles were occasionally broken up after their explosion too. But this breakage took place at later oscillations. This type of bubble breakage is interpreted to be caused by surface instabilities on the bubble wall and an non homogeneous pressure field around it.

5.3.2 Estimation of the conditions inside the bubble at the moment of ignition

In this section the composition of the gas mixture, the pressure and the temperature inside the bubble at the moment of ignition will be estimated. The estimations will be performed by theoretical calculations for which the experiments of this work will offer input data. For the calculations the bubbles created by injection of pure oxygen into the liquid cyclohexane are considered only. As already shown in §5.2, these bubbles contained a saturated gaseous mixture in cyclohexane already before the shock wave impact.

5.3.2.1 Composition of the gas mixture inside the bubble

As has been described in previous sections, after shock wave impact a bubble undertakes a process of compression prior to its ignition. On the other hand, the temperature increase inside the bubble results into a temperature increase of the bubble's surface also. Because of this and since relatively high temperatures can be achieved in the bubble, it seems at a first glance plausible, that the composition of the gaseous mixture inside the bubble could be significantly altered prior to its ignition.

The important question rises at this point, if, by diffusion from the surface of the shrinking bubble before the ignition, a considerable enrichment in gaseous cyclohexane can take place; or even if this process can go as far as to result into a new equilibrium of cyclohexane vapor inside the bubble that corresponds to the new temperature. This consideration is based on the assumption that the vaporization process is significantly faster than diffusion, and that eventual convection processes can be neglected (see §3.2).

In order to answer this question a rough estimation of the time needed for such an enrichment in vapor of cyclohexane inside the bubble is necessary. As explained in Appendix A, the process of molecular diffusion inside a spherical bubble has a characteristic time τ_D, which depends on the bubble size and the diffusion coefficient only. To estimate the value of τ_D the bubble size and the diffusion coefficient are necessary input data. The diffusion coefficient is the one of gaseous cyclohexane. For the bubble size the experimental values have to be taken into account.

During the experiments, bubbles with 2.4 to 7.2 mm in initial diameter were ignited. These bubbles were ignited at a compression level in the range of $0.20 < r_{ign}/r_0 < 0.56$. The characteristic time for diffusion τ_D inside the bubble at the moment of its ignition depends not only on

the size of the bubble, but because of the diffusion coefficient, also on the conditions inside it. The calculation, presented in Table 5-3, shows that τ_D remains in the range of tens of milliseconds at all the stages of bubble compression before the ignition. The calculation was performed for a spherical bubble of initial diameter 2 r_0 that is compressed and ignited when attained the radius r_{ign}. As initial temperature and pressure inside the bubble 300 K and 1 bar were assumed respectively. The composition of the gaseous mixture in the bubble was: C_6H_{12} / O_2 with an O_2 molar fraction of 0.87.

Even the minimum of the above mentioned characteristic times, i.e. 26.9 ms, is three orders of magnitude longer than the total compression time (15 μs - 60 μs). Thus, in the compressed bubble a new equilibrium corresponding to the new temperature cannot be reached by diffusion through the bubble wall.

In fact, as can be seen in Table 5-3, the molar fraction of cyclohexane inside the gaseous phase of the bubble, after this kind of enrichment, can not exceed the value of 18.3 % (initial concentration inside the bubble: 13 %). As this table shows, this level of cyclohexane enrichment would have been attainable only if a bubble of initially 2.4 mm in diameter would have been adiabatically compressed up to a diameter of about 1.3 mm; then the bubble should have remained at the levels of the minimum diameter for a time equal to the maximum observed ignition delay in the experiments; at the same time keeping its high temperature and pressure. In this respect the above calculated addition of 5.3 % in molar fraction of cyclohexane is a considerable overestimation.

It should be noted at this point, that the real amount of this type of enrichment is influenced also by effects that are not taken into account up to this point. These effects describe non ideal behaviors, which demonstrate themselves especially at high pressures. The most important of these effects seem to be the pressure dependence of the vapor pressure. This dependence is known (e.g. see [94], [95]) and can be calculated by the equation:

$$P_{v(P,T)} = P_{v(P_0,T)} \cdot e^{\frac{M \cdot (P - P_0)}{\rho_l \cdot R \cdot T}}, \qquad \text{(eq. 5-2)}$$

where M and ρ_l is the molecular weight and the density of the liquid respectively, P_v is the vapor pressure, P_0 the pressure at which the vapor pressure is known, T is the temperature and R the universal ideal gas constant. All units are in SI.

The above calculation of the pressure dependence of P_v is also called *Poynting correction* and its accuracy strongly depends on the foreign gas that mixes with the vapor [96]. In the case of the bubbles in discussion that gas would be oxygen.

From (eq. 5-2) it is calculated that the corrected vapor pressure of cyclohexane should be 321 bar at T = 785 K, P = 327 bar, with $P_{v(P_0,T)}$ = 216 bar; and 9.7 bar at T = 451 K, P = 8.6 bar, with $P_{v(P_0,T)}$ = 9.45 bar (see Table 5-3). These higher values of vapor pressures do not influence the conclusions of the above discussion. The maximum (and overestimated, as stated above) cyclohexane

addition into the bubble would reach now 5.5 % (i.e., 18.5 % total cyclohexane concentration, see Table 5-4) instead of 5.3 % previously calculated.

Two other effects that can influence the vapor pressure in the bubble are: (i) the fact that the pressured gas inside the bubble might dissolve into the liquid layer around the bubble and change its properties; and (ii) that gas-phase molecules might attract molecules out of the liquid by the process of *gas solvation*, the attachment of molecules to gas-phase species [95].

Apart from the effects that are related to the vapor pressure, other phenomena might create a deviation of the total pressure inside the bubble from the adiabatic value (P_{ad}), e.g. due to interaction between the molecules inside the gaseous mixture. The influence of all these effects is assumed to be negligibly small for the processes calculated here, and therefore it is ignored.

Thus, the conclusion of this section is that during the bubble compression, the composition of the gas mixture in the bubble (before the shock wave impact) can be assumed to remain the same. This means that this mixture was the one which exploded at the ignition point. This consideration ignores the influence of the jet penetration and the consequent evaporation of the generated droplets inside the bubble.

Table 5-3: Characteristic time for diffusion τ_D at the moment of bubble ignition and amount of enrichment in vapor of cyclohexane. The most extreme cases.

The calculation of the pressure P_{ad}, and of the temperature T_{ad}, in case of an adiabatic compression is presented in §5.3.2.2. The calculation of D at temperature T_{ad} and pressure P_{ad} was performed by (eq. 5-1). The calculation of τ_D and C_{av}/C_{eq} was performed by the corresponding eqations in Appendix A.

Initial bubble diameter $2\,r_0$ Mm	r_{ign}/r_0	T_{ad} K	P_{ad} bar	**D** cm2/s	τ_D (at r_{ign}) ms	t_{ign}/τ_D (t_{ign}= 60 μs)	C_{av}/C_{eq} %	P_{vapor} bar	**C_6H_{12}(g) in the bubble** %
2.4	0.56	452	8.6	0.01701	26.9	0.0022	0.055	9.45	18.3
7.2	0.56	452	8.6	0.01701	242.1	0.0002	0.037	9.45	16.6
2.4	0.20	785	327	0.00102	57.0	0.0010	0.045	216	15.4
7.2	0.20	785	327	0.00102	513.0	0.0001	0.036	216	14.9

Table 5-4: Amount of enrichment in vapor of cyclohexane taken into consideration the pressure dependence of the vapor pressure. The most extreme cases.

This table shows the results of the same calculation presented in Table 5-3, but with the difference that the values of the vapor pressure have been corrected according to (eq. 5-2) (Poynting-correction).

Initial bubble diameter $2\,r_0$ mm	r_{ign}/r_0	T_{ad} K	P_{ad} bar	**D** cm2/s	τ_D (at r_{ign}) Ms	t_{ign}/τ_D (t_{ign}= 60 μs)	C_{av}/C_{eq} %	P_{vapor} bar	**C_6H_{12}(g) in the bubble** %
2.4	0.56	452	8.6	0.01701	26.9	0.0022	0.055	9.7	18.5
7.2	0.56	452	8.6	0.01701	242.1	0.0002	0.037	9.7	16.7
2.4	0.20	785	327	0.00102	57.0	0.0010	0.045	371	17.5
7.2	0.20	785	327	0.00102	513.0	0.0001	0.036	371	16.6

5.3.2.2 Temperature and pressure inside the bubble

The next point of interest is to calculate the temperature and the pressure at which the gaseous mixture inside the bubble, which is assumed to have the composition estimated in §5.3.2.1, was ignited in the experiments. The upper limit of the gas temperature and pressure that can be reached inside the bubble during the compression and before the explosion, is the one calculated under the assumption of adiabatic compression.

An obvious question is if the assumption of adiabatic compression can adequately describe this process. In §3.2 the possible sources of heat losses from a hot bubble were briefly discussed. From this discussion heat conduction and radiation appear to be the two most relevant mechanism of heat losses for this consideration. The answer of the above question will be given by the three calculations that follow. First is the calculation of the pressure and the temperature inside the bubble under the assumption of adiabatic compression. Secondly the decrease of the temperature inside the bubble due to heat conduction will be calculated. And thirdly the additional influence of radiation will be estimated.

Calculation of the adiabatic temperature and pressure at the ignition point

For the calculation of the pressure and temperature inside the bubble under the assumption of adiabatic compression, the adiabatic index of the gas mixture, γ_{mixture} is an essential parameter. In §5.3.2.1 it was shown that the composition of the gaseous mixture inside the bubbles, during the time between the shock wave impact and the bubble ignition, was: C_6H_{12} / O_2 with an O_2 molar fraction of about 0.87. This information was shown to be valid for bubbles created by injection of pure oxygen into liquid cyclohexane and with the assumption that shock induced jet penetration does not occur.

As the bubble compression develops and the temperature increases, the adiabatic index is not constant. This effect was taken into account in the calculation shown Table 5-5. In this table the calculated temperature T_{ad} and pressure P_{ad} are presented for the case of an adiabatic bubble compression as a function of r/r_0. The calculation was performed with the help of (eq. 3-6) and (eq. 3-7) with n = 180, and $\alpha = 0.1$, i.e. from a bubble compression from $r/r_0 = 1$ to $r/r_0 = 0.1$ with 180 intermediate steps was calculated. The adiabatic index of the mixture $\gamma_{i,\,mixture}$ was calculated by the equation (eq. 7-21) with the help of the equations (eq. 7-16) – (eq. 7-18), presented in Appendix B for the above mentioned mixture of C_6H_{12} / O_2. The calculated values of the adiabatic index are presented in Table 5-5 and are valid for the corresponding calculated conditions inside the bubble.

Table 5-5: Calculated temperature T_{ad} and pressure P_{ad} in case of adiabatic bubble compression when the bubble contains the mixture C_6H_{12} / O_2 with an O_2 molar fraction of 0.87.

The shadowed cells denote the range of r/r_0 inside which bubble explosion was observed.

r/r_0	T_{ad} K	P_{ad} bar	$\gamma_{mixture}$	r/r_0	T_{ad} K	P_{ad} bar	$\gamma_{mixture}$
1.00	300.0	1.0	1.269	0.55	457.0	9.2	1.206
0.95	312.5	1.2	1.266	0.50	484.2	12.9	1.199
0.90	325.9	1.5	1.255	0.45	515.1	18.8	1.192
0.85	340.3	1.8	1.248	0.40	550.6	28.7	1.185
0.80	355.8	2.3	1.241	0.35	592.1	46.0	1.178
0.75	372.6	2.9	1.234	0.30	641.9	79.2	1.171
0.70	390.8	3.8	1.227	0.25	703.8	150.1	1.165
0.65	410.7	5.0	1.220	0.20	784.7	327.9	1.160
0.60	432.7	6.7	1.213	0.15	900.4	889.3	1.159
0.56	451.9	8.6	1.207	0.10	1100.2	3667.3	1.178

According to the experiments, the bubble ignition was observed at bubble compression levels in the range of $0.20 \leq r_{ign}/r_0 \leq 0.56$ (see §5.3.1.2). In case of adiabatic compression, and according to Table 5-5, this corresponds to a pressure and temperature in the range of (451.9 K and 8.6 bar) to (784.7 K and 327.9 bar). From the same table it is also obvious that an assumption of a constant adiabatic index $\gamma_{mixture}$ for the calculation of the temperature and the pressure inside the bubble for an adiabatic compression, would lead to significant errors. Assuming a constant value of for example 1.269 for $\gamma_{mixture}$ (which is valid for T = 300 K), one would calculate that at $r_{ign}/r_0 = 0.20$ the conditions inside the bubble would be 1100 K and 458 bar. These values are significantly higher than the above corresponding calculated values of 784.7 K and 327.9 bar.

The lower limits of the calculated pressure and temperature range inside which bubbles exploded (451.9 K and 8.6 bar) may have been decreased due to the phenomenon of 'premature' bubble ignition induced by a shock waves impact from other nearby bubble explosions. This phenomenon is observed experimentally and is reported in §5.3.3.1.

Apart from this, it is interesting that the two calculated temperatures at the moment of bubble ignition (452 K and 785 K) deviate in both directions from the known ignition temperature of cyclohexane in air, T_{ign} = 543 K [97]. It should be noted nevertheless, that this ignition temperature is measured by the standard method described in [98] and does not correspond exactly to the temperature inside the bubble at the point of its ignition. Some reasons that support this, are as follows. First of all, the ignition temperature is measured inside air, and not in other gaseous mixtures (e.g. pure oxygen). Apart from that the influence of the pressure on the ignition temperature has to be considered also. In the standard method a constant pressure of 1 bar is required, while the gas inside a shrinking bubble reaches much higher levels. Further, the standard method does not allow the determination of the exact composition of the gaseous mixture that ignites. In the bubbles the mixture is variable, but in principle definable. Finally a factor that could be important is the time scale of the two procedures. In the bubbles everything takes place in microseconds, while in the standard T_{ign} measurements the procedure takes time in the order of seconds or even minutes.

In order to define in which cases is the assumption of adiabatic compression reasonable for the calculation of the pressure and the temperature inside the bubble, an estimation of the deviation due to heat losses by conduction from a hot bubble, is necessary. This estimation is attempted in the section that follows.

Temperature decrease inside the bubble due to heat conduction

For the calculation of the temperature deviation from the adiabatic value, due to heat conduction, the following scenario will be used. A spherical bubble of initial diameter $2r_0$ = 2.4 or 7.2 mm is compressed until is ignited at r_{ign}/r_0 = 0.20 or 0.56. The initial temperature and pressure inside the bubble is 300 K and 1 bar respectively. The temperature of the surrounding liquid is T_l = 300 K and constant. At the moment of the ignition the bubble is assumed to have the corresponding temperature T_{ad} and pressure P_{ad} shown in Table 5-5. The composition of the gaseous mixture in the bubble is C_6H_{12} / O_2 with an O_2 molar fraction of 0.87. Time duration of the heat losses from the bubble: t_{ign} = 60 μs. This is the longest experimentally measured value of t_{ign} in this system.

With the help of the equations: (eq. 7-10), (eq. 7-12) – (eq. 7-20) presented in Appendix B, τ_C is calculated. The average temperature inside the bubble T_{av} is then calculated by (eq. 7-9). The results of the calculations are shown in Table 5-6. As it is shown in this table the maximum calculated deviation from the adiabatic value of the temperature inside the bubble is only 3.1 %.

The calculated deviation of the temperature depends on several parameters. Below the influence of some important parameters that can be varied during the experiments, is discussed.

(i) Addition of nitrogen into the gaseous mixture of the bubble

In case nitrogen is added into the mixtures of cyclohexane and oxygen, the calculation of the thermal conductivity, the heat capacity and the density of the mixture can be performed with the assumption that both the oxygen and the nitrogen molecules of the mixture behave as pure oxygen. This assumption is realistic because the thermal conductivity, the heat capacity and the density of nitrogen are very close to those of oxygen. Therefore, an addition of nitrogen would not influence the characteristic time of conduction τ_C. Thus, for both types of mixtures: a_1 C_6H_{12} – a_2 O_2 and a_1 ' C_6H_{12} – a_2 ' O_2 – a_3 N_2, the deviation from the adiabatic value of the temperature inside the bubble would be the same.

(ii) Influence of cyclohexane enrichment

Addition of cyclohexane in the gaseous mixture increases the density and the heat capacity of the mixture. On the other hand it decreases the thermal conductivity of the mixture, because pure cyclohexane has a lower thermal conductivity than oxygen. As a result the thermal diffusivity decreases and the characteristic time τ_C reaches higher values (see Table 5-7). In addition it should be noted that an addition of cyclohexane would decrease the value of the adiabatic index, so that for the same bubble compression levels the adiabatic temperature would reach significantly lower levels. This would further increase τ_C and reduce the deviation of the temperature from the adiabatic value.

(iii) Influence of the pressure inside the bubble

An increase in the pressure increases the density of the mixture inside the bubble (see (eq. 7-20)). The heat capacity of the mixture is not sensitive to a change of the pressure, since the c_p of ideal gases is independent of the pressure [99]. Therefore the increase of the density has as a result the decrease of the thermal diffusivity (see (eq. 7-12)) and thus an increased characteristic time of conduction τ_C that can be calculated by:

$$\tau_{C P_1} = \tau_{C P_0} \frac{P_1}{P_0}. \qquad \text{(eq. 5-3)}$$

In short, an increase of the pressure inside the bubble (e.g. by increasing the initial pressure P_0 before the initiation of the bubble compression) reduces the deviation from the adiabatic value of the temperature.

(iv) Influence of the temperature inside the bubble at constant composition

An increase in temperature can take place, e.g. by increasing the initial temperature of the bubble T_0, before the initiation of the compression process. In this case the heat capacity of the pure substances in the mixture would increase, and particularly the one of the cyclohexane (due to the higher number of atoms in it). Thus the heat capacity of the mixture increases too. The dependence on the temperature of

the heat capacities is described by (eq. 7-17) and (eq. 7-18). On the other hand, the thermal conductivity increases faster with the temperature as can be seen by (eq. 7-14) and (eq. 7-15). So, an increase in temperature increases the thermal diffusivity and finally decreases the characteristic time of conduction τ_C (see Table 5-7). As a result an increase in temperature inside the bubble leads to higher deviations from the adiabatic value.

(v) Influence of the bubble size

An increase in bubble size would according to (eq. 7-10) directly increases the characteristic time of conduction τ_C and therefore decreases the temperature deviation (e.g. see Table 5-6).

(vi) Influence of the bubble's shape

The heat losses due to conduction are taking place across the bubble wall, because the hot gas in the bubble is surrounded by a cold liquid. The rate of these losses depends on the area of the bubble's surface. A deformed bubble has a larger surface than a total spherical one with the same volume. The same conclusion is valid also between a bubble with an unstable, wobbling surface and one with a firmly stable surface. It follows that deformation and instabilities of the bubble's surface intensify the heat losses by conduction, thereby increasing the deviation from the adiabatic condition.

In the experiments many factors can lead to deviations and instabilities of the bubble's shape as compared to a spherical one. First, the bubbles of the sizes investigated in cyclohexane are typically of ellipsoidal, wobbling or oblate shape already from the time of their creation in the liquid. This was an expected feature of the system as theoretical calculation predicted [100]. Apart from that, instabilities of the interface between a liquid and a gas in an accelerating motion (the Taylor instability) are expected to exist on the bubble's surface. In case of a liquid jet penetration through the bubble, the bubble's shape is further deformed. In this case heat flows also into the heating and the evaporation of the liquid micro-droplets inside the bubble's volume, which are generated by this penetration.

(vii) Influence of jet penetration

A jet penetration would add new amounts of cyclohexane into the gas of the bubble and take energy from the bubble for the corresponding evaporation of these amounts. Apart from that the bubble's shape would be significantly deformed, thereby increasing its heat losses due to conduction. In this work the influence of an eventual liquid jet penetration through the bubble during its compression is not considered, although experiments indicate strongly the existence of the phenomenon. This consideration is planned for the near future, as the current experimental data are not adequate to support and validate a quantitative theoretical analysis.

Table 5-6: Calculation of the temperature T_{ad} and pressure P_{ad} for an adiabatic compression of a spherical bubble; the characteristic time of heat conduction τ_C, and the average temperature inside the bubble T_{av} after time t = 60 µs.

$2\,r_0$ mm	r_{ign}/r_0	T_{ad} K	P_{ad} bar	κ cm^2/s	τ_C ms	t_{ign}/τ_C (t_{ign} = 60 µs)	$\frac{T_{av}-T_1}{T_{ad}-T_1}$	T_{av} K	$\frac{T_{av}-T_{ad}}{T_{ad}}$ %
2.4	0.56	451.9	8.6	0.0378	18.99	0.00316	0.937	442.4	-2.1
7.2	0.56	451.9	8.6	0.0378	170.91	0.00035	0.962	446.1	-1.3
2.4	0.20	785	328	0.0026	35.53	0.00169	0.949	760.4	-3.1
7.2	0.20	785	328	0.0026	319.75	0.00019	0.963	767.2	-2.3

Table 5-7: Characteristic time for conduction τ_C for different mixtures of oxygen / cyclohexane at 1 bar and 300 K or 600 K.

	τ_C in ms			
r	0.13 C_6H_{12} + 0.87 O_2		0.3 C_6H_{12} + 0.7 O_2	
mm	at 300 K	at 600 K	at 300 K	at 600 K
0.5	2.57	0.76	3.90	1.15
1.0	10.26	3.03	15.59	4.60
1.5	23.09	6.81	35.08	10.36
2.0	41.04	12.11	62.36	18.41
2.5	64.13	18.92	97.44	28.77
3.0	92.34	27.24	140.31	41.43
3.5	125.69	37.08	190.98	56.39
4.0	164.17	48.43	249.44	73.65

Temperature decrease inside the bubble due to radiation

The maximum rate of temperature decrease due to radiation from the bubble $\dot{\Delta T}$ can be calculated by (eq. 7-24). For this calculation the same scenario that was used for the calculation of the temperature deviation inside the bubble from its adiabatic value, was used. The results are presented in Table 5-8.

The calculated values of $\dot{\Delta T}$ shown in this table assume a bubble that emits like a black body. Since the gas phase of the bubble is not a black body, it should be expected that in reality these rates are even smaller. Moreover, during the compression process the bubble has even lower temperatures as

the one than was used for the calculation. At lower temperatures $\dot{\Delta T}$ is also reduced. Consequently, the influence of radiation on the temperature of the bubble can be considered to be negligibly small for the time scale (less than 100 μs) of the phenomena observed in this work.

Table 5-8: Maximum rate of temperature decrease due to radiation $\dot{\Delta T}$ inside a spherical bubble of radius r_{ign}. The initial temperature inside the bubble is equal to T_{ad}.

Initial bubble diameter $2\,r_0$ mm	r_{ign}/r_0	T_{ad} K	$\dot{\Delta T}$ K/μs
2.4	0.56	452	- 0.001327
7.2	0.56	452	- 0.000442
2.4	0.20	785	- 0.001315
7.2	0.20	785	- 0.000438

5.3.3 Variation of parameters

In this section the influence of the variation of the following parameters of the system on the bubble explosion behavior during the first shock induced oscillation will be considered. The distance between neighboring bubbles, the composition of the gaseous mixture inside the bubble (variation through nitrogen addition), the initial pressure of the system, the initial bubble diameter and the organic liquid (variation of viscosity). Additionally the influence of the properties of the incident shock wave on the bubble explosion behavior is discussed.

5.3.3.1 Distance between bubbles

During the evaluation of the experiments in which bubble ignition in cyclohexane was recorded, a special attention was given to discover any evident interaction effects between neighboring bubbles that could influence their explosion behavior. The motivation behind this consideration is that such effects can provide additional information about the bubble explosion phenomenon under industrial conditions, i.e. in bubble columns where a much higher bubble concentration with a wide bubble size distribution exists. One obvious parameter that could reveal such interaction effects is the distance between bubbles.

In deed, the evaluation of the experiments showed that this distance can influence the explosion behavior of single bubbles significantly. To illustrate this effect, two experiments are presented here.

First, the experiment No. 96 in Fig. 5-15 is shown. The incident shock wave is recorded propagating in front of the observation window at 8 μs. Jet penetration during the compression phase

can be seen in the bubble No. 3 (at 22 μs). The same bubble is ignited at 30 μs. This bubble ignition is caused by the bubble compression. The spherical shock wave emitted by this explosion and also by the explosion of the bubble No. 1 (at 33 μs) meet at the position of the bubble No. 2 at 35 μs and -apparently instantaneously- ignite it. This bubble ignition is interpreted as a new kind of ignition, induced by the interaction with the two shock waves that impacted the bubble. This kind of ignition was observed also inside the bubble No. 4 which was ignited at 38 μs by the spherical shock wave from the explosion of bubble No. 2.

Some more detailed aspects of the ignition by other bubble explosions, can be seen in the experiment presented in Fig. 5-16. Also in this case the bubbles were created by pure oxygen and the liquid was cyclohexane. At 11 μs the incident shock wave is located at the middle of the observation window. The bubble explosion at 38 μs creates a shock wave. This shock wave reaches a group of nearby bubbles at 40 μs. From the angle of the recording it is not totally clear whether this group consists of two or three single bubbles. As the shock wave penetrates the volume of these bubbles, they are ignited (see frames at 41 μs, 42 μs and 43 μs). The pair of arrows on these frames indicate the position of the spherical shock wave (SW_b).

From the frames at 41 μs and 42 μs it is obvious that for 2 μs long the light emission inside the bubbles corresponds exactly to the penetration depth of the shock wave. This fact reveals that the shock wave which penetrated the gas phase of the bubbles is strong enough to create locally high temperatures. It is also interesting that the ignition took place not directly at the position of the first shock wave penetration near the bubble wall (at 41 μs), but rather when the shock wave penetration reached close to the bubble's center (at 43 μs). At the point of ignition, these bubbles were still in the compression phase. The bubble's center though is expected to be the bubble's hottest spot at that time, because it is the most remote position from the walls, where heat losses can take place. Further strong temperature increase due to local gas compression by the penetrated shock wave, makes this spot the most likely to initiate an ignition. This explains why in both Fig. 5-15 and Fig. 5-16 the bubble ignition appears to be in or very near the bubble's center.

The examination of the experiments indicate that bubble ignition due to shock wave impact from another nearby bubble explosion depends strongly on the distance that the emitted spherical shock wave has to travel before it will hit the bubble-target. This was expected, since such spherical pressure waves lose in amplitude as they propagate in the liquid [101]:

$$P_{SW_L} = P_{SW_0} \frac{r_{ign}}{L} \qquad \text{(eq. 5-4)}$$

where: P_{SW_0} is the initial pressure of the shock wave after the bubble explosion; P_{SW_L} is the pressure of the shock wave after distance L from the bubble's center, and r_{ign} is the radius of the bubble at the moment of explosion. The parameters of the above equation and the involved processes for the ignition are illustrated in Fig. 5-17.

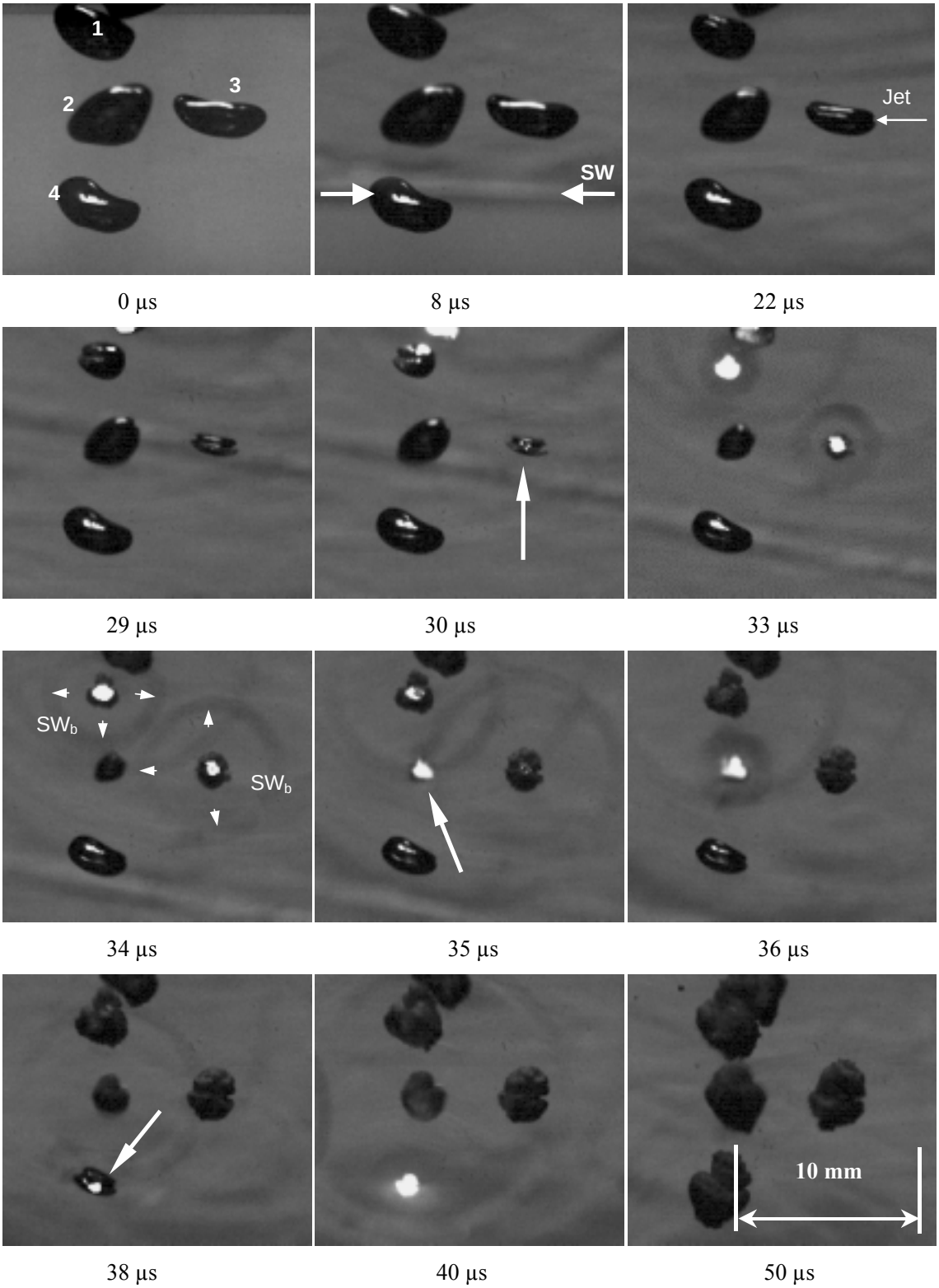

Fig. 5-15: Bubble ignition from the incident wave or from nearby bubble explosion.

The incident shock wave enters the observation window at 0 µs. The arrows at 34 µs indicate the position of the two spherical shock waves (SW_b). Framing rate of the camera: 1 000 000 fps. The bubbles were created by oxygen injection into the liquid. (Exp. No. 96)

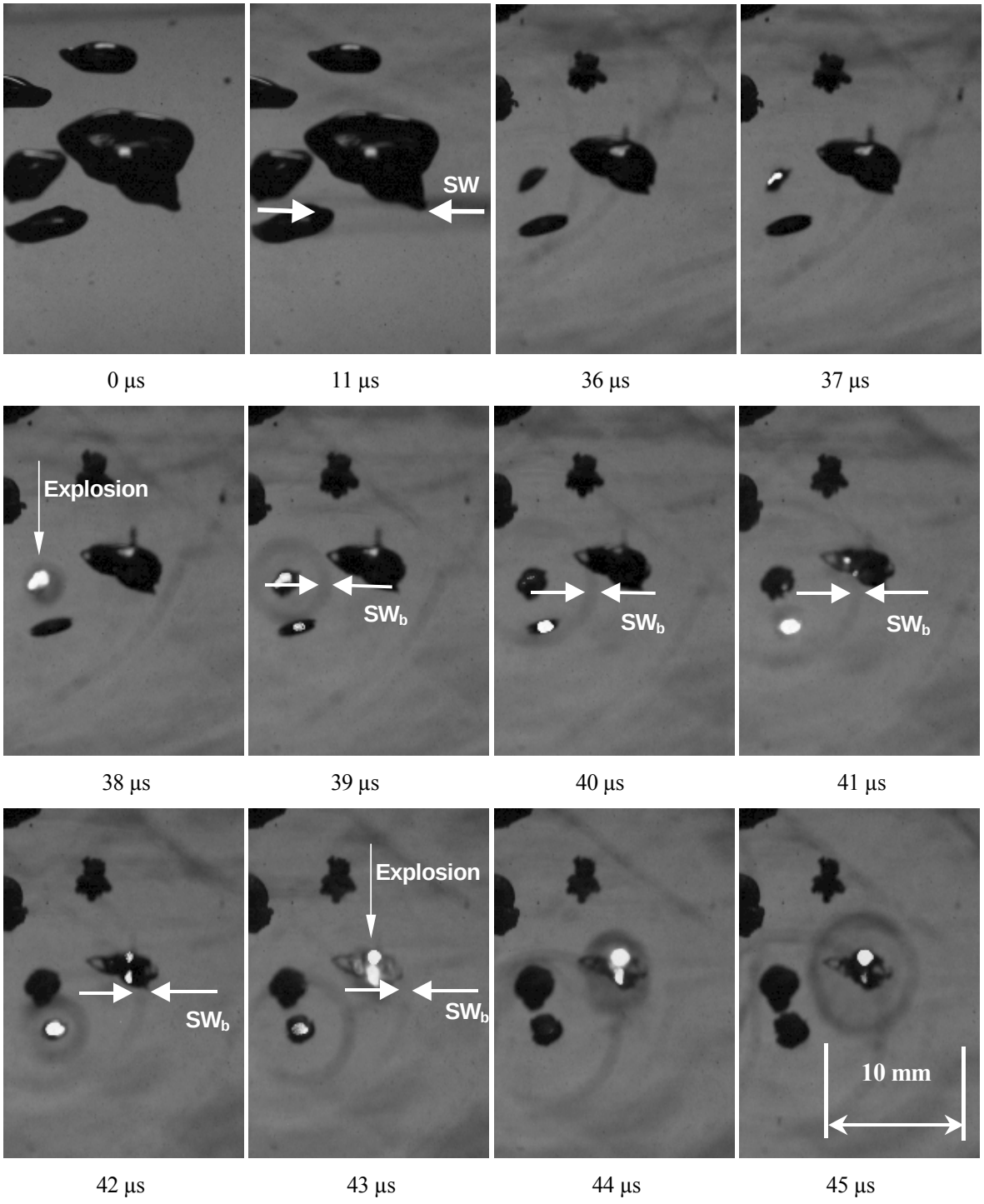

Fig. 5-16: Progressive bubble ignition induced by the shock wave emitted by a nearby bubble explosion.

The incident shock wave enters the observation window at 0 µs. The pair of arrows indicate the position of the spherical shock wave (SW_b). Framing rate of the camera: 1 000 000 fps. The bubbles were created by oxygen injection into the liquid. (Exp. No. 129)

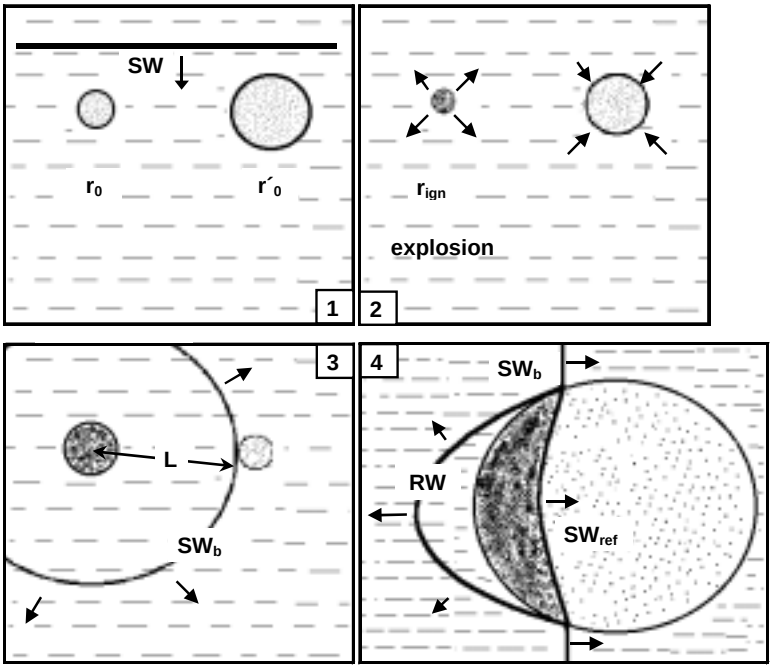

Fig. 5-17: Schematic of bubble ignition due to a nearby bubble explosion.

Two bubbles of different radius (r_0 and r'_0, respectively) are hit by a planar shock wave (1); later during the compression phase the smallest bubble explodes while the other bubble is shrinking (2); The spherical wave (SW_b) emitted by the bubble explosion impacts the still shrinking nearby bubble (3); This impact creates a refracted shock wave (SW_{ref}) inside that bubble and a rarefaction wave (RW) outside it (4). Behind the refracted wave ignition occurs.

According to the (eq. 5-4), the spherical shock wave is significantly weaker in pressure after a distance of a few bubble radii. In the present work the distance between the bubbles was not varied in a systematic and controlled way. By variation of the gas flow for the creation of the bubbles and due to stochastic deviations of the bubble spatial distribution in front of the observation window, it was possible to observe the bubble behavior at different inter-bubble distances.

The effect just described in Fig. 5-15 and in Fig. 5-16, according to which a bubble explosion can be induced by a shock wave from another, nearby single bubble explosion is observed experimentally for the first time and reported in the frame of this study [102]. The implications of this effect will be discussed in Chapter 6.

The principle possibility of bubble ignition due to shock wave refraction inside the bubble's volume was theoretically demonstrated by Mader [103] with the help of numerical analysis. More precisely, the author showed that a detonation process can in principle be initiated inside a bubble after shock wave impact, even without previous adiabatic compression of the bubble. The calculations were performed for the system acetylene / oxygen bubbles inside water (the bubble radius was assumed to be 2 mm). The results for this system showed that, when a shock wave with amplitude of 500 bar interacted with a bubble, the intensity of the wave refracted into the bubble was sufficient to initiate detonation in the vicinity of the bubble wall on the side of incidence of the shock wave.

According to the calculation, in the detonation-initiation zone arose an intense pressure peak with an amplitude of the order of 1 200 bar, which was much higher than the amplitude of the incident shock wave.

5.3.3.2 Nitrogen addition into the gas bubble

In order to observe the influence of inert gas addition on the bubble explosion, different N_2 / O_2 mixtures were used for the creation of the bubbles. These mixtures contained a N_2 molar fraction of 0.00, 0.30, 0.60, 0.79 and 0.90. The following experimental parameters were kept constant: (i) bubble equivalent diameter: 3 mm ± 0.5 mm; (ii) initial pressure of the system: 1 bar; (iii) initial temperature: the ambient one (20 ^{o}C – 25 ^{o}C), (iv) peak pressure of the incident shock wave: 85 bar ± 8.5 bar, and (v) liquid: pure cyclohexane. It is interesting to note that the adiabatic index γ of any gaseous mixture of N_2 / O_2 has a practically constant value, since both compounds are diatomic. Because of this the temperature in the bubbles should follow the same adiabatic curve during an adiabatic compression.

In Fig. 5-18 an experiment with bubbles containing a mixture of N_2 / O_2 with a N_2 molar fraction of 0.60 is presented. The first frame (0 μs) corresponds to the time exactly before the passage of the incident shock wave in front of the observation window. All the other frames in Fig. 5-18 were recorded after the shock wave impact on the bubbles. From the thirteen bubbles that are visible only four exploded (see the arrows). These explosions had ignition delays between 22 μs and 26 μs and the duration of the light emission was 2 μs or less (one frame).

In Fig. 5-19 the results of an other experiment are presented. Compared to the experiment described above, for this one a greater magnification was chosen, and the recording frame rate was doubled (1 000 000 fps), so that single bubbles can be observed better. The N_2 / O_2 gas mixture in these bubbles contained a N_2 molar fraction of 0.79. Like in the previous figure, here too the first frame (0 μs) corresponds to the time exactly before the passage of the shock wave in front of the observation window. As can be seen from the figure, the only bubble explosion that occurred (at 45 μs) had a very weak light emission. The black line that appears in the middle of that bubble, virtually dividing the illuminating area into two parts, is interpreted to be a penetrating liquid jet inside its volume. The ignition delay of this bubble explosion was 41 μs and the duration of its light emission was 1 μs or less (one frame).

Common features of the two experiments are that only a small fraction of the bubbles exploded and that when a bubble explosion did occur, its light emission was shorter and weaker compared to an exploding oxygen bubble. This behavior is in fact a general one. It was observed that the fraction of bubbles that explode decreases, as the molar fraction of nitrogen inside the bubbles increases (for example, compare the fraction of exploded bubbles in Fig. 5-14 and in Fig. 5-18).

Although in some experiments it was possible to ignite bubbles containing a N_2 / O_2 gas mixture with N_2 molar fraction as high as 0.79 (e.g. shown in Fig. 5-19), no bubble explosion was observed when a N_2 molar fraction of 0.90 was used.

Nitrogen addition into an oxygen gas bubble saturated in cyclohexane vapor, does not change the adiabatic index of the gaseous mixture. Therefore, it does not influence the temperature increase during the bubble compression. It follows that the absence of bubble explosion after a certain level of nitrogen addition, is a direct consequence of the fact that the gas mixture exceeds the explosion range.

Another information gained from the experiments is that often even bubbles created by pure oxygen did not explode, even though they were of the same diameter, compared to others that exploded, during the same experiment (see e.g. Fig. 5-14). This indicates the stochastic nature of the bubble ignition processes.

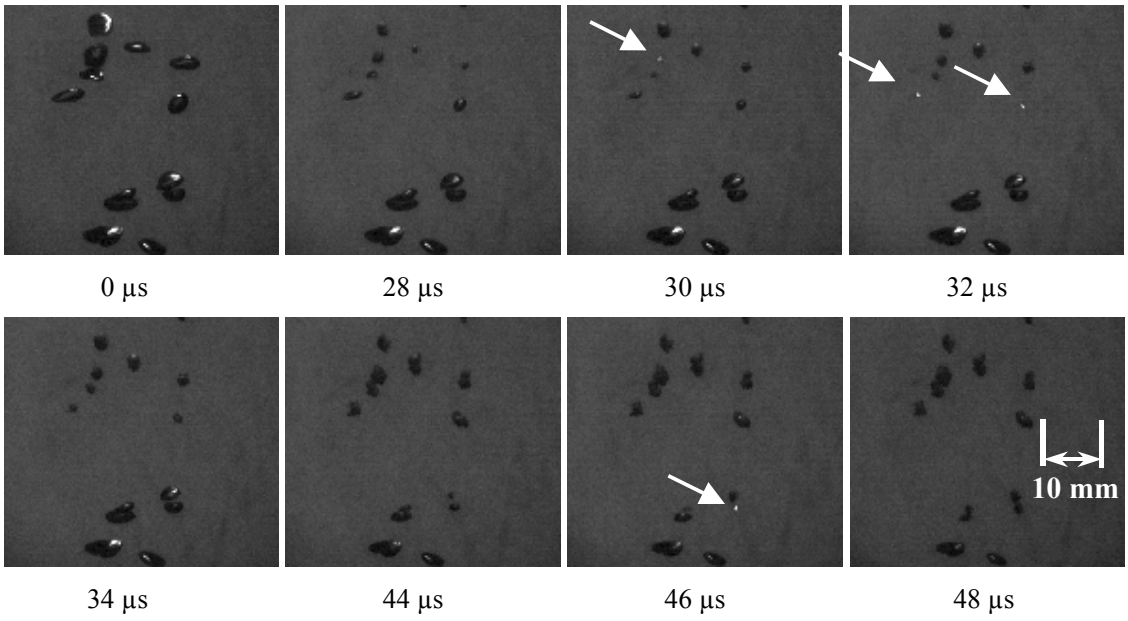

Fig. 5-18: Bubble explosions with weak light emission in cyclohexane.

Bubbles in cyclohexane under shock wave impact. For the bubbles the gaseous mixture of N_2 / O_2 with a N_2 molar fraction of 0.6 was used. The incident shock wave entered the observation window at t = 0 µs. The arrow shows bubble explosions. The framing rate of the camera was 500 000 fps. (Exp. No. 119)

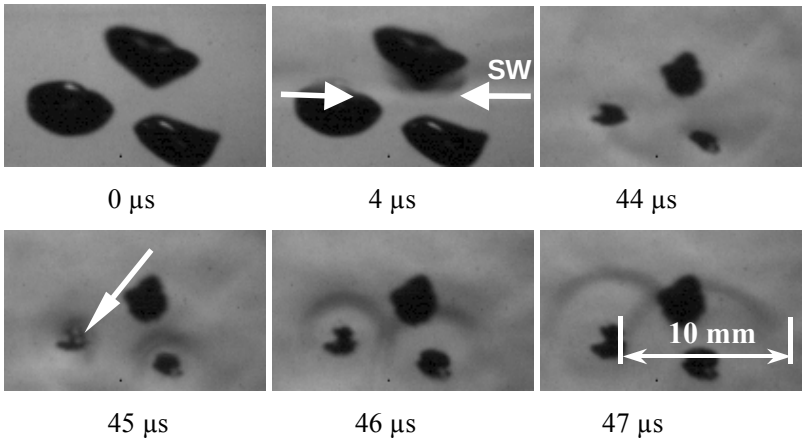

Fig. 5-19: Bubble explosion near the explosion limit.

Bubbles in cyclohexane under shock wave impact. For the bubbles a gaseous mixture of N_2/O_2 with a N_2 molar fraction of 0.79 was used. The shock wave entered the observation window at 0 μs. The arrow at 45 μs shows a weak bubble explosion. Framing rate of the camera: 1 000 000 fps. The pressure signal is presented in Fig. 5-21. (Exp. No. 139)

5.3.3.3 Incident shock wave pressure

As has been already mentioned, in order to ignite oxygen-containing bubbles inside organic liquid, the incident shock wave that was generated by the impact of the gas detonation on the liquid's surface was used. This section focuses on the question which properties of this shock wave influence the bubble explosions and can be extracted by the measured pressure signals. Then the experimentally measured values of these shock wave properties are reported.

Generally, a bubble containing an explosive gas phase will explode when its gas phase will reach a certain temperature and pressure. As it has been mentioned in many positions in this study, the increase of the temperature and pressure inside the bubble is caused by the pressure field of the incident shock wave. On the other hand, the recorded pressure of the incident shock wave show a very complicated oscillatory structure as will be described in §5.5.

In order to discuss the above question, a first approach that neglects this complicated structure and refers to an ideal situation is necessary. Assuming that a shock wave of the type illustrated in Fig. 5-20 impacts a bubble, the latter starts then to shrink. As the bubble shrinks, the temperature and the pressure inside the bubble's volume increase as function of the ratio, r/r_0 ; r being the radius of the bubble.

In the case of an adiabatic bubble compression, the minimum value of the ratio r/r_0 during the compression can be calculated by the equation (see §3.2.3):

$$\frac{r_{\min}}{r_0} = \left(\frac{P_{SW}}{P_0} \right)^{3\cdot\gamma} \qquad \text{(eq. 5-5)}$$

where:

- P_{SW} is the pressure of the shock wave,
- P_0 is the initial pressure of the system,
- and r the radius of the bubble.

In the ideal situation when the shock wave has the structure of the type shown in Fig. 5-20, the above equation can be used as a tool to discover those bubbles in the experiments, that independently of their initial radius, should finally reach the same level of internal temperature and pressure during an adiabatic compression. This is a necessary step for comparing the explosion behavior between different bubbles and in different experiments.

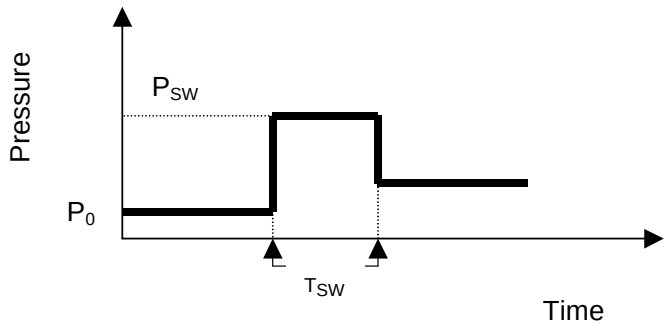

Fig. 5-20: Schematic of an one-step shock wave.

In the complicated structure of the real incident shock wave the definition of P_{SW} is not as obvious as in Fig. 5-20. Below, two possible solutions of this problem with their advantages and disadvantages are discussed.

One possibility is to define P_{SW} in (eq. 5-5) to be equal to the peak pressure of the incident shock wave, P_{SWmax}. This consideration requires the necessary condition that the duration τ_{SW} of the incident shock wave is long enough, i.e. it exceeds the compression time of the bubble under observation. In this case the role of the structure of the pressure signal behind the peak pressure is neglected.

The advantage of this solution is that the quantity P_{SWmax} characterizes the complete incident shock wave, i.e. if the number of the bubbles is sufficiently small, this quantity is independent of the properties and behavior of the bubbles in the liquid. Apart from that the quantity P_{SWmax} can be measured directly from the recorded pressure signals. The disadvantage on the other hand is the above mentioned condition that limits the applicability of the method.

Another possibility is to define P_{SW} in (eq. 5-5) as equal to the arithmetic average pressure in the liquid, P_{SWaver}. This quantity must be calculated for every bubble separately, because the bubble ignition delay t_{ign} varies between bubbles. The average pressure for each bubble is then the arithmetic

average of the pressure during the compression phase of that bubble. In this manner, the complicated structure of the pressure signal is partially taken into account.

Between the two above ways to define a value for P_{SW} in (eq. 5-5), the averaging of the pressure over the compression time will per definition produce values that are lower than the peak pressure, P_{SWmax}. In principle these lower values should give a more accurate picture of the reality. A weak point though is that the pressure measurements which are used for the calculation, are performed far away from the bubbles. Because of this the pressure structure may significantly differ from the one near the bubbles. This leads, of course, to sources of inaccuracies that could prove to be significant.

It is expected that the two values P_{SWaver} and P_{SWmax} define a range inside which the actual value that corresponds to the local conditions near the bubble should lay. To illustrate the difference between these two values the pressure signal from the experiment No. 139 is presented in Fig. 5-21. During this experiment only one bubble explosion was recorded (see Fig. 5-19). The ignition delay, t_{ign}, was 41 μs as denoted in Fig. 5-21. During that time the average pressure P_{SWaver} in the liquid was 47 bar, while the peak pressure of the signal P_{SWmax} reached the value of 81 bar.

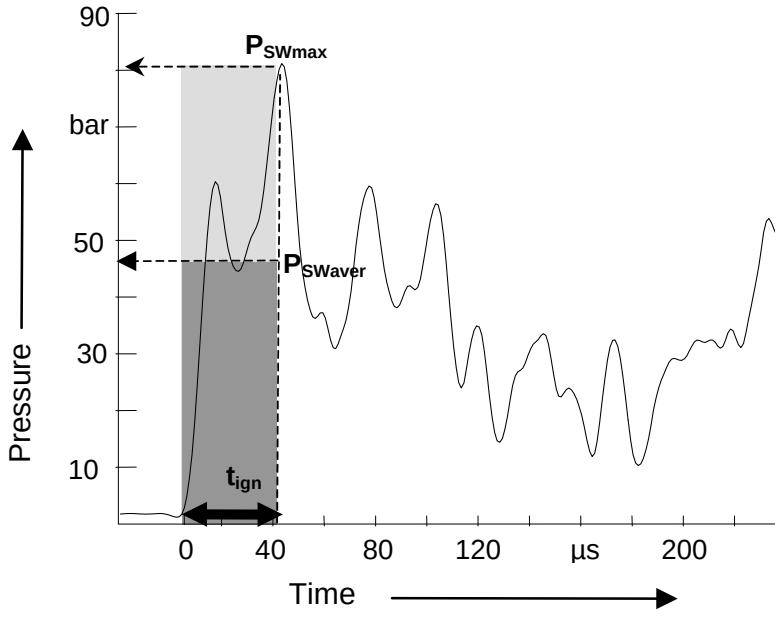

Fig. 5-21: The incident shock wave of the experiment presented in Fig. 5-19.

The ignition delay of the sole bubble explosion recorded in the experiment, was 41 μs. The ignition delay is denoted by a shadowed area on the pressure signal above. During this time the pressure had an average value, P_{SWaver}, of 47 bar (see upper end of the dark shadow). The shock wave had a peak pressure, P_{Swmax} , of 81 bar. (Exp. No. 139)

The examination of all the performed experiments at 1 bar initial pressure, shows that the minimum value of the peak pressure in the incident shock wave, $P_{SWmax,}$ was 50 bar. In the same experiments, the arithmetic average pressure P_{SWaver}, calculated for each bubble that exploded, was equal to or greater than 31 bar.

As a result of the above discussion it is clear that using only the peak pressure of the measured signals for the evaluation and interpretation of measurements with single bubbles is not advisable. The proposal of this study is to use instead a pressure range. This pressure range is limited by P_{Swaver} and P_{SWmax}.

5.3.3.4 Initial pressure of the system

A change in the initial pressure of the system resulted in a corresponding change in the incident shock wave's peak pressure. This is an inherent characteristic of the system investigated, because the initial pressure inside the bubbles was equal to the initial pressure of the explosive gas mixture used to generate the incident shock wave in the liquid. Apart from the experiments performed at initial pressure of 1 bar, experiments were performed also at 2 bar and at 3 bar. The experiments at 2 bar are not shown here.

In Fig. 5-22 two frames, from different experiments are presented. The frame on the left was recorded during the Exp. No. 90, which was performed at an initial pressure of 3 bar. The frame on the right was recorded during the Exp. No. 59. This experiment was performed at an initial pressure of 1 bar. In both experiments pure oxygen was used to create the bubbles and the liquid was pure cyclohexane. The incident shock wave had a peak value of $P_{SW\,max}$ = 52 bar in the Exp. No. 59 (P_0 = 1 bar) and 200 bar in the Exp. No. 90 (P_0 = 3 bar). The arrows in Fig. 5-22 show the position of the front of the incident shock wave. The propagation velocity of the shock wave was the same in both cases. In both experiments bubble explosions were recorded.

In terms of distance between the incident shock wave and the exploding bubble, it can be seen in Fig. 5-22 that the ignition delay on the left frame (P_0 = 3 bar) is significantly shorter than the one on the right frame (P_0 = 1 bar). The shortest ignition delay that was observed at an initial pressure of 1 bar is 14 μs and at 3 bar only 7 μs.

A change in the initial pressure influences the concentrations of the gases in the bubble, and therefore the value of the adiabatic index $\gamma_{mixture}$. This value has an influence to the temperature levels that will be reached during a certain level of bubble compression. Assuming an adiabatic compression, this temperature can be calculated by the formula $T/T_0 = (r_0/r)^{3\cdot\gamma-3}$ (see §3.2.3). To describe how the adiabatic index is influenced by the initial conditions, the case of an oxygen bubble in liquid cyclohexane is considered. If the bubble has enough time to reach the saturation levels, the cyclohexane concentration in the bubble will be limited by its vapor pressure. Therefore an increase of the initial pressure, P_0, will result into higher values of the adiabatic index $\gamma_{mixture}$. This means that at higher initial pressures, comparatively lower compression levels are necessary for the bubble to reach the ignition temperature which makes the explosion easier and the ignition delay shorter. This is therefore one reason why the ignition delays were shorter at higher initial pressures. Higher initial pressure also means that more oxygen moles exist in the same volume of bubble. Depending on the

introduction of cyclohexane into the bubble due to jet penetration the chemical energy that can be released may be higher.

A further explanation of the observations is related to the velocity of bubble compression. Generally, the slower the bubble compression is, the higher the diversion from the adiabatic conditions. The ignition delay of a shock induced bubble explosion is obviously proportional to the bubble compression (or collapse) time, $t_{collapse}$ after the shock wave impact. The collapse time can be estimated by (eq. 3-9):

$$t_{collapse} = 0.915 \cdot r_0 \cdot \sqrt{\frac{\rho_{liquid}}{P_{SW}}} .$$

In the experiments a higher initial pressure resulted into a higher absolute shock wave pressure in the liquid (e.g. P_{SW} = 200 bar at P_0 = 3 bar instead of P_{SW} = 50 bar at P_0 = 1 bar in Fig. 5-22). Although the ratio between the shock wave pressure and the initial pressure P_{SW} / P_0 is about the same, the ignition temperature will be reached in the bubbles faster in the case of stronger incident waves, because the bubble compression will be faster. Therefore the above equation gives a further explanation of the experimental observations, i.e. that incident shock waves with higher pressure peak resulted into bubble explosions with significantly shorter ignition delays.

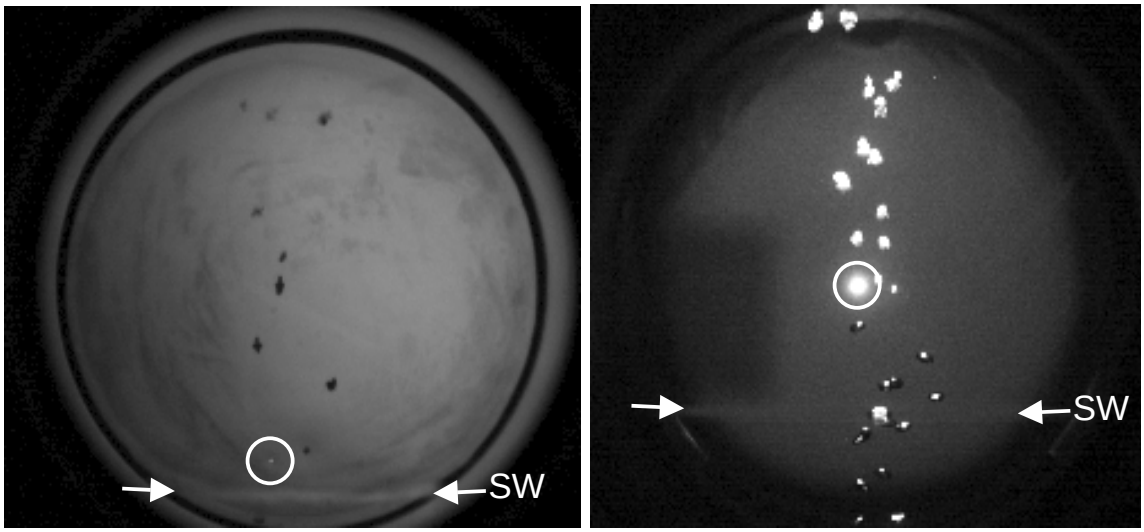

P_0 = 3 bar P_0 = 1 bar

Fig. 5-22: Bubble ignition at different initial pressures.

Bubble explosions at initial pressure of 3 bar (on the left) and 1 bar (on the right). Both experiments are recorded at a framing rate of 500 000 fps. $P_{SW\,max}$ = 52 bar (at P_0 = 1 bar), and 200 bar (at P_0 = 3 bar). (Exp. No. 90 and No. 59)

5.3.3.5 *Initial bubble diameter*

The dominant role of the bubble diameter on bubble explosion can be seen from the discussion about the heat losses during the compression phase (see §5.3.2.2). If a bubble is adequately small then the ratio of its surface to its volume is high enough that the heat losses during the compression do not allow its ignition. On the other hand, if a bubble is big enough its surface will have so many instabilities that its compression would be impossible without bubble breakage. In such a case bubble ignition may be impossible due to high heat losses induced by the process of breakage.

From the evaluation of the performed experiments with oxygen bubbles it was found that an incident shock wave with a peak pressure of 85 bar ± 8.5 bar can ignite oxygen bubbles with equivalent initial diameters between 2.4 mm and 7.2 mm. The experiments that correspond to these results were performed only in cyclohexane, at room temperature and at an initial pressure of 1 bar.

An example of an experiment with a single bubble with initial diameter at the maximum of the above range, i.e. 7.2 mm, is presented in Fig. 5-12. Bubble explosion at equivalent diameters below 1.5 mm was not observed in this study. From the conducted experiments it is impossible to draw a safe conclusion about the explosion of bubbles with initial equivalent diameters between 1.5 mm and 2.4 mm and above 7.2 mm.

5.3.3.6 *Viscosity of the liquid*

The role of the viscosity of the liquid phase to the phenomenon of bubble explosion was considered in the literature review in Chapter 2 (see §2.2.2). It was reported there that, according to experimental investigations, the critical shock wave pressure that can ignite a bubble through shock induced compression increases with diminishing viscosity of the liquid. Thus, a certain value of viscosity can be reached, after which bubble explosion is impossible. The explanation of this effect was that a decrease in viscosity, intensifies instabilities and perturbations on the bubble's surface during the compression phase. Because of this, bubble heat losses increase and as a result the critical parameters for bubble explosion are increased too.

In the frame of this study, eleven experiments were performed in which the viscosity of the liquid was handled as a parameter. In these experiments the liquid cyclohexane was substituted through one of the following organic liquids: methanol, cumene or 2-ethylhexanal.

The use of these liquids kept all the other parameters about constant: A saturated mixture of these solvents inside gaseous oxygen has about the same adiabatic index γ (1.35 for methanol; 1.38 for cumene; 1.39 for 2-ethylhexanal and 1.27 for cyclohexane). The calculation of these values was based on the method presented in Appendix B. Apart from that the surface tension of these four liquids was about the same. Under normal conditions (P = 1 bar, T = 293 K), an oxygen bubble saturated in vapor of methanol or cyclohexane contains an explosive gaseous mixture (see Table 5-9

and Table 5-10 respectively). The same is not valid in the case of 2-ethylhexanal and cumene. In this section the reactivity of the organic solvents related to the combustion processes is neglected. Cumene has a viscosity about three times higher than methanol as can be seen in Table 5-9.

Bubble explosion was observed in all above mentioned organic liquids (see Fig. 5-23). In the performed experiments with these three organic solvents, it was observed that the fraction of the bubbles that exploded was very high. This indicates that the critical value of viscosity below which the bubbles can not be ignited is not close to the range of 0.5 10^{-3} Pa s - 1.5 10^{-3} Pa s. The fact that bubble explosion was observed inside 2-ethylhexanal and inside cumene (see Fig. 5-23), i.e. inside bubbles which contained initially a non explosive fuel-lean mixture, is a clear indication that during the bubble compression enrichment in vapor of the surrounding liquid occurs. The evaluation of the experiments showed that like in cyclohexane this enrichment is induced by jet penetration.

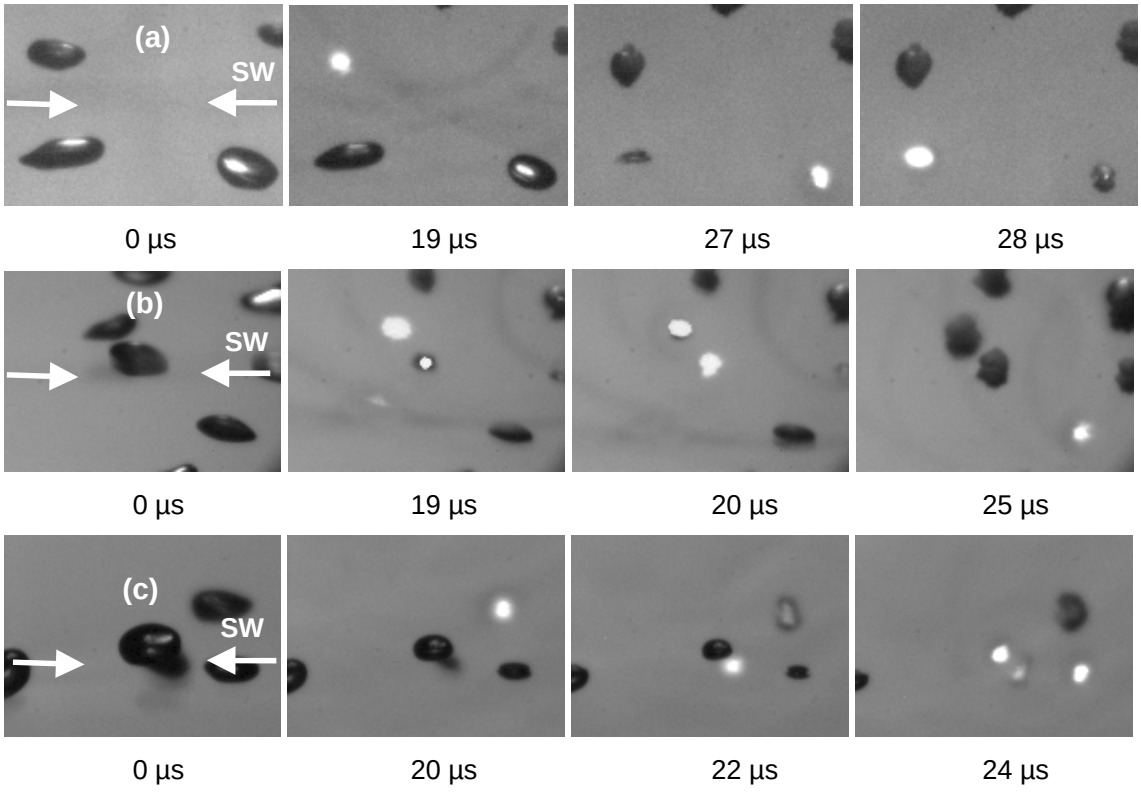

Fig. 5-23: Bubble explosions in different organic solvents.

Oxygen bubbles in three different organic liquids under shock wave impact. The shock wave is pointed by arrows at 0 µs. Framing rate of the camera: 1 000 000 fps. Liquid phase: (a) 2-ethylhexanal (Exp. No. 168); (b) methanol (Exp. No. 174) and (c) cumene (Exp. No. 175).

Table 5-9: Properties of the organic liquids investigated.

LEL = Lower Explosion Limit, UEL = Upper Explosion Limit, NA = No information available

Property	units	Organic compound			
		cyclohexane C_6H_{12}	methanol CH_4O	cumene C_9H_{12}	2-ethylhexanal $C_8H_{16}O$
Density (293 K)	kg/m^3	779 [a]	791 [a]	862 [a]	822 [a]
Viscosity (293 K)	10^{-3} Pa s	0.89 [b]	0.54 [b]	1.38 [b]	0.90 [c]
Surface Tension (293 K)	10^{-3} N/m	2.47 [b]	22.1 [b]	27.7 [b]	NA
Vapor pressure (293 K)	10^{-3} bar	102 [a]	129 [a]	4.3 [b]	2.3 [d]
Ignition temperature in air	K	533 [a]	713 [a]	693 [a]	458 [a]
Flash point in air	K	255 [a]	282 [a]	304 [a]	315 [a]
LEL in air, at 1 bar	%	1.0 [a] (293 K) 0.9 [a] (373 K)	6.0 [a] (293 K) 5.4 [a] (373 K)	0.8 [a] (NA)	0.85 [e] (NA)
UEL in air, at 1 bar	%	9.3 [a] (373 K)	50 [a] (373 K)	6.0 [a] (NA)	7.2 [e] (NA)
Adiabatic index (293 K)		1.08 [b]	1.23 [b]	1.06 [b]	1.03 [c]

a – CHEMSAFE® – Database for Recommended Safety Characteristics, BAM, PTB, DECHEMA, Germany, Update 2003;

b – Korea theromophysical properties databank, http://www.cheric.org/research/kdb/, last accessed on Nov. 2003;

c – L. Becker and J. Gmehling: Measurement of heat capacity for 12 organic substances by Tian-Calvet calorimetry, J. Chem. Eng. Data, 46, pp. 1638-1642 (2001);

d – Hawley's Condensed Chemical Dictionary, 14th Edition, John Wiley & Sons, Inc (2002);

e – International Chemical Safety Card No. 0621, http://www.cdc.gov/niosh/ipcsngrm/ngrm0621.html, last accessed on May 2004

5.3.4 Summary

Here a short overview of the main experimental results and conclusions of §5.3 (bubble explosion type I) is presented.

Stages of the bubble explosion behavior

The discussion of the experiments in §5.3.1, led to the conclusion that the shock induced bubble behavior has three general stages: The compression phase, i.e. initiation of bubble compression and jet penetration through the bubble; maximum bubble compression and eventually explosion; and bubble expansion phase. Following the shock wave impact, the bubble does not start to shrink immediately. This initial phase during which practically no bubble compression takes place, had a duration in the order of 10 μs. After this delay time, the bubble shrinks noticeably. During this compression step a jet may form, which penetrates the bubble. After the jet formation the bubble compression proceeds at higher rates, dr(t)/dt (r being the equivalent radius of the bubble), than before it. These higher rates were usually between 50 m/s and 100 m/s.

The jet was formed when the equivalent bubble radius reached the range: $0.5 \leq r/r_0 \leq 0.9$, (where r_0 is the initial equivalent bubble radius). Between the jet formation and the bubble ignition a time delay of between 2 μs and 18 μs was observed. This delay is generally longer when the jet is formed earlier.

The bubble radius during the compression phase of bubbles that did not explode, reached typically a minimum value that was between $0.2 \leq r/r_0 \leq 0.3$. Higher values were occasionally observed too. The bubble compression time can be estimated by the equation (eq. 3-9):

$$t_{collapse} = 0.915 \cdot r_0 \cdot \sqrt{\frac{\rho_{liquid}}{P_{SW}}}.$$

The experimental data are in good agreement with the corresponding calculated values of $t_{collapse}$.

Following or during the compression phase the bubble can break up into two parts, due to strong jet penetration. In any case an expansion phase follows the bubble compression. The bubble expansion ends when a maximum bubble size is reached, which is limited by the pressure level inside the liquid at that time. The experiments showed that bubbles which are very near to each other do not collide during the compression phase, such collision can though occur during the expansion phase that follows. Furthermore, spatial displacement and bubble breakage were occasionally observed also.

When ignition during the first shock induced oscillation was observed, the bubble was not previously broken up. The ignition of this type took place at a bubble compression level of $0.20 \leq r/r_0 \leq 0.56$. The measured ignition delays (time from the incident shock wave impact to bubble ignition) were in the range of 15 μs to 60 μs. A relationship between the length of the ignition

delay and the bubble radius was found. Between two bubbles with significant difference in size, the smaller one has the shorter ignition delay. On the other hand, the bigger the bubble is, the longer the compression phase lasts and the more asymmetric the compression process becomes.

The experiments showed that directly after the bubble ignition, light emission from the complete bubble volume and a strong spherical shock wave emission follows and results into the bubble expansion phase. The duration of this light emission was between 1 µs and 6 µs, and typically about 4 µs to 5 µs. In a few cases the bubble continued to shrink for 1 µs - 2 µs after its ignition, until the explosion front in the bubble reached the walls.

Often even initially pure oxygen bubbles did not explode, even though they were of the same diameter, compared to others that exploded, during the same experiment (see e.g. Fig. 5-14). This indicates the stochastic nature of the bubble ignition processes.

Estimation of the conditions inside the bubble at the moment of ignition

According to the calculations in §5.2 the bubbles in the experiments, i.e. with 2.4 to 7.2 mm in diameter, contained after a time between 130 µs (bubble 2 mm in diameter) and 1.57 ms (bubble 7 mm in diameter) an explosive gas phase. This time is considerably less than the at least 500 ms they needed to reach the middle level of the observation window. It was also shown that until the bubbles had reached this position, their gas phase was practically saturated in vapor of cyclohexane. At atmospheric pressure and at 300 K the molar fraction of cyclohexane in the bubble before the shock wave impact is 0.13. In this case the explosive mixture is nearly stoichiometric, if pure oxygen is used as oxidizer. Therefore the oxygen bubbles in these experiments contained an explosive mixture of cyclohexane / oxygen already before the shock wave impact.

The composition, the temperature and the pressure inside the bubble at the moment of ignition were estimated by calculations in §5.3.2. The corresponding phenomena were calculated for a time duration of 60 µs, which is the longest bubble ignition delay that was observed in the experiments. In the calculations the influence of the jet penetration and the consequent evaporation of the generated droplets inside the bubble were ignored.

It was shown by calculation that during the bubble compression, the further enrichment in cyclohexane vapor due to diffusion is in terms of molar fraction not more than 5.5 %. This means that the molar fraction of cyclohexane inside the bubble at the moment of ignition was in the range between 13 % and 18.5 % for the experiments with initial pressure 1 bar.

During the bubble compression process conduction is the governing process of heat losses. The calculation of the temperature decrease inside the bubble due to conduction showed that for the conditions of the experiments the deviation from the adiabatic value was not above 3.1%. Therefore, the process can be assumed adiabatic and the ignition temperature inside the bubble was equal to the adiabatic temperature that was caused by the bubble collapse during the experiments.

The bubble ignition was observed at bubble compression levels in the range of $0.20 \leq r_{ign}/r_0 \leq 0.56$, which corresponds to a pressure and temperature in the range of (434.1 K and 8.2 bar) to (674.2 K and 280.9 bar), in case of adiabatic compression.

It was demonstrated by calculation that the assumption of a constant adiabatic index of the gaseous mixture in the bubble $\gamma_{mixture}$ for the calculation of the temperature and the pressure inside the bubble during an adiabatic compression, would lead to very significant errors.

Apart from that, the following conclusions were drawn with the help of the equations for the calculation of the temperature deviation due to heat conduction, presented in this work:

(i) Addition of nitrogen into the gaseous mixture of the bubble would not influence the deviation of the temperature from the adiabatic value.

(ii) Cyclohexane addition into the gas of the bubble would reduce the deviation of the temperature from the adiabatic value.

(iii) Increase of the pressure inside the bubble (e.g. by increasing the initial pressure P_0 before the initiation of the bubble compression) would reduce the deviation from the adiabatic value of the temperature.

(iv) Increase in temperature (e.g. by increasing the initial temperature T_0 before the initiation of the bubble compression) leads to higher temperature deviations from the calculated adiabatic value.

(v) Increase in bubble size would decrease the temperature deviation.

(vi) Deformation and instabilities of the bubble's surface intensify the heat losses by conduction, thereby increasing the deviation from the adiabatic condition.

In this work the influence of an eventual liquid jet penetration through the bubble during its compression is not considered, although experiments indicate strongly the existence of the phenomenon. This consideration is planned for the near future, as the current experimental data are not adequate to support and validate a quantitative theoretical analysis.

The calculation of temperature decrease inside the bubble due to radiation during the bubble compression was also performed. It showed that the influence of radiation on the temperature of the bubble can be considered to be negligibly small for the time scale (less than 100 μs) of the phenomena observed in this work.

Variation of parameters

The influence of the following experimental parameters on the bubble explosion were discussed in §5.3.3: the distance between neighboring bubbles, the composition of the gaseous mixture inside the bubbles (variation through nitrogen addition), the properties of the incident shock wave, the initial pressure of the system and the initial bubble diameter.

By variation of the gas flow for the creation of the bubbles and due to stochastic deviations of the bubble spatial distribution in front of the observation window, it was possible to observe the bubble behavior at different inter-bubble distances. It was found that if the distance is short enough, then the shock wave caused by a bubble explosion can ignite nearby bubbles. This mechanism is proven experimentally for the first time.

Nitrogen addition into an oxygen gas bubble, which is saturated with cyclohexane vapor, influences the bubble explosion behavior too. The fraction of bubbles that explode decreases, as the molar fraction of nitrogen inside the bubbles increases. Bubbles saturated in cyclohexane vapor containing initially a N_2 / O_2 gas mixture with N_2 molar fraction 0.79 were ignited. No bubble explosion was observed when a N_2 molar fraction of 0.90 was used instead. The initial pressure of the system was 1 bar.

One problem for the evaluation of the experiments is to define the effective pressure of the incident shock wave P_{SW}. This quantity is needed for example for the calculation with (eq. 5-5). One possibility to define P_{SW} is for it to be equal to the peak pressure of the incident shock wave, P_{SWmax}. Another possibility is to define P_{SW} as equal to the arithmetic average pressure in the liquid, P_{SWaver}. This quantity must be calculated for every bubble separately. It is expected that the two values P_{SWaver} and P_{SWmax} define a range in which the actual value that corresponds to the local conditions near the bubble should lay.

Bubble explosions during the first shock induced oscillation (bubble explosion type I) were observed for all incident shock waves produced in the experiments with pure oxygen bubbles. At an initial pressure of $P_0 = 1$ bar, the examination of the experiments shows that the minimum value of the peak pressure in the incident shock wave P_{SWmax} was 50 bar. The minimum calculated value for the arithmetic average pressure P_{SWaver} for each bubble that exploded reached 31 bar.

The initial pressure inside the bubbles was equal to the initial pressure of the explosive gas mixture used to generate the incident shock wave in the liquid. Therefore a change in the initial pressure of the system resulted into a corresponding change in the shock wave's peak pressure. Experiments were performed at 1 bar, 2 bar, and 3 bar initial pressure. The experimental observations showed that incident shock waves with higher pressure peak resulted into bubble explosions with significantly shorter ignition delays. Two factors can explain this behavior.

First, a change in the initial pressure influences the concentrations of the gases in the bubble, and therefore the value of the adiabatic index $\gamma_{mixture}$. In the investigated system an increase of the initial pressure P_0 resulted into higher values of $\gamma_{mixture}$. This means that at higher initial pressures, comparatively lower compression levels are necessary for the bubble to reach the ignition temperature which makes the explosion easier and the ignition delay shorter.

Secondly, in gas detonations the peak pressure of the shock wave is about proportional to the initial pressure. Therefore, the ignition temperature was reached in the bubbles earlier in the case

of higher initial pressures, because the incident shock waves were stronger and therefore the bubble compression was faster (see §5.3.3.4).

Higher initial pressure also means that the amount of oxygen in the same volume of the bubble is bigger. Depending on the introduction of cyclohexane due to jet penetration the chemical energy that can be released may be higher.

The bubble diameter has a dominant role for the heat losses during the compression phase (see §5.3.2.2). If a bubble is adequately small then the ratio of its surface to its volume is high enough that the heat losses during the compression do not allow its ignition. On the other hand, if a bubble is big enough its surface will have so many instabilities that its compression would be impossible without bubble breakage. In such a case bubble ignition may be impossible due to high heat losses induced by the process of breakage.

In the experiments, an incident shock wave with a peak pressure of 85 bar ± 8.5 bar ignited oxygen bubbles with equivalent initial diameters between 2.4 mm and 7.2 mm. The experiments that correspond to these results were performed only in cyclohexane, at room temperature and at 1 bar. Bubble explosion at equivalent diameters below 1.5 mm was not observed. From the conducted experiments a conclusion about bubbles with initial equivalent diameters between 1.5 mm and 2.4 mm and above 7.2 mm can not be supported.

In the frame of this study eleven experiments were performed in which the viscosity of the liquid was handled as a parameter. In these experiments the liquid cyclohexane was substituted through one of the organic liquids: methanol, cumene, or 2-ethylhexanal. The use of these liquids kept all the other parameters about constant. The reactivity of the organic solvents related to the combustion processes is neglected. Under normal conditions an oxygen bubble saturated in vapor of cumene or methanol contains an explosive gaseous mixture (see Table 5-9). This is not valid in the case of 2-ethylhexanal.

Bubble explosion was observed in all above mentioned organic liquids (see Fig. 5-23). Cumene has a viscosity about three times higher than methanol as can be seen in Table 5-9. In the performed experiments with these three organic solvents, it was observed that the fraction of the bubbles that exploded was very high. This indicates that the critical value of viscosity below which the bubbles can not be ignited is not close to the range of $0.5\ 10^{-3}$ Pa s - $1.5\ 10^{-3}$ Pa s.

The fact that bubble explosion was observed inside 2-ethylhexanal and inside cumene (see Fig. 5-23), i.e. inside bubbles which contained initially a non explosive fuel-lean mixture, is a clear indication that during the bubble compression enrichment in vapor of the surrounding liquid due to jet penetration occurs. Evidence of another enrichment mechanism was not observed.

5.4 Bubble explosion type II

In the experiments during which the high speed video camera Kodak Ektapro HS was used, the observation time was much longer compared to that what the other two available cameras offered. This made the observation of the shock induced behavior of the bubbles for a longer time interval possible. In some cases, an unusual explosion behavior was observed inside the bubbles which did not explode during their first shock induced oscillation. This behavior is described and discussed in this section.

5.4.1 The observed explosion behavior

A shadow photograph of an oxygen bubble in liquid cyclohexane is shown in Fig. 5-24. These frames were recorded with the high speed video camera Kodak Ektapro HS. In this experiment the sensitivity of the optical measurements was not high enough to visualize the incident shock wave. Each frame had an exposure time of 37 μs. This time is about equal to the shock induced first oscillation of the bubble. The frame during which the bubble is suddenly altered, is interpreted to be the frame during which the shock wave impacted the bubble. Accordingly, the incident shock wave passed through the bubble at 0 μs. The pressure signal in the liquid phase is shown in Fig. 5-25. As shown in this figure the peak pressure of the incident shock wave was 74.3 bar.

After the shock wave impact, the bubble broke up into two new bubbles (see Fig. 5-24, frames at 0 μs to 593 μs). From these two bubbles the upper one remained in the position where the initial single bubble was situated and did not show any special behavior thereafter.

The second bubble was detached and removed away from the initial position during the frames at 0 μs – 593 μs. A simultaneous, spherical expansion at two edge positions of the bubble's volume was recorded during the frames at 926 μs to 1 037 μs. A new expansion is initiated at the center of the bubble's volume at 1 074 μs. At the end of this expansion the bubble is destroyed and disappears (see Fig. 5-24, frame at 2 259 μs). For reasons that are explained below, this behavior is interpreted as a two-step bubble ignition, i.e. a new type of bubble ignition and explosion. This new type is called bubble explosion type II.

This kind of bubble explosion was not coupled with a visible light emission, or the light emission was so weak that the camera could not clearly record it. Because of this, only the behavior of the bubble's volume can be used as a criterion to register this type of explosion. A difficulty rises from the fact that an expanding bubble is not necessarily an exploding one, since lower pressure in the liquid can also cause bubble expansion. Nevertheless based on Fig. 5-24 a clear argumentation can be given, as to if this behavior is caused by an explosion inside the bubble or not: As already described, in this experiment the initial bubble was broken into two parts. Of these two parts only one exploded. The fact that only this bubble expands while the other one nearby does not, shows that the pressure inside the liquid can not be the cause for this expansion.

This conclusion is justified also by the measured pressure signals (see Fig. 5-25), which did not register any rarefaction wave with a duration corresponding to the complete explosion behavior (i.e. about 400 μs). This leads to the conclusion that the observed bubble behavior should be caused by the pressure inside the bubble. This pressure rise must origin from a fast chemical reaction that releases considerable amounts of energy, i.e. an explosion.

The light shadow that remained in the position of the exploded bubble (see Fig. 5-25, frame at 2 259 μs) can be explained as soot inside the liquid, formed during the explosion. The ignition delay of the bubble explosion was determined by the optical measurements which showed a delay period of 25 frames, i.e. 926 μs, from the shock wave impact.

Experiments with the same system were conducted, during which more bubbles were simultaneously observed. Examples are presented in Fig. 5-26 and in Fig. 5-28 and are described below.

In Fig. 5-26 a group of four oxygen bubbles was recorded with shadow photography. The incident shock wave passed through the bubbles at 0 μs and had a peak pressure of 73.7 bar. One of these bubbles exploded according to the bubble explosion type II. The explosion behavior had the same stages as the one described above for the single bubble experiment.

In a similar experiment, which is presented in Fig. 5-28, a bigger cluster of bubbles was recorded. During the propagation of the detonation wave in the gas phase towards the surface of the liquid, both the bubbles and the liquid are becoming brighter. This effect reaches its maximum as the detonation wave reaches the surface of the liquid (Fig. 5-28, -99 μs) and is reduced rapidly thereafter, reaching an almost constant level. Bubble and liquid illumination caused by the light of the detonation wave propagating in the gas phase, was a common effect of the experiments investigating bubble explosions.

As in Fig. 5-26, each frame in Fig. 5-28 corresponds to 24.7 μs recording time. The frame during which the passage of the shock wave through the bubbles took place, is the first one in which the bubbles' form appears to be changed. Having identified the frame during which the detonation wave from the gas phase hits the liquid surface, the approximate time between these two events can be calculated. This time corresponds to the time calculated directly from the shock wave propagation velocity in the liquid and the distance between the surface of the liquid and the center of observation.

The incident shock wave passed through the bubbles at 0 μs and had a peak pressure of 104.4 bar. An unexpected expansion phase of the bubbles, i.e. bubble explosion, started at 741 μs. This expansion is evident in Fig. 5-28 (716 μs – 889 μs) and Fig. 5-30 (see curve A). It is interesting to note that as a result of the passage of the incident shock wave, breakage of all bubbles preceded this bubble behavior. Apparently all bubbles exploded. The ignition delay was 741 μs. The pressure signal that was measured in the liquid during this experiment is shown in Fig. 5-31.

For comparison with the experiments where pure oxygen was used as oxidizer, recorded by this high speed video camera, an experiment with nitrogen bubbles is presented in Fig. 5-29. The

light effect from the detonation wave in the gas phase reaches its maximum at the frame taken at 123 μs (Fig. 5-29), i.e. during this frame the detonation wave reached the surface of the liquid. The incident shock wave passed through the bubbles at 222 μs (frame not shown in Fig. 5-29). It had a peak pressure of 61.4 bar. Apart from bubble breakage (see Fig. 5-29, 296 μs - 420 μs), no special behavior was observed.

In Fig. 5-30 the change of total visible area of all oxygen bubbles as a function of the time from the shock wave impact is presented. This curve corresponds to the experiment of Fig. 5-28. The curve gives a qualitative information on the mean bubble diameter change as a function of the time. For comparison the corresponding curve from the experiment with nitrogen bubbles is also included in the diagram (curve (b)). It is interesting to note the two peaks that the curve for the oxygen bubbles presents. The existence of these two peaks on curve (a) may be connected with the two stages bubble explosion, that can be seen in Fig. 5-24 and Fig. 5-26.

From the examination of the relevant experiments it can be concluded that one characteristic feature of this type of bubble explosion is its two-steps ignition. The measured bubble ignition delays were typically above 600 μs, i.e. they are at least one order of magnitude longer than the ignition delays of bubble explosion type I.

The investigations did not reveal a range of bubble sizes inside which only one type of bubble explosion can take place in cyclohexane. On the other hand, according to the experimental results, the following three conditions were always fulfilled when the new type of explosion was observed:

i. the bubble did not ignite during the first shock induced oscillation (bubble explosion type I), and
ii. bubble breakage followed directly the incident shock wave impact, and
iii. there was an absence of a strong rarefaction wave in the liquid.

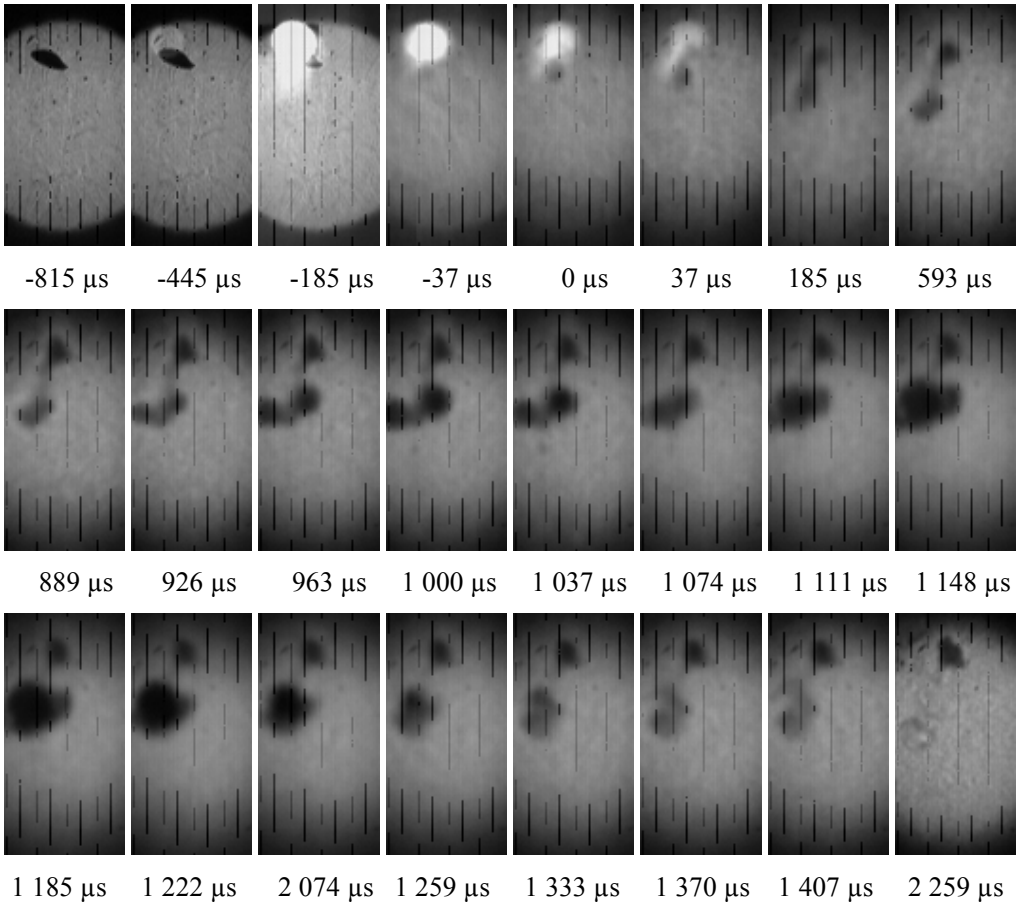

Fig. 5-24: The stages of a bubble explosion type II.

Shadow photography of a single oxygen bubble in liquid cyclohexane under shock wave impact. Incident shock wave impact on the bubble at 0 µs. Bubble ignition at 926 µs. Recording frame rate: 27 000 fps. The light emission that can be seen in the frames between –445 µs and 37 µs is caused by the reflection of the detonation wave on the surface of the liquid. The exposure time for each photo was 37 µs. The pressure signal is shown in Fig. 5-25. (Exp. No. 54)

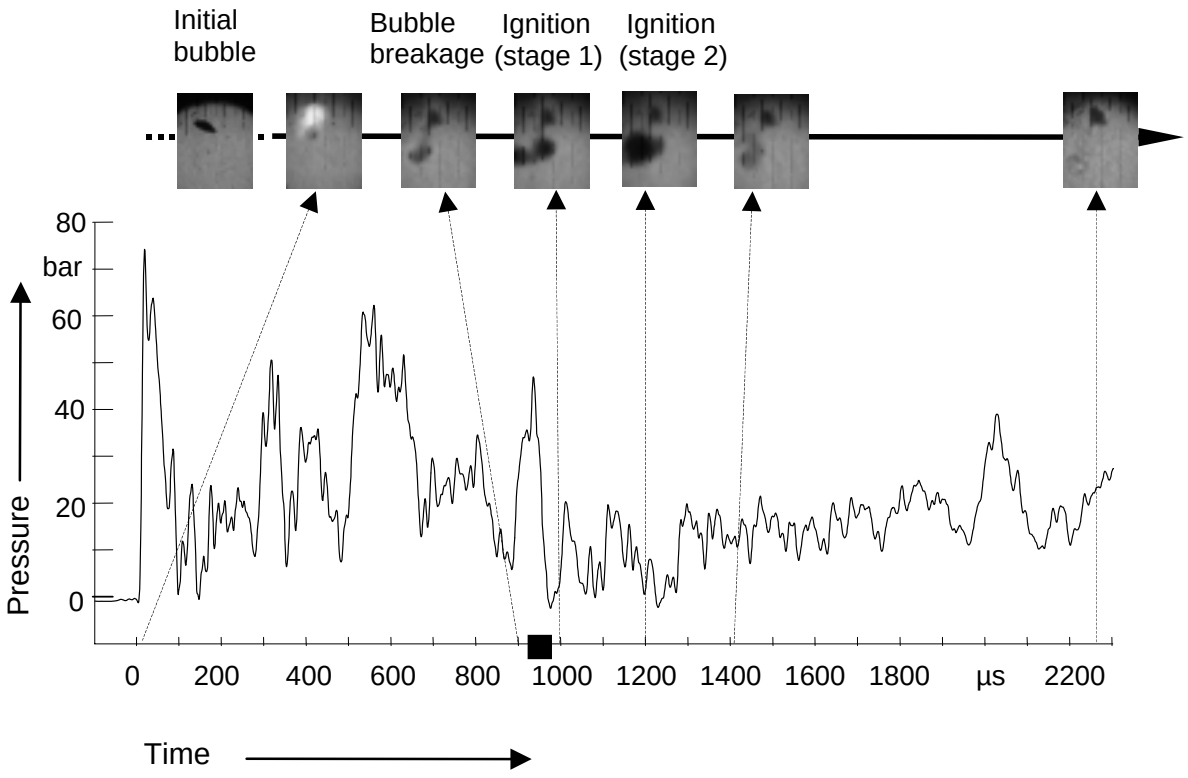

Fig. 5-25: Pressure signal from the experiment presented in Fig. 5-24.

The curve corresponds to the pressure in the liquid phase and was measured at the position 8.1 in Fig. 4-4. The time zero is the same as in Fig. 5-24, from which some frames are shown here too. The ignition moment at 926 µs is indicated by a rectangle. (Exp. No. 54)

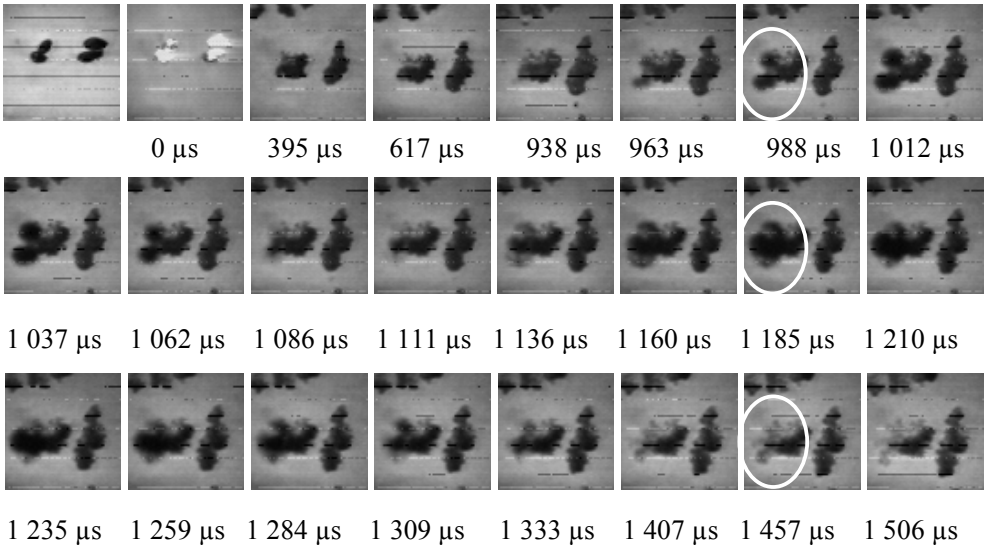

Fig. 5-26: Not all bubbles exploded (bubble explosion type II).

Shadow photography of four oxygen bubbles in liquid cyclohexane under shock wave impact. Incident shock wave impact on the oxygen bubbles at 0 µs. Bubble ignition delay: 963 µs. Peak pressure of the incident shock wave: 73.7 bar. Framing rate: 40 500 fps. Exposure time per frame: 24.7 µs. The pressure signal is shown in Fig. 5-27. (Exp. No. 101)

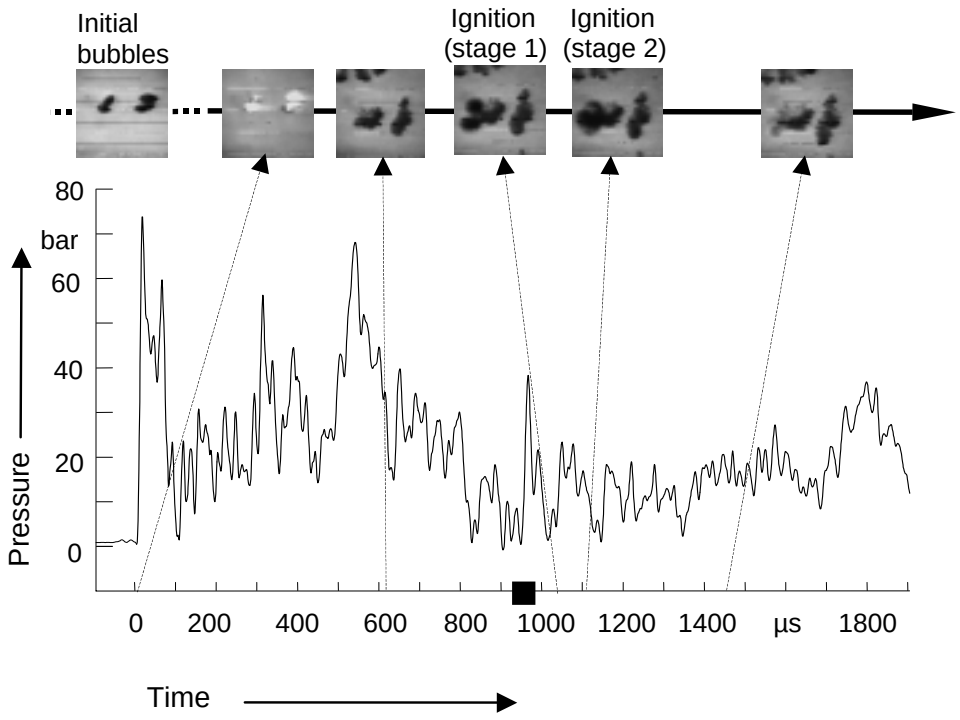

Fig. 5-27: Pressure signal from the experiment presented in Fig. 5-26.

The curve corresponds to the pressure in the liquid phase and was measured at the position 8.1 in Fig. 4-4. The time zero is the same as in Fig. 5-26, from which some frames are shown here too. The ignition moment at 963 µs is indicated by a rectangle. (Exp. No. 101)

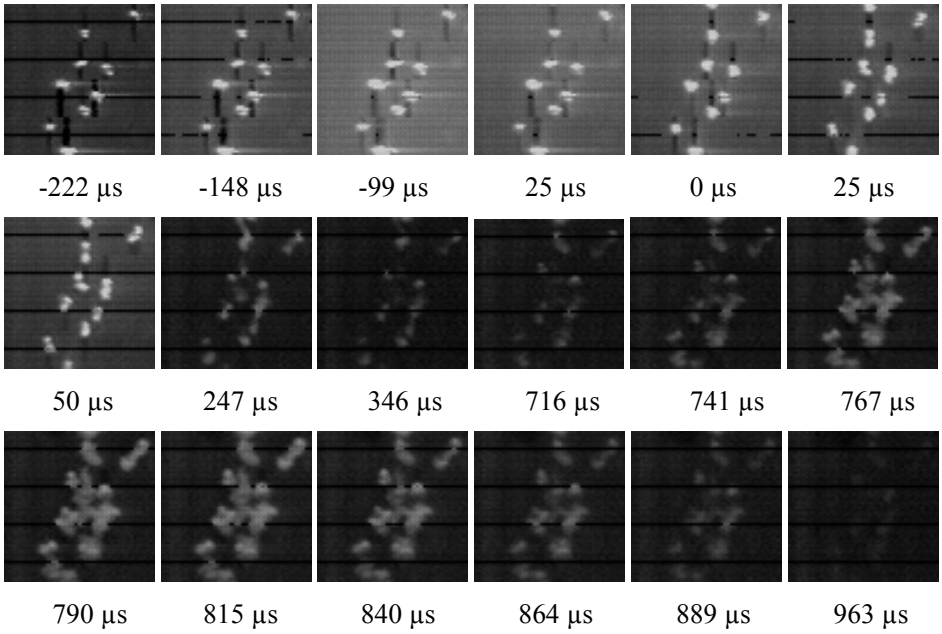

Fig. 5-28: A cluster of exploding oxygen bubbles in liquid cyclohexane (explosion type II).

High speed photography of a cluster of oxygen bubbles in liquid cyclohexane under shock wave impact. Shock wave passage through the bubbles at 222 µs. Peak pressure of the incident shock wave: 104.4 bar. Bubble ignition delay: 741 µs. Framing rate: 40 500 fps. Exposure time per frame: 24.7 µs. (Exp. No. 31)

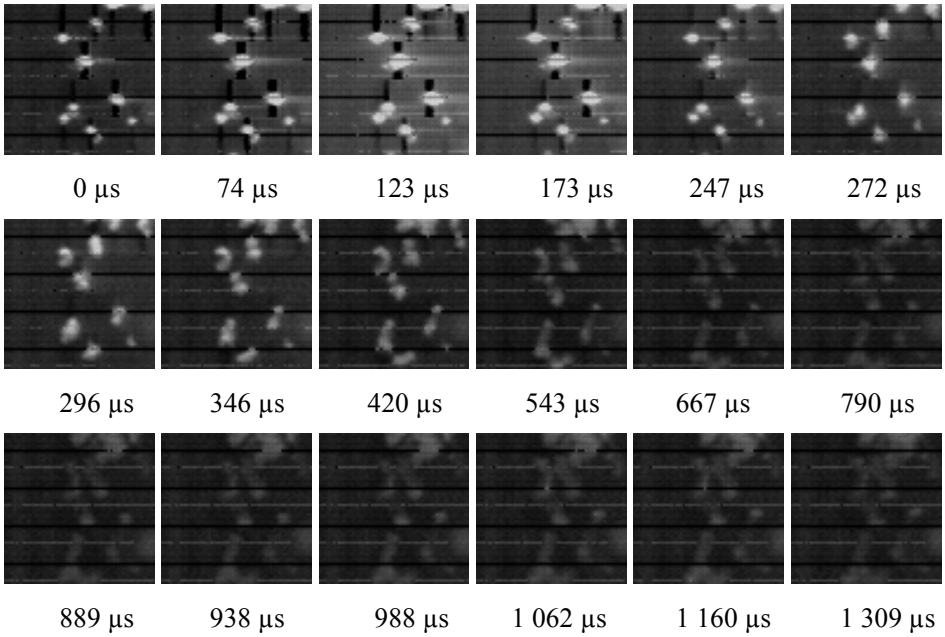

Fig. 5-29: A cluster of nitrogen bubbles in cyclohexane under shock wave impact.

Shock wave passage through the bubbles at 272 µs. Peak pressure of the incident shock wave: 61.4 bar. Framing rate: 40 500 fps. Exposure time per frame: 24.7 µs. (Exp. No. 45)

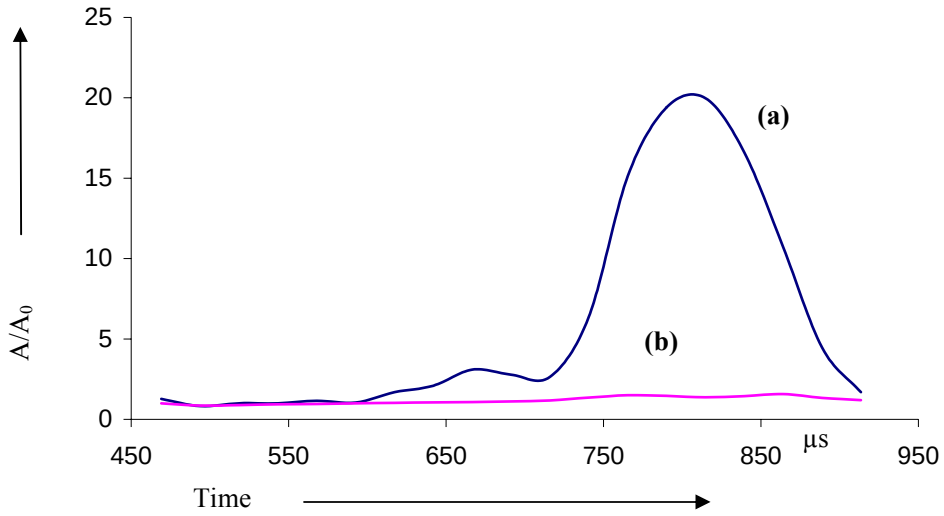

Fig. 5-30: Total bubble area as a function of time.

Diagram of total bubble area (A) divided with the initial bubble area (A_0), as a function of time after the shock wave impact for (a) the oxygen bubbles seen in Fig. 5-28 and (b) the nitrogen bubbles seen in Fig. 5-29. The total bubble area is defined as the sum of the projected area of all single bubbles on a recorded frame.

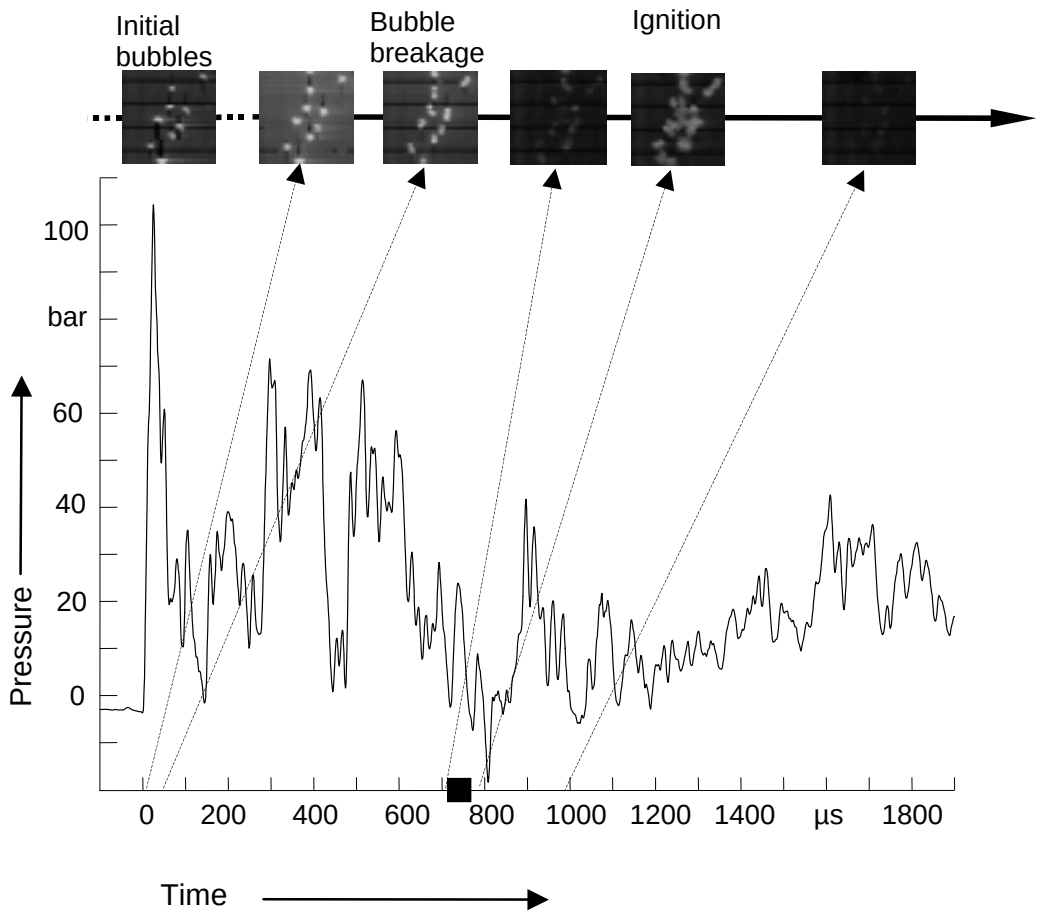

Fig. 5-31: Pressure signal from the experiment presented in Fig. 5-28.

The curve shows the pressure in the liquid phase and was measured at the position 8.1 in Fig. 4-4. The time zero is the same as in Fig. 5-28, from which some frames are shown here too. The ignition at 741 µs is indicated by a rectangle. (Exp. No. 31)

5.4.2 Discussion about bubble explosion type II

In this section the three observed conditions that always preceded the bubble explosion type II as well as its ignition delay will be discussed.

5.4.2.1 Bubble breakage before the explosion

The discussion at this point will start with the second of the three conditions mentioned in the last section. It is the observation that before a bubble explosion type II took place, shock induced bubble breakage always preceded. In §5.3.1 the experiments demonstrated that the direct result of a shock wave impact on a bubble is the mechanical compression of it. At some stage of this compression a penetrating jet may form. Investigations that are reported in the literature revealed that the jet size increases with shock wave amplitude and that the jet entrains the whole gas bubble when the pressure wave intensity is above a certain limit (see §2.1.2). If the jet formation is strong enough, its

penetration can result into the direct breakage of the bubble. An example of such a bubble breakage is shown in Fig. 5-11. Thus the second observed condition for bubble explosion type II, i.e. of bubble breakage, means that the incident shock wave was strong enough to divide the bubble through strong jet penetration.

5.4.2.2 Absence of bubble explosion type I

The first observed condition for the bubble explosion type II, is that the bubble was not ignited during the first shock induced oscillation (bubble explosion type I).

At this point the following scenario is considered. Two bubbles exist in the same system and are completely identical. Inside these two bubbles, after shock wave impact, a jet penetration takes place. Only one of them is broken by that penetration.

Based on the above discussion of the second condition of bubble explosion II to exist, it is reasonable to accept the following for the situation that corresponds to this scenario. The stronger of the two liquid jets, i.e. the one with more volume and faster propagation velocity, is that one which broke the bubble. Further it is reasonable to expect that inside the bubble with the stronger jet, i.e. the bubble that broke up, phenomena related to the jet penetration are more intense. These phenomena are related to mass and heat exchange processes and change of the gas concentration inside the bubble and are analyzed below.

Generally, penetration of any liquid jet through the bubble provides the inner part of it with amounts of the surrounding liquid in the form of micro-droplets (see Fig. 5-32). The number and the size of these micro-droplets depend on many parameters like the size of the jet, i.e. the area of the jet's surface, and its penetrating velocity. As reported in the literature review in Chapter 2, it is experimentally found that the propagation velocity of a shock induced jet inside a gas bubble is in the order of a few hundred of m/s. At these velocities the interaction between a gas phase and a surface of a liquid enriches the first with droplets having diameter in the range of 10 μm to 100 μm. This range has been calculated with the help of the semi-empirical equation in [104].

It is reasonable to expect that the high temperature inside the bubble during its compression, allows some or all of the liquid injected in the form of micro-droplets to be evaporated into the gas phase of the bubble. This means two things. First, because of the evaporation process, the temperature of the bubble's gas phase is reduced. Secondly, through the evaporation of the micro-droplets the gas phase is enriched in cyclohexane. These two phenomena intensify as the jet is stronger and produces more and smaller micro-droplets. As a result in a bubble the temperature is essentially lower and the amount of gaseous cyclohexane is significantly higher, compared to the case without strong jet formation and bubble breakage.

The explanation of the absence of ignition during the first shock induced oscillation, lies exactly on this point. Either the bubble's gas mixture is not explosive because it reaches the non explosive fat mixture area, or although it remains in the explosive area its temperature is not adequate

to initiate an ignition. This explains the absence of bubble explosion type I not only inside the bubble that broke up, but also inside the new bubbles formed after the bubble breakage.

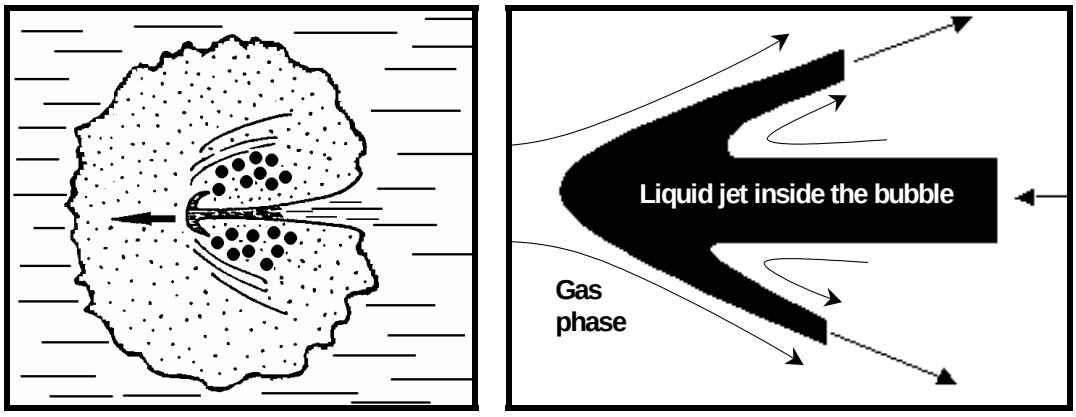

Fig. 5-32: Schematic of a liquid jet penetration through a bubble.

Drawing out of scale. The black spots represent clouds of micro-droplets produced by the penetration of the jet. The shape of the jet is drawn according to [105].

5.4.2.3 Long ignition delay

Before the discussion of the third -and final- observed condition for the bubble explosion type II, a reference on the observed relatively long ignition delay is useful at this point. In the experiments a relatively long time was needed (more than 600 μs) before the bubble explosion type II finally took place. It is an experimental fact that during this ignition delay the pressure in the liquid tends to reach lower levels. The pressure in the liquid at the moment of the ignition for the explosion type II, was in the experiments in the order of 10 bar – 20 bar (see for example Fig. 5-25).

Assuming a bubble saturated with cyclohexane vapor at initially high pressure, the decrease of the pressure in the liquid is transferred into a decrease in pressure inside the bubble. This means that the average bubble radius is becoming longer and therefore the gas temperature of the bubble is decreasing. Heat transfer phenomena on the bubble's surface (evaporation/condensation of cyclohexane, heat conduction) may also play a role. Mass transfer phenomena in both directions, i.e. evaporation and condensation, are expected to play an important role for these processes too. As the temperature decreases, the bubble loses amounts of gaseous cyclohexane which condenses.

Due to this condensation process even in the case of a non explosive fat mixture after the breakage, the gas phase of the bubble can become explosive again. The ignition can be initiated then by one of the pressure changes in the liquid (see for example the Fig. 5-25). It can be assumed that at the ignition point the bubble contains a very high fraction of gaseous fuel, that is limited by the vapor pressure of cyclohexane at the temperature of the gas phase inside the bubble.

In Fig. 5-33 the saturation concentration of cyclohexane in a bubble is shown at several temperatures and pressures. These concentrations were calculated by the equation [97]:

$$\ln(P_v) = -9.200978 \cdot \ln(T) - \frac{6354.898}{T} + 75.65058 + \frac{T^2}{7.374814} \cdot 10^6, \qquad \text{(eq. 5-6)}$$

where P_v is the vapor pressure of cyclohexane in kPa, and T is the temperature in K.

This equation is valid for temperatures between 280 K and 554 K. In this equation the influence of the curvature of the bubble's surface on the vapor pressure is neglected.

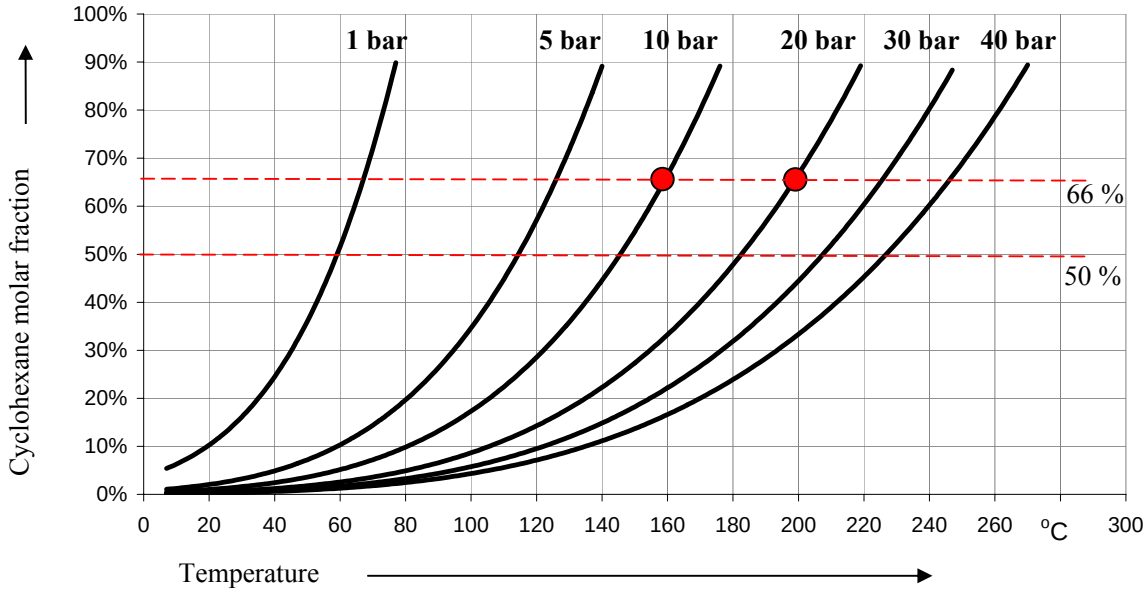

Fig. 5-33: Saturation concentration of cyclohexane in a bubble.

This graph shows the molar fraction of saturated cyclohexane inside an oxygen bubble at several temperatures and pressures. The lines at 66 % and 50 % denoted on the graph, correspond to the measured upper explosion limit at a temperature of 150 °C and at a pressure of 5 bar and 1 bar respectively.

5.4.2.4 Explosion limits inside the bubble

For the discussion of the experimental observations of bubbles containing gaseous oxygen and cyclohexane, it is useful to know the explosion limits of the corresponding gaseous mixture. Especially interesting is to know these limits at pressures in the range of 10 bar – 20 bar and at elevated temperatures, i.e. at the conditions at which the bubble explosion type II was initiated.

No explosion limit of cyclohexane inside pure oxygen is known in the literature. Because of this, in the frame of this work, the explosion limits of cyclohexane in oxygen were measured. The measurements were performed according to the standard device and procedures described in [106]. Details of these measurements are described in [107]. The conditions for the measurements were: A pressure of 1, 2, 3 or 5 bar at a temperature of 25 °C and 150 °C. The measured explosion limits in cyclohexane are summarized in Table 5-10.

These measurements show that the upper explosion limit increases with increasing pressures, at the same temperature. For example in Table 5-10 it can be seen that at 150 °C the

cyclohexane upper explosion limit in oxygen increases from a molar fraction of 50 % at 1 bar, to 66.2 % at 5 bar. The same kind of influence has also an increase of the temperature. Apart from that it was found that near the upper limits large amounts of soot were produced from the explosion.

Table 5-10: Explosion limits of cyclohexane in oxygen at 25 °C and 150 °C.

UEL stands for Upper Explosion Limit and LEL for Lower Explosion Limit. The composition given in molar fraction. NA stands for non applicable. The UEL at 25 °C exceeds the vapor pressure of cyclohexane.

Pressure	**Temperature**	**LEL**	**UEL**
bar	**°C**	**%**	**%**
1 - 5	25	1.1	NA
1	150	0.9	50.0
2	150	0.9	55.6
3	150	0.9	57.8
5	150	0.9	66.2

According to these results and because the bubble explosion type II corresponds to the ignition of cyclohexane-rich mixtures, the explosion should produce significant amounts of soot. Furthermore the upper explosion limit of cyclohexane inside the bubble's gas phase at the point of ignition (bubble explosion type II) must lie above the value of 66.2 % in molar fraction. This is valid only in the case that the trend for the pressure dependence of the UEL measurements continues in the pressure range above 5 bar.

5.4.2.5 Absence of rarefaction wave

The third observed condition for the bubble explosion type II was the absence of a strong rarefaction wave in the liquid (see §5.4.1). An investigation of the behavior of gas bubbles in such waves, was performed and is presented in §5.5.2. It was found that inside the pressure field of a rarefaction wave, a bubble expands homogeneously (see Fig. 5-40). Such an expansion results into a strong decrease of the temperature in the bubble. Without adequate levels of temperature the bubble then does not ignite, even if its mixture is explosive.

5.4.3 Summary

A new type of bubble explosion, not reported in the literature before, was described and discussed above. This type of bubble explosion takes place at a much later time after the first shock induced bubble oscillation. In this work it is named *bubble explosion type II* and it was observed in some of the experiments only.

This kind of bubble explosion was not coupled with a visible light emission, or the light emission was so weak that the camera could not clearly record it. Because of this, only the behavior of the bubble's volume can be used as a criterion to register it. The observations showed that bubble explosion type II took place only when:

i. the bubble did not ignite during the first shock induced oscillation (bubble explosion type I), and
ii. bubble breakage followed directly the incident shock wave impact, and
iii. there was an absence of a strong rarefaction wave in the liquid during the observation time.

One characteristic feature of the bubble explosion type II is its two-steps ignition. The measured bubble ignition delays were typically above 600 μs, which is at least one order of magnitude longer than the ignition delays of bubble explosion type I.

The condition of bubble breakage means that the incident shock wave was strong enough to violently divide the bubble due to strong jet penetration.

This strong jet penetration results also in the absence of ignition during the first shock induced oscillation. Either the bubble's gas mixture is not explosive because it exceeds the upper explosion limit, or although it remains in the explosive area its temperature is not adequate to initiate ignition. This is because inside a bubble, the temperature is essentially lower and the amount of gaseous cyclohexane is significantly higher, compared to the case without strong jet formation and bubble breakage. This explains the absence of bubble explosion also inside the new bubbles formed after the bubble breakage.

As the temperature inside the bubble decreases, the gas phase of the bubble loses amounts of gaseous cyclohexane by condensation. Due to this process even in the case of a non explosive fat mixture after the breakage, the gas phase of the bubble can become explosive again. A strong pressure perturbation inside the liquid at that time could result in a bubble ignition.

Since the bubble explosion type II corresponds to the ignition of cyclohexane-rich mixtures, experimental measurement of the explosion limits of gaseous cyclohexane-oxygen mixtures were performed. Near the upper explosion limit (UEL) the explosion produced significant amounts of soot. This is expected to take place also inside the bubble during the bubble explosion type II.

The explanation of the third observation that there was an absence of a strong rarefaction wave in the liquid, is as follows. Experiments showed that inside the pressure field of a rarefaction wave, a bubble expands homogeneously (see Fig. 5-40). Such an expansion results into a strong decrease of the temperature in the bubble. Without adequate levels of temperature the bubble then does not ignite, even if its gas is explosive.

5.5 Pressure behavior inside the liquid after shock wave impact

The present section differs fundamentally from the previous sections in two aspects. On the one hand, the discussion will be based not on an additional group of experiments, but on all groups of experiments that have been discussed up to this point. On the other hand, the discussion will be focused mainly on the behavior of the pressure in the investigated system.

The goal of the discussion in this section is to give an insight on the structure of the measured pressure signals in the liquid and that of the pressure field near the bubbles. The goal is to analyze and to understand how this structure was created in the experiments. For this reason the discussion is based not only on the pressure signals of the experiments, but also on optical recordings of experiments. Because of their importance in this study, the spherical shock waves created by the bubble explosions will be discussed in detail too.

At this point it is helpful to remind pieces of information that have already been mentioned in the work, and are useful for a better understanding of the discussion that follows. The discussion about the pressure behavior inside the system during the experiments was initiated in §5.1, when the detonation in the gas phase and the behavior of the liquid's surface after the detonation impact was discussed. In §5.3.3.3 the question of which properties of the incident shock wave in the liquid are related to bubble explosions and can be extracted by the measured pressure signals, was answered.

Apart from that information, the following should be noted as background information. The calculated propagation velocity of the shock wave inside the bubbly medium had a value in the experiments close to the sonic velocity of 1 280 m/s [93] in liquid cyclohexane. Some spread of this velocity between the experiments was observed too (see Appendix D, Table 7-7). This spread can be explained by the variation of the parameters that have an influence on it (e.g. the existence of bubbles, eventual temperature variation) and by eventual errors of the measurement method.

Another interesting information at this point is the fact that the shock wave in the liquid had always a higher pressure peak than the detonation wave in the gas phase. This is a result of the rebound of the detonation wave initially on the surface and later on the bottom of the autoclave. In the experiments the impact of the detonation wave on the surface created a shock wave in the liquid with peak pressure that was higher up to 2.3 times than the one in the gas phase. The reflection of this wave at the bottom of the autoclave generated a new shock wave with a peak pressure of up to 3.2 times more. These calculations are based on pressure measurement at the positions 4.2, and 8.1 and on the bottom of the autoclave as denoted in Fig. 4-4.

It is well known that the pressure of a reflected wave depends on the pressure of the shock wave (or detonation wave) that is reflected. The pressure after the reflection of weak shock waves on solid media is typically increased by a factor of 2 [78]. It should be noted here that the

refracted wave inside the second, more dense, medium has initially the same amplitude in pressure as the reflected wave.

In the case of a gas detonation impact on the liquid inside the autoclave, the surfaces between the gas and the liquid and the liquid and the bottom of the autoclave, denoted in Fig. 5-34 by (Pos. I) and (Pos. II) respectively, are the positions where the maximum loading is expected to appear. The measured pressures in the gas phase and in the liquid in front of the observation window and on the bottom of the autoclave are presented in Appendix D, Table 7-6.

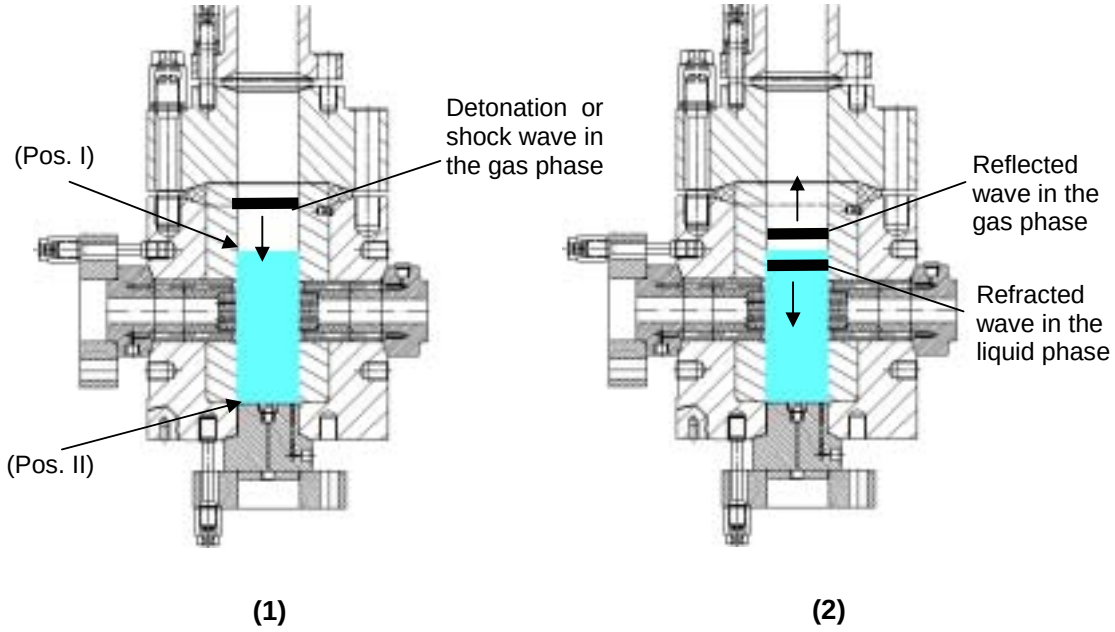

Fig. 5-34: Shock or detonation wave reflection on the surface of the liquid, inside the autoclave.

This drawing illustrates the system (1) before and (2) after the reflection of a shock wave on the surface of the liquid. The reflected wave has a pressure amplitude that is higher than the original shock wave that was reflected. The refracted wave inside the liquid has initially the same pressure as the reflected wave. In the experiments this effect took place not only at the surface between the gas and the liquid phase (Pos. I) but also at the surface between the liquid and the autoclave, at the bottom (Pos. II).

5.5.1 Pressure fields

In a discussion about the behavior of the pressure in the liquid, the interaction between the detonation wave in the gas phase and the autoclave's metallic walls can not be neglected. This interaction creates shock waves in the metallic walls of the autoclave during the propagation of the detonation wave in the gas phase, i.e. already before its reflection on the liquid's surface.

These waves propagate through the walls at sonic velocity, which is essentially higher than the propagation velocity of the detonation wave in the gas phase. In steel the sonic velocity is

about 6 000 m/s [93]. As a result, weak waves are constantly generated in the liquid before and after the arrival of the shock wave which is created by the detonation impact on the liquid's surface. In the experiments these waves were not strong enough to be clearly registered by the pressure sensors, but they were recorded optically when the optical method was sensitive enough. An example is presented in Fig. 5-35.

In this figure the overlapping of at least three different types of inhomogeneous pressure fields are shown. First a pressure field which exists in the liquid already before the ignition of the gas phase. It is created by the flow of the bubbles. The generated local pressure gradients are so weak that they were not visualized by the applied optical method. What was visualized in the photos, is the slow movement of the liquid due to this pressure gradients (see Fig. 5-35, 0 µs).

The second field is created by the shock waves emission from the autoclave's walls after the gas detonation, as described above and can be seen in Fig. 5-35 at 85 µs. The third is the structure of the incident shock wave (see Fig. 5-35, 185 µs). Because of the high sensitivity of the optical method in this experiment, and because of the complex structure of the incident shock wave, it is practically impossible to recognize the position or the shape of the bubbles after the passage of this wave. For this reason, the sensitivity of the optical method was adjusted to lower levels for the investigations of bubble explosions.

By adjusting the parameters of the optical method it is possible to visualize a fourth source of pressure waves too. The compression and expansion of the bubbles, with or without explosion, creates these additional pressure waves. For an example of such a shock wave emission by the expansion of a nitrogen bubble, see bubble No. 2 in Fig. 5-11, 38 µs. It should be noted that in the case of a bubble that explodes, the emitted spherical wave has a higher amplitude. This situation will be discussed below in more detail. The spherical pressure waves emitted by the bubbles are according to [101] of sinusoid-like form and have not only a positive but also a negative phase.

Indications for the negative phase of these pressure waves were recorded in many of the conducted experiments with exploding bubbles. One example is presented in Fig. 5-36. In this figure oxygen bubbles under shock wave impact are presented. At 0 µs the shock wave is near the first bubbles. At 28 µs a weak explosion of the bubble No. 1 is recorded. At 30 µs, 34 µs and 37 µs the bubbles No. 2; No. 3 at the same time with No. 5 and the bubble No. 4 exploded. The spherical shock waves that are emitted by the bubble explosions are also visible on these frames. At 45 µs cavitation micro-bubbles at their maximum diameter can be seen in the volume between the bubbles. At the same time the gas bubbles in the frame expand.

These cavitation bubbles are indicated by the white arrows on the frame and are interpreted to be a clear indication for an overlapping of the negative phase of the pressure waves emitted by the reported bubble explosions. At 64 µs the cavitation bubbles are not visible anymore, and also the expansion phase of the gas bubbles is completed, meaning that the negative phase of the pressure has been completed.

The term “negative pressure”, i.e. a pressure with negative amplitude, should not be confused with the term “under-pressure”, i.e. a pressure that is less than the one in the surrounding environment. The existence of negative pressure -and therefore of negative pressure waves- in liquids, is scientifically a well understood phenomenon. For more information see for example [108]. The influence of negative pressure in liquids to safety aspects in several different systems, has been investigated in many studies. Two examples of such studies can be found in [109] and [110]. The piezoelectric pressure sensors used in this work were not constructed to measure negative pressure and therefore it was not possible to investigate this phenomenon in the experiments.

Finally it should be noted that in the frame of this work the role of the inhomogeneous pressure field created by the bubbles movement in the liquid as well as the weak pressure waves emitted from the autoclave’s walls were not taken into consideration during the evaluation of the experiments. The reason for this, is that it was assumed that they have a negligible role to the bubble explosion behavior, which is the main topic of this study.

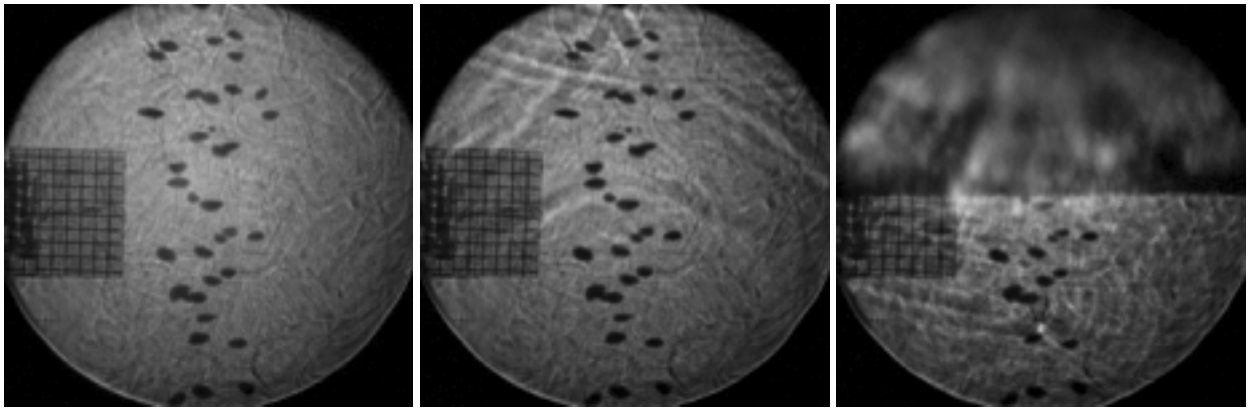

Fig. 5-35: Visualization of the complicated structure of the pressure field inside the liquid.

Oxygen bubbles under shock wave impact. The pressure field generated from the bubbles movement, the autoclave’s walls and the incident shock wave are visualized in these frames. Shadow photography was applied at a framing rate of 200 000 fps. (Exp. No. 58)

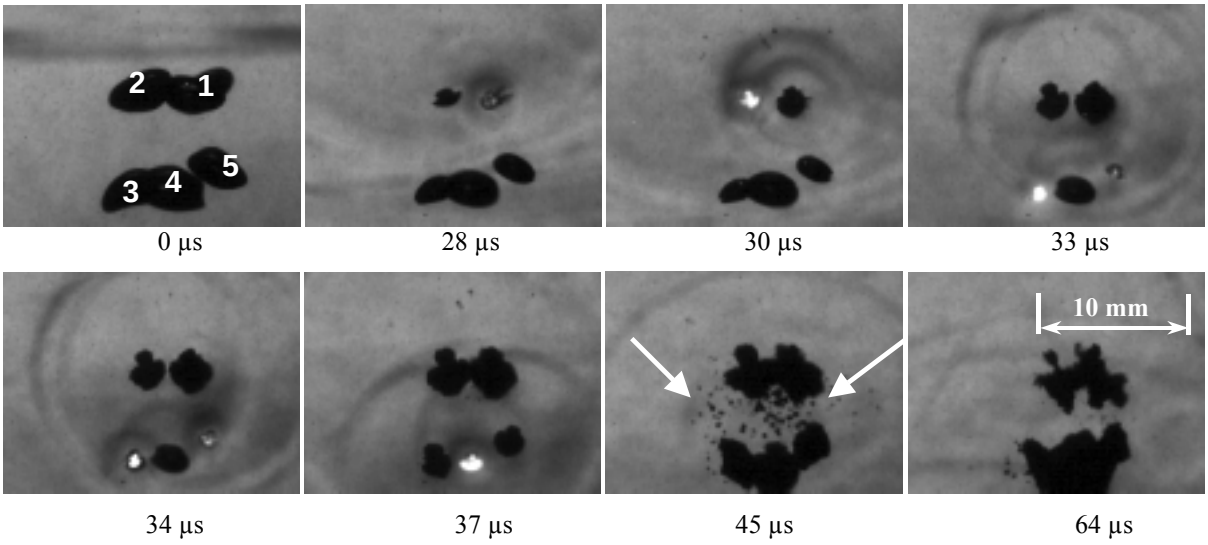

Fig. 5-36: Pressure waves created by bubble explosions.

Oxygen bubbles in cyclohexane. (0 µs) – The incident shock wave just before it contacts the first bubbles. The arrows at 45 µs indicate the liquid's volume containing cavitation micro-bubbles, at their maximum diameter. (Exp. No. 137)

5.5.2 Structure of the pressure signal in the liquid after shock impact

In the section just above, the different pressure fields that overlap inside the liquid and near the position of the bubbles, were discussed based on optical recordings. Here the measured pressure signals in the bubbly liquid will be discussed. More precisely, the discussion will focus on the structure of these signals and its influence on the behavior of the bubbles.

It is important to know as background information that a shock wave propagating in a liquid with bubbles, has an oscillatory structure. This is a known characteristic feature of bubbly liquids (see e.g. [59] - [61], [111]). This feature is illustrated in Fig. 5-37 for three different cases. In Fig. 5-37 (i) the evolution of a pressure step into its final steady form is sketched; Fig. 5-37 (ii) indicates the development of the shock wave into a train of solitons as a result of the action of a negative wave packet; Fig. 5-37 (iii) shows the evolution of a negative wave packet. Since the speed of the single peaks increases with amplitude, they move up the slope of the rarefaction wave.

As is already described in this work, after the impact of the detonation wave on the surface of the liquid, the generated shock wave inside the liquid propagates towards the bottom. It is then reflected as shock wave at this position, returning back to the surface. At the surface it is reflected as a rarefaction wave and returns to the bottom again. The next reflection at the surface creates a new shock wave. Given that the pressure waves propagate with the sonic velocity inside the liquid, i.e. 1 280 m/s [93], these reflections should create a periodic change between shock wave (positive phase) and rarefaction wave (negative or zero phase) inside the liquid until they fade out. And in deed this effect was observed in the experiments, independent of the existence of gas bubbles inside the

liquid. This is because although an adequate number of bubbles inside the liquid can change the structure of the pressure signal, as illustrated in Fig. 5-37, the existence of the subsequent positive – negative phases can not be prohibited. Because of space limitations, the discussion will now focus only on the case that the liquid contained bubbles.

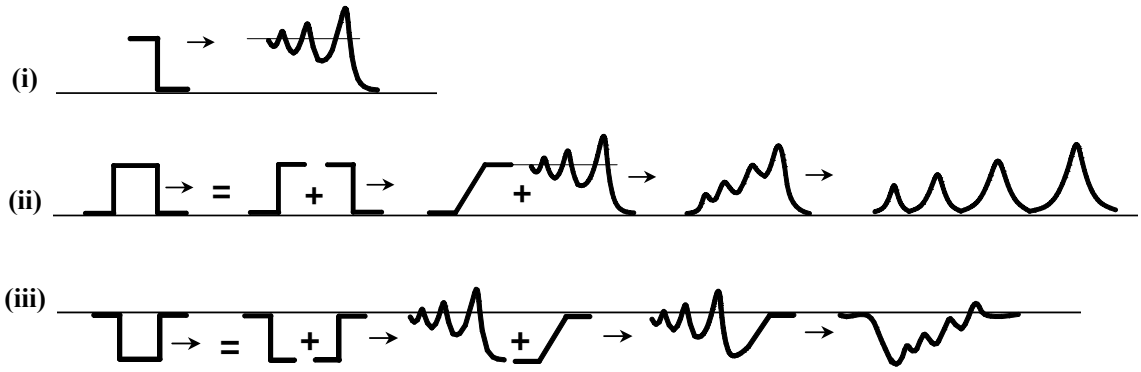

Fig. 5-37: Construction of wave shapes in a bubbly medium (inert bubbles).

(i) Steady positive step wave (shock wave); (ii) The positive wave packet finally develops into a train of (steady) solitons; (iii) Negative wave packet: Solitons finally creep up the slope of the rarefaction wave. The wave shapes correspond to the suggestion in [111].

An example of this type of pressure behavior in liquid cyclohexane with oxygen bubbles is presented in Fig. 5-39. In Fig. 5-38 a schematic of the autoclave showing the position of the liquid's surface and the positions of the pressure measurements is presented. The liquid was cyclohexane and the bubbles were created by injection of gaseous oxygen into the liquid.

In Fig. 5-39 the following parts of the signal can be recognized: The shock wave peak pressure that was created from the detonation impact on the surface propagating towards the bottom of the autoclave (pos. 1); the reflection on the bottom propagating towards the surface (pos. 2) first passing in front of the observation window (pos. 3). After the shock wave impact at the surface, it is reflected as rarefaction wave propagating towards the bottom. This rarefaction wave is recorded first by the pressure sensor at the level of the windows (pos. 4) and then by the sensor at the bottom of the autoclave (pos. 5). The structure is distorted after a few reflections as the pressure wave in the liquid becomes weaker and the influence of the pressure behavior in the gas phase, more important.

The existence of strong rarefaction waves with relatively long duration in the system, as the one shown in Fig. 5-39 for example, creates effects that should be taken in consideration during the evaluation of the experiments. An obvious effect is that, during the duration of such relatively strong rarefaction waves, cavitation bubbles can be produced inside the bubbly liquid. Such a behavior can be seen in Fig. 5-40. The behavior of the gas bubbles under these conditions was investigated. It was observed that during cavitation conditions the diameter of all gas bubbles is significantly altered. As a result of this change their inner temperature and pressure falls, making a bubble explosion impossible during cavitation.

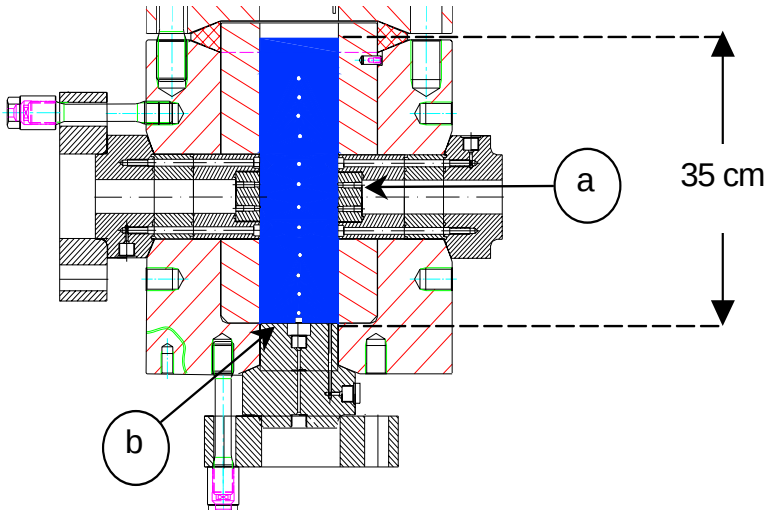

Fig. 5-38: Cut out of the autoclave.

This schematic shows the position of the pressure sensors for the pressure measurements during the Exp. No. 85, presented in Fig. 5-39.

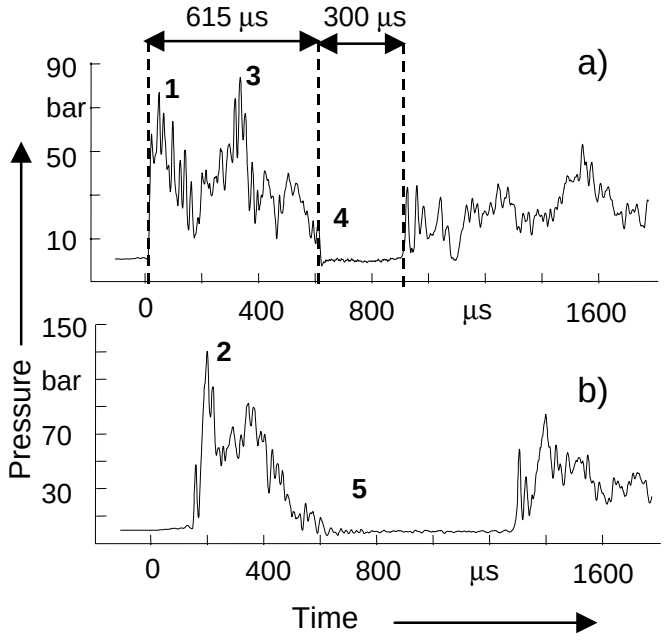

Fig. 5-39: Pressure signals recorded during an experiment were the bubbly liquid (O_2 bubbles in cyclohexane) had cylindrical volume.

The pressure curves (a) and (b) were measured at the positions (a) and (b) in Fig. 5-38 respectively. The numbers on both signals indicate the sequence of the pressure wave passage from the two pressure sensors. The geometry of the autoclave was cylindrical (windows length: 184 mm)and the height of the liquid 35 cm. (Exp. No. 85)

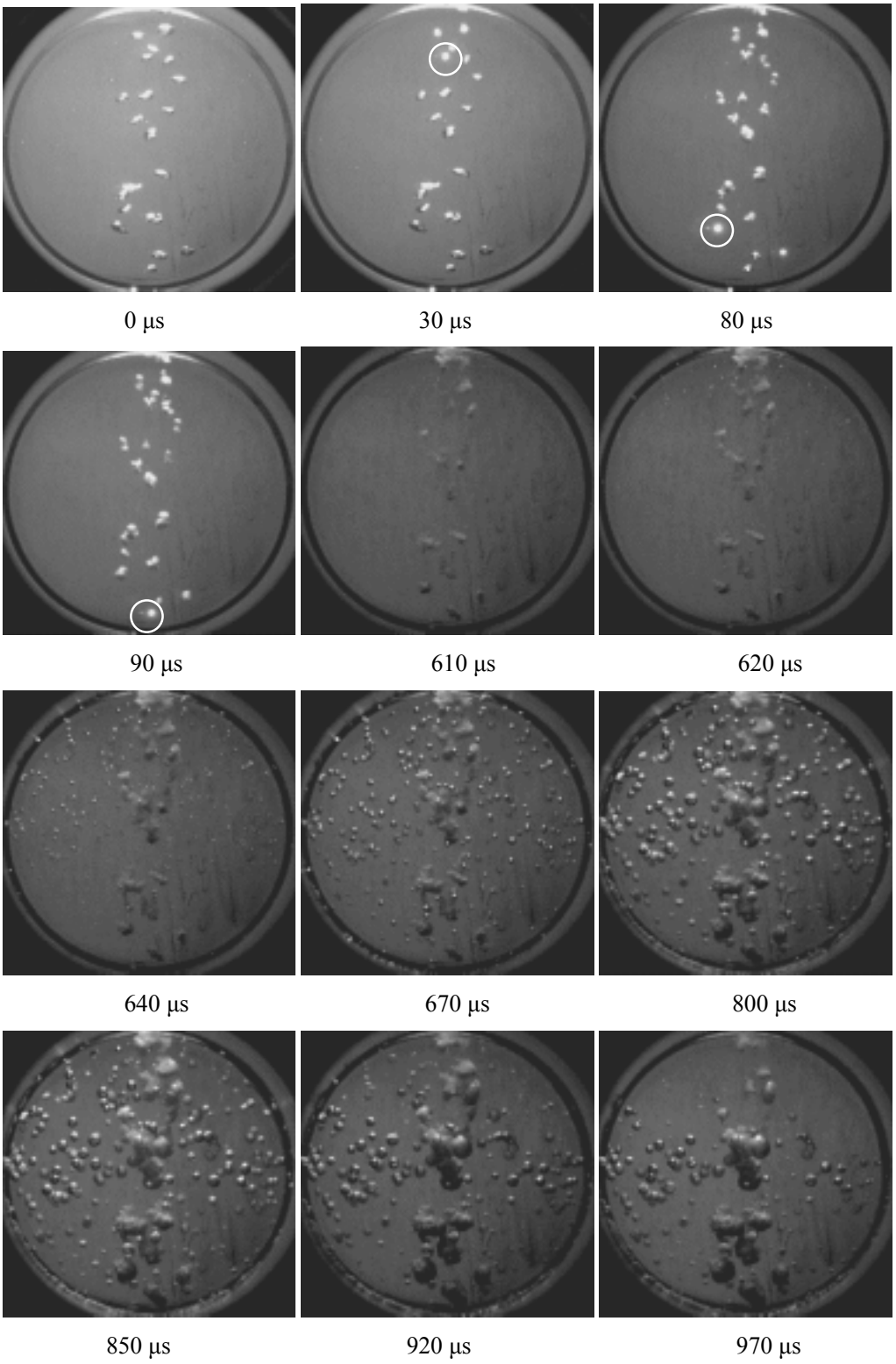

Fig. 5-40: Oxygen bubbles in cyclohexane under shock wave and subsequent rarefaction wave impact.

The white circles indicate exploding bubbles. The observation area had a diameter of 90 mm. Windows of type 3 were used (windows length: 184 mm, see Fig. 4-7). Time zero corresponds to the moment the shock wave entered the observation window. The pressure in the liquid is the curve (a) in Fig. 5-39. The cavitation bubbles appear (620 µs) and start to disappear (920 µs) together with the low pressure. (Exp. No. 85)

Influence of the geometry of the autoclave

The pressure structure in the liquid was discussed above only for the case in which the internal volume of the autoclave that contained the liquid was cylindrical, i.e. the windows that were used were of the type 3 (length: 184 mm), as denoted in Fig. 4-7. Of the 162 experiments that contained liquid (with or without bubbles), 90 experiments were performed with this type of windows. The rest of the experiments were performed with windows of type 2 (length: 144 mm, see Fig. 4-7) mounted, apart from 5 experiments in which windows of type 1 (length: 40 mm) were used.

In Fig. 5-41 the pressure signals measured in an experiment in which windows of type 1 (40 mm length) were used, is presented. The system consisted of liquid cyclohexane containing oxygen bubbles. In this figure it is not possible to clearly recognize parts of the signal that would correspond to the parts described for the pressure signals in Fig. 5-39. The pressure signals in Fig. 5-41 appear to be without a clear structure pattern, i.e. subsequent positive and negative (or zero) pressure phases were not registered. After the passage of the incident shock wave, the pressure inside the liquid tends to oscillate around -and finally reach- a value, which is the pressure of the gas phase after the detonation. In the experiments this value was about 10 bar to 30 bar at about 1 ms after the incident shock wave passage.

The optically recorded behavior of the system is presented in Fig. 5-42. In this figure the white circles indicate bubble explosions after the passage of the shock wave. In contrast to what was observed in Fig. 5-40, no cavitation bubbles were recorded in this experiment. This observation is in agreement with the absence of long negative (or zero) pressure levels that was observed in the pressure signals of the experiments, as described above.

Similar observations were made in all the experiments where the internal volume of the autoclave containing the liquid was not cylindrical. It is expected that the difference in the behavior is caused by the change of the geometry. This creates a more complicated pressure signal in the liquid due to more complex pressure wave reflections in the volume.

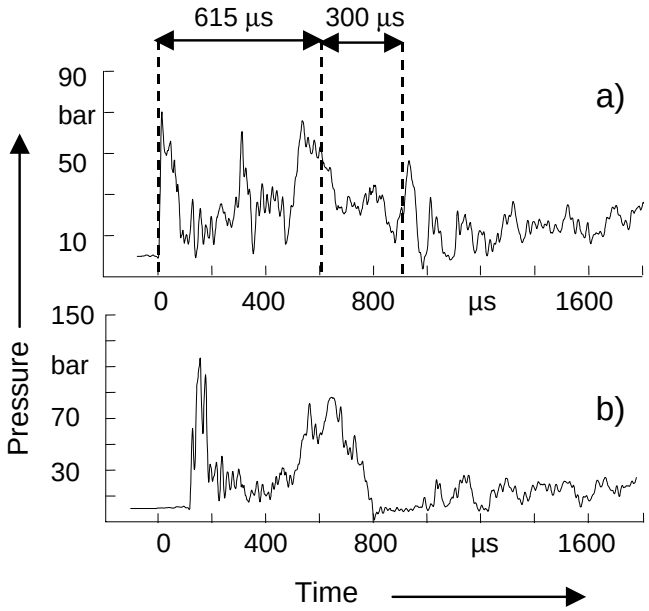

Fig. 5-41: Pressure signals recorded during an experiment during which the liquid had no cylindrical volume.

The pressure curves (a) and (b) were measured at the positions (a) and (b) in Fig. 5-38 respectively. The geometry of the autoclave was not cylindrical (windows length: 40 mm) and the height of the liquid was 35 cm. For comparison reasons with Fig. 5-39, the times 615 µs and 300 µs later have been pointed. (Exp. No. 100)

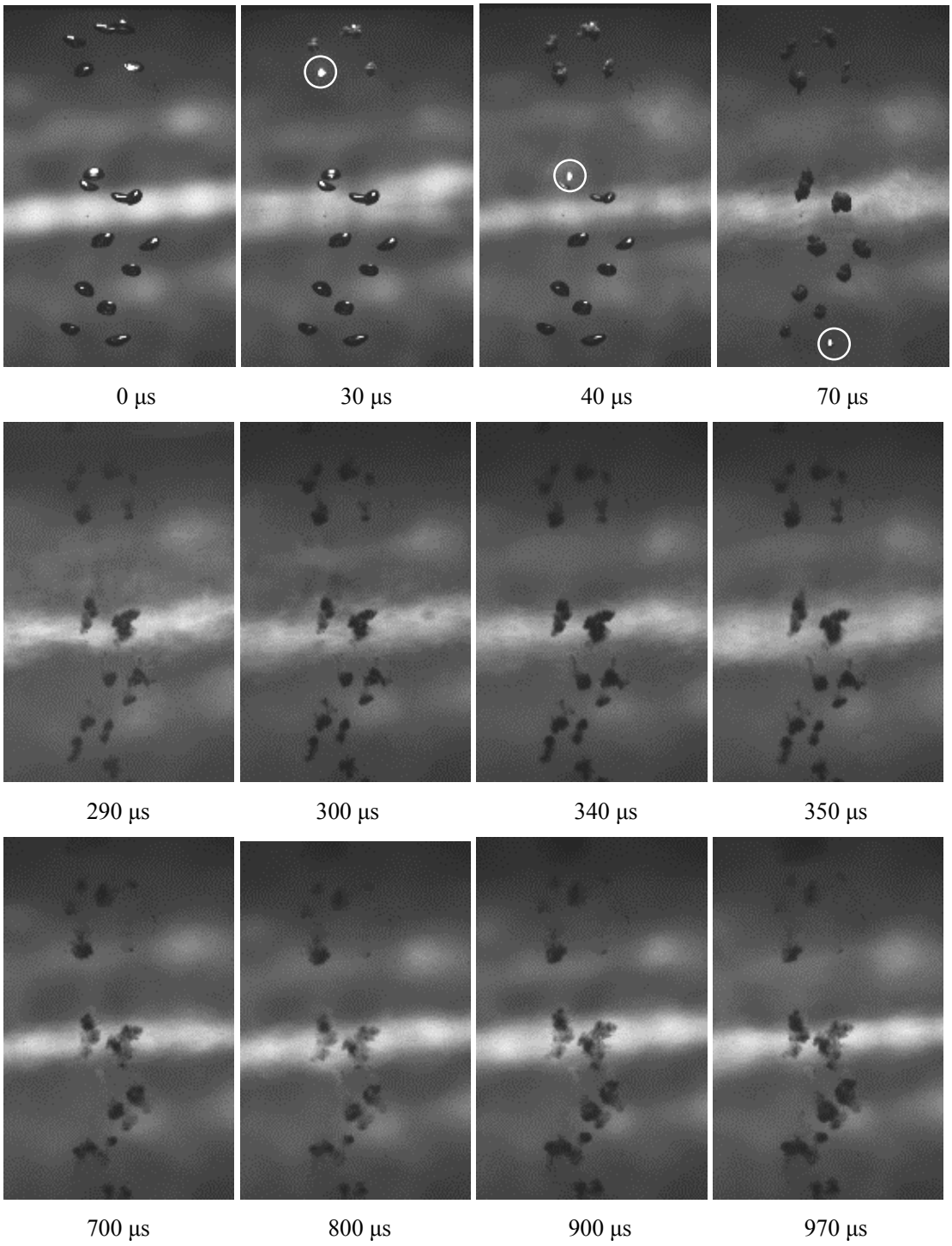

Fig. 5-42: Oxygen bubbles in cyclohexane under shock wave without subsequent rarefaction wave impact.

The white circles indicate exploding bubbles. The bubbles had an initial diameter between 3 mm and 3.5 mm. Windows of type 1 were used (windows length: 40 mm see Fig. 4-7). The framing rate was 100 000 fps. Time zero corresponds to the moment the shock wave entered the observation window. The pressure in the liquid is presented by the curve (a) in Fig. 5-41. (Exp. No. 100)

5.5.3 Shock waves caused by bubble explosions

In all the performed experiments, an identification by pressure measurements of the shock waves emitted by either of the two registered bubble explosion types was not possible. The reason for this must lay on the fact that the pressure waves from the single bubble explosion had to travel a relatively long distance (of the order of 5 cm) to meet the pressure sensors, making the damping effect important. The amplitude loss of the spherical pressure waves from the single bubble explosions as they propagate in the liquid can be described by the equation [101]:

$$P_{SW_L} = P_{SW_0} \frac{r^*}{L} \qquad \text{(eq. 5-7)}$$

where: P_{SW_0} is the initial pressure of the shock wave after the bubble explosion; P_{SW_L} is the pressure of the shock wave after distance L from the bubble's center and r^* is the radius of the bubble at the moment of explosion.

In order to understand the order of magnitude of this effect, it is assumed that a bubble of 3 mm in diameter explodes at $r/r_0 = 1/3$ and is situated 5 cm from the pressure sensor. These numbers correspond to a typical situation in the experiments. From (eq. 5-7) follows that less than 1 % of the initial pressure peak of this explosion will arrive at the pressure sensor. A measurement of this shock wave was practically impossible, because of the fact that the structure of the pressure inside the liquid (background pressure signal) had a very intense oscillatory structure. This structure is independent of the single bubble explosion shock waves. Stochastic processes have a strong influence in its properties too.

5.5.4 Summary

In the above sections of §5.5 the experimentally observed behavior of the pressure in the investigated system was presented and discussed.

First, the calculated properties of the propagating shock wave inside the gas and liquid phase of the system of (O_2 / N_2) bubbles in liquid cyclohexane, were presented. It was shown that the measured propagation velocity of the shock wave inside the bubbly medium had a value in the experiments close to the sonic velocity inside the pure liquid. Some spread of this velocity between the experiments was observed and is explained by the variation of the parameters that have an influence on it (e.g. the number and the spatial distribution of bubbles, fluctuation of the room temperature) and by eventual errors of the measurement method.

Secondly, in the experiments the impact of the detonation wave on the surface created a shock wave in the liquid with peak pressure that was higher up to 2.3 times than the one in the gas

phase. The reflection of this wave at the bottom of the autoclave generated a new shock wave with a peak pressure of up to 3.2 times more.

Thirdly, the evaluation of the experiments showed that during the observed bubble explosion behavior at least four different types of inhomogeneous pressure fields co-existed inside the liquid. These pressure fields were:

i. The pressure field which exists in the liquid already before the ignition of the gas phase and is created by the flow of the bubbles;
ii. the pressure field created by the shock waves emission from the autoclave's walls after the gas detonation;
iii. the pressure field created by the incident shock wave during its passage through the liquid; and
iv. the pressure field created by the spherical pressure waves which are emitted by the compression and expansion of bubbles. These waves are of sinusoid-like form and have not only a positive but also a negative phase. In the case of a bubble that explodes, the emitted spherical wave has a higher amplitude.

The inhomogeneous pressure field created by (i) the bubbles movement inside the liquid, as well as by (ii) the weak pressure waves emitted from the autoclave's walls, were not taken into consideration during the evaluation of the experiments. It is assumed that they had a negligible role to the bubble explosion behavior inside the investigated system.

The structure of the pressure inside the liquid during and after the incident shock wave's passage is also discussed. Its oscillatory structure is in agreement with the corresponding observations described in the literature. Apart from the oscillations, the positive to zero pressure level changes, i.e. the shock wave to rarefaction wave changes, and their duration are explained according to the sources of shock wave reflections inside the autoclave.

It was observed that during strong rarefaction waves with relatively long duration in the system cavitation bubbles can be produced inside the bubbly liquid. During cavitation conditions the diameter of all gas bubbles is significantly increased, making a bubble explosion impossible.

The influence of the internal geometry of the liquid's vessel was investigated experimentally. It was found that asymmetries in the volume, vertical to the propagation direction of a rarefaction wave, disturb or destroy the latter. Because of this reason, the variation of the windows length, resulted into significantly different pressure structures inside the liquid. The use of windows with a length of 40 mm (windows type 1) resulted into the absence of rarefaction waves and absence of cavitation bubbles.

Because of their importance, the spherical shock waves created by the bubble explosions were investigated in more detail. It was estimated that of the initial pressure peak of a bubble explosion only 1 % or less arrived at the pressure sensor. Even this 1 % could in principle be

recognizable by the pressure sensors that were used in the experiments. But such a recognition was practically impossible, because of the fact that the structure of the pressure inside the liquid caused by the passage of the incident shock wave (background pressure signal) had a very intense oscillatory structure. This structure is independent of the single bubble explosion shock waves. Stochastic processes have a strong influence in its properties too. These reasons did not allow the measurement of the bubble explosion pressure waves.

6 Conclusions and implications for safety engineering

The behavior of an organic liquid with or without the existence of bubbles, exerted to the impact of a detonation wave on its surface, was investigated. The experiments were performed in liquid cyclohexane, and in some experiments also in liquid cumene, 2-ethylhexanal, or methanol. The bubbles inside the liquid phase were created by the injection of pure N_2, or O_2, or mixtures of them. As was shown by calculation, the bubbles in the experiments were saturated in vapor of the surrounding liquid before the shock induced compression. High speed photography and pressure measurements were applied. Bubble explosions inside these organic liquids were investigated for the first time.

The evaluation of the experiments showed two different types of bubble explosion. These are called bubble explosion type I and type II respectively. A main difference between these two types is their ignition delay. The bubble explosion type I takes place during the first oscillation after the shock wave impact. The bubble explosion type II, on the other hand, takes place with much longer ignition delay.

Bubble explosion type I

The experiments for the bubble explosion type I showed that the ignition delay increases with increasing bubble size, but it remained always less than one hundred microseconds. The experimental observations showed also that an increase in the pressure of the shock wave which impacts the bubble leads to shorter bubble ignition delays. The ignition delay of single bubble explosions is important because it is connected with the properties of self-sustaining bubble detonation waves.

For the understanding of single bubble dynamics after shock wave impact, the pressure that forces a bubble to shrink and to ignite should be estimated for each bubble separately. A good estimation of this pressure is important also in order to define the critical pressure below which, bubble ignition does not occur. A method how to make this estimation is proposed in this study.

Apart from the pressure that compresses the bubbles, explosion ranges can be defined according to many other parameters also. Two of them are the bubble diameter and the composition of the gas inside the bubble. These parameters were among those systematically varied in this work.

It was found experimentally that an incident shock wave in liquid cyclohexane with a peak pressure of 85 bar ± 8.5 bar ignited oxygen gas bubbles saturated with cyclohexane vapor, with equivalent initial diameters between 2.4 mm and 7.2 mm. The experiments that correspond to these results were performed at room temperature. Explosion of bubbles with an initial equivalent diameter below 1.5 mm was not observed in this system.

Limits according to the nitrogen concentration inside an oxygen gas bubble, saturated with cyclohexane vapor were also measured in liquid cyclohexane. The fraction of bubbles that

explode decreases, as the molar fraction of nitrogen inside the bubbles increases. Bubbles saturated in cyclohexane vapor containing initially a N_2 / O_2 gas mixture with N_2 molar fraction 0.79 were ignited. No bubble explosion was observed when a N_2 molar fraction of 0.90 was used instead. The initial pressure of the system was 1 bar.

An interesting observation is that not all bubbles exploded, even though they were of the same diameter and of the same gas composition, compared to others that exploded during the same experiment. Because of this reason, any bubble explosion limits should be measured according to the behavior of groups of similar bubbles and not of single bubbles.

Another important finding from the experiments is that if the distance between two bubbles is short enough, then the generated shock wave after the explosion of the one can ignite the second. Optical recordings that show this kind of interaction between bubbles are presented and discussed for the first time. This behavior was observed in liquid cyclohexane.

These optical recordings prove the following. The penetration of a shock wave created by a bubble explosion into another bubble nearby, can create inside the latter such high temperatures that can ignite it. This information together with theoretical calculations allow a realistic estimation of the pressure amplitude of the spherical shock waves emitted by bubble explosions type I.

A rough estimation, which takes into account also the measured pressure signals in the liquid, was performed. According to this estimation, the spherical shock waves, at the moment of their emission from the corresponding exploding bubble, did not exceed the value of three to four thousand bar. It is expected that pressure waves of that amplitude pose locally a potential hazard for the corresponding equipment (e.g. due to surface destruction of materials).

The properties of the shock waves caused by bubble explosions could not be measured during the experiments. This was, on the one hand, due to the intensive damping of their peak pressure as they propagate; on the other hand, due to the simultaneous existence of additional sources of shock waves in the liquid. As a result the measured pressure signals had a very complex structure, inside which shock waves from bubble explosions could not be identified with confidence.

Additionally, the experimental finding that bubbles can be ignited by shock waves emitted from nearby bubble explosions, indicates that a process of synchronization of bubble explosions can occur. This synchronization process offers a better understanding of the propagation mechanism of self-sustaining bubble detonation waves inside bubbly media.

Apart from that, in the experiments where bubble explosion type I was investigated, ignition took place not only when the bubble contained initially an explosive gas mixture, but also in the case of an initially non explosive fuel-lean gas mixture. The explosion of these initially non explosive gas mixtures was observed in liquid 2-ethylhexanal or cumene at 1 bar and room temperature. The

corresponding experiments indicate that during the bubble compression an enrichment in vapor of the surrounding liquid through shock induced jet penetration occurs.

Bubble explosion type I was observed in liquid cyclohexane, 2-ethylhexanal, cumene and methanol. The differences in the values of their physical properties, most important of them being their viscosity, did not result to a significantly altered bubble explosion behavior.

Bubble explosion type II

The bubble explosion type II is a phenomenon that takes place in a much larger time scale than that of bubble explosion type I. It was observed occasionally in cyclohexane (it was not investigated in other liquids) and only under certain conditions. This type of explosion is reported for the first time.

The experiments showed that the mechanism of the bubble explosion type II is as follows. An initially explosive gas bubble is enriched with molecules of the organic solvent through shock induced jet penetration. This enrichment leads to the formation of a non explosive fuel-rich gas mixture inside the bubble. This gas mixture enters then the explosive range through condensation, before its ignition by a shock wave inside the liquid. This is the first experimental proof that bubbles can be ignited even if they contain at some stage a gas mixture that is above the upper explosion limit. It is expected that such an ignition mechanism will occur also inside bubbles of an initially non explosive fuel-rich gas mixture.

This proof combined with the finding described above from bubble explosion type I that a fuel-lean non explosive gas bubble can explode, leads to an important safety related conclusion. The conclusion is that a bubble explosion can be induced by shock wave impact independently if the bubble's gas phase is initially explosive or not. This result has an implication for the hazard assessment of the relevant systems, because the latter will have to include the phenomenon of bubble explosion, independently of the system conditions, provided that an organic solvent and an oxidizer co-exist in the system.

Because the bubble explosion type II has a relatively long ignition delay, it may be impossible for this type of explosion to cause the formation of a self-sustaining bubble detonation wave. This question remains though still open.

Shock induced behavior of the liquid's surface

In the experiments the shock induced behavior of the liquid's surface was also investigated. It was found that the existence of bubbles near the liquid's surface added local sources for aerosol creation. When the number of the bursting bubbles was adequate, a liquid film on the walls around the surface was observed too. These effects are important for the safety assessment of similar systems.

Behavior of the pressure inside the liquid phase

The experiments demonstrated also that the behavior of the pressure inside the liquid had some safety related features. One of them is the experimental observation that the shock wave in the liquid had always a higher pressure peak than the detonation wave in the gas phase. This is a result of the rebound of the detonation wave initially on the surface and later on the bottom of the autoclave. The impact of the detonation wave on the surface created a shock wave in the liquid with a peak pressure that was up to 2.3 times higher than that of the detonation wave in the gas phase. The reflection of this wave at the bottom of the autoclave generated a new shock wave with a peak pressure of up to 3.2 times higher than the one before the reflection. Such multiplication factors must be taken into consideration when safety aspects of multiphase systems are considered.

The rebound of the shock wave inside the liquid at the bottom of the autoclave and at the liquid's surface caused also another effect. Positive to zero pressure level changes, i.e. shock wave to rarefaction wave changes, were measured in the experiments in which the autoclave had a cylindrical internal volume. This effect can result into cavitation phenomena inside the system, as was optically recorded in the experiments.

The influence of the internal geometry of the liquid's vessel on the existence of cavitation was investigated. It was found that asymmetries in the cylindrical volume of the liquid, vertical to the propagation direction of a rarefaction wave, disturb or eliminate this wave. This finding may have practical application for the construction of equipment inside which the absence of cavitation is important.

7 APPENDIX

A. Enrichment of a gas bubble with vapor molecules due to diffusion

In this section, the process of molecular diffusion of solvent molecules in a bubble in liquid cyclohexane will be calculated. The calculation is based on the following assumptions:

(i) The bubble is a sphere with constant radius α.

(ii) The initial concentration of cyclohexane in the sphere is zero.

(iii) The diffusion process is radial.

(iv) At r = α interfacial equilibrium holds, i.e. the vaporization process is much faster than the difussion process.

(v) The molecular diffusion coefficient D and the equilibrium concentration of cyclohexane in the bubble C_{eql} are constant. C_{eql} is limited by the vapor pressure of the cyclohexane in the bubble.

(vi) The second Fick's law for diffusion applies.

For spherical coordinates and in the case of diffusion in the sphere, when the initial and surface conditions are such that the surfaces with the same mixture composition are concentric spheres and thus the cyclohexane concentration inside the sphere depends only upon the coordinates r and t, and Fick's law takes the form:

$$D \cdot \left[\frac{\partial^2 C}{\partial r^2} + \frac{2}{r} \cdot \frac{\partial C}{\partial r} \right] = \frac{\partial C}{\partial t} \qquad \text{(eq. 7-1)}$$

The solution for the concentration of cyclohexane in the bubble, C(r,t), under the above mentioned assumptions, can be derived by the (eq. 7-1). The solution of this type of equation can be found in the literature, (e.g. see p.233 (equation 4) in [112]), and is:

$$\frac{C(r,t)}{C_{eql}} = 1 + \frac{2 \cdot \alpha}{\pi \cdot r} \cdot \sum_{n=1}^{\infty} \frac{(-1)^n}{n} \cdot \sin \frac{n \cdot \pi \cdot r}{\alpha} \cdot e^{-D \cdot n^2 \cdot \pi^2 \cdot t / \alpha^2} \qquad \text{(eq. 7-2)}$$

In Fig. 7-1 (eq. 7-2) is graphically represented.

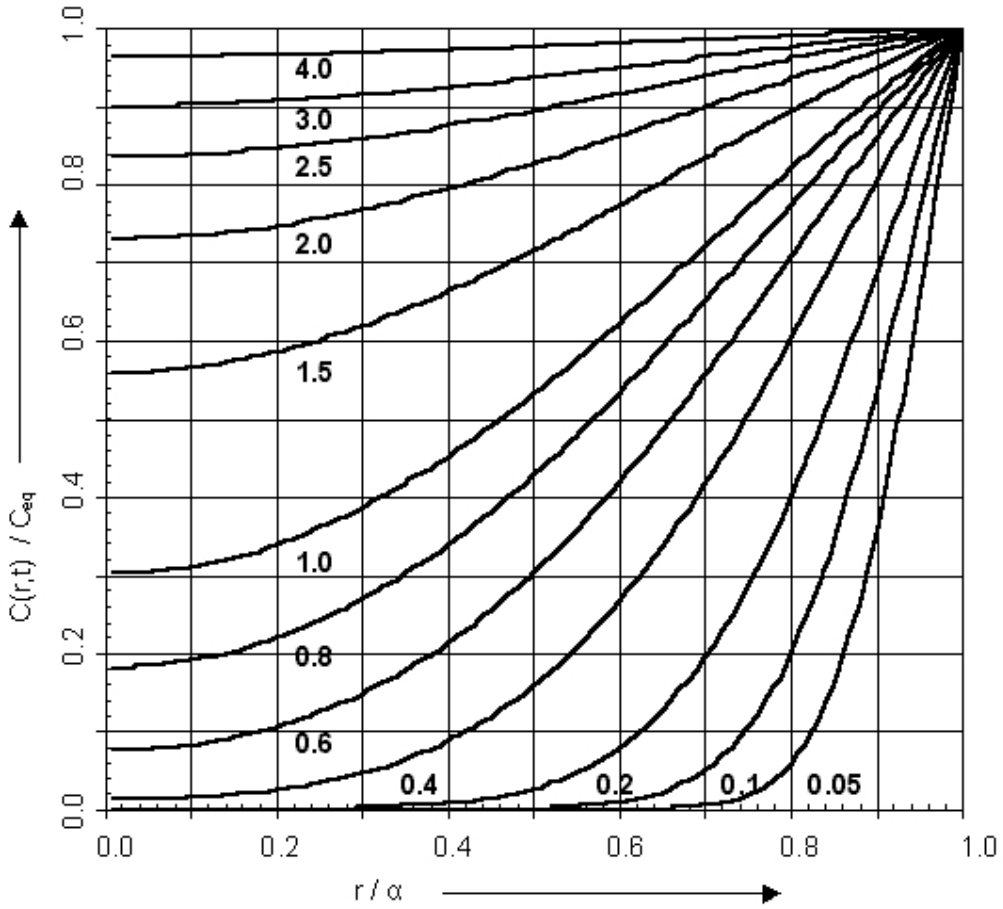

Fig. 7-1: Concentration distribution as a function of time and position

This graph presents the concentration distribution at various times in a sphere of radius α with zero initial concentration and equilibrium concentration C_{eql}. The number on the curves are the values of t/τ_D (t = time, τ_D = characteristic time - see text below).

It can be proven from (eq. 7-2) that the average concentration in the sphere, C_{av}, is:

$$\frac{C_{av}}{C_{eql}} = 1 - \frac{6}{\pi^2} \cdot \sum_{n=1}^{\infty} \frac{1}{n^2} \cdot e^{-n^2 \cdot \frac{t}{\tau_D}} \qquad \text{(eq. 7-3)}$$

where: $\tau_D = \frac{\alpha^2}{\pi^2 \cdot D}$ (eq. 7-4)

The time τ_D is called the characteristic time of the process. After time τ_D the average concentration in the bubble has reached about 77 % of the equilibrium point. After time $3\tau_D$, the average concentration in the bubble has reached 97 % of the equilibrium point, i.e. it is practically in equilibrium. In Table 7-1 calculated values of C_{av}/C_{eql} for some typical values of t/τ_D are presented.

Table 7-1: Calculated values of C_{av}/C_{eql} for some typical values of t/τ_D.

t/τ_D	C_{av}/C_{eql}	t/τ_D	C_{av}/C_{eql}
0.001	0.045	2.000	0.918
0.010	0.105	3.000	0.970
0.100	0.310	4.000	0.989
0.200	0.421	5.000	0.996
0.500	0.610	6.000	0.998
1.000	0.774	7.000	0.999

From (eq. 7-2) the concentration at the center of the spherical volume, C_{center}, can be shown to be:

$$\frac{C_{center}}{C_{eql}} = 1 + 2 \cdot \sum_{n=1}^{\infty} (-1)^n \cdot e^{-n^2 \cdot t/\tau_D} \qquad \text{(eq. 7-5)}$$

B. Temperature decrease inside a hot bubble due to heat conduction

The process of heat conduction from an initially hot bubble to the surrounding liquid will be described in this section. More precisely, equations will be derived that calculate the temperature at the center of the bubble and the average temperature of the bubble as a function of time. Apart from that, the characteristic time of the conduction process and important properties of the gaseous mixture inside the bubble at different conditions and gas compositions will be calculated. The calculation of heat conduction is based on the following assumptions:

(i) The bubble is a sphere with constant radius α.

(ii) The initial temperature T_0 is spatially uniform inside the bubble.

(iii) The surrounding liquid's temperature T_1 is constant, and $T_1 < T_0$.

(iv) The thermal diffusivity κ is constant.

(v) The conduction process is radial.

(vi) The Fourier's law for conduction applies:

$$dQ/dt = -\lambda \cdot A \cdot (dT/dx), \qquad \text{(eq. 7-6)}$$

where: dQ/dt is the rate of heat flow; A is the area at right angles to the direction in which the heat flows; $-dT/dx$ is the temperature gradient; and λ is called thermal conductivity and is a characteristic property of the material through which the heat is flowing and varies with temperature.

For spherical coordinates and in the case of heat flow in the sphere, when the initial and surface conditions are such that the isothermal surfaces are concentric spheres, and the temperature thus depends only upon the coordinates r and t, (eq. 7-6) takes the form [112]:

$$\kappa \cdot \left[\frac{\partial^2 T}{\partial r^2} + \frac{2}{r} \cdot \frac{\partial T}{\partial r} \right] = \frac{\partial T}{\partial t} \qquad \text{(eq. 7-7)}$$

The solution for the temperature inside the bubble, T(r,t), under the above mentioned assumptions, can derived by the (eq. 7-7). The solution of this type of equation can be found in the literature, (e.g. see p.235 in [112], equation of case IV, modified to correspond to T_2 surface temperature instead of zero):

$$\frac{T(r,t) - T_1}{T_0 - T_1} = -\frac{2 \cdot \alpha}{\pi \cdot r} \cdot \sum_{n=1}^{\infty} \frac{(-1)^n}{n} \cdot \sin \frac{n \cdot \pi \cdot r}{\alpha} \cdot e^{-\kappa \cdot n^2 \cdot \pi^2 \cdot t / \alpha^2} \qquad \text{(eq. 7-8)}$$

In Fig. 7-2, (eq. 7-8) is graphically represented.

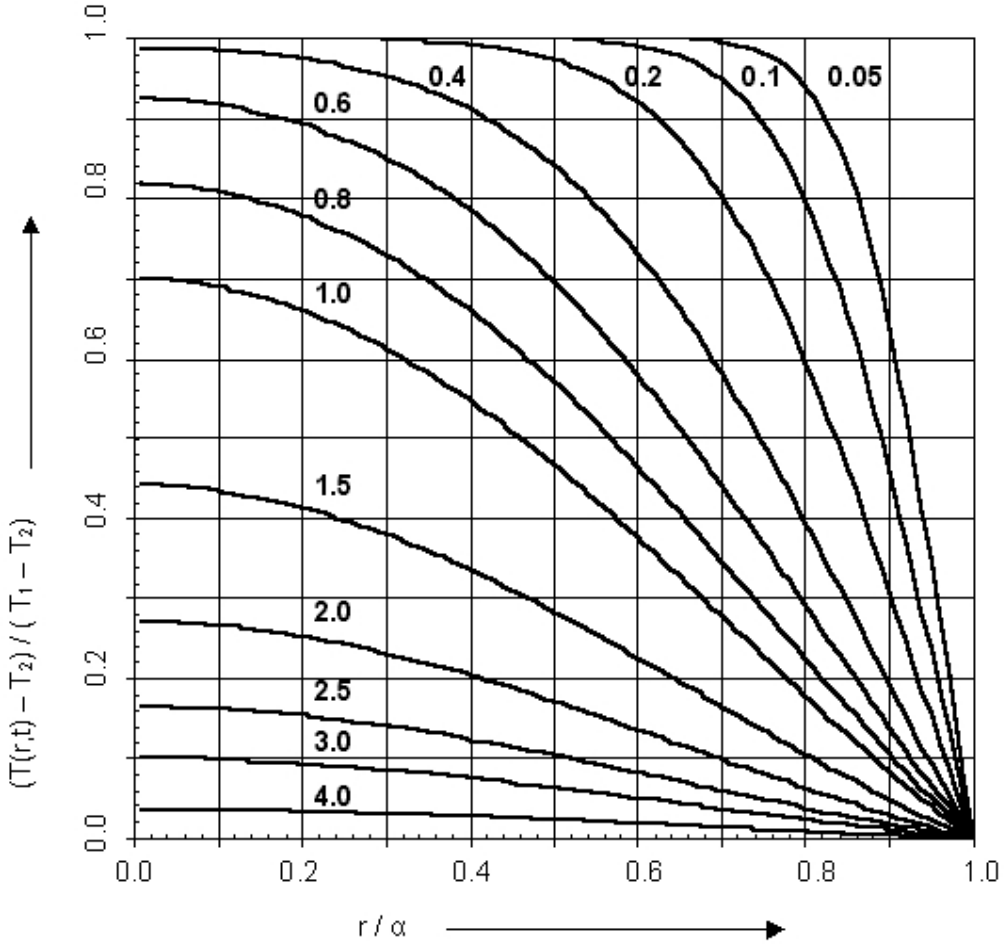

Fig. 7-2: Temperature difference distribution as a function of time and position

This graph presents the temperature difference distribution at various times in a sphere of radius α and at an initial temperature T_0, which is inside a liquid of temperature T_1. The number on the curves are the values of t/τ_C (t = time, τ_C = characteristic time - see text below).

It can be proven from (eq. 7-8) that the average temperature inside the sphere, T_{av}, is:

$$\frac{T_{av}-T_1}{T_0-T_1}=\frac{6}{\pi^2}\cdot\sum_{n=1}^{\infty}\frac{1}{n^2}\cdot e^{-n^2\cdot t/\tau_C} \quad , \qquad \text{(eq. 7-9)}$$

where: $\tau_C=\dfrac{\alpha^2}{\pi^2\cdot\kappa}$ (eq. 7-10)

After time equal to the characteristic time of the process τ_C the difference between the average temperature in the bubble and the constant temperature of the surrounding liquid is about 23 % of the initial one. After time $3\tau_C$, this difference is practically zero and the bubble has the equilibrium temperature, T_1. In Table 7-2 calculated values of $(T_{av}-T_1)/(T_0-T_1)$ for some typical values of t/τ_C are presented.

Table 7-2: Calculated values of $(T_{av} - T_1)/(T_0 - T_1)$ for some typical values of t/τ_C.

t/τ_C	$\frac{T_{av} - T_1}{T_0 - T_1}$	t/τ_C	$\frac{T_{av} - T_1}{T_0 - T_1}$
0.001	0.955	1.000	0.226
0.010	0.895	2.000	0.082
0.020	0.854	3.000	0.030
0.100	0.690	4.000	0.011
0.200	0.579	5.000	0.004
0.500	0.390	6.000	0.002

From (eq. 7-8) the temperature at the center of the spherical volume $T_{center,}$ is:

$$\frac{T_{center} - T_1}{T_0 - T_1} = -2 \cdot \sum_{n=1}^{\infty} (-1)^n \cdot e^{-n^2 \cdot t/\tau_C} \quad \text{(eq. 7-11)}$$

.

In Table 7-3 calculated values of $(T_{center} - T_1)/(T_0 - T_1)$ for some typical values of t/τ_C are presented.

Table 7-3: Calculated values of $(T_{center} - T_1)/(T_0 - T_1)$ for some typical values of t/τ_C.

t/τ_C	$\frac{T_{center} - T_1}{T_0 - T_1}$	t/τ_C	$\frac{T_{center} - T_1}{T_0 - T_1}$
0.2	1.000	1.5	0.441
0.3	0.998	2.0	0.270
0.4	0.988	2.5	0.164
0.5	0.964	3.0	0.100
0.6	0.925	4.0	0.037
0.7	0.875	5.0	0.013
0.8	0.819	6.0	0.005
0.9	0.759	7.0	0.002
1.0	0.699	10.0	0.000

At this point the characteristic time τ_C of the conduction in a hot gas bubble containing a gas mixture of the type: a_1 C_6H_{12} – a_2 O_2, at a given temperature and pressure will be calculated. For this

calculation, the thermal diffusivity needs to be known. The thermal diffusivity can be calculated by the equation [112]:

$$\kappa_{mixture} = \frac{\lambda_{mixture}}{\rho_{mixture} \cdot c_{p,mixture}}, \quad \text{(eq. 7-12)}$$

It follows that the thermal conductivity of the mixture must be known. Generally the thermal conductivity of a gas mixture of N components, $\lambda_{mixture}$, can be calculated by the equation [112]:

$$\lambda_{mixture} = 0.5 \cdot \left[\sum_{i=1}^{N} a_i \cdot \lambda_i + \frac{1}{\sum_{i=1}^{N} \frac{a_i}{\lambda_i}} \right], \quad \text{(eq. 7-13)}$$

where a_i is the molar fraction of the compound i.

The conductivity of the two gases can be calculated as function of the temperature from the equations [97]:

$$\lambda_1 = -0.008614 + 1.863 \cdot 10^{-5} \cdot T + 1.704 \cdot 10^{-7} \cdot T^2 - 7.249 \cdot 10^{-11} \cdot T^3, \text{ and} \quad \text{(eq. 7-14)}$$

$$\lambda_2 = -0.0003273 + 9.966 \cdot 10^{-5} \cdot T - 3.743 \cdot 10^{-8} \cdot T^2 - 9.732 \cdot 10^{-12} \cdot T^3, \quad \text{(eq. 7-15)}$$

where λ_1, λ_2 are the thermal conductivities in W / (m K) of the gaseous cyclohexane and oxygen respectively, and T is the temperature in K.

The average molar heat capacity of the mixture of N gases can be calculated by:

$$c_{p,mixture} = \sum_{i=1}^{N} a_i \cdot c_{pi}, \quad \text{(eq. 7-16)}$$

where c_{pi} is the molar heat capacity of the substance i. In the case of a mixture of cyclohexane and oxygen, c_{pi} can be calculated by (eq. 7-17) and (eq. 7-18) respectively:

$$c_{p1} = -63.73333 + 6.444021 \cdot 10^{-1} \cdot T - 2.633224 \cdot 10^{-4} \cdot T^2 - 3.784166 \cdot 10^{-8} \cdot T^3 + 3.795949 \cdot 10^{-11} \cdot T^4 \quad \text{(eq. 7-17)}$$

And

$$c_{p2} = 29.7045 - 9.895231 \cdot 10^{-3} \cdot T + 3.989792 \cdot 10^{-5} \cdot T^2 - 3.394227 \cdot 10^{-8} \cdot T^3 + 9.184016 \cdot 10^{-12} \cdot T^4 \quad \text{(eq. 7-18)}$$

where c_{p1}, c_{p2} are the molar heat capacities at constant pressure in J / (mol K) of the gaseous cyclohexane and oxygen respectively, and T is the temperature in K. These equations can be found in [97].

The average molar mass M of a mixture containing N gases can be calculated by:

$$M_{mixture} = \sum_{i=1}^{N} a_i \cdot M_i \qquad \text{(eq. 7-19)}$$

The density of the mixture can be calculated then from the law of ideal gases:

$$\rho_{mixture} = \frac{P \cdot M_{mixture}}{R \cdot T}. \qquad \text{(eq. 7-20)}$$

Although the adiabatic index is not needed for the calculation of the characteristic time of the conduction process in the bubble, it is an important parameter for the theoretical analysis of the experimental observations.

The calculation of the adiabatic index of a gaseous mixture containing N substances can be performed by the well known equation:

$$\gamma_{mixture} = \frac{c_{p,mixture}}{c_{p,mixture} - R}, \qquad \text{(eq. 7-21)}$$

where $c_{p,mixture}$ is the average molar heat capacity of the mixture, and is calculated by (eq. 7-16). R is the molar gas constant (R = 8.314 J / (mol K)).

The equations (eq. 7-12) – (eq. 7-21) can be used to calculate the properties of a gaseous mixture of cyclohexane - oxygen inside a bubble.

C. Temperature decrease inside a hot bubble due to heat losses from radiation

In this section the temperature decrease of a compressed bubble due to heat losses from radiation will be estimated. The bubble will be considered a blackbody, or ideal radiator of a spherical shape having a constant radius. It is also assumed that the process of heat loss is isotropic in the bubble.

The characteristic property of a blackbody is that the quality and intensity of the radiation it emits are completely determined by its temperature. The total radiative flux $\dot{Q}$ throughout a black surface of area *A* and absolute temperature *T* is given by the Stefan-Boltzmann law [91]:

$$\dot{Q} = A \cdot \sigma \cdot T^4 \qquad \text{(eq. 7-22)}$$

The Stefan-Boltzmann constant has the value: $\sigma = 5.67051 \cdot 10^{-8} \cdot \frac{W}{m^2 \cdot K^4}$ [93]

In the case of a sphere:

$$A = 4 \cdot \pi \cdot r^2 \qquad \text{(eq. 7-23)}$$

The heat losses from the bubble, $\dot{Q}$, will create a temperature difference in the bubble, which can be calculated by:

$$Q = m \cdot C_V \cdot \Delta T \Rightarrow$$

$$\Delta T = \frac{Q}{m \cdot c_V} \qquad \text{(eq. 7-24)}$$

where C_v is the specific heat capacity of the gas mixture, and m the mixture's mass.

Let $\sum_i a_i \cdot A_i$ be the chemical mixture in the gas phase of the bubble, where a_i is the molar fraction of the chemical substance A_i in the mixture. The molar heat capacity of the mixture can then be calculated by the equation: $c_{Vmixture} = c_{Pmixture} - R \Rightarrow$

$$c_{Vmixture} = \sum_{i=1}^{N} a_i \cdot c_{Pi} - R \qquad \text{(eq. 7-25)}$$

The mass of the mixture is:

$$m_{mixture} = \rho_{mixture} \cdot V\,, \qquad \text{(eq. 7-26)}$$

where: $\rho_{mixture} = \frac{P_0 \cdot M_{mixture}}{R \cdot T_0}$, with: $M_{mixture} = \sum_{i=1}^{N} a_i \cdot M_i$, and $V = \frac{4}{3} \cdot \pi \cdot r^3$

D. Detailed information about the performed experiments

Table 7-4: Important properties of the investigated system

Exp. Nr.	Bubbles	Liquid	Volume ml	Liquid's height mm	Windows mm	Initial P bar	Gas mixture
1	-	-	-	-	-	2	mixture 1
2	-	-	-	-	-	2	mixture 1
3	-	-	-	-	-	5	mixture 1
4	-	Ethanol	1,350	150	-	5	mixture 1
5	-	Ethanol	1,350	150	-	5	mixture 1
6	-	Ethanol	1,350	150	-	5	mixture 1
7	-	-	-	-	-	1	mixture 2
8	-	-	-	-	-	2.5	mixture 2
9	-	-	-	-	-	5	mixture 2
10	-	C_6H_{12}	1,350	150	-	1	mixture 2
11	-	C_6H_{12}	1,350	150	-	2.5	mixture 2
12	-	H_2O Dist,	4,400	350	-	1	mixture 1
13	-	H_2O Dist,	7,966		40	1	mixture 2
14	-	H_2O Dist,	3,960		40	1	mixture 2
15	air	C_6H_{12}	4,750	350	40	1	-
16	N_2	C_6H_{12}	4,750	350	40	1	mixture 2
17	O_2	C_6H_{12}	4,750	350	40	1	mixture 2
18	O_2	C_6H_{12}	4,750	350	40	1	mixture 2
19	O_2	C_6H_{12}	4,750	350	40	1	mixture 2
20	N_2	C_6H_{12}	4,750	350	40	1	mixture 2
21	-	-	-		-	1	mixture 2
22	-	C_6H_{12}	4,750	350	40	1	mixture 2
23	-	-	-		-	1	mixture 2
24	-	C_6H_{12}	4,750	350	40	1	mixture 2
25	O_2	C_6H_{12}	4,750	350	40	1	mixture 2
26	N_2	C_6H_{12}	4,750	350	40	1	mixture 2
27	O_2	C_6H_{12}	4,750	350	40	1	mixture 2

28	O_2	C_6H_{12}	4,750	350	40	1	mixture 2
29	O_2	C_6H_{12}	4,750	350	40	1	mixture 2
30	O_2	C_6H_{12}	4,750	350	40	1	mixture 2
31	O_2	C_6H_{12}	4,750	350	40	1	mixture 2
32	O_2	C_6H_{12}	4,750	350	40	1	mixture 2
33	-	C_6H_{12}	2,320	150	40	1	mixture 2
34	-	C_6H_{12}	2,320	150	40	1	mixture 2
35	-	C_6H_{12}	2,320	150	40	1	mixture 2
36	O_2	C_6H_{12}	4,750	350	40	1	mixture 2
37	O_2	C_6H_{12}	4,750	350	40	1	mixture 2
38	O_2	C_6H_{12}	4,750	350	40	1	mixture 2
39	O_2	C_6H_{12}	4,750	350	40	1	mixture 2
40	O_2	C_6H_{12}	4,750	350	40	1	mixture 2
41	O_2	C_6H_{12}	4,750	350	40	1	mixture 2
42	O_2	C_6H_{12}	4,750	350	40	1	mixture 2
43	O_2	C_6H_{12}	4,750	350	40	1	mixture 2
44	N_2	C_6H_{12}	4,750	350	40	1	mixture 2
45	N_2	C_6H_{12}	4,750	350	40	1	mixture 2
46	N_2	C_6H_{12}	4,750	350	40	1	mixture 2
47	N_2	C_6H_{12}	4,750	350	40	1	mixture 2
48	N_2	C_6H_{12}	4,750	350	40	1	mixture 2
49	N_2	C_6H_{12}	4,750	350	40	1	mixture 2
50	N_2	C_6H_{12}	4,750	350	40	1	mixture 2
51	N_2	C_6H_{12}	4,750	350	40	1	mixture 2
52	N_2	C_6H_{12}	4,750	350	40	1	mixture 2
53	O_2	C_6H_{12}	4,750	350	40	1	mixture 2
54	O_2	C_6H_{12}	4,750	350	40	1	mixture 2
55	O_2	C_6H_{12}	4,750	350	40	1	mixture 2
56	O_2	C_6H_{12}	4,750	350	40	1	mixture 2
57	O_2	C_6H_{12}	4,750	350	40	1	mixture 2
58	O_2	C_6H_{12}	4,750	350	40	1	mixture 2
59	O_2	C_6H_{12}	4,750	350	40	1	mixture 2
60	O_2	C_6H_{12}	4,750	350	40	1	mixture 2
61	O_2	C_6H_{12}	2,680	350	200	1	mixture 2
62	O_2	C_6H_{12}	2,680	350	200	1	mixture 2

63	O_2	C_6H_{12}	2,680	350	200	1	mixture 2
64	O_2	C_6H_{12}	2,680	350	200	1	mixture 2
65	O_2	C_6H_{12}	2,680	350	200	1	mixture 2
66	O_2	C_6H_{12}	2,400	350	200	2	mixture 2
67	O_2	C_6H_{12}	2,400	350	200	2	mixture 2
68	O_2	C_6H_{12}	2,400	350	200	2	mixture 2
69	O_2	C_6H_{12}	2,400	350	200	2	mixture 2
70	O_2	C_6H_{12}	2,400	350	200	2	mixture 2
71	O_2	C_6H_{12}	2,400	350	200	2	mixture 2
72	O_2	C_6H_{12}	2,400	350	200	2	mixture 2
73	O_2	C_6H_{12}	2,400	350	200	2	mixture 2
74	O_2	C_6H_{12}	2,400	350	200	2	mixture 2
75	N_2	C_6H_{12}	2,400	350	200	2	mixture 2
76	N_2	C_6H_{12}	2,400	350	200	2	mixture 2
77	-	C_6H_{12}	2,400	350	200	2	mixture 2
78	-	C_6H_{12}	2,400	350	200	3	mixture 2
79	O_2	C_6H_{12}	2,400	350	200	3	mixture 2
80	-	C_6H_{12}	2,400	350	200	1	mixture 2
81	O_2	C_6H_{12}	2,400	350	200	1	mixture 2
82	O_2	C_6H_{12}	2,400	350	200	1	mixture 2
83	O_2	C_6H_{12}	2,400	350	200	1	mixture 2
84	O_2	C_6H_{12}	2,400	350	200	1	mixture 2
85	O_2	C_6H_{12}	2,400	350	200	1	mixture 2
86	O_2	C_6H_{12}	2,400	350	200	2	mixture 2
87	O_2	C_6H_{12}	1,200	150	200	1	mixture 2
88	O_2	C_6H_{12}	1,200	150	200	1	mixture 2
89	O_2	C_6H_{12}	1,200	150	200	1	mixture 2
90	O_2	C_6H_{12}	2,400	350	200	3	mixture 2
91	O_2	C_6H_{12}	2,400	350	200	1	mixture 2
92	N_2	C_6H_{12}	2,400	350	200	1	mixture 2
93	O_2	C_6H_{12}	2,400	350	200	1	mixture 2
94	O_2	C_6H_{12}	2,400	350	200	1	mixture 2
95	O_2	C_6H_{12}	3,950	350	100	1	mixture 2
96	O_2	C_6H_{12}	3,950	350	100	1	mixture 2
97	O_2	C_6H_{12}	3,950	350	100	1	mixture 2

98	O_2	C_6H_{12}	3,950	350	100	1	mixture 2
99	O_2	C_6H_{12}	3,950	350	100	1	mixture 2
100	O_2	C_6H_{12}	4,700	350	40	1	mixture 2
101	O_2	C_6H_{12}	4,700	350	40	1	mixture 2
102	O_2	C_6H_{12}	4,700	350	40	1	mixture 2
103	O_2	C_6H_{12}	4,700	350	40	1	mixture 2
104	O_2	C_6H_{12}	4,700	350	40	1	mixture 2
105	O_2	C_6H_{12}	4,700	350	40	1	mixture 2
106	O_2	C_6H_{12}	4,700	350	40	1	mixture 3
107	O_2	C_6H_{12}	4,700	350	40	1	mixture 4
108	O_2	C_6H_{12}	4,700	350	40	1	mixture 4
109	O_2	C_6H_{12}	4,700	350	40	1	mixture 4
110	O_2	C_6H_{12}	2,400	350	200	1	mixture 4
111	O_2	C_6H_{12}	2,400	350	200	1	mixture 4
112	O_2	C_6H_{12}	2,400	350	200	1	mixture 2
113	O_2	C_6H_{12}	2,400	350	200	1	mixture 2
114	O_2	C_6H_{12}	2,400	350	200	1	mixture 2
115	O_2	C_6H_{12}	2,400	350	200	1	mixture 2
116	O_2	C_6H_{12}	1,200	150	200	1	mixture 2
117	$0{,}3N_2+0{,}7O_2$	C_6H_{12}	2,400	350	200	1	mixture 2
118	$0{,}6N_2+0{,}4O_2$	C_6H_{12}	2,400	350	200	1	mixture 2
119	$0{,}6N_2+0{,}4O_2$	C_6H_{12}	2,400	350	200	1	mixture 2
120	$0{,}79N_2+0{,}21O_2$	C_6H_{12}	2,400	350	200	1	mixture 2
121	N_2	C_6H_{12}	2,400	350	200	1	mixture 2
122	N_2	C_6H_{12}	2,400	350	200	1	mixture 2
123	O_2	C_6H_{12}	2,400	350	200	1	mixture 2
124	$0{,}79N_2+0{,}21O_2$	C_6H_{12}	2,400	350	200	1	mixture 2
125	$0{,}79N_2+0{,}21O_2$	C_6H_{12}	2,400	350	200	1	mixture 2
126	$0{,}79N_2+0{,}21O_2$	C_6H_{12}	2,400	350	200	1	mixture 2
127	$0{,}79N_2+0{,}21O_2$	C_6H_{12}	2,400	350	200	1	mixture 2
128	$0{,}9N_2+0{,}1O_2$	C_6H_{12}	2,400	350	200	1	mixture 2
129	O_2	C_6H_{12}	2,400	350	200	1	mixture 2
130	O_2	C_6H_{12}	2,400	350	200	1	mixture 2
131	O_2	C_6H_{12}	2,400	350	200	1	mixture 2
132	O_2	C_6H_{12}	2,400	350	200	1	mixture 2

133	O_2	C_6H_{12}	2,400	350	200	1	mixture 2
134	O_2	C_6H_{12}	2,400	350	200	1	mixture 2
135	O_2	C_6H_{12}	2,400	350	200	1	mixture 2
136	O_2	C_6H_{12}	2,400	350	200	1	mixture 2
137	O_2	C_6H_{12}	2,400	350	200	1	mixture 2
138	$0,79N_2+0,21O_2$	C_6H_{12}	2,400	350	200	1	mixture 2
139	$0,79N_2+0,21O_2$	C_6H_{12}	2,400	350	200	1	mixture 2
140	-	C_6H_{12}	1,200	150	200	1	mixture 2
141	O_2	C_6H_{12}	1,200	150	200	1	mixture 2
142	O_2	C_6H_{12}	2,400	350	200	1	mixture 2
143	O_2	C_6H_{12}	2,400	350	200	1	mixture 2
144	N_2	C_6H_{12}	2,400	350	200	1	mixture 2
145	N_2	C_6H_{12}	2,400	350	200	1	mixture 2
146	N_2	C_6H_{12}	2,400	350	200	1	mixture 2
147	N_2	C_6H_{12}	2,400	350	200	1	mixture 2
148	O_2	C_6H_{12}	2,400	350	200	1	mixture 2
149	O_2	C_6H_{12}	2,400	350	200	1	mixture 2
150	O_2	C_6H_{12}	2,400	350	200	1	mixture 2
151	N_2	C_6H_{12}	4,700	350	40	1	mixture 2
152	N_2	C_6H_{12}	4,700	350	40	1	mixture 2
153	N_2	C_6H_{12}	4,700	350	40	1	mixture 2
154	N_2	C_6H_{12}	4,700	350	40	1	mixture 2
155	N_2	C_6H_{12}	4,700	350	40	1	mixture 2
156	N_2	C_6H_{12}	4,700	350	40	1	mixture 2
157	N_2	C_6H_{12}	4,700	350	40	1	mixture 2
158	O_2	C_6H_{13}	4,700	350	40	1	mixture 2
159	O_2	C_6H_{14}	4,700	350	40	1	mixture 2
160	O_2	C_6H_{15}	4,700	350	40	1	mixture 2
161	O_2	C_6H_{16}	4,700	350	40	1	mixture 2
162	O_2	$C_8H_{16}O$	2,400	350	200	1	mixture 2
163	O_2	C_6H_{12}	2,400	350	200	1	mixture 2
164	O_2	C_6H_{12}	2,400	350	200	1	mixture 2
165	O_2	C_6H_{12}	2,400	350	200	1	mixture 2
166	O_2	$C_8H_{16}O$	2,400	350	200	1	mixture 2
167	O_2	$C_8H_{16}O$	2,400	350	200	1	mixture 2

168	O_2	$C_8H_{16}O$	2,400	350	200	1	mixture 2
169	O_2	$C_8H_{16}O$	2,400	350	200	1	mixture 2
170	O_2	$C_8H_{16}O$	2,400	350	200	1	mixture 2
171	O_2	CH_4O	2,400	350	200	1	mixture 2
172	O_2	CH_4O	2,400	350	200	1	mixture 2
173	O_2	CH_4O	2,400	350	200	1	mixture 2
174	O_2	CH_4O	2,400	350	200	1	mixture 2
175	O_2	C_9H_{12}	2,400	350	200	1	mixture 2
176	O_2	C_9H_{12}	2,400	350	200	1	mixture 2

Mixture 1 = H_2 / O_2, with H_2 mole fraction of 0.66

Mixture 2 = C_2H_2 / O_2, with C_2H_2 mole fraction of 0.25

Mixture 3 = C_2H_2 / O_2 / He, with C_2H_2 mole fraction of 0.20 and O_2 mole fraction of 0.60

Mixture 4 = C_2H_2 / O_2 / He, with C_2H_2 mole fraction of 0.10 and O_2 mole fraction of 0.30

Table 7-5: The cameras and optical methods used in each experiment

Exp. Nr.	Cordin fps	Opt. Method	Kodak fps	Opt. Method	Other camera fps	Opt. Method (light)
16	-	-	4,500	Diffused light	-	-
17	-	-	4,500	Diffused light	-	-
19	-	-	18,000	Diffused light	-	-
20	-	-	27,000	Diffused light	-	-
29	-	-	13,500	in angle with opt, axis	-	-
30	-	-	27,000	in angle with opt, axis	-	-
31	-	-	40,500	in angle with opt, axis	-	-
34	25,000	Shadowphot,, 100W Hg	-	-	-	-
35	50,000	Shadowphot,, 100W Hg	-	-	-	-
36	-	-	27,000	Diffused light	-	-
37	50,000	Shadowphot,, 100W Hg	40,500	in angle with opt, axis	-	-
38	50,000	Shadowphot,, 100W Hg	-	-	-	-
39	-	-	40,500	in angle with opt, axis	-	-
40	50,000	Shadowphot,, 100W Hg	40,500	in angle with opt, axis	-	-
41	75,000	Shadowphot,, 100W Hg	40,500	in angle with opt, axis	-	-
42	100,000	Shadowphot,, 100W Hg	40,500	in angle with opt, axis	-	-
43	100,000	Shadowphot,, 100W Hg	40,500	in angle with opt, axis	-	-
45	100,000	Shadowphot,, 100W Hg	40,500	in angle with opt, axis	-	-
47	50,000	Shadowphot,, 100W Hg	27,000	in angle with opt, axis	-	-

48	50,000	Shadowphot,, 100W Hg	-	-	-	-
50	100,000	Shadowphot,, 100W Hg	27,000	in angle with opt, axis	-	-
52	-	-	27,000	Shadowphot,, 100W Hg	-	-
53	-	-	27,000	Shadowphot,, 100W Hg	-	-
54	-	-	27,000	Shadowphot,, 100W Hg	-	-
55	-	-	27,000	Shadowphot,, 100W Hg	-	-
56	100,000	Shadowphot,, 100W Hg	40,500	in angle with opt, axis	-	-
57	-	-	-	-	200,000	Shadowphot,, 100W Hg, ISIS Camera
58	-	-	40,500	in angle with opt, axis	200,000	Shadowphot,, 100W Hg, ISIS Camera
59	-	-	-	-	500,000	Diffused light, 500W, ISIS Camera
60	-	-	40,500	Diffused light	-	-
61	-	-	40,500	Diffused light	-	-
62	-	-	40,500	Diffused light	-	-
63	-	-	40,500	Diffused light	500,000	USS16 Camera with photointensifier
64	-	-	40,500	Diffused light	500,000	USS16 Camera without photointensifier
65	-	-	40,500	no light source,low light sensitivity	800,000	USS16 Camera
66	100,000	Flash Lamp	40,500	Flash Lamp	-	-
67	-	-	40,500	Flash Lamp	-	-
68	-	-	40,500	Flash Lamp	-	-
69	100,000	Flash Lamp	40,500	Flash Lamp	-	-
70	100,000	Flash Lamp	40,500	Flash Lamp	-	-
72	100,000	Flash Lamp	40,500	Flash Lamp	-	-

73	100,000	Flash Lamp	40,500	Flash Lamp	-	-
74	100,000	Flash Lamp	40,500	Flash Lamp	-	-
75	100,000	Flash Lamp	40,500	Flash Lamp	-	-
76	100,000	Flash Lamp	40,500	Flash Lamp	-	-
77	100,000	Flash Lamp	13,500	Flash Lamp	-	-
78	100,000	Flash Lamp	13,500	Flash Lamp	-	-
79	100,000	Flash Lamp	40,500	Flash Lamp	-	-
80	100,000	Flash Lamp	13,500	Flash Lamp	-	-
81	100,000	Parallel light	40,500	Parallel light	-	-
82	-	-	40,500	Parallel light	1,000,000	Parallel, ISIS Camera
83	-	-	40,500	Flash Lamp	1,000,000	Diffused light, Flash Lamp, ISIS Camera
84	-	-	40,500		100,000	Diffuse light, 500 Watt, ISIS Camera
85	-	-	40,500		100,000	Diffuse light, 500 Watt, ISIS Camera
86	-	-	40,500		100,000	Diffuse light, 500 Watt, ISIS Camera
87	-	-	40,500	Flash Lamp	-	-
88	-	-	40,500	Flash Lamp	100,000	Diffused light, Flash Lamp, ISIS Camera
89	-	-	40,500	Flash Lamp	500,000	Diffused light, Flash Lamp, ISIS Camera
90	-	-	40,500	Flash Lamp	500,000	Diffused light, Flash Lamp, ISIS Camera
91	-	-	-	-	500,000	Diffuse light, 500 Watt, ISIS Camera

92	-	-	-	-	500,000	Diffuse light, 500 Watt, ISIS Camera
93	-	-	-	-	1,000,000	Diffuse light, 500 Watt, ISIS Camera
94	-	-	-	-	1,000,000	Diffuse light, 500 Watt, ISIS Camera
95	-	-	-	-	500,000	Diffuse light, 500 Watt, ISIS Camera
96	-	-	-	-	1,000,000	Diffuse light, 500 Watt, ISIS Camera
97	-	-	-	-	1,000,000	Diffuse light, 500 Watt, ISIS Camera
98	-	-	-	-	100,000	Diffuse light, 500 Watt, ISIS Camera
99	-	-	-	-	100,000	Diffuse light, 500 Watt, ISIS Camera
100	-	-	-	-	100,000	Diffuse light, 500 Watt, ISIS Camera
101	-	-	40,500	Shadowphot,, 100W Hg	-	-
102	-	-	40,500	Shadowphot,, 100W Hg	-	-
103	-	-	40,500	Shadowphot,, 100W Hg	-	-
104	-	-	40,500	Shadowphot,, 100W Hg	-	-
105	-	-	40,500	Shadowphot,, 100W Hg	-	-
106	-	-	40,500	Shadowphot,, 100W Hg	-	-
107	-	-	40,500	Shadowphot,, 100W Hg	-	-
108	-	-	40,500	Diffused light	-	-
109	-	-	40,500	Diffused light	-	-

110	-	-	40,500	Diffused light	-	-
111	-	-	40,500	Diffused light	-	-
112	-	-	40,500	Shadowphot,, 100W Hg	-	-
113	-	-	40,500	Shadowphot,, 100W Hg	-	-
114	-	-	-	-	-	-
115	50,000	Parallel light	40,500	Shadowphot,, 100W Hg	-	-
116	100,000	Flash Lamp	-		-	-
117	-	-	-	-	500,000	Diffuse light, 2000 Watt, ISIS Camera
118	-	-	13,500	Diffused light	500,000	Diffuse light, 2000 Watt, ISIS Camera
119	-	-	13,500	Diffused light	500,000	Diffuse light, 2000 Watt, ISIS Camera
120	-	-	13,500	Diffused light	500,000	Diffuse light, 2000 Watt, ISIS Camera
121	-	-	13,500	Diffused light	500,000	Diffuse light, 2000 Watt, ISIS Camera
122	-	-	13,500	Diffused light	500,000	Diffuse light, 2000 Watt, ISIS Camera
123	-	-	13,500	Diffused light	500,000	Diffuse light, 2000 Watt, ISIS Camera
124	-	-	13,500	Diffused light	1,000,000	Diffuse light, 2000 Watt, ISIS Camera
125	-	-	13,500	Diffused light	1,000,000	Diffuse light, 2000 Watt, ISIS Camera
126	-	-	13,500	Diffused light	1,000,000	Diffuse light, 2000 Watt, ISIS

						Camera
127	-	-	-	-	500,000	Diffuse light, 2000 Watt, ISIS Camera
128	-	-	-	-	500,000	Diffuse light, 2000 Watt, ISIS Camera
129	-	-	-	-	1,000,000	Diffuse light, 2000 Watt, ISIS Camera
130	-	-	-	-	1,000,000	Diffuse light, 2000 Watt, ISIS Camera
131	-	-	-	-	1,000,000	Diffuse light, 2000 Watt, ISIS Camera
132	-	-	-	-	1,000,000	Diffuse light, 2000 Watt, ISIS Camera
133	-	-	-	-	1,000,000	Diffuse light, 2000 Watt, ISIS Camera
134	-	-	-	-	1,000,000	Diffuse light, 2000 Watt, ISIS Camera
135	-	-	-	-	1,000,000	Diffuse light, 2000 Watt, ISIS Camera
136	-	-	-	-	1,000,000	Diffuse light, 2000 Watt, ISIS Camera
137	-	-	-	-	1,000,000	Diffuse light, 2000 Watt, ISIS Camera
138	-	-	-	-	1,000,000	Diffuse light, 2000 Watt, ISIS

						Camera
139	-	-	-	-	1,000,000	Diffuse light, 2000 Watt, ISIS Camera
140	-	-	-	-	100,000	Diffused light, Flash Lamp, ISIS Camera
141	-	-	-	-	100,000	Diffused light, Flash Lamp, ISIS Camera
142	-	-	-	-	500,000	Diffuse light, 2000 Watt, ISIS Camera
143	-	-	13,500	Diffused light	-	-
144	-	-	13,500	Diffused light	-	-
145	-	-	13,500	Diffused light	-	-
146	-	-	13,500	Diffused light	-	-
147	-	-	13,500	Diffused light	-	-
149	-	-	13,500	Diffused light	-	-
152	-	-	40,500	Diffused light	-	-
153	-	-	40,500	Diffused light	-	-
154	-	-	40,500	Shadowphot,, 100W Hg	-	-
155	-	-	40,500	Shadowphot,, 100W Hg	-	-
156	-	-	40,500	Shadowphot,, 100W Hg	-	-
157	-	-	27,000	Shadowphot,, 100W Hg	-	-
158	-	-	27,000	Shadowphot,, 100W Hg	-	-
159	-	-	27,000	Shadowphot,, 100W Hg	-	-
160	-	-	27,000	Shadowphot,, 100W Hg	-	-
161	-	-	27,000	Shadowphot,, 100W Hg	-	-
164	-	-	13,500	Diffused light	100,000	Diffuse light, 500 Watt, ISIS Camera
165	-	-	13,500	Diffused light	500,000	Diffuse light, 2000 Watt, ISIS Camera

166	-	-	13,500	Diffused light	500,000	Diffuse light, 2000 Watt, ISIS Camera
168	-	-	-	-	1,000,000	Diffuse light, 2000 Watt, ISIS Camera
169	-	-	13,500	Diffused light	1,000,000	Diffuse light, 2000 Watt, ISIS Camera
170	-	-	-	-	1,000,000	Diffuse light, 2000 Watt, ISIS Camera
172	-	-	40,500	Diffused light	1,000,000	Diffuse light, 2000 Watt, ISIS Camera
173	-	-	40,500	Diffused light	1,000,000	Diffuse light, 2000 Watt, ISIS Camera
174	-	-	40,500	Diffused light	1,000,000	Diffuse light, 2000 Watt, ISIS Camera
175	-	-	-	-	1,000,000	Diffuse light, 2000 Watt, ISIS Camera
176	-	-	-	-	1,000,000	Diffuse light, 2000 Watt, ISIS Camera

Only those experiments that produced optical measurements are listed in the above table.

Table 7-6: Overview of the pressure measurements

Exp. Nr.	Sensor position: 4.1		Sensor position: 4.2		Sensor position: 8.1		Sensor position: 8.2		Sensor position: Bottom	
	SW	Pmax	SW	Pmax	SW	Pmax	SW	Pmax	SW	Pmax
7	57.6	57.6	40.2	45.5	26.5	31.3	31.1	44.0		
8	122.9	122.9	81.3	81.3	66.3	85.9	66.6	104.8		
9	181.1	181.1	182.0	182.0	155.7	187.7	150.2	200.0		
10	77.0	77.0	35.6	40.7	33.5	58.9	61.1	92.7		
11	132.9	132.9	128.5	128.5	90.0	151.8	169.2	220.8		
13	28.3	39.5	33.0	53.9	129.8	129.8	60.0	60.0		
14	35.0	35.0	35.1	35.1	74.5	74.5	67.2	81.0		
16	42.7	46.8	88.8	88.8	79.6	112.7	59.0	86.6		
17	28.0	62.4	93.9	93.9	90.7	90.8	93.6	93.6		
18	41.6	63.0	103.5	103.5	107.5	107.5	68.1	79.3		
19	47.8	61.0	113.7	113.7	76.5	93.6	60.2	96.1		
20	28.3	65.1	94.6	94.6	85.4	85.4	84.8	84.8		
21	53.3	53.3	33.7	34.9	27.8	35.0	27.7	39.5	74.3	75.7
22	34.8	52.4	92.4	92.4	127.1	127.1	101.9	137.5	191.9	191.9
23	51.3	51.3	43.5	43.5	31.4	35.6	30.5	39.8	64.2	76.3
24	49.5	50.4	59.4	63.5	119.8	119.8	97.1	125.4	154.4	179.0
25	37.3	57.6	55.3	55.3	65.4	119.4	18.7	131.3	185.4	185.4
26	86.6	86.6	50.6	57.1	13.4	119.6	22.8	121.3	43.1	147.2
27	66.6	69.6	49.6	49.6	76.0	76.0	71.2	86.2		
28	53.1	53.1	48.9	48.9	76.8	76.8	83.7	83.7	82.0	143.9
29	60.4	60.4	46.1	46.1	108.0	108.0	82.8	89.9	92.0	141.2
31	61.0	61.0	51.9	53.2	104.4	104.4	85.5	85.5	100.4	155.6
32	75.9	75.9	58.6	58.6	103.0	103.0	85.7	101.4	147.3	147.3
33	61.0	61.0	34.9	36.0	32.0	44.5	64.2	81.9	146.0	146.0
34	64.0	64.0	49.4	49.4	40.7	52.1	79.0	79.6	118.5	119.8
35	49.0	49.0	33.2	34.3	32.8	43.7	63.7	82.4	137.2	137.2
36	74.2	74.2	39.0	39.0	78.3	78.3	55.1	78.4	89.2	115.9
37	62.0	62.0	42.5	42.5	66.7	71.6	55.2	74.0	87.0	109.3
38	75.3	75.3	38.3	38.3	61.1	68.2	56.5	77.1	70.0	109.3

39	93.1	93.1	42.4	42.4	32.1	102.5	22.0	67.4	38.5	126.4
40	74.3	74.3	43.6	43.6	74.3	74.3	58.3	71.6	75.8	122.6
41	66.7	66.7	47.3	47.3	68.6	71.2	56.7	74.4	71.1	121.6
42	46.3	46.3	41.9	41.9	65.3	65.3	55.3	63.1	62.7	128.2
43	66.3	66.3	36.0	39.2	50.4	91.0	77.9	77.9	79.1	138.5
45	64.2	64.2	35.4	40.6	61.4	61.4	47.7	63.0	62.7	93.6
46	69.5	69.5	33.5	40.2	46.4	64.5	36.6	62.9	78.5	88.8
47	66.4	66.4	37.6	39.0	56.9	65.3	43.3	69.8	64.9	106.9
48	71.5	71.5	37.5	40.0	76.2	76.2	64.2	68.3	74.5	110.4
49	79.7	79.7	51.2	51.2	69.4	69.4	57.5	76.8	66.9	105.3
50	69.2	69.2	36.2	36.7	56.3	58.9	51.5	68.8	73.7	114.6
51	35.3	35.3	23.5	26.2	46.1	46.1	35.3	44.5	52.1	62.9
52	52.0	52.0	32.5	35.9	55.0	69.8	41.2	73.6	70.0	105.4
53	76.9	76.9	40.6	40.6	66.9	66.9	59.7	73.9	69.1	104.3
54	70.5	70.5	39.2	39.2	74.3	74.3	56.1	73.3	68.1	119.1
55	57.0	57.0	36.3	38.8	53.1	76.7	47.8	74.0	78.9	110.3
56	78.2	78.2	36.9	42.1	62.0	71.2	46.5	85.5	70.9	108.3
57	62.3	62.3	38.4	38.4	64.7	66.5	55.5	79.2	85.1	120.5
58	47.4	47.4	35.6	36.9	55.1	75.2	39.8	67.6	63.3	154.9
59	44.3	51.2	34.1	37.3	52.3	88.0	39.3	72.5	79.9	124.0
60	84.0	84.0	53.1	53.1	79.3	79.3	59.8	87.0	68.9	160.9
61	48.1	66.9	45.1	50.0	55.5	114.8	90.0	98.2	73.4	145.9
62	76.2	76.2	47.4	47.4	66.8	98.4	59.2	106.4	57.1	148.1
63	55.7	55.7	50.5	50.5	108.6	108.6	60.4	103.1	58.7	173.0
64	100.6	100.6	76.2	76.2	88.6	127.9	65.3	136.0	60.6	181.6
65	50.4	76.6	146.1	146.1	101.5	124.5	74.9	126.1	77.6	188.5
67	58.9	78.2	59.5	59.5	99.5	141.0	75.3	151.5	117.3	211.3
68	100.5	100.5	88.0	88.0	121.6	159.9	89.9	158.7	73.6	207.1
69	56.5	76.4	55.1	55.2	89.2	127.7	60.9	139.0	66.6	193.7
70	65.3	82.3	71.3	71.3	103.4	142.9	69.9	156.4	97.3	213.9
71	66.1	82.1	67.0	67.0	98.5	155.3	70.0	177.0	100.2	226.8
72	86.1	86.1	89.3	89.3	131.3	160.7	96.2	171.5	215.5	224.6
73	63.8	80.8	63.2	63.2	127.6	154.6	73.8	158.3	100.3	206.2
74	63.2	85.3	63.3	63.3	93.5	161.3	121.6	152.9	107.1	198.5
75	74.5	86.4	65.4	74.6	101.5	149.4	69.2	169.6	95.0	245.2

76	61.3	70.2	62.8	62.8	98.4	135.0	71.6	155.7	95.3	212.9
77	79.9	80.3	63.5	64.2	136.3	153.6	103.1	169.9	159.4	233.8
78	98.7	109.8	93.6	93.6	196.4	214.0	178.8	228.0	219.1	308.9
79	94.2	114.3	96.0	96.0	155.4	217.6	165.9	227.3	221.3	334.3
80	62.1	62.1	32.2	34.7	65.1	75.3	71.1	87.4	78.0	118.3
81	66.6	66.6	48.8	48.8	61.5	79.9	43.1	87.1	41.6	115.0
82	76.2	76.2	40.2	40.2	61.4	82.4	46.9	94.1	39.2	135.9
83	76.9	76.9	38.4	38.6	60.0	78.7	49.2	87.2	46.3	138.1
84	65.7	65.7	54.5	54.5	73.1	73.1	54.7	95.6	38.0	146.5
85	79.5	79.5	37.7	37.7	57.2	83.2	43.9	91.2	47.6	130.6
86	66.3	87.5	62.1	62.1	131.1	152.3	113.5	159.8	131.4	230.6
87	65.3	65.3	33.0	33.4	34.0	67.5	59.5	94.9	73.8	221.6
88	64.5	64.5	48.3	48.3	39.3	70.4	73.6	89.8	67.2	216.9
89	69.4	69.4	30.8	34.8	31.1	57.8	55.6	88.3	69.3	159.0
90	112.8	143.7	95.0	101.7	199.6	228.1	160.4	218.6	223.3	300.5
91	67.5	67.5	33.7	38.8	57.3	81.1	40.7	86.2	48.2	118.7
92	58.2	58.2	33.4	39.3	54.1	78.3	37.7	82.4	44.6	107.7
93	77.9	77.9	41.8	41.8	69.8	85.8	39.8	87.5	129.1	149.9
94	69.6	69.6	31.6	36.1	54.7	76.0	38.3	63.3	45.7	127.8
95	74.5	74.5	34.5	34.5	49.9	80.6	38.3	72.0	53.1	96.6
96	63.5	63.5	33.8	37.5	57.5	63.1	41.6	63.1	60.3	112.4
97	78.1	78.1	49.3	49.3	59.4	93.7	30.2	66.6	38.8	102.0
98	59.0	59.0	48.1	48.1	73.7	77.2	48.5	103.1	25.5	92.2
99	66.2	66.2	39.8	39.8	52.4	62.4	36.4	66.3	50.1	97.1
100	92.9	92.9	52.8	52.8	71.5	71.5	55.4	67.8	62.6	117.2
101	78.8	78.8	53.1	53.1	73.8	73.8	54.6	65.7	55.4	103.3
102	66.9	66.9	32.3	37.9	67.8	71.1	70.5	70.5	82.8	95.7
103	73.8	73.8	35.7	35.8	54.5	73.0	42.5	69.0	67.2	107.2
104	60.8	60.8	32.8	39.2	53.2	71.2	35.9	76.7	63.9	136.3
105	62.2	62.2	32.3	37.3	55.9	70.6	39.0	65.7	60.1	126.1
106	35.9	39.0	37.8	37.8	75.3	75.3	57.1	73.2	69.2	126.1
107	18.8	32.4	20.7	26.1	109.0	109.0	66.7	69.8	113.3	113.3
108	10.8	13.5	11.8	13.4	13.1	19.1	10.2	20.0	14.8	24.7
109	10.2	11.1	10.5	12.9	11.3	15.4	10.9	13.7	13.2	16.2
110	23.8	46.5	16.1	28.7	110.0	107.0	95.6	115.0	179.3	179.3

111	13.9	17.9	11.7	15.2	12.0	24.4	11.4	25.2	20.4	39.0
112	37.7	39.0	34.9	35.6	70.1	80.1	47.2	83.5	50.3	121.8
113	33.6	40.5	42.2	42.2	71.1	95.6	52.4	94.4	39.9	137.8
114	47.5	47.5	38.7	38.7	54.4	82.5	41.9	90.1	38.4	123.6
115	35.1	38.1	39.7	39.7	74.9	74.9	57.2	102.9	43.9	133.4
116	28.1	36.9	37.0	37.0	37.9	70.4	70.6	102.8	63.4	162.3
117	57.9	57.9	46.7	46.7	66.5	83.6	52.9	89.8	40.8	126.7
118	62.9	62.9	37.0	37.0	56.6	78.1	46.5	91.7	50.6	117.6
119	58.6	58.6	33.6	36.7	58.5	79.8	39.2	87.1	41.2	120.3
120	74.4	74.4	43.3	43.3	71.3	76.8	48.4	87.9	38.7	111.1
121	77.0	77.0	40.0	40.0	59.0	75.3	48.0	92.1	41.8	104.0
122	70.1	70.1	39.4	39.4	61.1	81.2	40.5	94.3	48.7	116.3
123	50.9	50.9	34.0	37.7	56.0	85.2			44.1	131.5
124	75.8	75.8	37.3	37.3	56.1	81.7	43.5	89.9	50.7	107.8
125	92.2	92.2	41.7	41.7	63.1	87.0	54.2	93.4	51.7	112.5
126	75.3	75.3	38.6	39.0	58.2	86.6	47.3	91.7	51.6	115.2
127	76.8	76.8	37.0	37.3	56.8	77.2	45.8	87.8	50.5	111.8
128	86.6	86.6	37.5	37.5	62.5	75.8	47.1	92.7	49.9	116.2
129	89.7	89.7	40.0	42.4	55.4	98.4			35.9	140.8
130	86.7	86.7	39.5	39.5	40.0	81.5	33.0	99.0	29.1	143.8
131	64.6	64.6	45.4	45.4	64.3	110.7	49.9	120.8	31.5	137.3
132	77.6	77.6	37.5	47.3	55.6	84.4	34.7	88.1	30.6	137.5
133	79.6	79.6	38.3	39.2	63.8	75.0	44.3	99.8	22.8	128.1
135	65.6	65.6	37.3	38.1	60.7	80.6	44.5	95.3	52.1	123.4
136	93.8	93.8	49.5	49.8	68.3	83.8	50.0	80.8	41.0	126.5
137	62.5	62.5	40.4	40.4	73.1	79.4	45.9	87.1	50.3	99.0
138	95.4	95.4	51.7	51.7	52.3	86.0	36.4	93.3	46.4	118.3
139	76.7	76.7	34.2	41.0	60.1	80.9	37.5	87.1	41.1	108.3
140	95.8	95.8	43.2	43.2	41.0	75.3	65.1	102.1	119.2	282.2
141	112.3	112.3	64.1	64.1	49.1	96.3	100.8	126.3	39.7	262.4
142	58.9	58.9	37.1	41.1	21.7	108.0	17.4	74.0	16.1	154.4
143	80.0	80.0	37.3	43.0	49.0	99.5	27.0	111.1	42.1	152.7
144	85.4	85.4	37.7	37.7	39.9	79.9	33.4	83.9	32.9	130.0
145	102.9	102.9	44.8	44.8	67.6	90.4	29.3	80.6	29.9	105.9
146	86.3	86.3	44.9	44.9	10.7	78.1	25.6	81.6	13.8	105.3

147	86.6	86.6	58.2	58.2	62.4	98.3	27.7	85.1	10.4	137.9
148	70.6	70.7	39.6	43.3	13.4	91.7	11.0	95.5	39.6	135.2
149	98.9	98.9	65.4	65.4	24.3	92.2	22.8	106.4	23.6	149.9
150	113.7	113.7	72.5	72.5	66.8	105.5	23.0	113.8	25.0	221.0
151	64.5	64.5	52.5	52.5	58.1	73.2	36.5	59.5	29.9	99.2
152	60.3	60.3	36.0	38.1	47.1	63.1	30.6	63.9	38.4	91.5
153	75.1	75.1	35.8	40.1	34.1	75.4	24.4	60.7	32.5	104.4
154	61.4	61.4	34.7	40.8	39.1	70.7	25.8	63.2	38.4	91.2
155	61.8	61.8	34.5	42.5	40.3	73.2	27.6	61.6	23.0	122.6
156	61.9	61.9	36.3	42.5	50.1	81.2	28.8	68.8	22.5	121.4
157	60.6	63.8	92.9	92.9	63.8	96.3	41.6	95.6	29.6	135.0
158	63.0	63.0	43.4	43.4	45.1	97.2	26.3	85.6	51.1	115.9
159	64.5	64.5	36.0	43.9	29.9	92.8	19.3	88.9	77.4	106.4
160	77.7	77.7	43.8	43.8	42.7	87.4	73.7	74.5	49.7	121.0
161	70.8	70.8	39.2	46.5	40.5	88.0	24.8	72.9	37.7	137.4
163	47.5	47.5	33.3	38.8	38.8	74.9	28.6	83.5	109.8	109.8
164	69.3	69.3	40.7	40.7	68.3	87.5	52.8	100.5	144.0	144.0
165	77.7	77.7	38.9	38.9	63.5	88.1	47.4	103.6	21.3	183.1
167	58.8	58.8	33.1	33.3	61.3	73.8	44.1	79.6	20.1	187.4
168	50.4	50.4	34.3	38.2	57.9	76.9	44.8	89.0	23.4	178.7
169	42.2	42.2	27.5	32.0	48.5	71.0	36.5	83.7	133.9	133.9
170	55.6	55.6	34.2	34.2	64.9	73.2	43.9	78.2	161.8	161.8
172	70.4	70.4	45.1	49.9	82.0	90.3	62.1	105.4	196.4	196.4
173	47.1	47.1	36.5	37.5	60.8	92.2	45.0	86.6	134.7	134.7
174	40.2	43.7	33.6	33.6	50.7	71.6	36.9	75.0	155.0	155.0
175	56.4	56.4	33.3	33.3	45.6	83.6	32.7	76.9	20.1	124.2
176	65.9	65.9	41.4	41.4	55.8	78.8	33.2	81.7	40.6	147.3

Only the experiments that produced pressure measurements are listed in the above table. SW: The peak pressure of the incident shock wave. P_{max} : The peak pressure of the complete pressure signal. All pressures are in bar.

Table 7-7: Overview of the calculated shock wave propagation velocities in m / s

Exp. Nr.	Pos. 4.1->4.2 (in the gas phase)	Pos. 8.1 -> bottom (in the liquid phase)
7	2,585	
8	2,376	
9	2,585	
10	2,882	
11	2,705	
13	2,442	
14	3,084	
16	3,084	
19	3,084	
20	3,447	
21	2,511	2,400
22	2,705	1,312
23	2,442	2,400
24	2,835	1,312
25	2,664	430
26	2,664	633
27	2,790	
28	2,882	1,322
29	2,747	1,312
31	2,835	1,312
32	2,980	1,322
33	2,376	1,471
34	2,624	1,483
35	2,344	1,459
36	2,476	1,303
37	2,511	1,303
38	2,511	1,294

Exp. Nr.	Pos. 4.1->4.2 (in the gas phase)	Pos. 8.1 -> headon (in the liquid phase)
92	2,511	1,294
93	2,476	881
94	2,476	1,294
95	2,511	1,285
96	2,442	1,303
97	2,747	1,303
98	2,548	1,285
99	2,548	1,294
100	2,882	1,312
101	2,021	1,312
102	2,476	1,303
103	2,511	1,303
104	2,835	1,303
105	2,511	1,303
112	2,835	1,331
113	2,930	1,312
114	2,747	1,303
115	3,031	1,312
116	2,624	1,495
117	2,548	1,322
118	2,476	1,322
119	2,476	1,312
120	2,624	1,322
121	2,511	1,303
122	2,476	1,322
123	2,197	1,312
124	2,511	1,303

39	2,585	1,294
40	2,511	1,303
41	2,442	1,303
42	2,476	1,294
43	2,442	1,303
45	2,548	1,276
46	2,511	1,294
47	2,511	1,285
48	2,476	1,285
49	2,835	1,294
50	2,548	1,294
51	2,548	1,303
52	2,511	1,276
53	2,664	1,303
54	2,624	1,285
55	2,476	1,285
56	2,585	1,285
57	2,511	1,294
58	2,548	1,285
59	2,476	1,276
60	2,664	1,285
61	2,705	1,285
62	2,790	1,276
63	3,139	1,294
64	3,139	1,267
65	85	1,285
66	2,511	1,294
67	2,511	1,312
68	2,511	1,322
69	2,511	1,303
70	2,548	1,303
74	2,548	1,312
75	2,511	1,312
76	2,548	1,322
77	2,044	1,331

125	2,511	1,312
126	2,548	
127		1,303
128	2,442	1,312
129	2,476	1,303
130	2,511	1,861
131	2,408	1,312
132	2,442	1,285
133	2,476	1,285
135	2,548	1,322
136	803	1,312
137	2,511	1,322
138	2,835	160
139	2,442	1,312
140	2,442	
141	2,548	1,403
142	2,376	873
143	2,705	738
144	2,442	1,294
145	2,585	1,241
146	2,476	385
147	2,705	396
148	2,476	414
149	3,084	490
150	2,442	368
151	2,930	1,267
152	2,585	1,267
153	2,548	1,267
154	2,548	1,249
155	2,548	1,249
156	2,624	1,258
157	3,381	1,249
158	3,031	1,276
159	2,585	1,249
160	2,664	1,276

78	2,511	1,361
79	2,585	1,351
80	2,408	1,312
81	2,408	1,824
82	2,548	1,312
83	2,548	1,303
84	2.747	1.312
85	2.548	1.312
86	2.511	1.322
87	2.344	1.459
88	2.408	1.495
89	2.376	1.495
90	2.585	1.771
91	2.476	1.303

161	2,705	1,258
163	2,442	1,249
164	2,476	1,241
165	2,511	1,241
167	2,408	1,249
168	2,408	1,241
169	2.118	1.258
170	2.476	1.241
172	2.408	1.112
173	2.476	1.119
174	2.442	1.092
175	2.376	1.294
176	2.442	1.249

Only the experiments in which the velocity measurement was possible are presented. Categories of experiments in which velocity measurement was impossible:

1. Experiments with deflagration above the liquid (Exp. No. 106 - 111)
2. When no pressure signal was available
3. When the structure of the signal did not allow a clear definition of a reference point

References

[1] Wolf-Dieter Deckwer: Bubble Column Reaktors. John Wiley & Sons, Chichester New York Brisbane Toronto Singapore, (1992)

[2] Loison, R.: The propagation of deflagration in a tube covered with an oil film, C. R. Acad. Sci. 234, pp. 512-513 (1952)

[3] Burgoyne, J. H. and Cohen, L.: Effect of drop size on flame propagation in liquid aerosols, Proc. R. Soz., London, A225, pp. 375-392 (1954)

[4] Plewinsky, B. et al.: Surface Detonations and Indirect Ignition Processes; Progress in Astronautics and Aeronautics, Vol. 133, pp. 279-294 (1990)

[5] Hofmann, M.: Auswirkungen von Hindernissen auf Oberflächedetonationen, Dissertation, BAM/TU Berlin (2001)

[6] Hieronymus, H., et. al.**:** Characterisation of surface explosions**,** Archivum Combustionis, vol. 21, pp. 117-125 (2001)

[7] Glinka, W., et. al.: Detonations in model foams, Archivum Combustionis, vol. 14, pp. 97-110 (1994)

[8] Henschen, Ph.: Untersuchung von Oberflächen- und Schaumdetonationen; Dissertation BAM/TU Berlin (1999)

[9] Henschen, Ph., et al.: Explosions and Detonations of Foams., Proceedings of the 9th Int. Symposium on Loss Prevention and Safety Promotion in the Process Industries, pp. 632-640 (1998)

[10] Solouhkin, R. I.: Bubble mechanism of shock ignition in a liquid, Dokl. Akad. Nauk. SSSR. 1961, 136 (2), pp. 311-312 (1961)

[11] T.Hasegawa, T.Fujiwara: Detonation in Oxyhydrogen Bubbled Liquids. Nineteenth Symposium on Combustion, pp. 675-683 (1982)

[12] A.I.Sychev: Shock-Wave Ignition of liquid-gas Bubble Systems, Combustion, Explosion and Shock Waves, Vol. 21, N. 2, pp. 250-253 (1985)

[13] Villermaux, J.: Future challenges for basic research in chemical engineering, Chem. Engng. Sci., 48 (14), pp. 2525-2535 (1993)

[14] Ullmann's Encyclopedia of Industrial Chemistry. 5th Ed., Vol. A8, pp. 219; VCH Verlagsgesellschaft mbH, (1987)

[15] Howell, J.A., Leslie, S.W., Kenneth, J.: Oxidation of cyclohexane, GB Patent Nr. 1025752, 14. Apr. 1966

[16] Greene, M. I, Summer, C., Gartside, R.J. : Cyclohexane oxidation, US Patent Nr. 6,008,415, 28. Dec. 1999

[17] A.I.Sychev, A.V. Pinaev: Self-Sustaining Detonation in Liquids with bubbles of Explosive Gas , Zournal of applied mechanics and technical physics, N. 1, pp.119-123 (1986)

[18] E. Wlodarczyk: Analysis of the efficiency of initiation of detonation by 'hot spots' generated by shock compression of gas bubbles included in the explosive. Part I. Analysis of the experimental data. J. of Tech. Phys., 33, 1, 35-61 (1992)

[19] E. Wlodarczyk: Analysis of the efficiency of initiation of detonation by hot spots generated by shock compression of gas bubbles included in the explosive. Part II Theortical Analysis. J. of Tech. Phys., 33, 2, 133-166, (1992)

[20] Kornfeld, M. & Suvorov: On the destructive action of a cavitation. J. Appl. Phys. 15, 495 (1944)

[21] Naude & Ellis: On the mechanism of cavitation damage by non-hemispherical cavities collapsing in contact with a solid boundary. Trans. ASME D: J. Basic Engng 83, 648-656 (1961)

[22] Benjamin, T. P. & Ellis, A. T. : The collapse of cavitation bubbles and the pressures thereby produced against solid boundaries. Phil. Trans. R. Soc. Lon. A 260, 221 – 240 (1966)

[23] Brunton, J. H. : Erosion by liquid shock. Proc. 2nd Intl Conf. On Rain Erosion (ed. A. A. Fyall & R. B. King), Royal Aircraft Establishment, UK, p. 291 (1967)

[24] Lauterborn, W. : Liquid jets from cavitation bubble collapse. Proc. 5nd Intl Conf. On Erosion by Liquid and Solid Impact (ed. J. E. Field), Cavendish Lab., Cambridge, UK, paper 58 (1979)

[25] A. E. Beylich and A. Gülhan: On the structure of nonlinear waves in liquids with gas bubbles, Phys. Fluids A 2, 1412 (1990)

[26] A.V.Pinaev, A.I.Sychev: Structure and Properties of Detonation in a Liquid-Gas Bubble System Combustion, Explosion and Shock Waves, Vol. 22, N. 3, pp. 360-368 (1986)

[27] A.I.Sychev: The Effect of Bubble Size on the Detonation Wave Characteristics. Combustion, Explosion, and Shock Waves, vol.31, no.5, pp.577-584 (1995)

[28] Gabrielle, DuPre: Explosive properties of energetic systems: application to technological hazards and industrial safety, Invited Lecture (Chair: J. Lee),17th International Colloquium on the Dynamics of Explosions and Reactive Systems, July 25 - 30, Heidelberg, Germany, (1999)

[29] Y.Tomita, A.Shima, T.Ohno: Collapse of multiple gas bubbles by a shock wave and induced impulsive pressure. J. Appl. Phys. Vol.56 No.1, 125-131, (1984)

[30] J. P. Dear & J. E. Field: A study of the collapse of arrays of cavities, J. Fluid Mech., 190, pp. 409-425, (1988)

[31] A. Shima: Studies on bubble dynamics. Shock Waves, Volume 7, Issue 1, pp. 33-42 (1996)

[32] Plesset, M. S. & Prosperetti, A.: Bubble dynamics and cavitation. Ann. Rev. Fluid Mech. 9, pp. 145, (1971)

[33] Mørch, K. A.: Dynamics of cavitation bubbles and cavitation liquids, in Erosion. (Ed. C. M. Preece), pp. 309-353, Academic (1979)

[34] Tomita, Y., Shima, A.: mechanisms of impulsive pressure generation and damage pit formation by bubble collapse. J. Fluid Mech. 169, 535-564

[35] Hickling, R. & Plesset, M. S.: Collapse and rebound of a spherical bubble in water. Phys. Fluids 7, 7-14 (1964)

[36] Bruckert, B., Frost, D., Meidani, A., Chue, R. and Brouillette, M.: Dynamics of a single reactive gas bubble. In: Morioka, S. and van Wijngaarden, L. (eds), Proc. IUTAM Symp. on Liquid/Gas and Liquid/Vapour Two-Phase Systems, Kyoto, Japan pp281-292 (1994)

[37] Plesset, M. S. & Chapman, R. B.: Collapse of an initially spherical vapour cavity in the neighbourhood of a solid boundary. J. Fluid Mech. 47, 283 (1971)

[38] Mader, Ch.L.: Numerical modeling of detonation. in: Los Alamos Ser. in Basic and Applied Sci., Univ. of California Press (1979)

[39] Brennen, Christopher E.. Fission of Collapsing Cavitation Bubbles. Presented at CAV2001:Fourth International Symposium on Cavitation, California Institute of Technology (USA). June 20-23, 2001. http://resolver.library.caltech.edu/cav2001:sessionA5.006

[40] Chaudhri, M. M., Almgreu, L.A. & Perrson, A.: High speed photography of the interactions of shocks with voids in condensed media. Proc. 15th Intl Conf. On High Speed Photography and Photonics, SPIE, vol. 348, p. 388 (1982)

[41] T.Fujiwara, T.Hasegawa: Shock Propagation in Liquid-Gas Media. Proceedings of 13th International Symposium on shock tubes and Waves, pp. 724-732 (1981)

[42] T.Hasegawa, T.Fujiwara: Shock wave Deformation of a Nonspherical Gas Bubble in Liquids. Proceedings of 13th International Symposium on Space Technology and science, pp. 583-591 (1982)

[43] Nakroyakov, V.E., Donstov, V.E.: Pressure Waves interaction in a liquid with gas bubbles and bubble fragmentation" In: Proc. Int. Symp. Two-Phase Flow Modeling and Experimentation, Vol.2, Rome, Italy, pp. 951-958 (1995)

[44] V.K.Kedrinskii, C.L.Mader: Accidential Detonation in Bubble Liquids, in: Shock Tubes and Waves, H.Gronig [Ed], VCH, pp.371-376 (1987)

[45] T. Hasegava, T. Fujiwara: Propagation velocity and mechanism of bubble detonation. In:

Dynamics of Shock Waves, Explosions, and Detonations (Progress in Astronautics and Aeronautics, Vol. 94), American Institute of Aeronautics and Astronautics, pp. 309-319 (1984)

[46] A.I.Sychev: Detonation Waves in a liquid-gas Bubble System. Combustion, Explosion and Shock Waves, Vol. 21, N. 3, pp.365-371 (1985)

[47] A.I.Sychev: Bubble Detonation in Polydisperse Media. Combustion, Explosions and Shock Waves, vol.33, No.3, pp.339-343 (1997)

[48] Gülhan, A.and Beylich, A. E.: Detonation wave phenomena in bubbled liquid Proc. 17th Int. Symp. on Shock Tubes & Waves, July 1989, Bethlehem, USA

[49] Beylich, A. E. and Gülhan, A.: Waves in reactive bubbly liquids in:Meier, G. and Thompson, P. (eds), Proc. IUTAM Symp. on Adiabatic Waves in Liquid-Vapour Systems, Göttingen, Germany, pp. 39-48 (1989)

[50] Rubach, T.; Blum, C.; Schecker, H. G.: On the vibration behavior of gas bubbles exploding in suspensions and in diluted polymer solutions, Acustica, 78(2), 93-100 (1993)

[51] A.V.Pinaev, A.I.Sychev: Effects of Gas and Liquid Properties on Detonation-Wave Parameters in Liquid-Bubble Systems., Combustion, Explosion and Shock Waves, Vol. 23, N. 6, pp.735-742 (1987)

[52] A.I.Sychev: Energy Limits For the Existence of Detonation Waves in bubbly Media. Combustion, Explosion, and Shock Waves, vol.30, no.1, pp. 86-90 (1994)

[53] A.I.Sychev: Structure of a Bubble-Detonation Wave. Combustion, Explosion, and Shock Waves, vol.30, no.4, pp.517-521 (1994)

[54] E. Brandes and W. Möller: Sicherheitstechnische Kenngrößen, Vol. 1, PTB, Wirtschaftverlag NW (2003)

[55] A.I.Sychev: Structure and properties of detonation in the systems liquid-gas bubbles (Struktura i svoistva detonazii v sistemah zidkost'-puzir'ki gaza), Novosibirsk, Lavrent'ev Institute of Hydrodynamics, Siberian Division of USSR Academy of Sciences, dissertation, 135 pages (1988)

[56] Lewis, B. and von Elbe, G.: Combustion, Flames and Explosions of Gases, Academic Press, Orlado Florida (1987)

[57] I. J. Campbell and A. S. Pitcher: Shock waves in a liquid containing gas bubbles, Proc. R. Soc. London Ser. A, 243, 534 (1958)

[58] Shock Waves in Mixtures of Liquids and Air Bubbles. L.Noordzij; Dissertation Technische Universität Twente (1973)

[59] Noordzij, L., van Wijngaarden, L.: Relaxation effects, caused by relative motion, on shock waves in gas-bubble/liquid mixtures. J. Fluid Mech. 66, 115-144 (1974)

[60] Borisov, A.A., Gelfand, B.E., Timofeev, E.I.:Shock waves in liquid containing gas bubbles. Int. J. Multiphase Flow 9, 531-543, (1983)

[61] Wave Propagation in Gas-Liquid Media. V.E.Nakroyakov, B.G.Pokusaev, I.R.Schreiber, CRC Press (2000)

[62] L.van Wijngaarden: On the structure of shock waves in liquid-bubble mixtures. Appl. Sci. Res. 22, pp.366-381 (1970)

[63] Nigmatulin, R.I., Shagapov, V. Sh. : Structure of shock waves in a liquid containing gas bubbles. Izvestiya Akademii Nauk SSR, Mekhanika Zhidkosti i Gaza, vol. 6, p. 30-41 (1974)

[64] V.K.Kedrinskii: Wave Processes and Structure dynamics in inhomogeneous media under pulsed loading. Journal of Applied Mechanics and Technical Physics, Vol.38, No.4, pp. 598-624 (1997)

[65] A. E. Beylich: Pressure waves in bubbly liquids. In: IUTAM Symp. on Waves in Liquid/Gas and Liquid/Vapor Two-Phase Systems, Kyoto, Japan, Eds: K.Morioka and L.van Wijngaarden, pp.87-106. Kluwer Academic Publishers, Dordrecht, NL (1995)

[66] Overhoff, K. H.; Schecker, H. G.; Fellensiek, J.; Onken, U.: Explosion behavior of bubbles ignited under water, DECHEMA-Monogr., 111(Fortschr. Sicherheitstech. 2), 221-35; ISSN: 0070-315X (1988)

[67] Kedrinskii, V.K. and Zamaraev, F.N.: Wave amplification in chemically active bubble medium. In: Kim, Y.W. (ed.), Proc. 17th Int. Symp. On Shock Waves & Shock Tubes, Bethlehem, USA, pp. 51-62 (1989)

[68] Scarinci, T., Bassin, X., Lee, J.H.S. and Frost, D.L.: Propagation of a reactive wave in a bubbly liquid. in: Takayama, K. (ed.) Proc. 18th Int. Symp. on Shock Waves, Sendai, Japan, Springer-Verlag, Berlin, Vol. 1, pp. 481-484 (1991)

[69] Barbone, R. and Frost, D. L.: Propagation of a Reactive Wave in a Weakly Confined Bubbly Liquid, Proceedings of the 16th International
Colloquium on the Dynamics of Explosions and Reactive Systems, Krakow, Poland, Wydawnictwo Akapit (publishers), p. 615 (1997)

[70] European Standard: EN-1127-1 (1997)

[71] International standard ISO/FDIS 13943: Fire safety-vocabulary (1999)

[72] Christen, H. R.: Grundlagen der allgemeinen und anorganischen Chemie, Otto Salle Verlag, Berlin (1985)

[73] Hieronymus, H.; Plewinsky, B; Anwendbarkeit sicherheitstechnischer Kenngrößen zur Beschreibung der Explosionsgefahren im heterogenen System organisches Lösemittel/gasförmiges Oxidationsmittel; 8. Kolloquium zu Fragen der chemischen und physikalischen Sicherheitstechnik; BAM/PTB; Berlin (1999)

[74] Gaseous Detonations. M.A.Nettleton; Chapmann and Hall (1987)

[75] Combustion Fundamentals. R. A. Strehlow, International Student Edition, McGraw-Hill Book Co., ISBN: 0070622213 (1984)

[76] Brandes et. al. in: §3.1, Handbook of Explosion Prevention and Protection, M. Hattwig, Wiley-VCH (2003)

[77] McGraw-Hill Dictionary of Scientific and Technical Terms, McGraw-Hill Professional Publishing, ISBN: 007042313X (2002)

[78] D.Bjerketvedt, J.R.Bakke, K.van Wingerden: Gas Explosion Handbook. Journal of Hazardous

Materials 52, pp. 1-150 (1997)

[79] Fluid Mechanics (Landau and Lifshitz Course of Theoretical Physics, Vol. 6),L.D. Landau, E.M. Lifshitz., Butterworth-Heinemann, 2nd edition (1995)

[80] H. J. Pasman, A. A. Pekalski and M. Braithwaite: Getting better grip on gas phase hydrocarbon oxidation processes; the EU SAFEKINEX project. Proceedings of the 11th Int. Symp. Loss Prevention, pp.- PG2101-PG2108 (2004)

[81] Berechnung von Druckbehältern, AD B0, Verband der Technischen Überwachungs-Vereine e.V. (1986)

[82] Schrauben, AD B7, Verband der Technischen Überwachungs-Vereine e.V. (1986)

[83] Flansche, AD-Merkblatt B8, Verband der Technischen Überwachungs-Vereine e.V. (1998)

[84] BAM Qualitätssicherungs-Handbuch OE II.2902, Arbeitsanweisung: Kalibrierung von Druckmessketten mit piezoelektrischen Druckaufnehmern, in preparation

[85] Gavrilenko, T.P.: Transition of combustion into detonation in mixtures based on acetylene. Fizika Goreniya i Vzryva, Vol. 16, No. 5, (1980) 148-149 (in Russian)

[86] The shock tube in high-temperature chemical physics. A. C. Gaydon, I. R. Hurle, Chapman and Hall Ltd, London (1963)

[87] Dengel, J., Vorarbeiten zur Untersuchung des Explosions- und Detonationsverhaltens von Sauerstoffblasen in organischen Lösemitteln, Studienarbeit, TU-Berlin / BAM-Berlin, Sept. 2000

[88] A. Sam, C.O. Gomez, J.A. Finch: Axial velocity profiles of single bubbles in water/frother solutions. Int. J. Miner. Process. 47 177-196 (1996)

[89] Li Chen, Suresh V. Garimella, John A. Reizes, Eddie Leonardi: The development of a bubble in a viscous liquid. J. Fluid Mech. 61-96 (1999)

[90] R. Krishna, M.I. Urseanu, J.M. van Baten, J. Ellenberger: Wall effects on rise of single gas bubbles in liquids. Int. Comm. Heat Mass Transfer, Vol 26, pp 781-790, 1999

[91] Perry's Chemical engineers' handbook, seventh edition, McGraw-Hill, ISBN 0-07-115448-5 (1997)

[92] R. Brdicka, Grundlagem der physikalischen Chemie, VEB Deutscher Verlag der Wissenschaften, Berlin (1982)

[93] CRC Handbook of Chemistry and Physics, 81th edition, CRC Press (2000)

[94] Stephan Mayinger: Thermodynamik. Grundlagen und technische Anwendungen, 13 Auflage, band 2, Springer-Verlag (1991)

[95] P. W. Atkins: Physical Chemistry, 5th edition, Oxford university press (1994)

[96] see Table 66 in: Einführung in die chemische thermodynamik. G. Kortüm, Vandenhoeck & Ruprecht Gmbh, Göttingen, (1960)

[97] Korea theromophysical properties databank, http://www.cheric.org/kdb/ (Last accessed: Aug. 2004)

[98] DIN 51 794, Bestimmung der Zündtemperatur, Jan. 1978

[99] Einführung in die chemische Thermodynamik. G. Kortüm, Vandenhoeck & Ruprecht GmbH, Göttingen, (1960)

[100] Clift, R; Grace, J. R.; Weber, M. E.: Bubbles, Drops and Particles; Academic Press, New York, 1978

[101] Ya.B.Zel'dovich and Yu.P.Raizer: Physics of Shock Waves and High – Temperature Hydrodynamics Phenomena I., Editor: W. D. Hayes and R. F. Probstein, Academic Press, New York (1966)

[102] K. Mitropetros, B. Plewinsky, J. Steinbach, H. Hieronymus:
First oscillation shock induced oxygen bubble dynamics and ignition inside a cluster of a monodispersed bubbly organic liquid
Proceedings of the 19th International Colloquium on the Dynamics of Explosions and Reactive Systems, July 27 - August 1, 2003, Kanagawa, Japan

CD ISBN 4-9901744-1-0 C3053, Article number 96.

[103] Ch. L. Mader, Numerical modeling of detonation, in: Los Alamos Ser. In Basic and Applied Sci., Univ. of California Press (1979)

[104] S. M. Frolov, B. E. Gel´Fand, and E. I. Timofeev: Interaction of a liquid film with a high-velocity gas flow behind a shock wave. Combustion, Explosion and Shock Waves, Vol. 20, N. 5, pp.573-579 (1984)

[105] The theory of jets in an ideal fluid. Gurevich, International series of monographs in pure and applied mathematics, Vol. 93, Pergamon press, London (1966)

[106] Norm prEN 1839: Bestimmung der Explosionsgrenzen von Gasen und Dämpfen; Methode ‚B' (Bombenmethode), Version Feb. 2001

[107] Apel, W., Bestimmung von Explosionsgrenzen von Cyclohexan in reinem Sauerstoff, Studienarbeit TU Berlin / BAM Berlin, Jun. 2003

[108] Liquids Under Negative Pressure. A.R.Imre, H.J. Maris and P.R. Williams (edit.), NATO science series, II. Mathematics, physics and chemistry, Vol. 84, ISBN 1-4020-0896-1, Kluwer Academic publishers, London (2002)

[109] Kedrinskii VK: Negative pressure profile in cavitation zone at underwater explosion near a free surface. Acta Astronautica 3: 623-632 (1976)

[110] T.Krauthammer, A.Altenburg: Negative Phase blast effects on glass panels. International Journal of Impact Engineering 24, pp.1-17 (2000)

[111] Beylich, A. E. and Gülhan, A.: On the structure of nonlinear waves in liquids with gas bubbles. Phys. Fluids A 2, 1412 (1990)

[112] H.S. Carslaw, J.C. Jaeger: Conduction of Heat in Solids, Second edition, Clarendon Press, Oxford (2001)

List of figures

List of tables

List of equations